Transactions

of the

ASME

MAY, 1951

VOL. 73, NO. 4

Transactions

of The American Society of Mechanical Engineers

Published on the tenth of every month, except March, June, September, and December

---

Published monthly by The American Society of Mechanical Engineers. Publication office at 20th and Northampton Streets, Easton, Pa. The editorial department is located at the headquarters of the Society, 29 West Thirty-Ninth Street, New York 18, N. Y. Cable address, "Dynamic," New York. Price $1.50 a copy, $12.00 a year for Transactions and the *Journal of Applied Mechanics*; to members and affiliates, $1.00 a copy, $6.00 a year. Changes of address must be received at Society headquarters four weeks before they are to be effective on the mailing list. Please send old as well as new address. . . . By-Law: The Society shall not be responsible for statements or opinions advanced in papers or . . . printed in its publications (B13, Par. 4). . . . Entered as second-class matter March 2, 1928, at the Post Office at Easton, Pa., under the Act of August 24, 1912. . . .

The Manufacture of Small Ice[1]

By CROSBY FIELD,[2] BROOKLYN, N. Y.

Small ice may be defined as water frozen in the form of ribbons, strips, fragments, cubes, or relatively small pieces, whether regular or irregular in shape, or pieces compounded thereof, or compounded of crushed ice. With the exception of ice cubes frozen in the domestic electric or gas refrigerator, it is only at the beginning of its third decade of successful commercialization. The daily production of small ice is now a substantial tonnage, a growth from less than 10 tons per day at the time of the visit of the Metropolitan New York Section of the American Society of Refrigerating Engineers to the author's first commercial plant in 1928 (1).[3] Although the reasons for this growth will be mentioned briefly, this paper will be limited to an abbreviated description of the numerous developments of processes and machinery for freezing small ice, including those in commercial operation today. No mention will be made of the equally numerous methods of freezing large cakes of ice and then crushing, sawing, or grid or wire-melting them into small ice, the product of which has not been included in the production stated.

History of Development

FOR all its commercial youth, small ice has a most extensive history, as a brief glance at the References will show.

Astonishing as it may now seem, the first ice to be made and sold was small ice. This took place long before the commercial use of compression or absorption of volatile gases to produce subfreezing temperatures. Siemens (2)[4] obtained a 30 F temperature drop by the controlled dissolving of calcium chloride in water and used it to freeze ice, but it remained for Tosselli[5] to get a 40 F drop by using ammonium nitrate and water. His machine comprised an "ice can containing several slightly tapering molds of circular cross section of various sizes. The molds being filled with water are introduced into the freezing mixture; and in a few minutes ice is formed around the edges to the thickness of nearly 1/8 in. The rings or tubes of ice are then removed and placed one within the other forming a small stick of ice."[6] In this type of process the salt was recovered by evaporating the solution to dryness and re-using it.

Siemens and Tosselli were not the first, as we are informed that in the period 1630–1660 frozen lemonade was peddled in the streets of Paris (4). Of course, Lord Bacon, who died in 1626, used snow or ice with saltpeter to produce subfreezing temperatures. Snow and ice became quite a trade in France in the reign of Henri III, and Greece, Rome, and India all enjoyed snow-cooled wine in the times of the ancients.[7] As, however, we have no record of the ice having been man-made, no further discussion of this phase is included.

With improved methods of producing refrigeration for ice making, a short recrudescence occurred in 1907 in the form of a conical drinking cup made wholly of ice, called an "ice goblet," invented by H. D. P. Huiser of the Netherlands (5).

U. S. Patent 1941 issued January 23, 1841, to T. B. Smith of St. Louis, Mo., proposed a method of freezing by exposure to the atmosphere when the circumambient air was below freezing, of water in laminae or increments, of 1/8 to 1/4 in. in thickness and which might have been used to obtain small ice.

In 1755 Dr. William Cullen[8] introduced the "vacuum process" of refrigeration, using water as the refrigerant, and in 1810 Leslie greatly improved it by combining the vacuum pump with the use of sulphuric acid to absorb the water vapor. He produced from 1 to 1 1/2 lb of ice at a single operation. This operation was improved by others, such as Vallence, and years later (1850) Edmund Carré invented a machine for the manufacture of small quantities of ice for domestic purposes.[9]

About this time there entered the competition of a new refrigerating cycle, Dr. John Gorrie's cold-air or dense-air machine (U. S. Patent 8080, May 6, 1851).[9] In England this type was improved, and T. B. Lightfoot[10] invented improvements and introduced it into extensive general use, beginning about 1882.

Block or Small Ice

Although this paper deals with small ice, major developments in the field of primary refrigeration to produce ice, block or small, may not be entirely ignored, but references will be as condensed as possible.

In 1834 the first experimental machine using the compression process—today so universal—was built by John Hague from designs by Jacob Perkins. Volatile liquids to be used were methylene ether, sulphur dioxide, volatile derivatives of coal tar.[11] Note a little later the statement could be made, "anhydrous ammonia, which may now be obtained as an article of commerce, used for refrigeration in Germany and the United States."[12] Perkins used mechanical paddles to produce clear ice by means of agitation. Because of historic interest, plates 53 and 54 of Lightfoot's paper are reproduced here as Figs. 1 and 2. Note also Perkins (English Patent No. 6662, August, 1834) and our own Prof. A. C. Twinning of New Haven, Conn. (U. S. Patent 10,221, November, 1853) (7).

In the 1860's P. E. Carré of France invented a compression system using "ether, sulphuret of carbon, etc.," and an ammonia absorption system,[11] obtaining U. S. Patent 30,201, issued October 2, 1860. In 1868 the Louisiana Ice Company started operation of an ice plant, using his absorption system, and produced 25-lb blocks of ice.[13] Beginning in 1867, Rees Reece, Stanley, Ponti-

[1] The author is aware of the human tendency to be overcritical of the work of others in one's own field. Therefore, throughout this paper all statements regarding the work of others have been taken directly from the sources indicated. The author has intentionally withheld any opinions and criticisms of these statements except where there is conflict between the statements and the author's work and experience—and even then such comments and criticisms are expressed only where omission would be misleading.

[2] President, Flakice Corporation. Fellow ASME.

[3] Numbers in parentheses refer to the Bibliography at the end of the paper.

[4] Reference (2), p. 203.

[5] Ibid., p. 203; also reference (3).

[6] Ibid., p. 203.

Contributed by the Process Industries Division and presented at the Annual Meeting, New York, N. Y., November 26–December 1, 1950, of The American Society of Mechanical Engineers.

Note: Statements and opinions advanced in papers are to be understood as individual expressions of their authors and not those of the Society. Manuscript received at ASME Headquarters, Oct. 31, 1949. Paper No. 50—A-5.

[7] Reference (4), p. 447.

[8] Reference (2), p. 206; reference (6), p. 329.

[9] Reference (6), p. 330.

[10] Reference (2), pp. 223-238.

[11] Ibid., p. 210.

[12] Ibid., p. 216.

[13] Reference (7), p. 68.

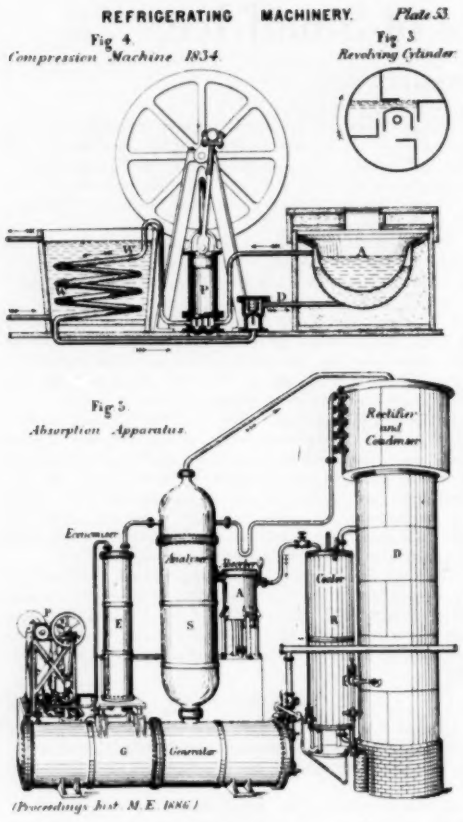

FIG. 1 EARLY COMPRESSION AND ABSORPTION REFRIGERATING MACHINES
(Courtesy British Institution of Mechanical Engineers.)

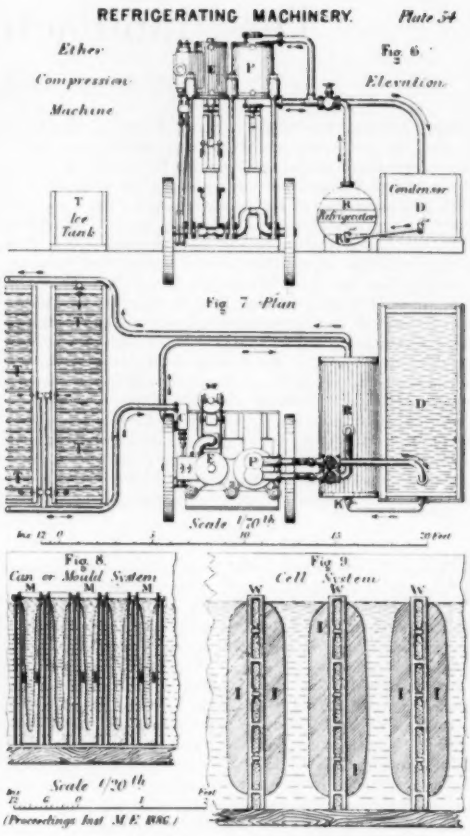

FIG. 2 MORE EARLY ICE-MAKING MACHINES
(Courtesy British Institution of Mechanical Engineers.)

fex, and Wood of England invented their improvements, and 1869 saw the invention in Sydney, Australia, by Morl and Nicolle of the Binary absorption system, using ammonia and water.[11]

Competition between the several methods of producing primary refrigeration for ice making and for cooling then became accelerated. During 1876–1877, Carl von Linde of Munich, Germany, produced his ammonia compression machine. In 1878 Franz Windhausen of Berlin patented a compound vacuum pump and in 1881 he brought out such a machine to produce 12 to 15 tons of ice per 24 hr, using sulphuric acid, but his system could be used without it. On February 16, 1869, a U. S. Patent (No. 87,084) was issued to Dr. P. H. Vander Weyde, of Philadelphia, Pa., which included the adaptation to ice manufacture of "naphtha, gasoline, rhigolene, petroleum, ether, or the condensed petroleum-gas or chimogene." He also produced ice in the form of long cylinders by freezing in tubes.

On September 26, 1869, U. S. Patent No. 95,347 was issued to Daniel L. Holden, thus introducing one of the foremost names in small-ice development, whose long hard struggle ended in tragic failure. Between that date and March 4, 1913 (see Fig. 3), numerous patents were issued to him. He installed plants in Newark, Baltimore, and other places, each of which was, he thought, technologically satisfactory, but which commercially proved a failure. Several hypotheses have been advanced as reasons for these failures, in which it is believed the inferior thermal and physical characteristics of ice so made play a large part.

Our old friend Dr. Vander Weyde moved from Philadelphia to New York and obtained U. S. Patent No. 108,851 on November 1, 1870, showing a method of building up an ice slab by freezing crusts, each $\frac{1}{2}$ in. thick, by intermittent additions of precooled water. He states he has "attempted to imitate Nature, and freeze water from above," but he must have offended her as well by recommending that his machine "be used for ether, bisulphide of carbon, methylic ether, or any other appropriate liquid"; this just after mentioning chymogene or cryogene!

An approach to small ice, although we do not know how near he actually came, is shown in U. S. Patent No. 177,845 issued May 23, 1876, to A. Jas of New Orleans, La.

Among the early patents is that to C. L. Riker, No. 191,256

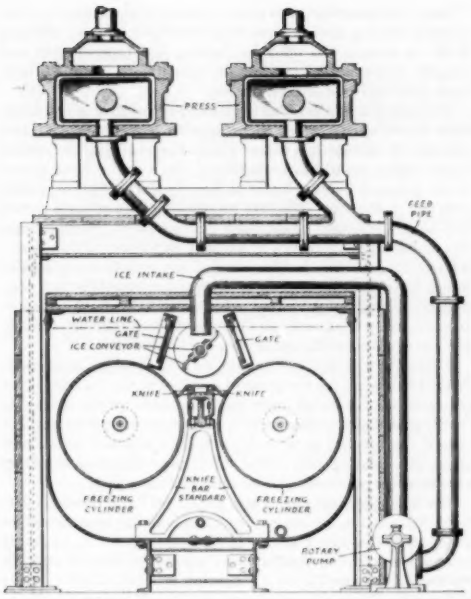

FIG. 3 ONE OF THE HOLDEN SLUSH ICE AND BRIQUETTING PRESSES

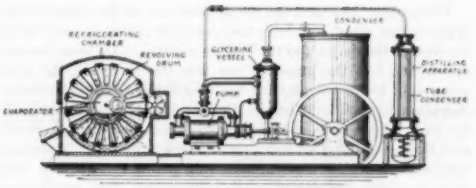

FIG. 4 ONE OF LINDE'S ICE MACHINES

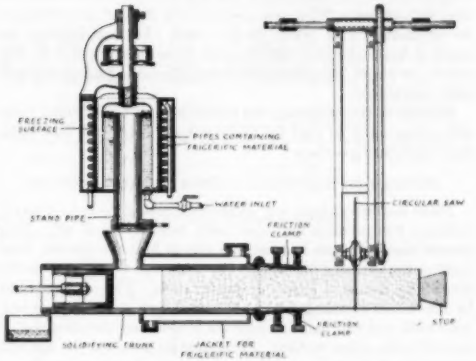

FIG. 5 ANOTHER OF HOLDEN'S ICE MACHINES

issued May 27, 1877. Another possible producer of small ice is shown in the U. S. Patent No. 228,364, issued June 1, 1880, to C. P. G. Linde of Munich, Germany, already well known for his work on low temperatures (see Fig. 4). His invention comprised a refrigerated revolving drum "with radial ice collecting coils, to enable the ice to be formed in thin films or layers, and thereby rendered transparent." (We know this to be a non sequitur today.)

We dare not pass over this period without an occasional reference to Holden, so we note his Patent No. 530,526 issued December 11, 1894 (see Fig. 5). Here we find a refrigerated vertical cylindrical vessel freezing ice on its sides, which is scraped off by slowly revolving scrapers or cutters, floats to the top of the contained water, overflows into a downspout leading to a piston-type press, where it is pressed into a large cake to be cut into smaller blocks by a swinging circular saw.

G. H. Abrams (No. 654,576, July 24, 1900) froze ice in jacketed molds mounted on wheels and pushed into a room where cold air was circulated through the jackets and the room. Water was fed to the molds periodically to form strata of ice, making large blocks which were then thawed free by admitting steam to the jackets. S. N. Smith of Philadelphia, Pa. (No. 703,353) shows two refrigerated revolving cylinders submerged in a tank turning in opposite directions with cutters intended to produce slush to be compacted (Fig. 6).

W. E. Crane (No. 763,089, June 21, 1904) shows a rather complicated machine, and G. K. Davol (No. 988,316, April 4, 1911), proposed freezing a block of ice built up by laminae on a mercury-freezing surface. The period ends with No. 1,054,771 issued to Daniel L. Holden, March 4, 1913 (Fig. 3). The twin refrigerated submerged drums of Smith (supra) have been adopted, cutters, pumps, presses, etc., have been improved. Holden is reported to have built machines according to this patent and to have made ice in large opaque blocks.

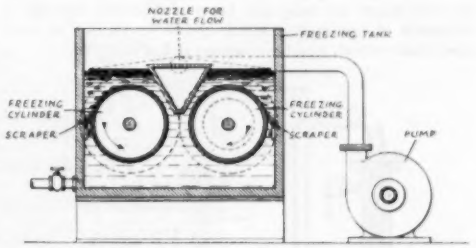

FIG. 6 S. N. SMITH'S SLUSH ICE MACHINE OF THE YEAR 1902

AUTHOR'S FIRST DEVELOPMENTS IN FIELD

In 1915 the author started his developments in the small-ice field, which have continued to the present and are now progressing at a highly accelerated rate.

The author's first small-ice machine comprised a vertical pipe, ammonia refrigerated by means of a bayonet pipe insert, on which water was sprayed. The ice thus produced was cut off by cutters pivoted within ring brackets which were carried up and down by a chain somewhat similar to the soot collectors on the old-fashioned Green economizers (for steam boilers). The pipe was also operated submerged in water.

These experiments were interrupted by the rumor that Holden had built plants for the manufacture of small ice. Why develop when you can buy? So a hunt for Holden was started, but both he and all his plants had completely disappeared, even his freezing drums from the "reclaimed metalman's" junk heap.

The author then took the drums from one of the several drum driers in his plant and built and operated (1916) a plant along the lines of the Smith and the Holden schemes. He found several difficulties, but the principal one was the fact that the large amount of water entrained in ice thus formed requires another operation to remove it before the ice can be used economically for most purposes, as was apparently recognized by both Smith and Holden, as they added a press to their freezers. Numerous calorimeter tests, extending over long periods, show that such slush ice, after draining at room temperature, until equilibrium is established with meltage, has a heat-absorption figure of about 102 Btu per lb; in other words, the entrapped water amounts to over 29 per cent. When compressed, it is difficult commercially to eliminate water below 10 per cent. For comparison, ice cracked from subcooled 300-lb cakes of ice runs about 126 Btu per lb, or about 12½ per cent water, depending upon size and other conditions.

Because of the foregoing, the author set out to develop a form of ice that could be used for many purposes just as it was taken from the freezing surface.

Problem of Removing Ice From Freezing Surface

There had never been any difficulty freezing ice onto a metal surface; the problem had ever been, how to get it off. Two general methods were known; one was to heat the surface, thus melting the adhering film of ice; the other was to cut some of the film off by means of knives or similar tools. The cutting could be done either submerged or in the atmosphere. The author had tried both and had found it impossible to obtain the most useful form of ice by either method. Therefore he invented the method of freezing the water on a flexible surface, and separating the ice thus formed by changing slightly the configuration of the surface. Ice thus frozen and subcooled, has proved both by test and by thousands of tons in commercial use, to be superior in heat-absorption content, long-time storage, and in other ways.

Since that invention, two other methods of separating ice from a metal freezing surface have been developed; one by wedging it off the surface, the other by freezing in a tapered mold and (usually hydraulically) pressing the cake from the mold surface. Both these will be discussed further.

The author next proceeded to make a large number of machines, each based upon one of the numerous embodiments of this principle of dislodging a frozen product by changing the outline of the surface on which it was frozen, and a few of these appear in the group of patents issued to him April 17, 1923, beginning with No. 1,451,901. The first Patent Office Examiner's Action had been a rejection based upon statements to the effect that this invention was contrary to the laws of nature. Fortunately, some of the machines had been tested at Cornell, during part of which tests some professors of impeccable standing had been present, so their affidavits caused a withdrawal of the rejection. In our country apparently all that's needed are affidavits enough, and any law can be changed, even a law of nature!

A machine was installed, and the ice from it sold commercially. Soon the demand for the product resulted in the building of an enlarged plant operated under test conditions by the author, so that large-scale experimental work in connection with the application of the product to all possible users continued for a dozen years (8). During this period, of course, numerous machines were leased or purchased and installed by others (10).

The first machines were water peeled (WP) as shown in No. 1,451,903; that is, the ice was detached from the freezing surface under water (see also Fig. 7). It was found later that ice frozen on a submerged freezing surface and then carried into the air while freezing is continued gave a subcooled product of 150 or more Btu per lb of heat-absorbing capacity, which has many advantages in subsequent handling, storage, and use.

This air-peeled (AP) product is made on a machine such as described in U. S. Patents No. 2,005,734 (June 25, 1935) and No. 2,257,904 (October 7, 1941). The essentials are shown in

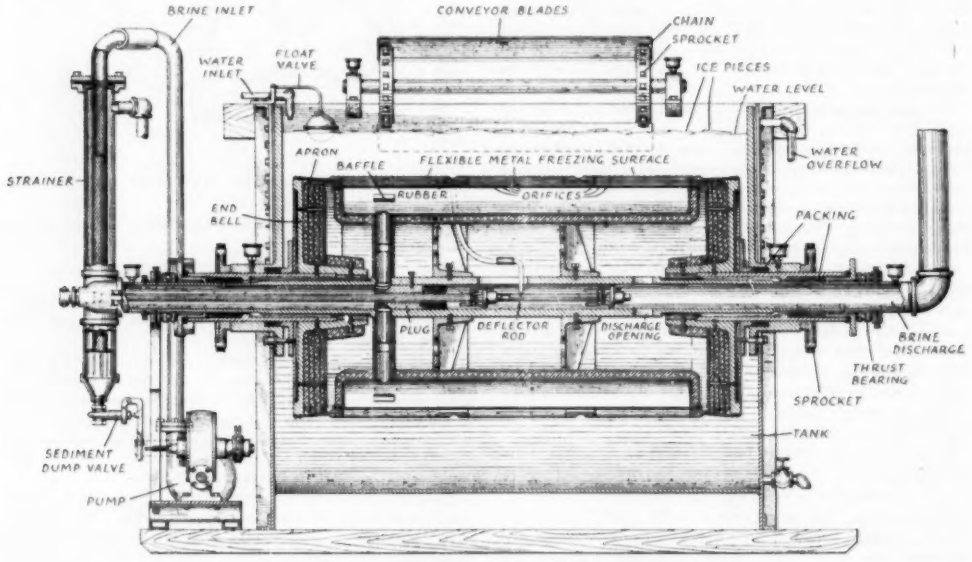

Fig. 7 Machine to Manufacture Water-Peeled Ice Ribbons

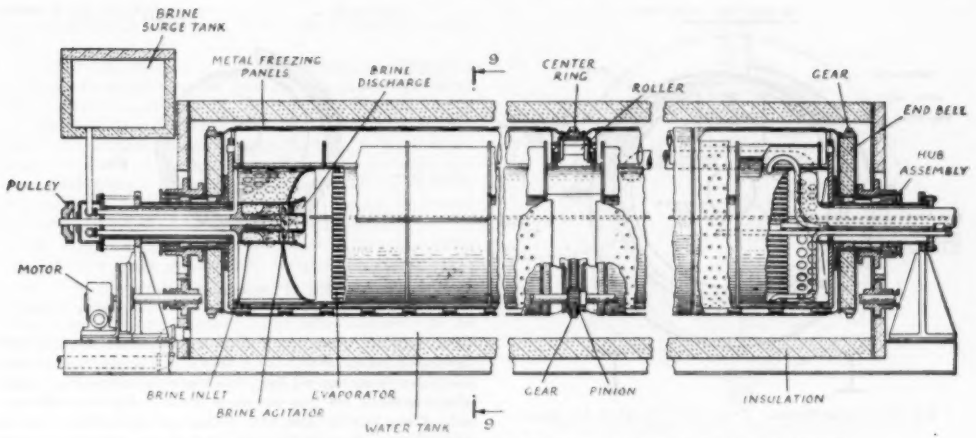

FIG. 8 ONE TYPE OF MACHINE FOR MANUFACTURING SUBCOOLED FLAKICE FROZEN WATER RIBBONS
(Note internal brine cooler.)

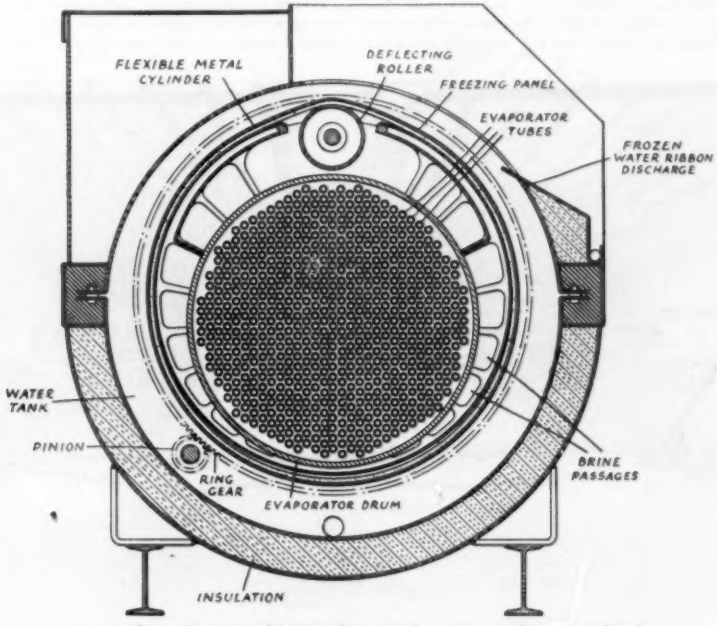

FIG. 9 CROSS SECTION OF MACHINE SHOWN IN LONGITUDINAL SECTION IN FIG. 8

Figs. 8 and 9. It is believed that the operation is obvious from a glance at Fig. 10 and its schematic simplification Fig. 11, bearing in mind that no knives or scrapers of any kind are used and that the separation is due entirely to the difference in elasticity between the ice and the cylinder metal to which it has frozen, and to the slight change in shape of the latter as it passes over the deflecting roller. Many tons of the subcooled FlakIce Frozen Water Ribbons thus produced may be stored in a properly designed bin without their freezing together (Fig. 12).

OTHER DEVELOPMENTS

It was not long, however, before others entered the field. One small company, the IXL, sold a very few machines cutting fine spicules of ice off the part in the air of a partly submerged

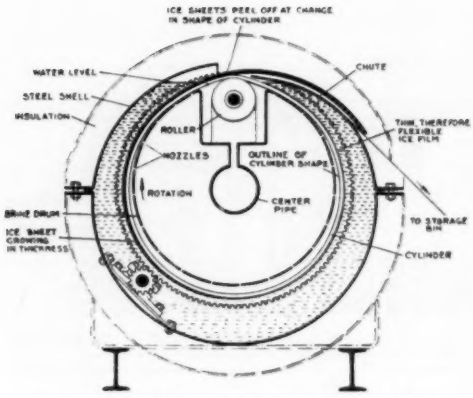

FIG. 10 CROSS-SECTION TYPE BRC FLAKICE MACHINE

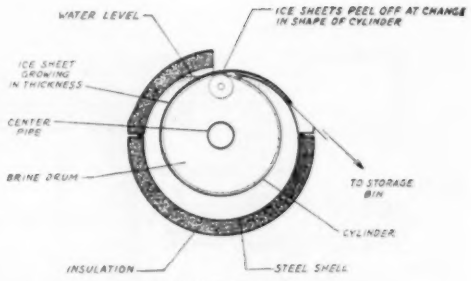

FIG. 11 SCHEMATIC DESIGN
(How Frozen Water Ribbons peel from the flexible freezing surface.)

revolving refrigerated drum. Gay, in co-operation with Carrier, experimented with a refrigerated drum, presumably along the lines of his patents No. 1,963,842, June 19, 1934, and No. 1,931,347, October 17, 1933, but more substantial progress was made by W. H. Taylor (9), whose "Pak Ice" machines shave the ice in a fashion similar to Holden, but which are much further developed mechanically. As is shown in Fig. 13, the machine comprises "a corrugated liner, fitted into an outer casing, liquid ammonia being fed into the space between the two. The inside of the liner is filled with circulating water which freezes rapidly on the liner surface and is constantly removed by tool steel scrapers" (Fig. 14). In order to adapt this product to certain uses Taylor developed a briquetter (Fig. 15).

Several inventors had by now entered the field, including the well-known Glenn Muffly, to whom Patent No. 2,145,773 was issued January 31, 1939, showing the "float or fall method of

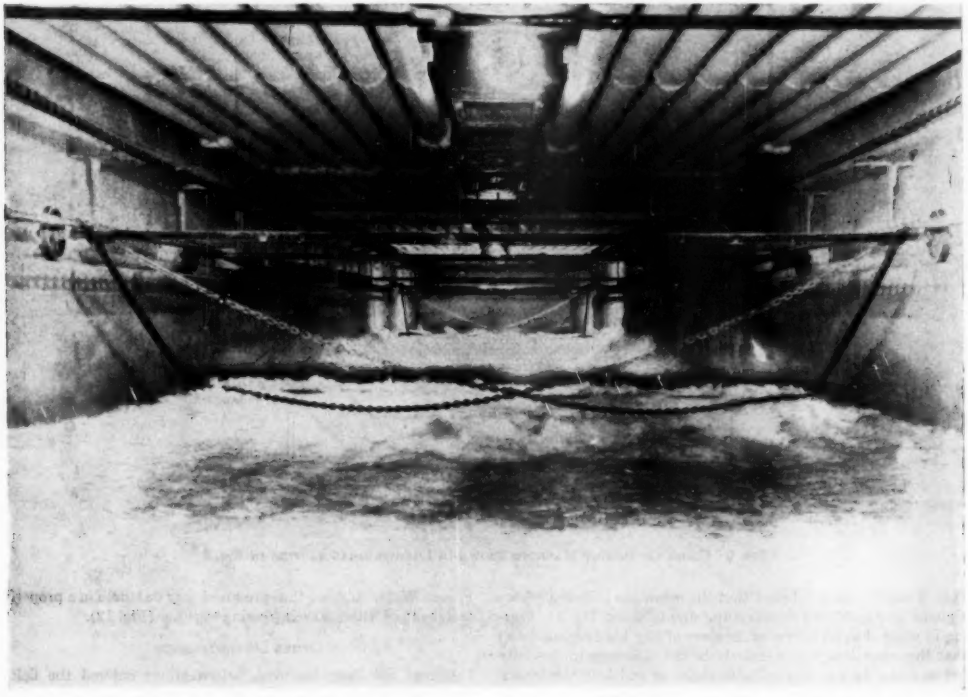

FIG. 12 AUTOMATIC STORAGE BIN FOR STORAGE OF LARGE TONNAGE OF FLAKICE FROZEN WATER RIBBONS

harvesting ice plus automatic control of cycles, quantity and size of ice."

The next type of machine to become commercialized uses the principle of wedging a narrow band or strip off the layer of ice adhering to the metal surface. The first large-sized machine to be built of this type is shown in Figs. 16, 17, and 18, taken from Patent No. 2,310,468, issued January 29, 1938, to Frank Short. Many thousands of machines operating on this principle have been made, using a special form of helical cutter, as shown in Fig. 19, taken from Patent No. 2,308,541, issued to Francis M. Raver, January 19, 1943, and modifications thereof.

Now enter the tapered freezing-chamber inventors, showing many improvements over our old friend Riker of the 1870's (*vide supra*), Patent No. 2,133,521 issued October 18, 1930, to Reinhard Wussow of Charlottenburg, Germany, and Fritz W. Fechner of Hamburg, Germany. The initial adherence of the ice body to the freezing surface is destroyed "by temporarily heating the latter," or the tube may be so designed, it is stated, that this adhesion is overcome "by the pressure produced by the expanding ice in the lower extension of the tube." Glenn Muffly in other patents shows machines utilizing this and similar principles. John R. Watt has described his machine using this tapered tube for freezing and a hydraulic ram for harvesting.

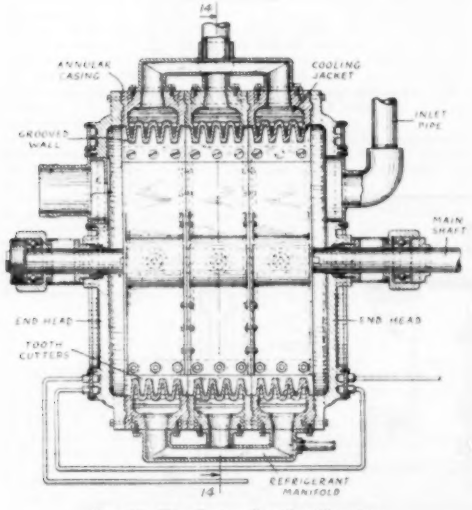

Fig. 13 The Taylor Pak Ice Machine

His machine has two features of importance. First, the freezing in laminae or "incremental films," as he calls them, and next, his design permits the rapid manufacture of large sizes of ice blocks or cakes. For further details refer to the inventor's 1948 paper (11).

The manufacture and sale of machines under the Flakice Corporation patents by the York Corporation, and the manufacture and sale of machines under the Pak Ice Patents by the Vilter Company have naturally created a situation inviting competition from other methods. Of these the only one to date to have become commercial is the Henry Vogt & Company Tube Ice machine, which freezes ice within long vertical tubes. Harvesting is obtained by heating the tubes periodically for a short

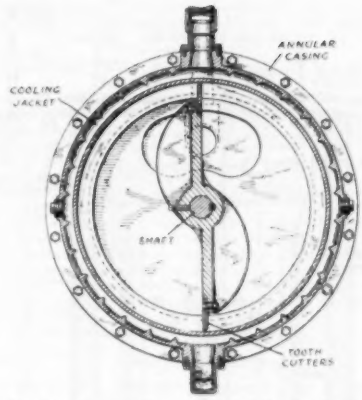

Fig. 14 Another View of Taylor Pak Ice Machine

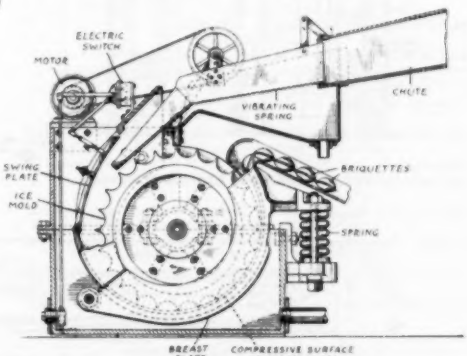

Fig. 15 The Taylor Slush Ice Briquetter

time; as the rods of ice fall they are cut into short lengths by a special form of cutter (12).

A flexible belt type of ice-making machine is shown in Patent No. 2,412,621 issued December 17, 1946, to Frank W. Knowles, and recently considerable activity has been evident in the development of other small-ice freezers. As authentic information about their commercial operation has not been made public, to the author's knowledge, further details cannot be given here.

The advent of the York Automatic Cube Ice Maker, which freezes ice in vertical square cross-sectioned tubes and releases the ice by heating the tubes in one of several different ways, has been followed by the development of several competing devices.

Space is not available for a full survey of the foreign field, from which has come little of note recently, nor to permit detailed discussion of the advantages claimed by various processes. This paper is more a historical and descriptive narrative than a critical review of the art.

Conclusion

An attempt has been made to tell briefly the complete story of the development of the small-ice field—known years ago,

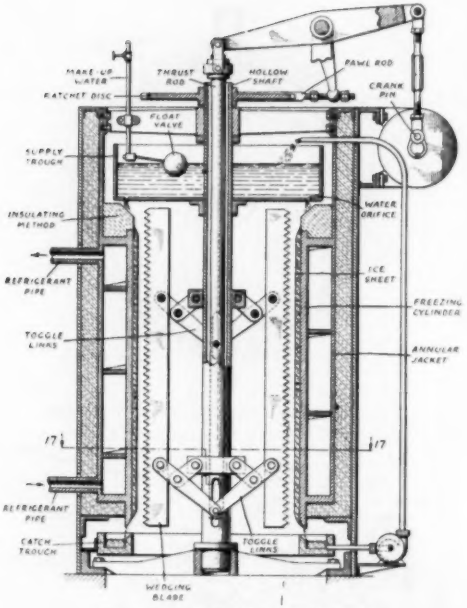

FIG. 16 THE SHORT CHIPICE MACHINE

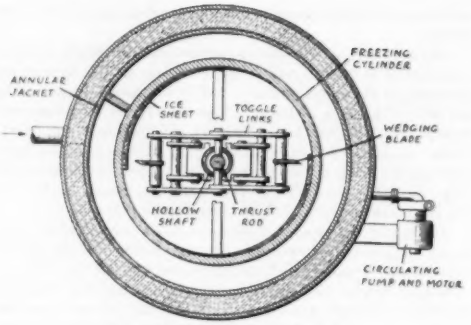

FIG. 17 CROSS SECTION OF FIG. 16

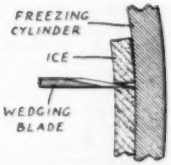

FIG. 18 ENLARGED VIEW OF ICE CHIPPING POINT

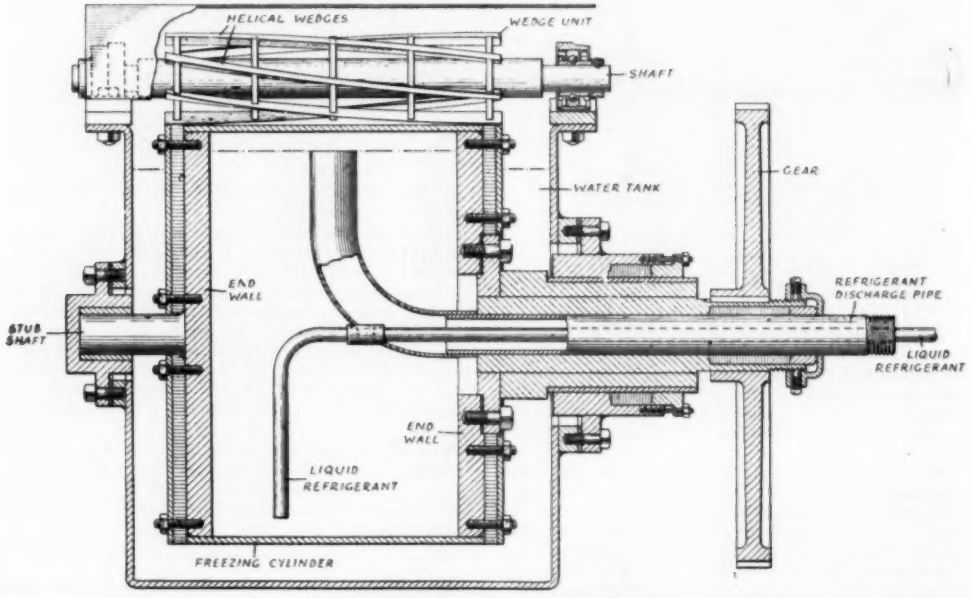

FIG. 19 THE RAVEN ICE-MAKING MACHINE

yet forgotten commercially or entirely unknown a bare two decades ago. Now it is a rapidly growing industry of real stature and a bright future.

BIBLIOGRAPHY

1 "Machinery for Continuous Ice Production," by Crosby Field, paper delivered before the 1928 Annual Meeting of the American Society of Refrigerating Engineers; *Refrigerating Engineering*, vol. 17, February, 1929, pp. 35–40; also in *Refrigerating World*, vol. 64, February, 1929, pp. 12–17; see also *Power*, vol. 69, March 19, 1929, pp. 474–475, and *Ice and Cold Storage*, vol. 32, May, 1929, pp. 119–120.

2 "Refrigerating and Ice-Making Machinery," by T. B. Lightfoot, Proceedings of The Institution of Mechanical Engineers (British), 1886, pp. 201–241.

3 "An Ice Machine," *Journal of The Franklin Institute*, vol. 84, 1867, pp. 80–81.

4 "History of Refrigeration," by J. C. Goosmann, *Ice and Refrigeration*, vol. 66, May, 1924, p. 448.

5 "Ice Goblets," *Scientific American*, vol. 100, May 15, 1909, p. 374; also *Ice and Refrigeration*, vol. 36, June, 1909, pp. 299–302.

6 "History of Refrigeration," by J. C. Goosmann, *Ice and Refrigeration*, vol. 67, 1925, p. 328–330.

7 "Development of Refrigeration in the United States," by J. F. Nickerson, *Journal of the American Society of Refrigerating Engineers*, vol. 2, November, 1915, pp. 66–82.

8 "FlakIce, New Developments," by Crosby Field, *Refrigerating Engineering*, vol. 22, October, 1931, pp. 227–233; also "FlakIce" Proceedings of the American Institute of Refrigeration, 22nd Annual Meeting, 1933, pp. 265–275; "Ice in Ribbons," *Refrigerating Engineering*, vol. 28, September, 1934, p. 141; *Steel*, vol. 96, March 11, 1935, pp. 40–42; "FlakIce Frozen Water Ribbons," *Ice and Refrigeration*, vol. 89, October, 1935, pp. 179–181; also "Installation of FlakIce Equipment," by A. Adams and R. E. Miller, *Ice and Refrigeration*, vol. 96, pp. 281–283; "FlakIce, Its Manufacture and Use," Trans. of the American Institute of Chemical Engineers, vol. 24, 1930, pp. 16–33; discussion, pp. 33–36.

9 "The Pak Ice Machine," by W. H. Taylor, *Refrigerating Engineering*, vol. 22, December, 1931, no. 5, p. 307, et seq. See also *Ice and Refrigeration*, vol. 81, December, 1931, pp. 434–438, and *Power*, vol. 74, November 3, 1931, p. 647.

10 "FlakIce Machines in Units," by C. P. Holley, *Refrigerating Engineering*, vol. 43, January, 1943, pp. 23–24.

11 "Ice Making by the Extrusion Process," by J. R. Watt, *Mechanical Engineering*, vol. 71, January, 1949, pp. 17–20 and discussion, *Mechanical Engineering*, June, 1949, pp. 519–522.

12 "Development in the Manufacture of Ice," by B. F. Kubaugh, *Mechanical Engineering*, vol. 63, December, 1941, pp. 875–888.

Additional References

"Ice Machine That Created Interest in 1878," *Power House*, vol. 17, October 5, 1924, p. 27. Brief illustrated description of Holden ice machine

"FlakIce," by E. Joelson, Kholodil'noe Delo, no. 7, 1931, p. 12 (in Russian). Reviews Holden machine, American FlakIce process, and German processes.

"Refrigerating Progress During 1931," by D. L. Fiske, *Refrigerating Engineering*, vol. 22, December, 1931, pp. 371–378.

"Tankless Ice-Making System," by R. S. Wheaton, *Power*, vol. 75, March 29, 1932, pp. 476–477.

"New 'Kolderol' Ice Molds," *Ice and Refrigeration*, vol. 83, November, 1932, p. 242.

"PakIce, the Continuous and Tankless System for Manufacturing Ice," by H. Sloan and W. H. Taylor, *American Institute of Refrigeration Proceedings*, 22nd Annual Meeting, 1933, pp. 276–287.

"Pak-Ice Briquette Press," by W. H. Taylor, *Refrigerating Engineering*, vol. 30, October, 1935, pp. 205–206 and 228.

"Vilter Builds New Pacicer Unit," *Ice and Refrigeration*, vol. 96, January, 1939, pp. 93–94.

"Tube-Ice, a New Sized Ice," *Ice and Refrigeration*, vol. 97, November, 1939, pp. 339–340.

"Vergleichende Übersicht uber neue Verfahren zur Eiserzeugung," by H. Pahl, *Zeitschrift für die gesamte Kalte-Industrie*, vol. 46, June, 1939, pp. 107–111.

"Automatic Tube-Ice Machine," *Refrigerating Engineering*, vol. 38, November, 1939, pp. 285 and 318.

"Ice Cubes, Walnut or Egg?" by F. E. Kunkel, *Refrigerating Engineering*, vol. 40, August, 1940, p. 94.

"Development of Refrigerating Equipment," by H. Sloan and W. B. Vilter, *Ice and Refrigeration*, vol. 101, July, 1941, pp. 25–26.

"New Forms of Ice," *Refrigerating Engineering*, vol. 101, July, 1941, pp. 36–37.

"Processed Ice," *Ice and Refrigeration*, vol. 103, August, 1942, pp. 93–94.

"Neues Verfahren und neue Vorrichtungen zum Erzeugen von Eis in Stangen odor Wurfelform," by J. Fuss, *Zeitschrift für Eis und Kalte-Industrie*, vol. 36, 1943, p. 1.

"New Ways of Making Ice," by J. R. Watt, Texas University, College of Engineering, *Journal of Architecture, Engineering, and Industry*, vol. 7, July, 1946, pp. 8–14.

"High-Speed Production of Ice," by J. R. Watt, *Ice and Refrigeration*, vol. 110, May, 1946, pp. 17–19.

"Chip Ice Production—Continuous Output Plant," *Modern Refrigeration*, vol. 49, October, 1946, pp. 277–278.

"Mechanical Refrigeration—Its American Birthright," by W. R. Woolrich, *Refrigerating Engineering*, vol. 53, March, 1947, pp. 196–199, 246, 248, 250; April, 1947, pp. 305–308, 346, 348.

"Business and the Sovereign State," by Crosby Field, *Refrigerating Engineering*, October, 1934.

"Icette," *Ice and Refrigeration*, April, 1949.

Books for Reference

"Refrigerating Data Book," American Society of Refrigerating Engineers, vol. 1, 1939.

"Eis und Kalteerzeugungs-Maschinen," by G. Behrend, fourth edition, Wilhelm Knapp, Halle a. S., Germany, 1900.

"Encyclopedia Americana, New York, N. Y., vol. 23, 1947.

"Seventy-Five Years of Progress," Frick Company, Inc., Waynesboro, Pa., 1928.

"Kaltemaschinen und ihre Anlagen," by G. Gottsche, fifth edition, Verlag fue Kalte-Industrie, Hamburg, Germany, 1912–1915.

"Air Conditioning and Refrigeration," by B. H. Jennings and S. R. Lewis, second edition, International Textbook Company, Scranton, Pa., 1944.

"Refrigeration and Air Conditioning," by R. C. Jordan and G. B. Priester, Prentice-Hall, Inc., New York, N. Y., 1948.

"Kaltemaschinen und ihre thermodynamischen Grundlagen," by M. Krause, Walter de Gruyter & Company, Berlin, Germany, 1932.

"Refrigerating Machinery," by A. R. Leask, second edition, Simpkin, Marshall & Company, Ltd., London, England, 1901.

"Refrigerating Engineering," by H. J. Macintire, John Wiley & Sons, Inc., New York, N. Y., 1937.

"Refrigeration," by J. A. Moyer and R. U. Fitts, second edition, McGraw-Hill Book Company, Inc., New York, N. Y., 1932.

"New International Encyclopaedia," second edition, University Press, Cambridge, Mass., vol. 19, 1916.

"Chemical Engineers' Handbook," by J. H. Perry, editor, second edition, McGraw-Hill Book Company, Inc., New York, N. Y., 1941.

"Machinery for Refrigeration," by N. Selfe, H. S. Rich & Company, Chicago, Ill., 1900.

"Refrigeration, Cold Storage and Ice Making," by A. J. Wallis-Taylor, third edition, D. Van Nostrand Company, Inc., New York, N. Y., 1912.

"Handbook of Refrigerating Engineering," by W. R. Woolrich and L. H. Bartlett, third edition, D. Van Nostrand Company, Inc., New York, N. Y., 1948.

Discussion

R. T. Brizzolara.[14] In his review of the developments associated in the field of producing small ice, the author refers to his own developments, using a flexible cylinder which through line distortion of the cylinder curvature peels the ice from its thin cylindrical freezing surface.

While the writer is not unfamiliar with his machine development, it has been noted that the flexing of the thin drum cylinder imposes a strain in the metal which strain in all probability is beyond the elastic limit.

It would be interesting to secure factual data from the author, as to the length of life secured with such panels from actual operation by the users of this equipment. It would also be interesting to be informed as to the fabrication methods adopted for these panels—particularly relating to securing uniform thickness and

[14] Advisory Engineer, New York, N. Y.

the method adopted to secure continuity of metal structure at joints and without incurring incipient points of weakness.

G. F. GRAY.[15] The text of this paper tells the technical story of the birth of a new industry in great detail but omits the "romance and adventure" which is so much a part of it. If the author could be induced to review that aspect of the subject, it would prove to be not only interesting but thrilling to the younger members of the Society, who may themselves be launching a career of pioneering in industry.

For instance, consider the "David and Goliath" story of the struggling inventor trying to give the ice-making industry a better tool with which to serve the public, and finally succeeding in spite of the united opposition of a number of older and richer competitors who, as the writer heard it, not only joined forces to suppress this threat to their vested interests, but even succeeded (temporarily) in enlisting the aid of the Government itself in that un-American endeavor. This is discussed in one of the author's earlier papers,[16] but is worth recalling, both as warning and encouragement, to others hoping to bring other new products to public acceptance.

J. W. MARTIN.[17] It is not clear to the writer why ice frozen and subcooled on a flexible cylinder should be superior in quality to the ice frozen on a rigid cylinder and chipped from it in accordance with some of the other machines described in the text of the article. Will the author please clarify this statement?

AUTHOR'S CLOSURE

The paper just presented covers 35 years of constant experimental work on its subject, and the presentation of the paper itself is an experiment, on which we would like your comments. This paper was written on request of a responsible committee of your Society who want your assistance in getting the answers to certain problems of presentation. The questions to be answered by the presentation are as follows:

1 Can the history of a young industry be completely condensed into a single paper within the space and time limitations imposed by the excessive demands upon our Society, which paper will be of value as a background for future papers describing still further advances? You may note the extensive bibliography yet the complete patent analysis originally in the manuscript would have required in addition over one half of the text. For this and other reasons it was omitted. Similarly for the same reasons you may note the omission of heat-transfer data, as a mere summary of our work would require approximately three pages of text, and perhaps another page for the changes with temperature in the coefficient of heat-conductivity of ice itself—strange to say, this coefficient is not a constant.

2 Can such a paper be written by one active in the industry and be fair to competitors? Judging from the protests I have already had from some of my associates, this question may have already been answered, at least in part.

3 Can such a paper be given without harm to the interests of the author or his company? What is the balance between the duties of a professional engineer and the demands of his employer in the delicate matter of making public information acquired by expensive research? A previous attempt of mine, a paper on "Steel Wool Manufacture" presented in 1927 before this Society, involved me and my company in patent litigation for many years. In my belief, the principal reason was that I accepted for purposes of the paper, with neither question nor sneer, patent published statements of my competitors as facts, which was not always the case. I was, therefore, embarrassed in the denial that I had confirmed or approved these statements. How can a professional engineer talk about the work of other engineers and maintain a professional bearing, neither belittling nor advocating?

4 The final facet of this experiment is the attempt to use colored slides. It is one of the worst subjects for that purpose, in that because of the other phases just mentioned, only the original patents are shown and these do not lend themselves to color as well as diagrams made for the purpose. The selection of colors is in turn an experiment; for example, I assure you red for ice was selected for contrast, not because of its present ideology.

Referring now to Mr. Gray, just as this development was becoming commercialized, the unbelievable happened; the Congress of the United States in an instant threw the nation back into the Middle Ages by the passage of the National Recovery Act. President Franklin D. Roosevelt signed many so-called "Codes of Fair Practice," in which the small manufacturer was placed at the mercy of his large competitor. The vast majority of these codes contained "Birth-Control Clauses" which as practiced prohibited the installation of newly developed products and equipment. An ice-industry trade association promptly took advantage of this opportunity to outlaw the new and very young competition of FlakIce Frozen Water Ribbons. The National Recovery Administration outdid the mediaeval guilds in their suppression of the individual. The exact parallelism of many of the regulations in these codes with guild statutes proved their origin, as was acknowledged to me privately by one of the Code Administrators. The story of one man's fight to preserve Americanism before the NRA was declared unconstitutional by the Supreme Court is given in the reference[16] "Business and the Sovereign State."

Referring to Mr. Brizzolara's question, the distortion of the metal necessary to peel the ice depends upon the thickness of the ice and some other operating conditions, but the strains due to this distortion are nowhere near the yield point. The design provides for a maximum strain due to the deflection of less than half the fatigue-endurance limit, which in turn is less than one third of the ultimate strength, so the design "factor of safety" as we used to call it, is greater than 6 on ultimate tensile strength.

In 1947 we studied the data from all flexible freezing cylinders that had been made in 1937. We had complete data on 94½ per cent of all such cylinders; the others had been shipped abroad, or otherwise track had been lost of them. Of this 94½ per cent there were still in operation after nine years 94 per cent (88 per cent of the total made). Those which failed in less than nine years of service life did so in almost every case because of freeze up or similar mechanical accident. Factory accelerated tests are stopped at the equivalent of ten years' service life and the fact that so many reach ten years or more in customers' plants confirms the accelerated test.

It should be pointed out, however, that these flexible freezing cylinders are belts, and as is the case with any belt, if due to wear or accident the roller or guides cause any misalignment, the strains in the cylinder increase very rapidly, with consequent great decrease in service life.

Referring to Mr. Martin's question, ice ribbons ⅛ in. or more thick, subcooled, dry, and peeled from an arcuate flexible surface, are superior to other forms of ice, in that their physical and heat absorptive characteristics can be controlled economically in production to suit the requirements of most ice-consuming operations. In general, it has been found possible to perform the same heat absorptive duty with FlakIce Frozen Water Ribbons having

[15] Vice-President, Pratt & Gray Company, Inc., Norwalk, Conn. Mem. ASME.

[16] "Business and the Sovereign State—Refrigeration Under the National Recovery Act," by Crosby Field, *Refrigerating Engineering*, vol. 28, October, 1934, pp. 175–180.

[17] Consulting Engineer, New York, N. Y.

a weight of 75 per cent or less of the block or can ice that is cracked or crushed before using.

In order to accomplish these results, and to provide large tonnage storage, with or without automatic or automatically measured discharge, the ribbons must be free flowing. To be free flowing, ice ribbons must:

(*a*) At *all times* before final consumption be dry and subcooled.

(*b*) Kept free from all moisture, even condensation from wet air.

(*c*) Be of a thickness sufficient to prevent breaking while handling into too small fragments ($^1/_8$ in. has been found the minimum practicable thickness, 0.14 in. to 0.16 inch is preferred).

(*d*) Have the long dimension of the fragment arcuate, not straight. This permits the fragment to ride like a sleigh on the pieces underneath. (Note the difference in behavior between a sleigh on a cold, dry morning and the same sleigh dragged through a thawing ice-water mixture. To date the only process commercialized for producing large quantities of ice of the foregoing characteristics is to freeze ice on a flexible surface and peel it therefrom by distorting the surface.)

In addition to the foregoing, it is possible by peeling the ice rather than scraping, wedging, or melting it off the freezing surface, to control the amount of heat absorptive capacity of each and every pound of subcooled ice to plus or minus one Btu. Thus ice may be produced at 150 Btu per lb, stored for long periods in a properly designed and operated bin (held at 20 F or lower), and then consumed absorbing 150 plus or minus one Btu per lb, with either very high or very low melting rates, depending upon the desired duty. This uniformity of heat-absorptive capacity and control of rate of melting is of great value in certain chemical-plant processes, and in concrete dam construction, etc.

Referring to Fig. 10, the desired subcooling is maintained by the relative positions of the water level, the deflection roller, and the brine nozzles. The omission of nozzles near the roller reduces the rate of heat transfer during the subcooling part of the cycle, thus tempering the ice without adding heat for that purpose. This, together with the flexible shape of the belt, prevents the cracking and shattering of the ice, which would occur on a rigid cylinder at similar low temperatures.

Referring to Mr. W. F. Friend's question, the economic factors of superiority of dry and subcooled ribbon ice may be summarized by saying that there is a large saving in the amount of ice needed for a definite operation, frequently a betterment in the product to which the ice is applied, such as an increase in yield of some chemicals or an absence of physical injury to boxed fish, a large saving in the space required for a plant of a given output, a saving in first cost of installation, and a smaller but still appreciable saving in the cost of production per ton of ice.

Referring now to the question from the floor, about two years after the 1936 shipment to Russia of the five-ton flexible freezing surface portable unit, we were informed by an American engineer recently returned from Russia that it was then operating, but since that time it has not been heard from. Negotiations for larger units were broken off because of war preparations.

The application was unique and may be of interest. The unit was designed to be taken into vegetable fields for prompt "dunking" in Flaklce Frozen Water Ribbons immediately upon "plucking." Tests had proved that by this method 100 per cent of the ascorbic acid (vitamin C) in the vegetable could be retained for a long period; a result not obtainable with other methods of preservation.

Referring to Mr. Gates' discussion, we have found that the change in heat-transfer coefficient is due not only to air inclusion, but is present also when no appreciable air has been frozen into the ice—it seems to be truly a function of the temperature of the ice itself.

Carbide High-Velocity Turning

By LEIF FERSING,[1] SPRINGFIELD, VT.

The term "carbide high-velocity turning," has lately come into use to indicate higher turning speeds than heretofore have been considered economical or practical for machining steel. Turning speeds of 350 to 400 fpm were generally considered high, whereas today turning speeds for steel from 400 to 1400 fpm are actually used in production with great success. This paper deals with factors affecting turning of steel and presents measurements of chip temperatures, loads on tools, effect of chip breakers, and the effect of turning speeds on the quality of finished surfaces. Illustrations of tools in cut at surface speeds up to 2400 fpm are shown. Descriptions of instruments are included, together with references to parts now being machined in the "high-velocity turning range" in production.

Introduction

FOR a given pair of materials, rate of wear between them is a function of surface finish, load, rubbing speed, hardness, and temperature. When turning steel, machinability becomes a very important variable. Correlating available information and extensive tests under actual production conditions, improvements in tool materials and machinability of steel, machine design and methods are problems which continuously confront the tool engineer. The wear at the tool point must be kept within economical range as speeds and feeds are increased if the increase in production is to result in a reduction in total cost.

Most tool-load data in this paper are obtained from turning cuts on $3^1/_2$-in-diam solid bars and on two types of normalized steel, SAE-C-1118, cold-rolled, and SAE-8747, hot-rolled. The cuts were taken on a J&L No. 5 ram-type turret lathe provided with a 15-hp motor. Spindle speeds 123, 253, 365, 510, 734, 1041, and 1500 rpm and feeds 0.007, 0.011, 0.015, and 0.022 in. per revolution (ipr) were used for a representative range of cuts with carbide tools. Photomicrographs of the structures and analyses are shown in Fig. 1. These steels were chosen as their machinability is fairly representative of steels used in manufacture today. All turning cuts were taken with tools having the cutting edge perpendicular to the axis of the work and a 0.015-in. nose radius, when not otherwise stated.

Average Temperature of Chips

An interesting phenomenon when cutting steel without coolant is the change in color of a chip as cutting speed is varied. For example, when machining C-1118 steel at 2400 fpm using 0.015-in. feed and a tool having 10-deg positive side rake angle, the chip discolors only slightly to a light straw color. As the cutting speed is reduced to below 1000 fpm, the chip starts to darken, turning purple-blue between 200 and 300 fpm, whereafter the chip again becomes lighter, showing only a slight discoloration at 100 fpm, Fig. 2. A similar though much less pronounced condition exists when 8747 steel is machined under the same conditions. The mean temperature of this chip is higher and rapid oxidation takes place, producing a purple-blue color as the chip is left in the air to cool.

C-1118 Steel

C	0.15	P	0.013
Mn	1.24	S	0.115
Si	0.11	Bhn	107–110

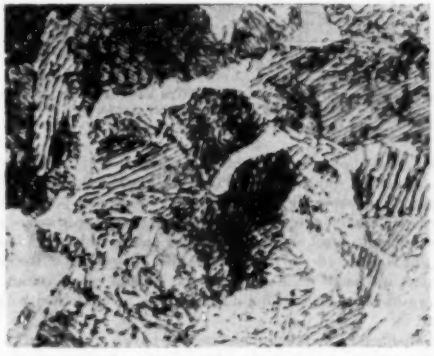

8747 Steel

C	0.47	S	0.012
Mn	0.91	Cr	0.51
Si	0.34	Ni	0.60
P	0.013	Mo	0.21
		Bhn	185–195

FIG. 1 MICROSTRUCTURES AND ANALYSES OF STEELS USED IN TOOL-LOAD TESTS
(Nital etch; ×1500.)

The calorimeter method was used for determining the average temperatures of chips at various cutting speeds. Some results of such tests are shown in Fig. 3. The average temperature of the chips as cutting speed is increased above 450 fpm remains approximately constant. The variation in color of the chips at high cutting speeds is probably due to variations in the thickness of chips and in the rate of air cooling at different speeds. The calorimeter method required the development of a chip breaker

[1] Experimental Engineer, Jones and Lamson Machine Company. Mem. ASME.

Contributed by the Production Engineering Division and presented at the Annual Meeting, New York, N. Y., November 26–December 1, 1950, of THE AMERICAN SOCIETY OF MECHANICAL ENGINEERS.

NOTE: Statements and opinions advanced in papers are to be understood as individual expressions of their authors and not those of the Society. Manuscript received at ASME Headquarters on October 20, 1950. Paper No. 50—A-127.

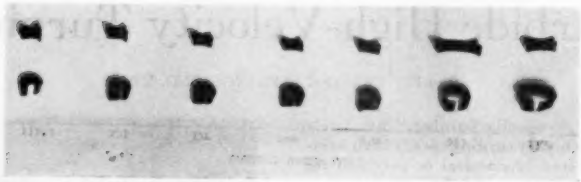

FIG. 2 COLOR COMPARISON OF CHIPS FORMED WITHOUT COOLANT AT VARIOUS SPEEDS, C-1118 STEEL
(0.015 in. feed per revolution, 0.150 in. depth of cut.)

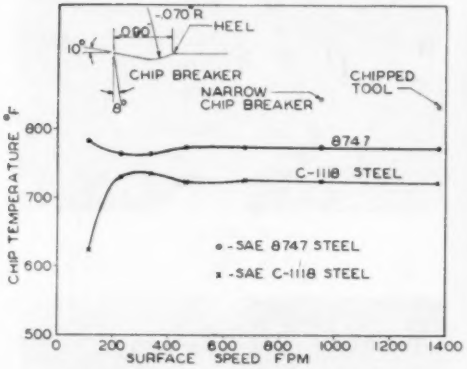

FIG. 3 AVERAGE TEMPERATURE OF CHIPS VERSUS CUTTING SPEEDS FOR C-1118 STEEL AND 8747 STEEL
(0.015 in. feed per revolution, 0.150 in. depth of cut.)

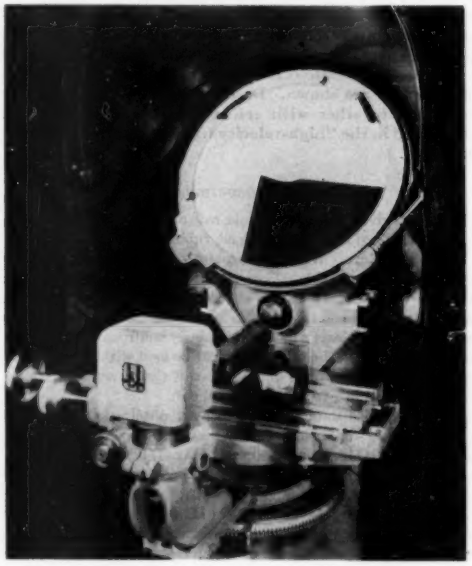

FIG. 4 METHOD FOR INSPECTING RADIUS, RAKE, AND WIDTH OF CHIP BREAKER ON COMPARATOR

which would break the chips of both types of steel at all speeds into somewhat similar shapes, Fig. 2. A cross section of the chip breaker is shown in Fig. 3. The temperature of each point on the curves is the average of three tests. It was necessary to keep close dimensional control of the chip breaker and to maintain a sharp cutting edge in order to duplicate results. Inspection of the chip breaker was made on a comparator at 31.25:1 magnification as shown in Fig. 4, permitting dimensions to be controlled within 0.001 in.

Chip breakers and rake angles on tools have a great influence on the average temperature of a chip. In Fig. 5 chips are shown formed at various speeds by a slightly narrower chip breaker. The thickness and the width of these chips are plotted in Fig. 6. The average temperatures of the chips from 8747 steel followed approximately the curve shown in Fig. 3, whereas for C-1118 steel the average temperature of the chips increased very rapidly when cutting speed was reduced to below 250 fpm, reaching a temperature of about 780 F at 112.5 fpm. This chip breaker was definitely of a poor design for C-1118 steel at low cutting speeds as evidenced by the shapes of the chips and their purple-blue color.

When cutting conditions were alike, the cross section of a chip from 8747 steel was always smaller both in width and thickness than of a chip from C-1118 steel. A chip is more or less trapezoidal in cross section and always thicker than the feed and wider than the depth of cut, although this effect is reduced as speed is increased. Furthermore, the average temperature of a chip taken at a certain speed and feed increases when a tool breaks the chips into smaller parts and/or forms a heavier cross section.

MEASUREMENTS OF TOOL LOADS

SR-4 type bonded-wire strain gages were used to measure deflections in a specially designed toolholder. Three components of the load as shown in Fig. 7 were recorded simultaneously with the help of direct-inking oscillographs.

Figs. 8 and 9 show the loads on a tool with the same chip breaker and for the same feed and depth of cut as used in Fig. 3, for C-1118 and 8747 steels, respectively. The load curves are similar to the average heat curves. Above a certain speed, about 450 fpm, the temperature of the chips remained approximately constant, whereas tool loads, especially for C-1118 steel, continued to drop.

The effect of coolant (50 parts water to 1 part wetting agent) on tool loads is plotted in dot-and-dash lines. All tool loads increased when coolant was used. It is obvious from these curves that the coolant had no lubricating value, but that a quenching of the chips took place. The cooling effect was excellent as all chips remained silver-white. The chips became more broken and slightly smaller in cross section than when turning dry. In order to complete the picture, loads on a tool with 10-deg side rake, no chip breaker, and without coolant are plotted in dotted lines. Note that at certain speeds for C-1118 steel the loads on the tool without the chip breaker are greater than on the tool with the chip

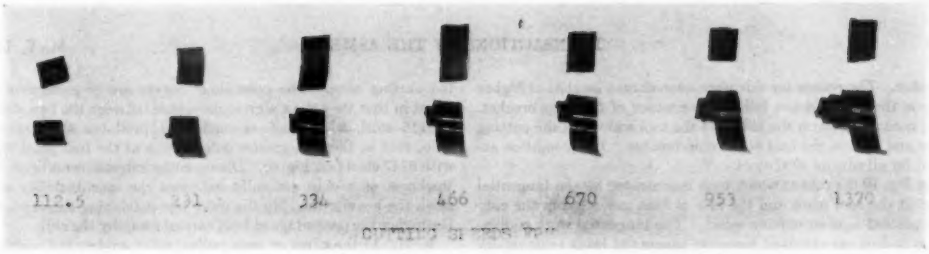

8747 Steel

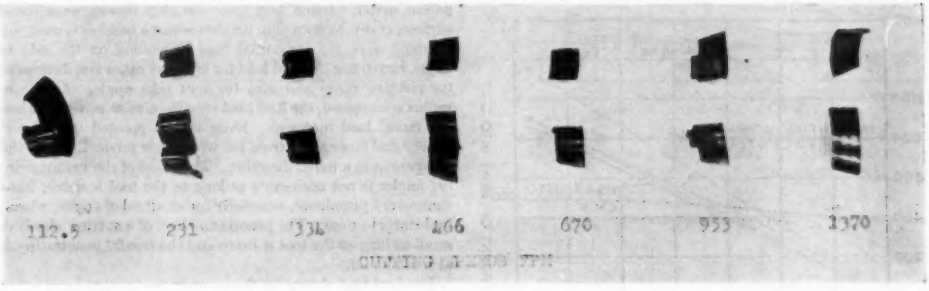

C-1118 Steel

FIG. 5 COMPARISON OF CHIP FORMATIONS AT VARIOUS SPEEDS. C-1118 AND 8747 STEELS; NARROW CHIP BREAKER
(0.015 in. feed per revolution, 0.250 in. depth of cut.)

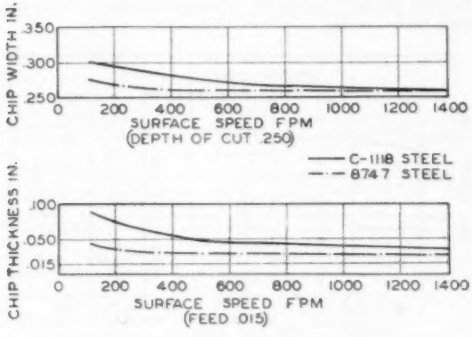

FIG. 6 VARIATION IN WIDTH AND THICKNESS OF CHIPS VERSUS CUTTING SPEED; NARROW CHIP BREAKER
(0.015 in. feed per revolution, 0.250 in. depth of cut.)

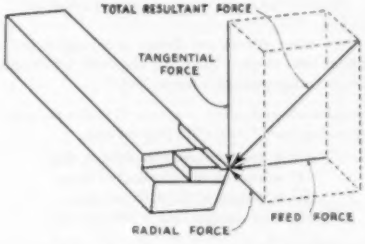

FIG. 7 COMPONENTS OF TOOL LOAD

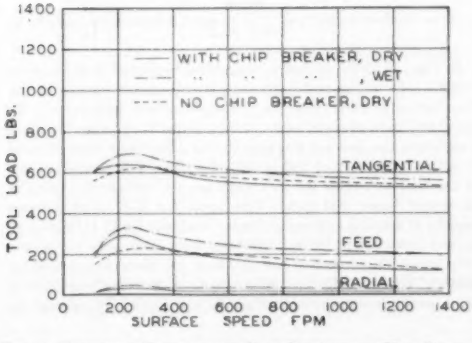

FIG. 8 EFFECT OF COOLANT AND CHIP BREAKER ON TOOL LOADS; C-1118 STEEL
(10-deg side rake angle, chip breaker as in Fig. 3, 0.015 in. feed per revolution, 0.150 in. depth of cut.)

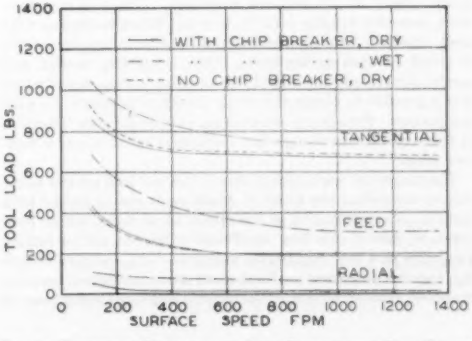

FIG. 9 EFFECT OF COOLANT AND CHIP BREAKER ON TOOL LOADS; 8747 STEEL
(10-deg side rake angle, chip breaker as in Fig. 3, 0.015 in. feed per revolution, 0.150 in. depth of cut.)

breaker. The reason for this phenomenon may be that at higher speeds the chip did not follow the contour of the chip breaker. The contact between the chip and the tool was along the cutting edge and against the heel of the chip breaker. This condition existed for all cuts on 8747 steel.

In Fig. 10 the rate at which heat is generated by the tangential load at the tool point and the rate of heat generated in the chip are plotted against cutting speed. The tangential work equivalents in Btu are obtained from the tangential loads (cutting dry with chip breaker) in Figs. 8 and 9, and the "heat into chips" from the temperature rise of chips, used for plotting curves in

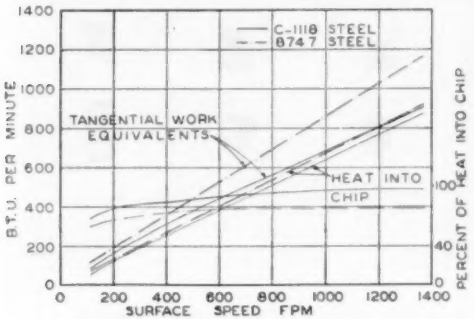

FIG. 10 CUTTING HEAT VERSUS SPEED; CHIP BREAKER, FIG. 3 (0.015 in. feed per revolution, 0.150 in. depth of cut.)

Fig. 3. Two other curves are shown and represented as "per cent" of heat into chips. They are obtained by dividing heat into chips by "tangential work equivalent."

Tangential work equivalent = power/$\frac{1}{778}$, Btu per min.
Heat into chips = $(T - t)\,CW$, Btu per min.

where $T - t$ = temperature rise of chips, deg F
C = average specific heat of chips
W = weight of chips, lb per min
Power = tangential load × feet per min

Friction between the tool and the chip, deformation of the chip by the chip breaker, and heat going into the workpiece and the tool are variable factors accounting for the difference in the "percentage" curves. In this connection it may be pointed out that the difference in machinability of the two steels was quite noticeable during test cuts. The C-1118 steel was very free-machining (note sulphur content, Fig. 1), and the limitation on speed and feed for the desired depth of cut was the capacity of the motor (30 hp at 100 per cent overload). The test cuts were short, however, ranging from $\frac{1}{2}$ to 1 in. When machining 8747 steel, especially with positive rakes, difficulties in tool life started at about 700 fpm cutting speed. Only by paying constant and careful attention to the lapped finish on the cutting edge of a tool was it possible to obtain the stable condition necessary for solid comparison. Five-degree negative rake angles gave no difficulties in this respect even though tool loads were higher than for positive rakes.

The tangential work equivalent and the tool load are two of the factors controlling the speed at which steels can be turned with carbide. A combination of the effects of pressure, speed, temperature, rate of chip flow, coefficient of friction and/or surface roughness on a tool, tool angles, duration of cut, and rate of cooling, together determine a critical speed above which heat becomes excessive, causing pitting of the carbide and rapid breakdown of the cutting edge. The percentage curves are of particular interest in that they show a great difference between the two steels. C-1118 steel, which is freer-machining, produces the heaviest chip, that is, there is greater deformation at the tool point than with 8747 steel (see Fig. 6). Disregarding extreme conditions, the thickness of a chip generally indicates the machinability of a steel, the heavier the chip the more free-machining the steel and the higher the percentage of heat carried away by the chip.

In Fig. 11 the effect of nose radius, relief angles, and width of chip breaker on load components are shown. The feed load has four components; penetration load forcing the tool point into the parent metal, friction load from the chip flowing over the tool surface, crowding by a chip breaker where a breaker is used, and a component of the tangential load depending on the side rake angle, increasing the feed load for negative rakes and decreasing it for positive rakes and zero for zero rake angle. As the nose radius is increased, the feed load remains almost constant whereas the radial load increases. Even with a pointed tool, the chip widens and flows away from the work, thus producing a frictional component in a radial direction. The effect of the variation in relief angles is not noticeable as long as the tool is sharp, but becomes very prominent, especially for small relief angles, when the tool starts to wear. The penetration load of a cutting edge is very small as long as the tool is sharp and the frontal penetrating area at a minimum.

The feed load shown by the curve is the friction force between the tool and the chip as the rake angle is 0 deg.

The importance of carefully designed chip breakers is emphasized by the marked effect of breaker dimensions on feed loads as shown at the right in Fig. 11. All combinations of width and depth broke the chip.

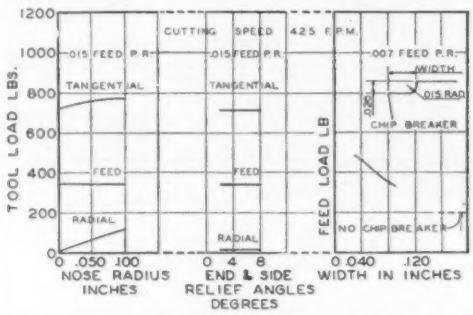

FIG. 11 EFFECT OF NOSE RADIUS, SIDE RELIEF AND END RELIEF ANGLES, AND WIDTH OF CHIP BREAKER ON TOOL LOADS; C-1118 STEEL (0.150 in. depth of cut, 425 fpm. Cutting speed, 0 deg side rake angle 3.2 in. OD of work.)

In Figs. 12 to 20, inclusive, tangential loads and feed loads for various rake angles and feeds are plotted against cutting speed. The test cuts were taken by holding constant first the spindle speed and then the feed rate. After a series of test cuts had been completed, the first cut was repeated and the loads were checked to insure that the tool had remained sharp. The characteristics of the load curves for the two steels are very different, especially at speeds below 500 fpm. The loads for 8747 steel increase rapidly as speed is reduced, whereas the loads for C-1118 steel go up and down except for negative rake tools. All radial loads were only about 10 per cent of the feed load and therefore are not included. Undoubtedly the surface finish on tools and variation in stock produce some irregularities in tool loads. Of special in-

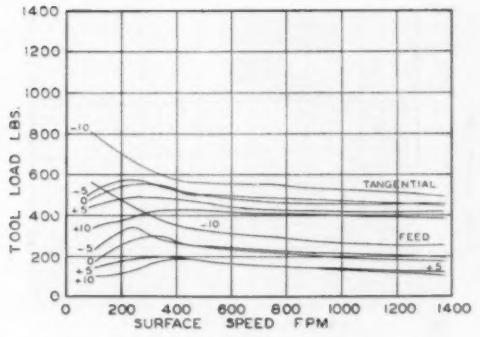

FIG. 12 TANGENTIAL AND FEED LOADS VERSUS CUTTING SPEED FOR VARIOUS SIDE RAKE ANGLES; C-1118 STEEL
(0.011 in. feed per revolution, 0.150 in. depth of cut.)

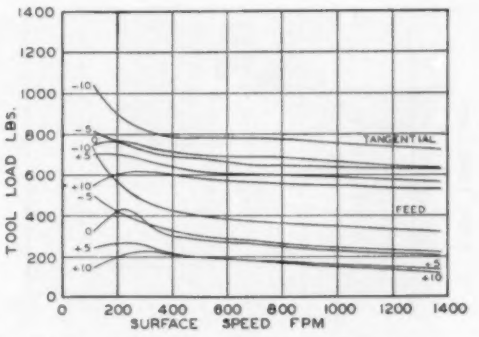

FIG. 13 TANGENTIAL AND FEED LOADS VERSUS CUTTING SPEED FOR VARIOUS SIDE RAKE ANGLES; C-1118 STEEL
(0.15 in. feed per revolution, 0.150 in. depth of cut.)

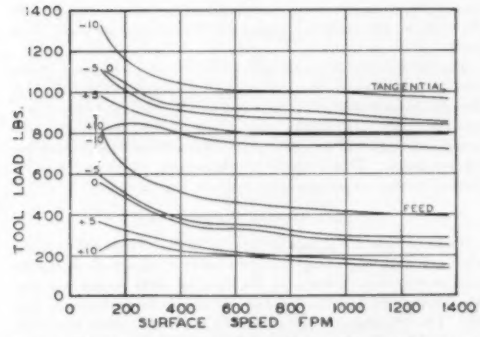

FIG. 14 TANGENTIAL AND FEED LOADS VERSUS CUTTING SPEED FOR VARIOUS SIDE RAKE ANGLES; C-1118 STEEL
(0.022 in. feed per revolution, 0.150 in. depth of cut.)

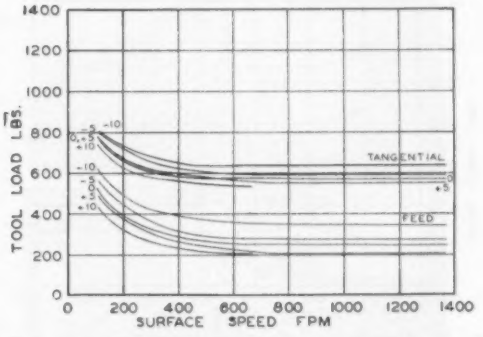

FIG. 15 TANGENTIAL AND FEED LOADS VERSUS CUTTING SPEED FOR VARIOUS SIDE RAKE ANGLES; 8747 STEEL
(0.011 in. feed per revolution, 0.150 in. depth of cut.
NOTE: Test for 10-deg side rake angle incomplete.)

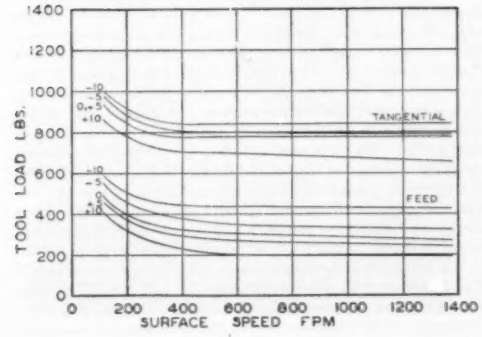

FIG. 16 TANGENTIAL AND FEED LOADS VERSUS CUTTING SPEEDS FOR VARIOUS SIDE RAKE ANGLES; 8747 STEEL
(0.015 in. feed per revolution, 0.150 in. depth of cut.)

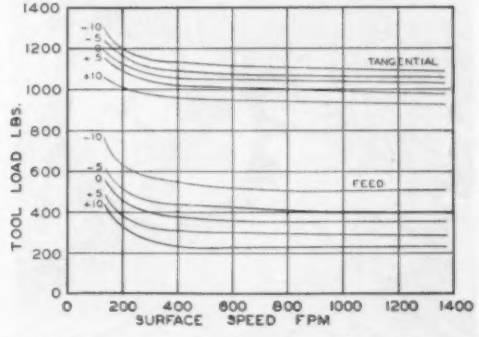

FIG. 17 TANGENTIAL AND FEED LOADS VERSUS CUTTING SPEED FOR VARIOUS SIDE RAKE ANGLES; 8747 STEEL
(0.022 in. feed per revolution, 0.150 in. depth of cut.
NOTE: Tool breakdown is rapid at 1370 fpm.)

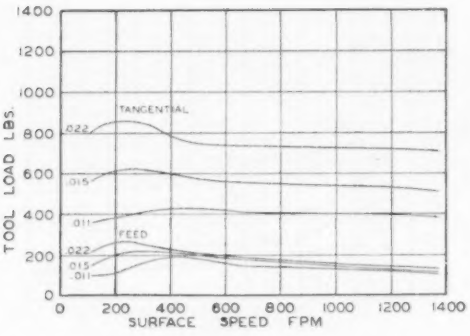

FIG. 18 TANGENTIAL AND FEED LOADS VERSUS CUTTING SPEED AT VARIOUS FEED RATES; C-1118 STEEL
(10-deg side rake angle, 0.150 in. depth of cut.)

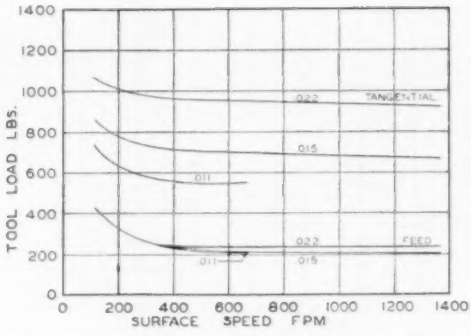

FIG. 19 TANGENTIAL AND FEED LOADS VERSUS CUTTING SPEED AT VARIOUS FEED RATES; 8747 STEEL
(10-deg side rake angle, 0.150 in. depth of cut.)

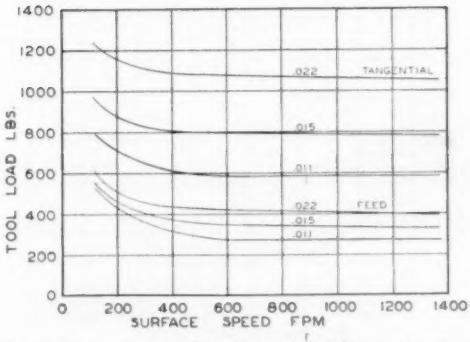

FIG. 20 TANGENTIAL AND FEED LOADS VERSUS CUTTING SPEED AT VARIOUS FEED RATES; 8747 STEEL
(—5 deg side rake angle, 0.150 in. depth of cut.)

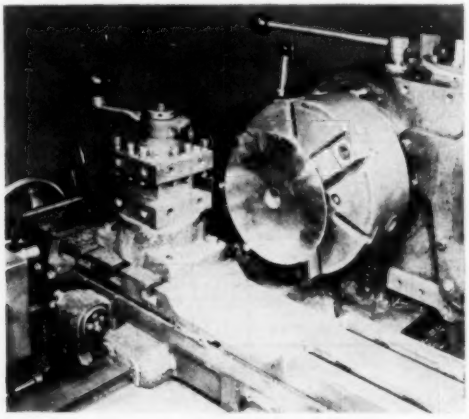

FIG. 21 SETUP ON TURRET LATHE FOR SLOW-MOTION PICTURES

terest is the slight change in feed load for 10-deg positive rake, Fig. 19, as feed was increased from 0.011 to 0.022 ipr and the almost proportional increase for 5-deg negative rake angle, Fig. 20. As a whole, the loads are higher for 8747 steel than for C-1118 steel.

Fig. 26 shows the tensile strength and the yield point of the two steels at elevated temperatures. Indications are that the difference between tensile strength and yield point affects the thickness of chips. Obviously, since temperature determines the tensile strength and the yield point, it has considerable influence on tool loads. This probably explains some of the adverse effects of coolant on tool loads as shown in Figs. 8 and 9.

SLOW-MOTION PHOTOGRAPHS

Tools in cuts are shown in Figs. 22 to 25. These illustrations were taken during facing cuts at various cutting speeds with a 16-mm slow-motion camera at the rate of 3000 frames per sec. The arrangement of the tool and the workpiece is shown in Fig. 21. The photographs are enlargements of the films when the tools had been in the cut 3 sec. The actual height of the tool was 1 in. When making the enlargements, the emulsified side of the film was kept closest to the photographic paper in order not to reduce sharpness, and the enlarged photographs are therefore shown in reverse.

There is no indication at any cutting speed either on the enlargements or on the film that the work splits ahead of the cutting edge. The chip flows across the cutting edge at a slower speed than the work is moving since the chip cross section is greater than the product of depth of cut and feed. The chip cross section is not uniform because of the shearing, compression, and variation in friction in the cutting process. As work speeds are increased, the chip tends to become thinner and more uniform in cross section. The dark spot at the very tip of the tools is caused by change in color due to heat, and the size of this dark spot shows how far the heat has flowed into the tool in the short time of 3 sec. The difference in the amount of heat going into the tip when machining C-1118 steel and 8747 steel can readily be appreciated by comparing the upper left-hand picture in Fig. 25 where C-1118 steel is machined at 2400 fpm and the lower right-hand picture in Fig. 22, where 8747 steel is machined at 1200 fpm, both tools having a 5-deg positive back rake angle. Another interesting comparison is the difference in chip thickness and the proportion of heat going into the tool when machining 8747 steel with 5-deg positive, 0-deg, and 5-deg negative rake angles at 1200 fpm cutting speed. The 5-deg positive rake angle shows the tool starting

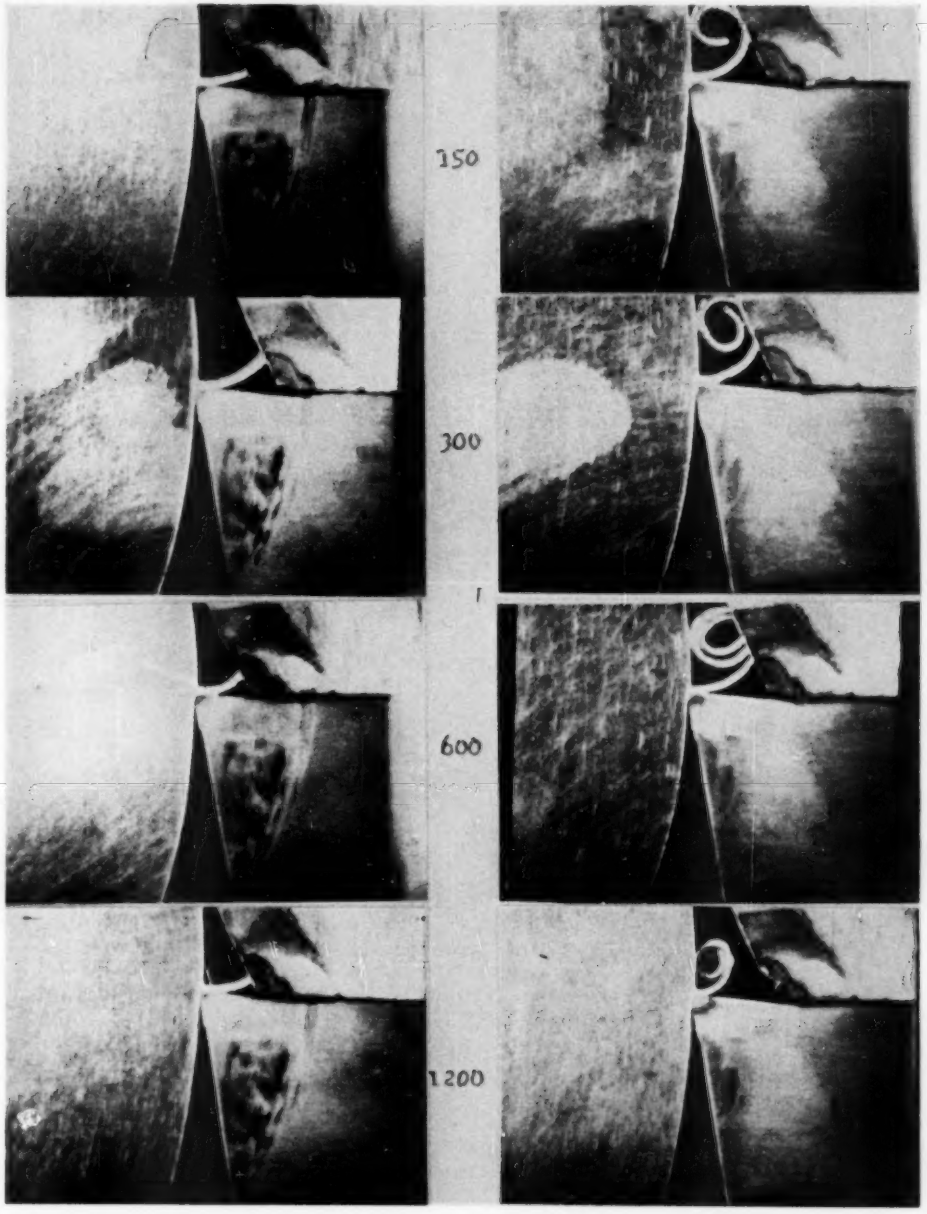

C-1118 Steel 8747 Steel

FIG. 22 FACING CUTS ON C-1118 AND 8747 STEELS AT 150, 300, 600, AND 1200 SFPM
(0.015 in. feed per revolution; 5 deg back rake.)

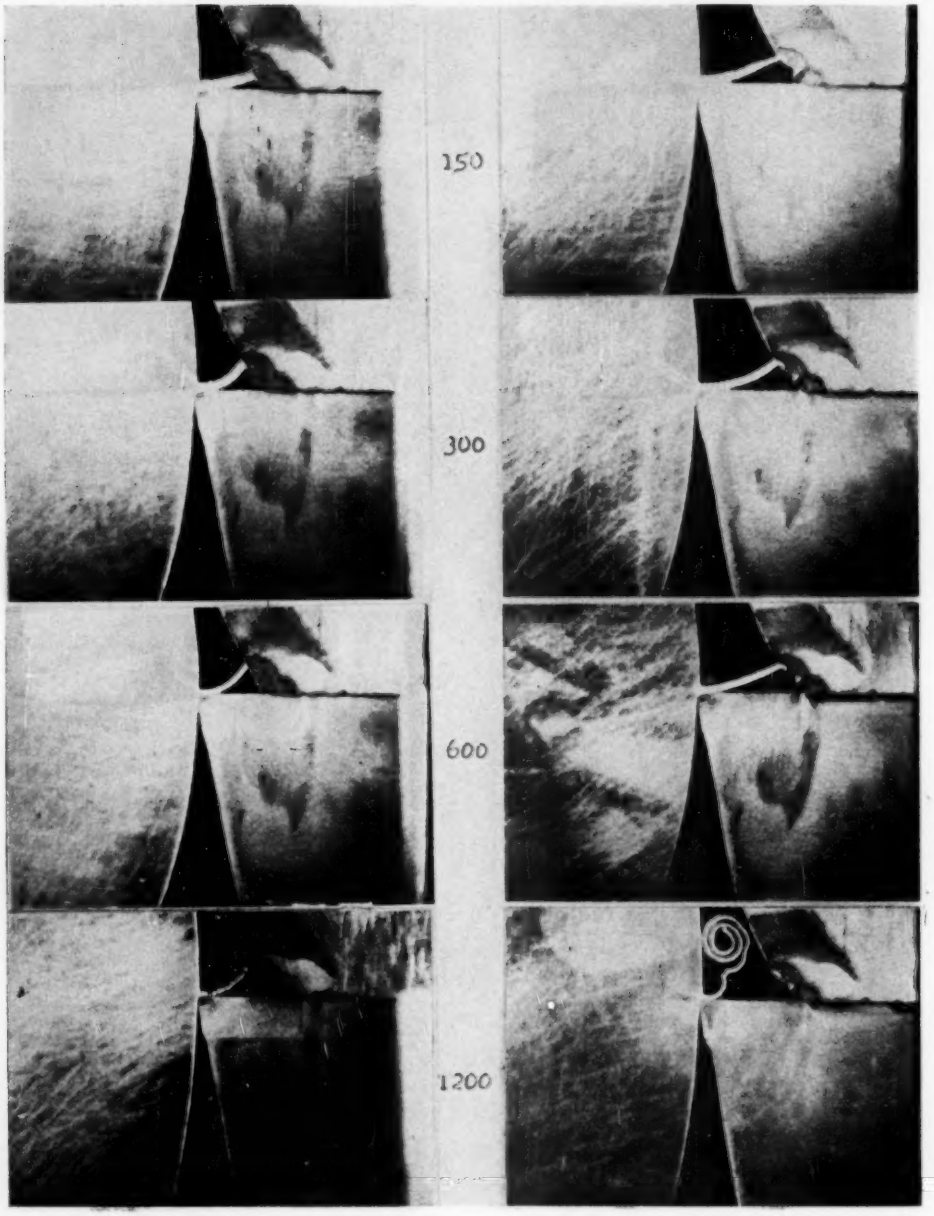

C-1118 Steel 8747 Steel

FIG. 23 FACING CUTS ON C-1118 AND 8747 STEELS AT 150, 300, 600, AND 1200 SFPM
(0.015 in. feed per revolution; 0 deg back rake.)

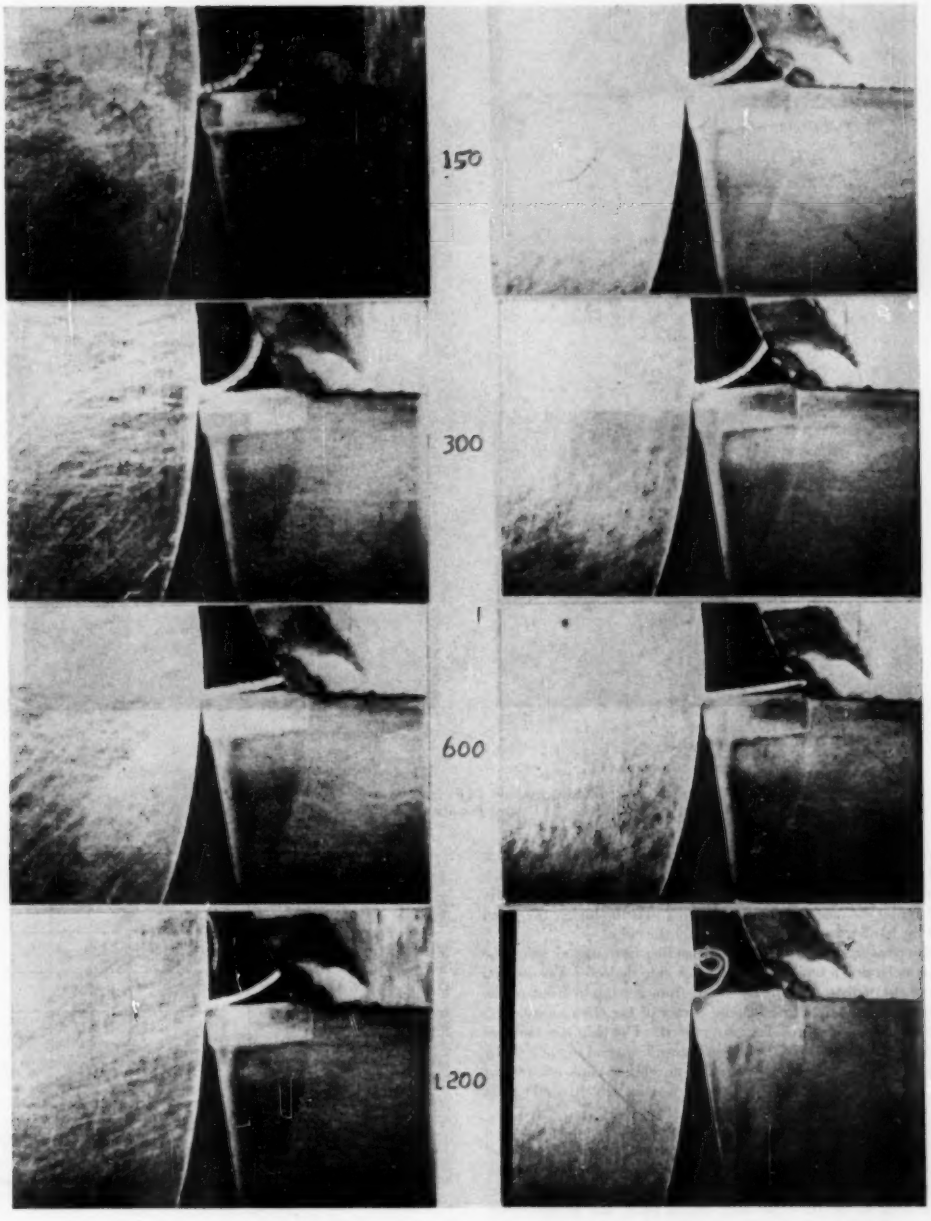

C-1118 Steel 8747 Steel

FIG. 24 FACING CUTS ON C-1118 AND 8747 STEELS AT 150, 300, 600, AND 1200 SFPM
(0.015 in. feed per revolution; —5 deg back rake.)

C-1118 steel
Back rake angle 5 deg
Feed 0.015 ipr
Speed 2400 fpm

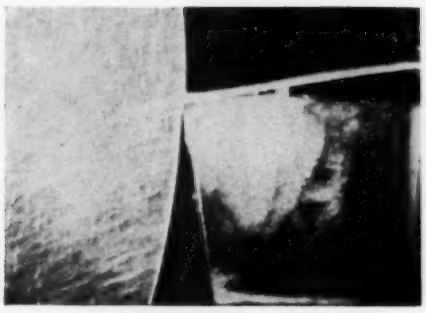

8747 steel
Back rake angle —5 deg
Feed 0.015 ipr
Speed 300 fpm
Chip deflector removed

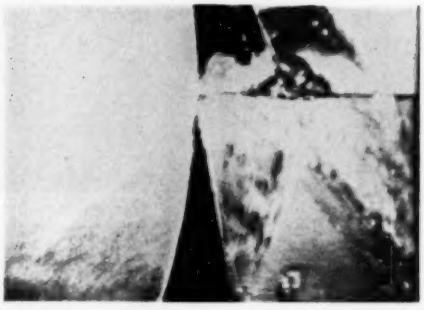

C-1118 steel
Back rake 5 deg
Feed 0.015 ipr
Speed 150 fpm with coolant

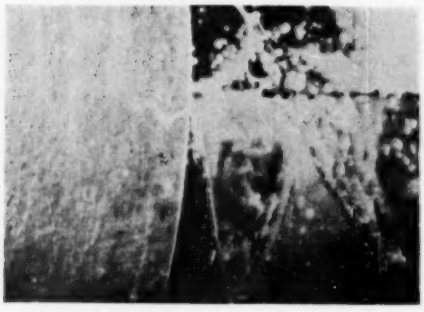

C-1118 steel
Back rake 5 deg
Feed 0.015 ipr
Speed 1200 fpm with coolant

FIG. 25 FACING CUTS ON C-1118 STEEL AT 2400 SFPM, AND AT 150 AND 1200 SFPM WITH COOLANT AND ON 8747 STEEL WITH CHIP DEFLECTOR REMOVED

to crater, whereas the 5-deg negative rake angle shows least heat and no cratering and the thinnest chip. The influence of cutting speed and material on the thickness of a chip can be seen easily and agrees with measured data, showing that the higher the speed and the harder the material the thinner the chip.

The photographs are slightly misleading in that they show the chips as having a tendency to curl. A chip deflector was used on top of the tool to prevent the chips from getting in front of the camera. In the upper right-hand corner of Fig. 25 a photograph is shown with the chip deflector removed. The chip is coming off straight along the top of the tool and even riding on top of a curler ground into the tip. The tendency of the chip to come off straight was always apparent until an object was hit which would start the curling.

The two lower photographs in Fig. 25 were taken while a transparent coolant was sprayed on the disk toward the tool and forming a sheet of coolant on one side of the tool only. In both pictures the heat at the tip of the tool is very noticeable. Quenching of the tip is actually taking place and is very detrimental to carbide. The volume and the force of the coolant are small and could not be directed at the tool for ideal conditions because of photographic limitations. A coolant should be directed against a cutting edge both from top and bottom.

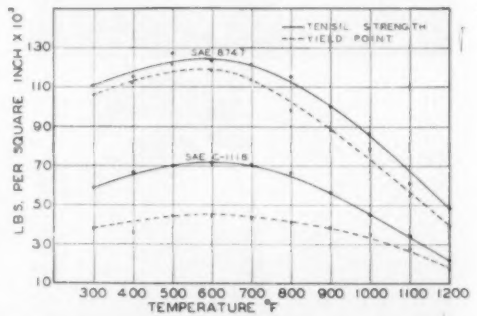

FIG. 26 ELEVATED-TEMPERATURE TEST OF TENSILE STRENGTH AND YIELD POINT OF NORMALIZED C-1118 AND 8747 STEELS

SUBFACE DEFORMATION

Cutting speed also affects the amount of deformation at and below the finished surface of a turned piece. In Figs. 27 and 28

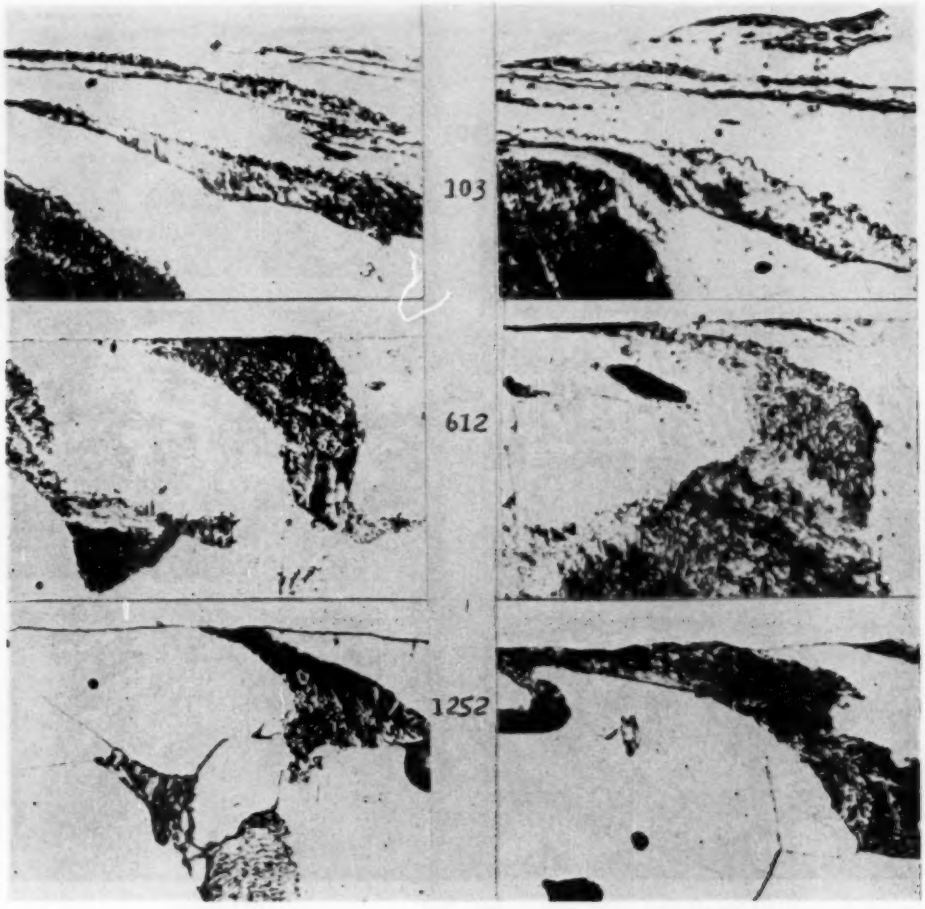

Without Coolant Speed Fpm With Coolant

FIG. 27 MICROSTRUCTURAL STUDIES OF SURFACE DEFORMATION ON C-1118 STEEL, MACHINED AT VARIOUS SPEEDS WITH AND WITHOUT COOLANT; ×1500
(0.015 in. feed per revolution; 0.150 in. depth of cut, 0.050 in. nose radius, and 10 deg side rake on tool.)

microstructural studies of deformations at various speeds with and without coolant are shown. The steels are the same as in previous tests with the exception that the C-1118 steel has not been normalized. Although the greatest deformation penetrates only 0.001 to 0.002 in. below the surface, it is clearly demonstrated that the cutting speed influences the surface structure. Deformation decreases with increased speed, this being less pronounced in the high-velocity range, is less without coolant than with coolant, and is less for steel with higher tensile strength, Figs. 1 and 26.

PRODUCTION APPLICATIONS

Test results and experimental work give the engineer a good base to work from for planning future developments and improvements. In machining, the variables are many and results often contradictory because components of many factors are hard to control and difficult to evaluate. Hence the ultimate value of pioneering work is determined on the production line rather than in the laboratory. Although cutting without coolant has shown certain advantages in the laboratory, these are generally far outweighed by disadvantages appearing on the production line such as heat expansions, preventing holding close dimensions, tool life, handling of hot workpieces and chips, and so forth. There are occasions, however, when cutting dry is the most practical solution, for example, when intermittent cuts are taken at high cutting speeds where the repeated quenching of a carbide tip by coolant quickly shatters a cutting edge.

Cutting speeds in the high-velocity range already have proved themselves on the production line. An amazing example is the

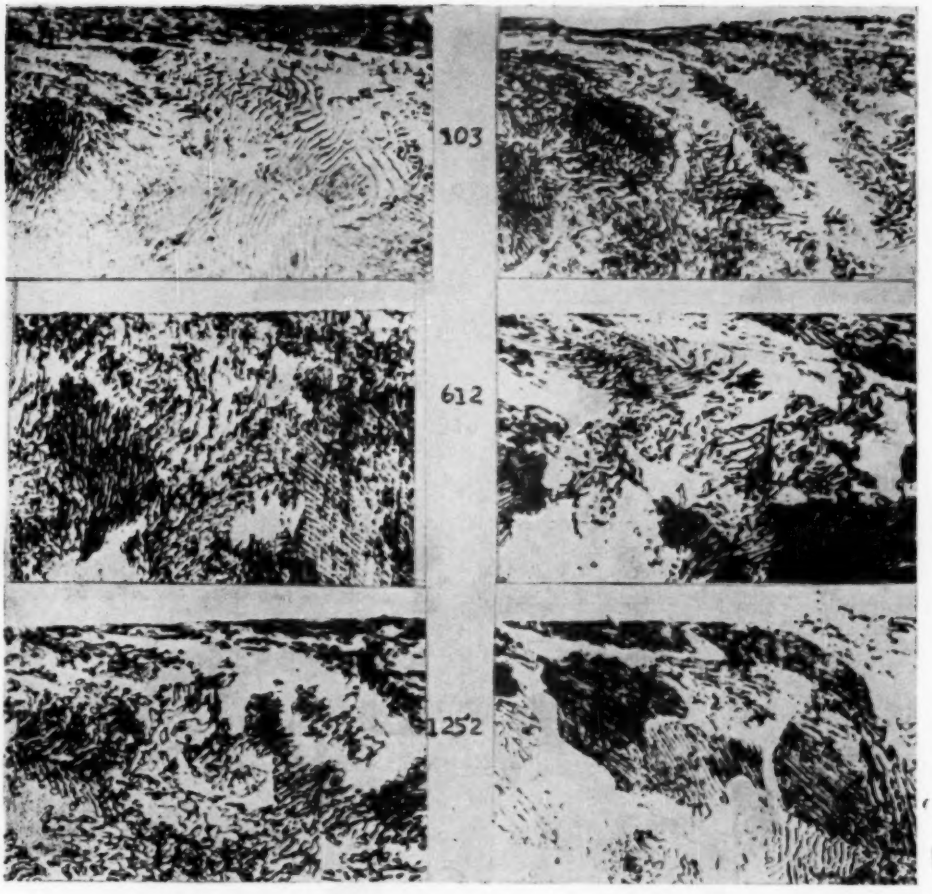

Without Coolant Speed, Fpm With Coolant

FIG. 28 MICROSTRUCTURAL STUDIES OF SURFACE DEFORMATION ON 8747 STEEL, MACHINED AT VARIOUS SPEEDS WITH AND WITHOUT COOLANT; ×1500

(0.015 in. feed per revolution; 0.150 in. depth of cut, 0.050 in. nose radius, and 10 deg side rake on tool.)

turning of automotive drive pinion forgings with the tooling shown in Fig. 29, on a 16-in. Fay automatic lathe shown in Fig. 30. The forging (SAE 8620 steel Bhn 176) is driven by a chisel drive and completely machined in 8.5 sec, as follows:

Spindle speed	1200 rpm
Cutting speed (max)	1185 fpm
Turning feed	0.0148 ipr
Facing feed	0.012 ipr
Cutting time	8.5 sec
Floor-to-floor time	17 sec
Maximum stock removed	3/8 in. total, 2 lb (approx.)
Maximum horsepower	66

Improvements in tool life after a year's production are still being made and some remarkable results are worth mentioning. As many as 660 pieces per index have been obtained on the square insert turning the large tapered diameter of the pinion, and over 1000 pieces per index on several of the triangular inserts. Note that all tools are of the carbide-insert type, requiring a minimum time for tool changes, and that toolholders are built as heavy as space permits. The coolant is supplied through holes integral with the toolholders and thus always forcibly directed at the cutting edges of a tool. To gain full advantage of cutting speeds in the high-velocity range other refinements than maximum rigidity and quick tool change become vital engineering problems. The loading time in this setup is reduced to a minimum in the following way: The operator puts the forging which has been faced to correct length and centered in both ends on the two brackets shown underneath the finished piece and pushes a buttom (see Fig. 34), which starts the entire automatic cycle. The ram, with a live center, moves forward, catching the forging on centers, forcing the knife-edges into the face of the forging by hydraulic pressure

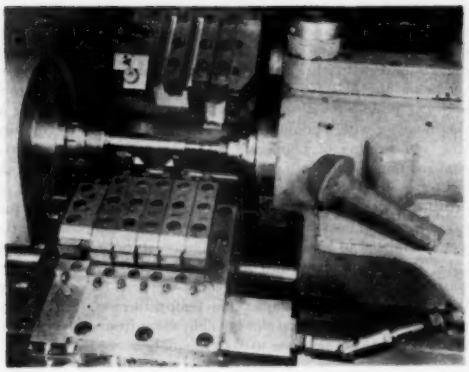

FIG. 29 TOOLING FOR AUTOMOTIVE DRIVE PINION FORGING ON A 16-IN. FAY AUTOMATIC LATHE

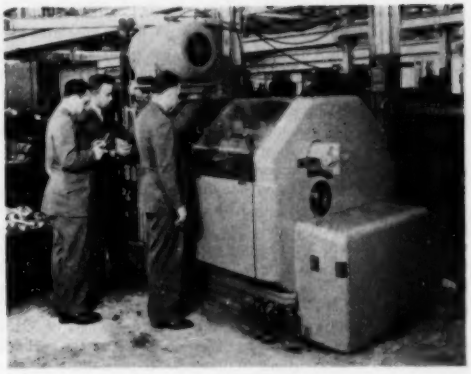

FIG. 30 16-IN. FAY AUTOMATIC LATHE FOR MACHINING AUTOMOTIVE DRIVE PINION FORGING

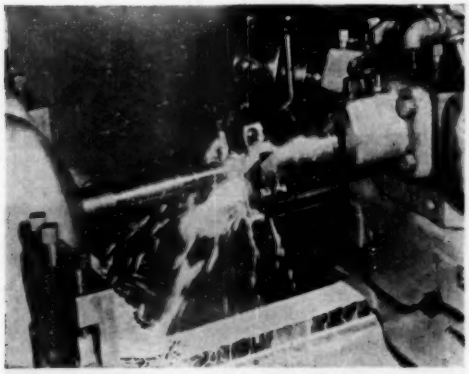

FIG. 31 THREADING BOLT AT 2000 RPM WITH CARBIDE CHASERS IN A TANGENT DIE HEAD

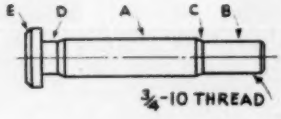

		OPERATION	SPINDLE RPM	SURFACE SPEED	FEED
1		STOCK STOP			
2		POINT	2000	714	HAND
3		TURN A	2000	714	.015"
4		TURN B	2000	422	.015"
5		THREAD B	2000	390	.100"
	REAR	FORM C, D & E	2000	714	HAND
	FRONT	CUT OFF	2000	714	.0035"

FIG. 32 OPERATION DATA FOR MACHINING BOLT SHOWN IN FIG. 31

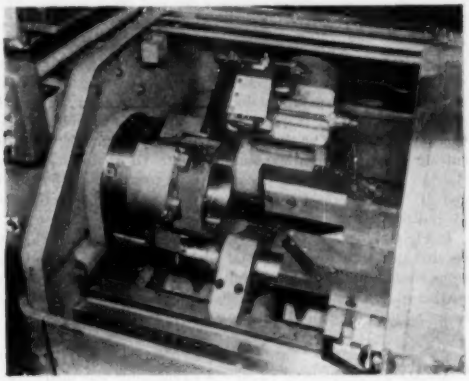

FIG. 33 BORING AND FACING OF BEARING FORGING SHOWING SPLASH GUARD WITHDRAWN

to provide the drive, the splash guard closes (see Fig. 34), and the spindle starts. When the piece is finished-machined, the spindle stops, the hood opens, the ram withdraws, and the finished piece drops down on the two brackets to be replaced with a new forging by the operator. Stopping and starting the spindle without appreciable loss of time is in itself a problem. The spindle comes to full speed in less than $1^1/_2$ sec and at maximum production $3^1/_2$ times per min. The kinetic energy of rotating parts is about 10,000 ft-lb per start, or 35,000 ft-lb per min, which has to be dissipated as heat between the clutch and brake surfaces of reasonable size without excessive wear. A total of 100,000 stops and starts is considered a short life.

The importance of tool-point surface finish is emphasized in another example from the production line shown in Fig. 31, with machining operations, feeds, and speeds shown in Fig. 32. The cutting of the $1^1/_4$-in-long thread at B is made with carbide chasers in about $^1/_2$ sec cutting time. It used to be necessary to resharpen the chasers after every 250 pieces, but the chasers are now provided with superfinished cutting surfaces, and 700 pieces are made without resharpening. The material in the bolt is SAE 1040 steel.

A steel considered difficult to machine is SAE 52100, commonly used in antifriction bearings. This steel has a machinability rating, using the drill method of penetration, of about 40 per cent lower than 8747 steel. The tooling for boring and facing an outer race is shown in Fig. 33. The ring forging is approximately 12 in. diam and $11\frac{1}{4}$ in. long with $\frac{3}{16}$ in. of stock coming off on the side. The race is finished-machined with only one cut taken on each surface in two operations, at cutting speeds of 594 fpm at 0.015-in. feed per revolution for boring and 655 fpm at 0.020-in. feed per revolution for turning the outside diameter in 3.35 and 2.76 min cutting time, respectively, and with a tool life of 17 to 20 pieces for boring with a shank tool and 25 to 30 pieces per index for turning with a round insert. Tool-setting gages permit replacing of shank tools in about $1\frac{1}{2}$ min a piece. Therefore any gain in tool life from reduced speeds would have to be considerable to increase production.

In Fig. 35 is shown a ball-bearing outer race, also of 52100 steel, which for several years has been machined by the author's company in three operations to demonstrate possibilities in carbide high-velocity turning. The ball groove 0.161 in. deep is machined in the third operation by a form tool at 945 fpm cutting speed and 0.006 in. feed in $2\frac{1}{2}$ sec cutting time, using about 50 hp. The average number of pieces per tool grind is about 220. The groove has been machined in only $1\frac{1}{2}$ sec by increasing feed and without appreciable reduction in tool life. The gain in floor-to-floor time was, however, so small from 15 to 14 sec, that no gain was made in a day's production on account of a few extra changes of tools. To increase production it would be necessary to reduce chucking time rather than cutting time. Similar grooving operations are run on the production line by bearing manufacturers at cutting speeds between 500 and 600 fpm. Of further interest is the fact that the grooving operation is run successfully both wet and dry since the tool is in the cut too short a time to become overheated.

In Fig. 34 is shown a modern automatic lathe with push-button control and with workpiece and tools totally enclosed under a transparent sliding hood, permitting coolant to be directed at cutting edges of tools in all directions without flooding operator or floor and providing ample protection against flying chips.

Test Arrangements

Average Temperature of Chips. A calorimeter was made from thin tin, double-walled with $\frac{1}{2}$-in. asbestos insulation between the walls. A square hole in one side fitted snugly around the tool, and a round hole in an adjacent side permitted the workpiece to enter with a slight clearance to prevent rubbing (see Fig. 36). Two covers were used, one during the cut, and one made from wood and insulated with felt. This latter cover fitted inside the calorimeter below the hole for the workpiece and underneath the tool and was provided with a small hole in its center, permitting a thermometer with 5 graduations per deg F to be inserted for stirring and reading of temperatures. The two covers were exchanged immediately after a cut had been taken. The length of cut for each speed was 1 in. and depth, 0.150 in. One pound of distilled water was used for each test, providing a depth in the calorimeter of about 2 in. Temperatures of all component parts were permitted to level off at room temperature before each test cut. The peak temperature of the water after each cut was recorded while the stirring took place and was used for determining the temperatures of the chips. The temperature would rise very rapidly, level off, and drop slowly. The chips from each cut were weighed and the weight was used in calculations.

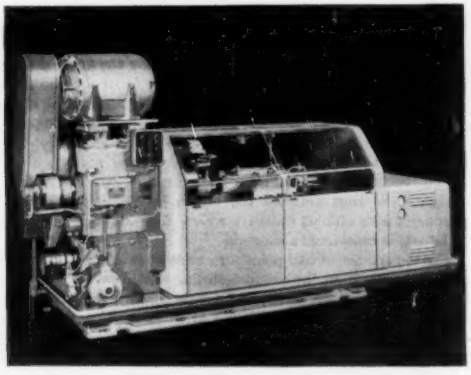

Fig. 34 Lathe Showing Push-Button Control and Complete Coolant Enclosure

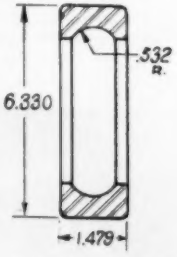

Fig. 35 Outer Bearing Race

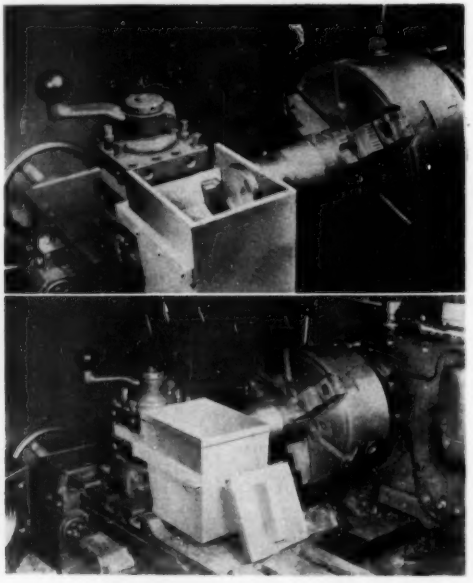

Fig. 36 Calorimeter

The calorimeter was calibrated by heating chips of both steels from a number of cuts to various measured temperatures. The chips were heated in covered Inconel trays provided with a thermocouple connected to a millivoltmeter calibrated directly into degrees F. The procedure for obtaining the temperature of the mixture of chips and water was the same as for a cut. The difference between the recorded temperature rise of the water and the theoretical temperature rise of an equal amount of water for perfect heat transfer was accepted as the loss in the calorimeter. The mean specific heats of steels of similar compositions within the known temperature ranges were used in the calculations and later for plotting the curves in Fig. 3. The heat loss of the calorimeter was approximately proportional to the temperature rise of the chips. Radiation and vaporization losses were neglected when computing various temperatures. These errors are small, though greatest at slow cutting speeds. The quantity of heat was obtained from

$$\text{Heat units} = CW(T - t)$$

where

C = specific heat of material (average)
W = weight of material
$T - t$ = temperature rise

The specific heat of C-1118 steel increases from 0.116 to 0.143 as temperature is increased from 120 F to 750 F, and of 8747 steel from 0.114 to 0.142 (Metals Handbook, American Society for Metals).

Components of Tool Loads. In developing a special toolholder for measuring components of tool loads, emphasis was placed on rigidity without loss of sensitivity and accuracy. Furthermore,

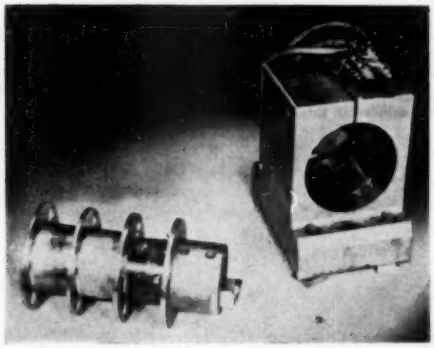

FIG. 37 TOOLHOLDER AND TOOL POST

recording instruments were desirable. The toolholder and tool post are shown in Fig. 37. The toolholder was provided with four integral diaphragms. The slotted, viselike tool post was provided with a round hole made to receive the outside diameter of the diaphragms. A sturdy sheet-steel cover with ample clearance around the toolholder was used for protection of strain gages and wiring and also for preventing chips from producing undue loads on the holder. Sets of sensitive SR-4 strain gages were cemented to the holder in such a way as to measure only one component of a tool load per set. The tangential load on the tool was indicated by two gages placed on top and bottom of the holder, and the feed load by two gages placed on the sides of the holder. The radial or shank load was indicated by a set of gages on a cantilever in juxtaposition with the rear end of the toolholder, Fig. 39. The surface of this cantilever was square with the axis of the toolholder and concentric with the rear diaphragm. The cantilever was slightly preloaded against the ball in order to assure good contact. The position of the ball was chosen so that bending loads on the toolholder would have minimum effect on radial tool loads. Only the three rear diaphragms were clamped in the tool post, the diaphragm closest to the tool being an extra protection for the electrical components. The toolholder was provided with a square hole to receive 1-in. × 1-in. tools, and located so that the cutting edge of the tool always could be located on the axis of the holder, thus reducing errors from torque interferences between components of tool loads to a minimum. The toolholder was hollow except for the part where the tool was clamped and at the rear end where a pressed-in plug was used for holding the ball. The three sets of strain gages on the toolholder were connected to universal analyzers and direct-inking oscillographs. All three components of a tool load were recorded simultaneously, Fig. 38.

FIG. 38 UNIVERSAL ANALYZERS AND DIRECT-INKING OSCILLOGRAPHS

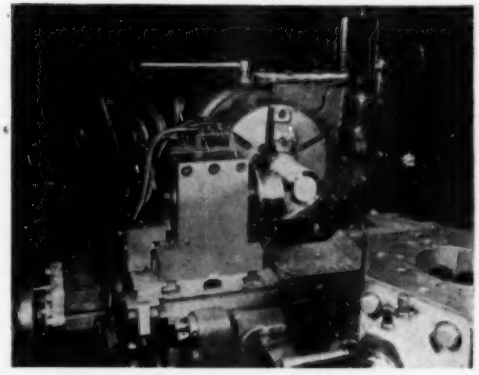

FIG. 39 TOOL POST WITH TOOLHOLDER, MOUNTED ON TURRET LATHE
(Sheet-steel cover removed, showing pickup for radial loads.)

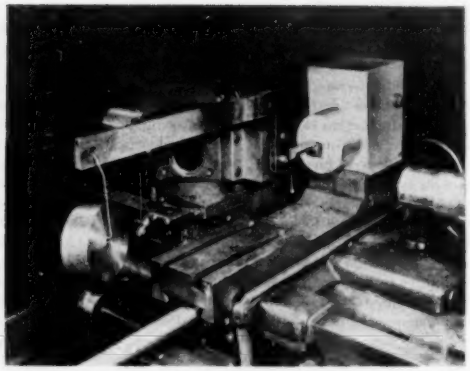

FIG. 40 CALIBRATION OF RADIAL TOOL LOADS
(Sheet-steel cover in place.)

The calibration of the instruments was made with known loads applied in the same direction as the components of the tool loads as shown in Fig. 40.

The lever arm was supported by a fulcrum point on the turret with a link abutting against or pulling on the tool. The width of engagement between the link and the cutting edge of the tool was made equal to the depth of the cut to be tested except for radial loads. Before a known weight was attached to the lever, the systems were balanced electrically, thus eliminating the lever and permitting use of loads in round figures for calibration, for example, 100 or 500 lb. Any cross-effect of one calibration load upon the other two sets of strain gages was recorded and compensated for when calculating loads. To calibrate with weights was necessary only once for each depth of cut as the instruments were provided with an auxiliary electrical calibration system which could be switched in at any time to check for drift. Full gain of the analyzers was always used and the lowest attenuation which would keep the inking pen inside the chart paper.

CONCLUSIONS

Both production experience and experimental tests have shown that higher cutting speeds for machining steels have many advantages, such as lower tool loads and less surface deformation on finished parts; and that tool life can be very economical even though the rate at which heat is generated at a tool point is practically proportional to cutting speed. Improvements in the quality of tools, coolants, machine construction, materials, methods, and controls have resulted in higher permissible cutting speeds with increased production and possibilities for greater economical benefits. It is not suggested that cutting speeds should or can be doubled or tripled on present equipment without careful attention to all factors involved nor that the limit in production capacity has been reached in examples from the production line. The various tests show that there are no drastic changes in tool loads and chip temperatures as cutting speeds are increased from 300 to about 1400 fpm, that tool finish and angles have a vital effect on tool life, and that chip breakers and cutting angles on tools should be modified to suit both cutting speed and type of steel for obtaining highest efficiency in chip removal. A few years ago when carbide was introduced, most machine tools lacked power, speed, and rigidity for efficient use of carbide tools. The recent successes in the high-velocity range indicate that a similar era is approaching when a large proportion of existing machine tools are rapidly becoming obsolete.

ACKNOWLEDGMENTS

The author wishes to express his appreciation to Lester Sheehan, chief metallurgist, Harold L. Murch, chief optical engineer, David N. Smith, research engineer, and William Moeser, research engineer, all of the Jones and Lamson Machine Company, for their collaboration in the preparation and presentation of the data included in this paper.

High-Speed Aerodynamic Problems of Turbojet Installations

By H. LUSKIN[1] and H. KLEIN,[2] SANTA MONICA, CALIF.

The possibility of supersonic flight in turbojet-powered aircraft is shown, and the resulting thrust requirements for the engine are estimated. The performance requirements of a turbojet installation are considered from the point of view of an aerodynamicist. Afterburning, inlet-pressure recovery and drag, matching of inlet size and engine, and the effect of exit and cooling losses are considered. Speed stability and jet problems are discussed briefly.

Nomenclature

The following nomenclature is used in the paper:

A_0 = free-stream tube area of air entering engine, sq ft
A_1 = area of inlet scoop, sq ft
A_{1x} = component of A_1 directed forward, sq ft
C_{d_s} = incremental scoop-drag coefficient, based upon area A_{1x} and q_0
C_{p1} = pressure coefficient at inlet, $\frac{p_1 - p_0}{q_0}$
c_v = specific heat of air at constant volume, Btu/lb deg F
D_s = incremental scoop drag, lb
F_g = engine gross thrust, lb
F_n = engine net thrust, lb, $F_n = F_g - \frac{W_a V_0}{g}$
L/D = lift-to-drag ratio
M = Mach number, $\frac{\text{velocity}}{\text{velocity of sound}}$
M_0 = ratio, $\frac{\text{velocity}}{\text{velocity of sound at sonic section}}$
p = pressure, psf
P_t = stagnation or total pressure, psf
q_0 = free-stream dynamic pressure, psf, $q_0 = \frac{1}{2}\rho_0 V_0^2$
T = temperature, deg R
T_t = stagnation or total temperature, deg R
V_0 = airplane velocity, fps
V_0' = velocity of air relative to airplane behind oblique shock, Fig. 12, fps
V_j = jet velocity relative to airplane, fps
W = gross airplane weight, lb
W_{F+PP} = weight of fuel plus power plant, lb
γ = ratio of specific heats, taken as 1.40
δ_1 = angle of inclination of flow entering scoop
η_c = compressor adiabatic efficiency
η_t = turbine adiabatic efficiency
η_n = nozzle adiabatic efficiency
ρ = density, slugs per cu ft

Subscripts:

0 = free stream
1 = scoop entrance
2 = compressor entrance
3 = compressor exit
4 = turbine entrance
5 = turbine exit
6 = afterburner exit
7 = nozzle exit

Other symbols are defined where used.

General Considerations

In the 11 years which have passed since the first flight of an aircraft powered with a turbojet, that type of propulsion device has shown a marked superiority in high-speed flight operations. Turbojets have powered each of the airplanes which broke the world's speed record during that time,[3] and the latest such craft, the USAF F-86, is, in addition, in operational military use. These speed records have increased at a rapid rate, which, when extrapolated into the future, promise considerably greater speeds. Fig. 1 reviews the history of aircraft speed records, shows the present superiority of the turbojet, and shows two recent predictions (1, 2)[4] for future speed possibilities. It is evident that there is at least hope that aircraft record speeds soon will be supersonic.

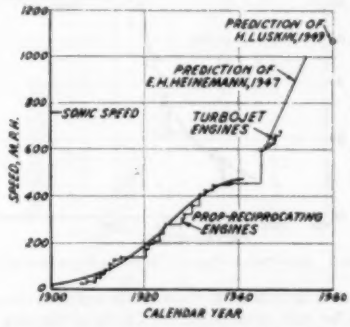

Fig. 1 History of Sea-Level Airplane Speed Records Together With Several Predictions

The turbojet has been considered as a possible power plant for supersonic flight because of its present marked superiority for fast

---

[1] Aerodynamics Research Engineer, Douglas Aircraft Company, Inc.

[2] Aerodynamics Engineer, Douglas Aircraft Company, Inc.

Contributed by the Aviation and Gas Turbine Power Divisions, and presented at the Annual Meeting, New York, N. Y., November 26–December 1, 1950, of The American Society of Mechanical Engineers.

Note: Statements and opinions advanced in papers are to be understood as individual expressions of their authors and not those of the Society. Manuscripts received at ASME Headquarters, October 9, 1950. Paper No. 50—A-102.

[3] Flights past the speed of sound in the X-1 are not recognized as official speed records by the FAI. Their regulations require the record-breaking airplane to take off from the ground and make a certain number of passes at low altitude before landing.

[4] Numbers in parentheses refer to the Bibliography at the end of the paper.

aircraft, and because it is still in a primitive state of development thus offering great potentialities for improvement. Analyses of the technical aspects of propulsion systems for aircraft have supported this view (3, 4). There will, of course, be many aerodynamic problems associated with the turbojet installations in these future high-speed airplanes. The consideration of several of these problems is the purpose of this paper. The speed range to be discussed goes up to $2^1/_2$ times the speed of sound.

Difficult technological problems must be solved to achieve useful supersonic flight. Of greatest concern here is the problem of the enormous power required to fly at those speeds. Even present-day aircraft can be considered to be large-output power stations, since the engines of modern transport airplanes, for example, have a maximum total output near 15,000 hp. For such an airplane (with no increase in power-plant size and weight) to fly supersonically, the power required would be greater by a factor between 10 and 100. For any such increase in power, the resulting engine weight and bulk would be hopelessly incompatible with that allotted in the airplane. Obviously, supersonic aircraft or their propelling devices, or both, must be greatly superior to those acceptable subsonically. Consideration of the power requirements for supersonic airplanes will thus be important for both airplane and engine designers.

The power required for flight is dependent on the airplane drag. The drag will be made up of the profile drag and the drag due to lift. Both parts of the drag must be low if the required power is to be kept down. Further large improvement of the profile-drag cleanness at subsonic speeds is apt to be difficult. This was shown recently by data of E. J. Richards (5), rearranged and plotted in Fig. 2. As used by Richards, the profile-drag cleanness factor is defined as the ratio of the turbulent skin-friction drag of a flat plate at operating speed to the profile drag at operating speed. The flat-plate chord is the same as the mean wing chord, while the flat-plate area is the gross wetted area. In that figure a ratio of 1 would be reached by an airplane with only drag due to skin friction at the wing's turbulent friction coefficient acting on all wetted areas,[5] i.e., no aerodynamic interference, no boundary-layer separation, and no cooling or leakage drag, etc. It is felt that although the profile-drag cleanness factor may continue to improve, for supersonic speeds it will do so starting at a new and lower level. This will be the result of large pressure drags associated with supersonic shock-wave systems which must be added to the subsonic drags. These supersonic pressure drags can be large. Well-shaped fuselages, for example, will have a supersonic profile drag increase of at least 50 per cent, while wing-wave drag at zero lift may increase by an even greater fraction. These effects are shown in Fig. 2 for a hypothetical supersonic airplane considered by Jones (6). It is suggested that the value shown may not be directly comparable since Jones' main purpose was apparently to point out favorable aerodynamic shapes and hence his design is aerodynamically optimized largely from consideration of wing and fuselage drags. Thus no drag allowance was made for longitudinal stability and control, scoops, air conditioning, cooling, canopies, and other items which always make up a significant fraction of the profile drag. Furthermore, the minimum profile drag was used since that at operating speed was not known. The value of the cleanness factor for the supersonic airplane therefore may be optimistic.

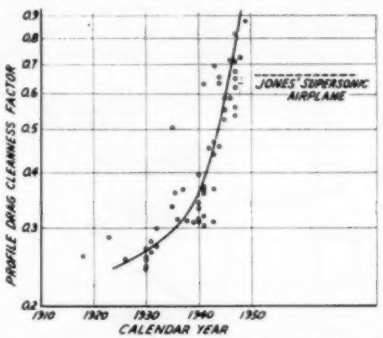

FIG. 2 GROWTH OF PROFILE-DRAG CLEANNESS FACTOR

The drag which varies with lift also inherently tends to be greater at supersonic speeds. The effect of this portion of the drag, when combined with that of the profile drag, is conveniently described by the maximum lift-drag ratio. Values of that parameter generally representative of modern subsonic practice are shown in Fig. 3 and compared to Jones' supersonic design.

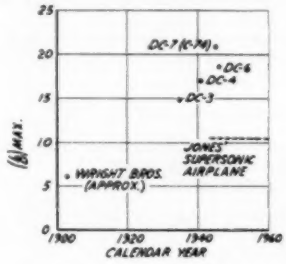

FIG. 3 GROWTH OF MAXIMUM LIFT-DRAG RATIO

A reduction in lift-drag ratio by about a factor of 2 is seen to result from a comparison of Jones' airplane at supersonic speeds to conventional airplanes at subsonic speeds. Consideration of the other drags (cooling, etc.) mentioned previously, as well as losses in induced-drag efficiency neglected by Jones, may make the factor approach 3 or even 4.

This reduction in lift-drag ratio has important effects on the requirements for supersonic power plants: (*a*) Since the drag level is already seriously increased, the engine and its installation must contribute as little as possible to the resistance. (*b*) Since for level unaccelerated flight the lift L essentially equals the weight W, and the thrust F_n equals the drag D, one can say

$$\left(\frac{L}{D}\right)\left(\frac{W_{F+PP}}{W}\right) = \left(\frac{W_{F+PP}}{F_n}\right)$$

where W_{F+PP} is the weight of fuel and power plant. It is reasonable to expect that the fraction of gross weight allowed for fuel and power plant, (W_{F+PP}/W), will not increase greatly supersonically, if at all. Assuming it remains unchanged in magnitude, it is seen that the power plant plus fuel weight to thrust ratio will be proportional to the lift-drag ratio. Hence the supersonic reduction by a factor of 3 or 4 in lift-drag ratio necessitates a similar change in power plant plus fuel weight-thrust ratio. If a further rough assumption is made that the fraction of weight allotted to fuel does not change, then it can be said that in order to make level supersonic flight possible, power plants must be made for supersonic speeds with 3 to 4 times more thrust per

[5] Values above 1 could be obtained by having laminar flow over portions of the wetted area, or by considering the reduction of fuselage friction coefficient from that of the wing. The latter effect results from the greater Reynolds number of the fuselage.

pound of weight than is acceptable subsonically on conventional aircraft.

While the design and development of sufficiently powerful but light and aerodynamically clean turbojets is without doubt the main goal to be reached in order to make economical supersonic flight possible, many other difficult problems also must be faced. The remainder of this paper is devoted to a consideration of several performance and operational problems, in particular those which fall into the fields of interest to the aerodynamicist.

Performance Considerations

The thrust actually developed by a turbojet engine installed in an airplane depends not only upon the engine design, but also upon the installation in the airframe. This is true at any airplane speed, but the installation becomes increasingly important as the speed of the aircraft increases, as will be seen presently. The performance of the engine itself is of course greatly influenced by such design quantities as the compressor pressure ratio, the temperatures through the cycle, and the component performances and efficiencies. The matter of the optimum selection of the pressure ratio and temperatures, and the influence on these quantities and of the component efficiencies on the thrust and fuel consumption has been dealt with extensively in the literature (9), and will not be reviewed here.

Afterburning, and the effect of aircraft speed on its desirability, is so crucial that it deserves some consideration here, although more complete studies have been made elsewhere (10). Peak combustion temperatures preceding the turbine are limited by metallurgical considerations, but it is possible to burn additional fuel to obtain very high temperatures in an afterburner which follows the turbine. These high temperatures increase the jet exit velocity and, consequently, increase the gross thrust of the engine, which is defined as the product of jet velocity and the exit-gas flow rate. It may be shown that with an initial ratio of airplane to jet velocity of V_0/V_j, an increase in gross thrust of an engine brought about by an increase in jet velocity gives rise to a net thrust increase given by the equation

$$\frac{\Delta F_n/F_n}{\Delta F_g/F_g} = \frac{1}{1-(V_0/V_j)}$$

where all quantities are defined in the nomenclature. This relationship is plotted in Fig. 4 and shows that a given fractional gross thrust increase, $\Delta F_g/F_g$, is accompanied by a larger fractional net thrust increase, $\Delta F_n/F_n$, and that the amount of this net thrust increase is higher the higher the ratio V_0/V_j. The ratio V_0/V_j may be expressed in explicit form as a function of the variables M_0, (P_{t2}/P_0), (P_{t2}/P_{t2}), η_c, η_t, η_n, and (T_{t4}/T_0). Values of V_0/V_j were calculated and are plotted in Fig. 5 for various assumed engine cycle parameters as given in Table 1.

TABLE 1 ENGINE CYCLE PARAMETERS

Engine	Compressor pressure ratio	Engine temperature ratio	Efficiencies
A	5.0	5.0	0.80
B	5.0	5.0	1.00
C	5.0	4.0	0.80
D	16.0	5.0	0.80

The data in Fig. 5 for the assumed engine A with pressure and temperature ratios of 5.0, and with assumed compressor, turbine, and nozzle efficiencies of 0.80, have been used to add a scale of airplane Mach number to Fig. 4. It may be noted that a given fractional increase in gross thrust under static conditions will yield an equal fractional increase in net thrust, but at Mach number 2.0, for example, the fractional increase in net thrust is 4 times the assumed fractional gross thrust increase. Thus if an afterburner reaches a temperature that yields a 0.50 increase in thrust statically, this increase in the thrust of the basic engine A is 2.00 (tripled thrust) at Mach number 2.0. It is evident that the high-speed airframe designer is anxious for even a small increase in afterburner augmentation.

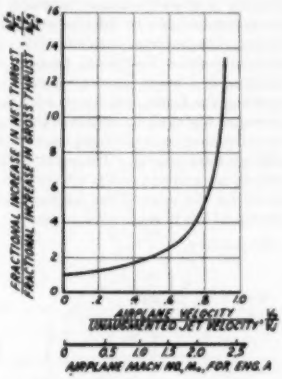

Fig. 4 Ratio of Net to Gross Thrust Increase for Change in Jet Velocity

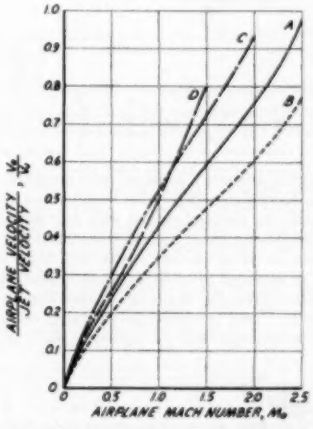

Fig. 5 Ratio of Airplane to Jet Velocity for Several Assumed Nonafterburning Engines

The engine design parameters, including the afterburner augmentation ratio, are beyond the control of the airframe designer, generally, once the selection of an engine has been made. There are several items that influence engine performance which are within the control of the airframe designer, and it is these items which are to be discussed here. The airframe designer is given an engine with certain performance capabilities under ideal conditions, and he must install it in an airframe to come as close as possible to realizing this ideal thrust. Losses are impossible to avoid, however, and it is proposed to discuss these losses, their magnitude, and their variations with airplane Mach number at some length.

Inlet Stagnation Pressure Losses. An inlet can adversely affect the thrust of a turbojet engine by losing an appreciable proportion of the isentropic stagnation pressure available. This loss in stagnation pressure comes about through frictional losses and, in the case of supersonic flows, shock losses. This pressure reduction affects the thrust in two distinct ways: (*a*) Since a compressor is essentially a constant-volume machine, reducing the pressure at the compressor face by inlet losses reduces the mass air-flow rate through the machine proportionally. (*b*) Reducing the compressor-inlet pressure lowers the pressure ahead of the exit nozzle, resulting in a lower jet exit velocity. An accurate method of evaluating the thrust loss due to inlet losses has been given (7) for an engine where all the details of the engine cycle are known. A derivation may be made along somewhat similar lines but with simplifying assumptions. These are sufficiently accurate for the present use and enable the following explicit expression to be derived for the ratio of the fractional change in net thrust to the fractional loss in stagnation pressure

$$\frac{\frac{\Delta F_n}{F_n}}{\frac{\Delta P_{t2}}{P_{t2}}} = 1 + \frac{\gamma-1}{2\gamma} \cdot \frac{\left(\frac{p_0}{p_{t2}}\right)^{\frac{\gamma-1}{\gamma}}}{\left[1-\left(\frac{p_0}{P_{t2}}\right)^{\frac{\gamma-1}{\gamma}}\right]} \cdot \frac{1}{\left\{1-\sqrt{\frac{\frac{\gamma-1}{2}M_0^2}{\frac{T_{t2}}{T_0}\eta_n\left[1-\left(\frac{p_0}{P_{t2}}\right)^{\frac{\gamma-1}{\gamma}}\right]}}\right\}}$$

where

$$\left(\frac{p_0}{P_{t2}}\right)^{\frac{\gamma-1}{\gamma}} = \frac{\left(\frac{P_{t2}}{P_{t2}}\right)^{\frac{\gamma-1}{\gamma}}}{\left(1+\frac{\gamma-1}{2}M_0^2\right)\left\{1-\left(1+\frac{\gamma-1}{2}M_0^2\right)\frac{T_0}{T_{t2}}\frac{1}{\eta_c\eta_t}\left[\left(\frac{P_{t2}}{P_{t2}}\right)^{\frac{\gamma-1}{\gamma}}-1\right]\right\}}$$

This equation assumes a constant ratio of specific heats, and neglects the fuel weight. Fig. 6 has been plotted from the foregoing equation for assumed engines with four assumed pressure ratios, temperature ratios, and efficiencies according to Table 1.

The results are given for each engine with and without afterburner. The assumed afterburner gives a temperature ratio, T_{t2}/T_0, of 9.0. From Fig. 6 it may be noted that for each of the engines, except C and D without afterburning, neither of which happens to be very well fitted for supersonic flight, the parameter

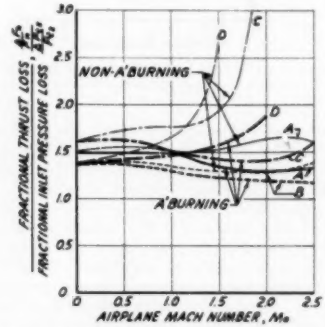

Fig. 6 Loss in Thrust Due to Inlet-Pressure Loss

$(\Delta F_n/F_n)/(\Delta P_{t2}/P_{t2})$ varies only moderately with Mach number. Also, one may draw the conclusion that for the rather large spread of parameters selected in Table 1 there is only a relatively small variation in the loss ratio in Fig. 6 for the engines suitable for high-speed flight. Such spread as is observed in Fig. 6 indicates the following conclusions:

(*a*) An engine with high component efficiencies suffers less thrust loss due to inlet loss, other things being equal.

(*b*) An engine with high turbine-inlet temperature suffers less thrust loss due to inlet loss, other things being equal.

(*c*) An engine with a very high pressure ratio suffers high thrust loss due to inlet loss, other things being equal (assuming no afterburner).

(*d*) An engine with an afterburner suffers less thrust loss due to inlet loss, other things being equal.

It may also be noted that the magnitude of the losses is such that a 1 per cent loss in total pressure at the compressor inlet causes, roughly, a 1½ per cent loss in engine thrust.

In order to see the thrust-loss variation with airplane Mach number, an inlet has been assumed which has a total pressure loss of 0.05 of the stagnation pressure to an airplane Mach number of 1.44, and at high Mach numbers has a loss equal to that of a normal shock at the free-stream Mach number. Such an inlet suffers the fractional losses in stagnation pressure indicated in Fig. 7. Fig. 7 also shows the resulting fractional thrust loss for an engine having the thrust loss-inlet loss relationship indicated in Fig. 6 for engine A with afterburning. For this case, the inlet causes a loss of 0.09 of the ideal thrust that would be available from a no-loss inlet at Mach number of 1.5, a fractional loss of 0.36 at M_0 = 2.0, and of 0.66 at a Mach number of 2.5. These losses are, of course, enormous at high speeds and illustrate that satisfactory inlets assume an ever-increasing importance for flight at high Mach numbers. An efficient inlet can very well spell the difference between successful economic flight at supersonic speeds and the inability to reach these speeds.

The losses in stagnation pressure in Fig. 7 apply to an inlet that is about average subsonically. The reason that the fractional loss in stagnation pressure is assumed constant rather than assuming a constant ram efficiency is that, with a fixed-area inlet, the mass-flow ratio of the inlet becomes more favorable with increasing airplane speed, thus improving the ram-recovery ratio. The normal shock inlet stagnation pressure losses assumed in Fig. 7 can be reduced considerably by using one or more oblique shocks to decelerate the entering air before passing through a normal shock. Many calculated and experimental results are availa-

ble on this type of inlet. Fig. 8 gives the results of theoretical calculations (11) for the type of inlet indicated. It may be noted that the loss in inlet stagnation pressure may be reduced very much by using two or more shocks instead of one.

Most unclassified work done on supersonic inlets to date has been done with a view of applying the results to ramjets, and not from the point of view of a turbojet-equipped supersonic craft. There are two very serious difficulties which occur when one at-

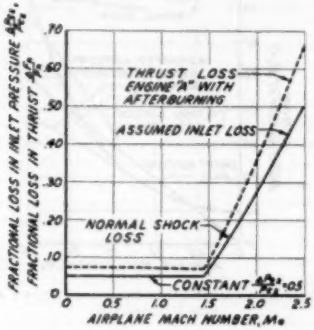

FIG. 7 LOSS IN INLET PRESSURE AND CORRESPONDING THRUST LOSS AS A FUNCTION OF AIRPLANE MACH NUMBER

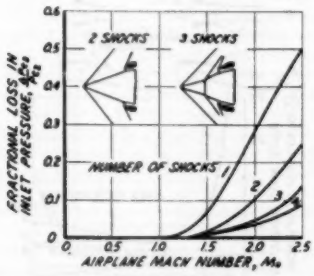

FIG. 8 FRACTIONAL INLET-PRESSURE LOSS FOR OPTIMUM OBLIQUE SHOCK SYSTEM

tempts to use an inlet of the type shown in Fig. 8 on a turbojet-equipped aircraft. The first one is the matter of arrangement. A conical inlet as shown in Fig. 8 is suitable for a nacelle or a nose installation, either of which may be undesirable. The second difficulty is the matter of off-design operation. A ramjet-equipped missile can be operated at constant or near-constant flight speed without seriously compromising the vehicle, whereas an airplane inlet geometry must be capable of functioning reasonably satisfactorily over a range of aircraft speeds from take-off to maximum. The compromises this requirement causes will be discussed in more detail shortly. Furthermore, if one did require a ramjet to operate efficiently over a range of speeds, satisfactory inlet operation could be arranged by using either fuel-flow control or an adjustable exit nozzle to keep the inlet shock positioned at or near the location for optimum inlet performance. On a turbojet-equipped aircraft on the other hand, both the fuel-flow and exit-nozzle settings are dictated by the requirement of keeping the engine performance optimum, and any adjustment to position the inlet shock system must come from a variable-inlet geometry.

Inlet Incremental Scoop Drag. It has been shown how an inlet geometry can adversely affect the performance of a turbojet-equipped aircraft by decreasing the engine thrust, and how this loss becomes more important at higher speeds due to the high inlet losses. Another way an inlet can decrease aircraft performance is by increasing the drag.

The net accelerating force along the flight path can be divided into a defined net thrust and into the resulting drag expression using the steady-state momentum equation (12). The vehicle considered is a general configuration with no special symmetry, and is indicated in Fig. 9. The figure may be interpreted as applying to either subsonic or supersonic flow conditions.

It can be shown (12) that at subsonic flight speeds the only drag forces that need be considered are those due to viscosity and lift, and that for a nonlifting fuselage in an inviscid fluid, there is no

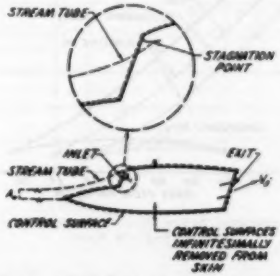

FIG. 9 AIRPLANE CONSIDERED TO ESTIMATE INCREMENTAL SCOOP DRAG

drag force to be considered. The proof of this for a fuselage with an intake and exhaust opening is shown to be merely an extension of D'Alembert's paradox which states the drag of a closed nonlifting body in a perfect fluid is zero. It is important to note that this conclusion is entirely independent of conditions at the scoop entrance, and of the size of the scoop. A larger scoop merely causes the stagnation point, in Fig. 9, to move further inside the scoop and modifies the pressure distribution on the external surfaces of the airplane, but the integrated pressure drag on the airplane skin remains zero.

At supersonic flight speeds it is no longer true that the drag of a closed nonlifting body in inviscid fluid is zero, and it follows that a pressure drag must be considered on the fuselage. In (12) the total momentum, pressure plus momentum flux, is integrated over the closed control surface (shown dotted in Fig. 9), to find an expression for the force acting on the airframe. It is found that in addition to the pressure integral over the exterior skin of the airplane, the difference in total momentum between the scoop inlet and engine exhaust must be taken. Since the engine thrust is defined as the difference in total momentum of the air entering the engine between the free-stream state and the engine exhaust, it follows that, in addition to the integrated pressure drag over the external airplane skin and the engine thrust, an additional term giving the difference in total momentum between the scoop inlet and free stream must be added. This term is defined as incremental scoop drag, and is given by

$$D_s = C_{d_s} q_0 A_{1_0}$$

The coefficient C_{d_s} is based on free-stream dynamic pressure and the forward projection of the inlet scoop area A_{1_0}, and is given by

$$C_{d_s} = C_{p1} - 2\frac{A_0}{A_{1_0}}\left(1 - \frac{M_{s1}}{M_{s0}}\cos\delta_1\right)$$

Fig. 10, from (12), gives the incremental scoop-drag coefficient as a function of the inlet mass-flow ratio. It may be noted that small mass-flow ratios, which mean that the amount of air aspirated by the engine is small relative to the size of the scoop, give large drag coefficients and large incremental scoop drags. This means that the scoop size relative to the engine-aspirating qualities affects the drag, and that an oversize scoop causes very large drags on a supersonic airplane. It will be shown that the required scoop size for an inlet will decrease with airplane Mach number, so that an adjustable inlet becomes almost a necessity for high-speed supersonic flight.

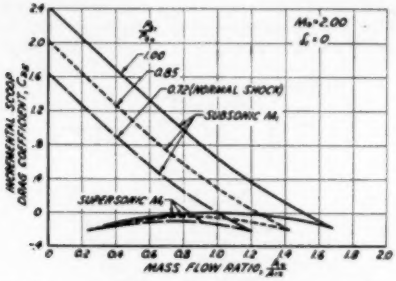

Fig. 10 Incremental Scoop-Drag Coefficient as a Function of Mass-Flow Ratio

Effect of Airplane Speed on Inlet-Engine Matching. It has been shown how it is increasingly important that the inlet and engine be commensurate in size at supersonic airplane Mach numbers. This section will demonstrate the principal factors involved, and how these factors indicate some kind of adjustable inlet scoop becomes necessary for efficient high-speed flight.

A turbojet has the approximate characteristic of being a constant-volume machine at fixed rotational speed. This relationship simply means that the velocity diagram of the flow at the inlet to the first compressor stage tends to remain constant at a fixed rotational speed. It follows that the weight-air-flow rate aspirated by the engine is directly proportional to the stagnation density of the air at the compressor inlet. Based upon this assumption, Fig. 11 gives the variation in air flow relative to the static air flow as a function of airplane Mach number at a fixed altitude. This has been done, assuming zero inlet losses at subsonic flight speeds, and for inlets with three different supersonic performances. The isentropic (zero loss) inlet gives the highest density of air at the compressor face and, consequently, the highest increase in engine air flow due to airplane speed. This inlet provides, at an airplane Mach number of 2.5, 7.6 times the air-flow encountered at static conditions. As a contrast, a normal shock inlet (geometry A) is considered which has the fractional loss in stagnation pressure below the isentropic indicated for a one-shock system in Fig. 8, and the same fractional loss in engine air flow relative to the isentropic inlet. This loss in air flow due to the normal shock is approximately 0.5 at M_0 of 2.5. Intermediate between these two extremes, an inlet (geometry B) is considered which consists of a 10-deg wedge, causing an oblique shock and followed by a normal shock. The engine-aspirating characteristics for this case are indicated in Fig. 11 where sketches of geometries A and B are also given. Since an isentropic inlet demands an area which varies with airplane Mach number, and since the consequences of fixed inlet geometry are being considered, geometries A and B will be discussed in more detail.

Consider geometry A. the inlet which has no oblique shocks. Define as the "swept air-flow rate," the product $\rho_0 V_0 A_1$. This product represents the rate at which air would pass through an area A_1 moved at velocity V_0 in the free stream. By dividing the swept air-flow rate by the engine air flow at static conditions,

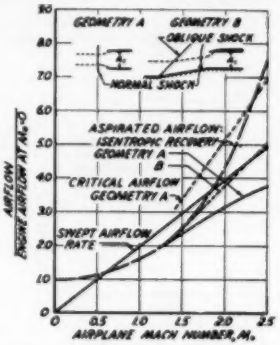

Fig. 11 Comparison of Engine-Aspirated Flows and Scoop-Size Parameters

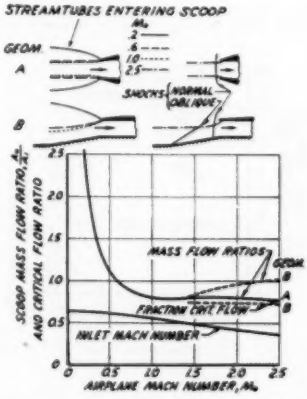

Fig. 12 Scoop-Mass Flow Ratio and Critical-Flow Ratio as a Function of Airplane Mach Number for Two Geometries

the swept air-flow rate is given in units suitable for plotting in Fig. 11. The swept air-flow rate is seen to be linear with the airplane Mach number M_0, and the slope of the line in Fig. 11 will be proportional to the scoop area. Now, if the swept air-flow rate is equal to the engine air-flow rate, then the stream tube approaching the inlet suffers no change in area, and the Mach number of the flow passing through area A_1 is equal to that of the free stream. Since the loss in the inlet duct increases rapidly with increasing Mach number at the inlet entrance, there is a lower limit to the allowable size of the inlet. If an inlet area A_1 is selected such that the swept air-flow rate curve crosses the engine-aspirated air-flow curve at an airplane Mach number of 0.6, then it insures that the Mach number entering the inlet is also 0.6 at this airplane Mach number, and that the scoop-entrance Mach number M_1, will decrease with increasing airplane Mach number approximately as shown in Fig. 12.

Having selected area A_1 on this basis, we may then examine the variation of the ratio of the engine-aspirated air to the swept air-flow rate as a function of airplane Mach number. This quantity, called the "mass-flow ratio," has been computed from Fig. 11 and is plotted for geometry A in Fig. 12. It may be noted that the inlet mass-flow ratio is very large at low airplane speeds, giving the type of streamline pattern sketched for M_0 of 0.2. At an airplane Mach number of 0.6, the mass-flow ratio becomes unity, and the streamline pattern is as indicated. At supersonic Mach numbers the mass-flow ratio is nearly constant at 0.8. Under these conditions, 0.2 of the "swept air flow" must spill around the inlet, giving rise to a flow pattern as indicated, and to the large incremental scoop drags mentioned in a previous section.

Consider now an inlet with an oblique shock preceding the normal shock as indicated in Figs. 11 and 12, geometry B. The geometry chosen has a 10-deg wedge preceding the normal shock. This improves the inlet recovery, and results in the engine aspirating more air at supersonic speeds than did geometry A. This comparison may be noted from Fig. 11 where each assumed inlet's effect on the engine breathing capacities is given.

As before, the swept air-flow rate is defined by $\rho_0 V_0 A_1$, and the ratio of engine-aspirated air-flow rate to swept air-flow rate, called mass-flow ratio, was computed. Since the swept air-flow rates are equal for the two assumed geometries (equal values of A_1 dictated by the limit on M_1), it follows that the mass-flow ratio for the geometry B is higher at supersonic speeds since the engine aspirates more air with geometry B. Thus at an airplane Mach number of 2.5, inlet B has a mass-flow ratio of 1.02.

The inlet flow patterns corresponding to geometry B have been sketched in Fig. 12. It is particularly interesting to note that at a free-stream Mach number of 2.5, the mass-flow ratio is 1.02, and yet there is a normal shock ahead of the inlet, and some air spills around the inlet, causing an incremental scoop drag. At supersonic airplane speeds, unity mass-flow ratio loses its subsonic significance of parallel entering streamlines, and a term is defined which has some of the significance of mass-flow ratio at subsonic speeds. This term is the "fraction of critical flow" and its meaning may be explained as follows: A "critical air flow" may be defined by the expression $\rho_0' V_0' A_1 \cos \delta_1$, where the density and velocity are taken in the flow behind the oblique shock. Since the mass velocity ρV is greater behind the oblique shock than in the free stream, it follows that this critical air flow is greater than the previously defined swept air-flow rate by the ratio, $[(\rho_0' V_0')/(\rho_0 V_0)] \cos \delta_1$. The critical flow rate gets its name from the fact that this is the maximum air-flow rate that can enter the inlet, and that the air speed is supersonic at the inlet when this flow is entering. From this follows directly the definition of the fraction of critical air flow, as the ratio of the engine breathing air-flow rate to the critical flow rate.

Fig. 11 shows the critical air flow derived from the swept air-flow rates by multiplying by the ratio of mass velocities, the latter calculated by means of charts for oblique shock flows (8). Fig. 12 gives the fraction of critical flow as a function of airplane Mach number for geometry B and also for geometry A (where the fraction of critical flow is identical to the mass-flow ratio). It may be noted that the fraction of critical flow is approximately 0.74 for geometry B, and is less than for geometry A. The remaining 0.26 fraction of the critical flow must flow around the inlet lip, and gives rise to the stream pattern shown, Fig. 12, at Mach number of 2.5, and causes large incremental scoop drags similar to those in Fig. 10 for a mass-flow ratio of 1.02.

It follows from the foregoing examples that in both inlets considered, a fixed area results in inlet areas that are undesirably high at high airplane Mach numbers, if the conditions of reasonably small take-off and low-speed inlet losses are to be met. It further follows that such undesirably large inlet areas at supersonic speeds will cause high airplane supersonic drags, and that, therefore, some type of adjustable inlet is necessary. The types of adjustable inlets which may be considered are as diverse as the designer's ingenuity makes them, and will not be considered here.

Outlet-Nozzle Installation and Cooling. As airplane speeds increase, the sensitivity of the airplane net thrust to losses in the exit nozzle also increases. This may be readily seen by reference to Fig. 4. A fractional reduction in velocity coefficient[4] reduces the gross thrust by the same fraction. The corresponding reduction in net thrust may be read from Fig. 4, knowing the ratio of airplane to jet velocity, V_0/V_j. The added scale of airplane Mach number for engine A without afterburning applies as before. From Fig. 4 it may be noted that a nozzle velocity coefficient of 0.90 causes a loss in thrust of 0.10 at static conditions, but at an airplane Mach number of 2.0 this loss becomes 0.40. It is thus apparent that outlet-nozzle losses, just as inlet losses, become increasingly important at high speeds.

The pressure ratio across the exit nozzle of a turbojet, expressed as a fraction p_0/P_{t1}, decreases rapidly with airplane Mach number, M_0. This is due to the rise in pressure level through the engine caused by ram. Fig. 13 gives the pressure ratio across the exit nozzle for each of the engines previously considered. It may be noted that for engine A at static conditions the pressure ratio across the exit nozzle is 0.41, while at an airplane Mach number of 2.5 this ratio becomes 0.075. As a consequence of this great reduction in the fractional nozzle pressure ratio p_0/P_{t1} at high Mach numbers, and since the nozzle losses become more important at high airplane speeds, it has often been suggested that a convergent-divergent nozzle be used for high airplane speeds to reduce the losses in thrust attendant upon the incomplete expansion of the nozzle (see Fig. 17). It has been pointed out recently (13) that provision of a convergent-divergent nozzle is desirable only if the losses due to incomplete expansion are greater than those that would occur in the diverging section of a nozzle. Fig. 14 gives the regions of velocity coefficient and pressure ratio where a divergent section to the nozzle is desirable

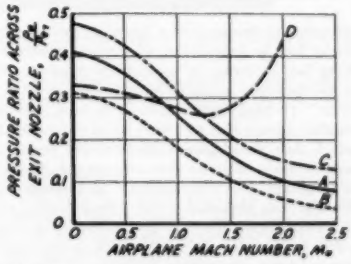

FIG. 13 PRESSURE RATIO ACROSS EXIT NOZZLE FOR SEVERAL ASSUMED ENGINES

(13). It may be noted that for low fractional pressure ratios across the nozzle, and high velocity coefficients, a convergent-divergent nozzle becomes desirable. Thus, for the example of a nozzle at a pressure ratio of 0.075, if the velocity coefficient is

[4] Velocity coefficient is defined as the following ratio:
Velocity of gases leaving nozzle at certain pressure ratio and temperature
Velocity of gases leaving ideal frictionless nozzle at same pressure ratio and temperature

less than 0.90, more thrust could be achieved with a convergent than with a completely expanded nozzle. Fig. 14 assumes that the velocity coefficient is the same for the convergent section of a convergent nozzle, and for the completely expanded nozzle used for comparison. The validity of this assumption may be questionable, but the trend is believed correct.

Reliable data on nozzle velocity coefficients are sparse indeed, and such data as are available indicate a spread between very low values and values greater than unity. It would appear that

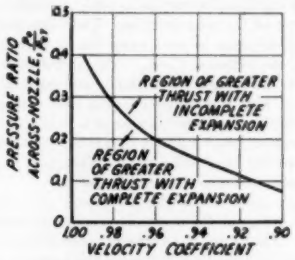

FIG. 14 DIVIDING LINE BETWEEN COMPLETE AND INCOMPLETE EXPANSION FOR MAXIMUM THRUST

some careful measurements on representative geometries would be desirable.

The design of the exit nozzle of the engine is, of course, accomplished by the engine designer. The problem of insuring adequate air to cool the external portions of the engine, and parts of the airplane structure in proximity to hot portions of the engine, has usually fallen to the airframe designer. Such cooling is often accomplished in flight by an air supply that utilizes ram due to flight speed. For ground and take-off cooling, the usual expedient is to have the air flow discharge into a shroud which surrounds the engine. This arrangement utilizes the main discharge from the engine as the motivating fluid to draw a flow through the cooling system by a "jet-pump" action.

The minimum requirements of a desirable cooling system are that sufficient flow be provided at all airplane speeds, and that any resulting loss in thrust be as small as possible. Woefully little data are presently available on the effect of jet pumps on engine thrust. Statically when there is no ram, such few data as are available indicate that the pumping of the cooling flows required (which may be as high as 0.05 times the engine air flow) causes losses in thrust of about this same magnitude (0.05 times the engine thrust) in some installations. Most designs on which information has been published utilize a fixed cooling configuration. That arrangement tends to give a cooling air flow which increases sharply with increasing flight speeds and ram. Such a flow increase, due to an increase in flight velocity, results in a compounded penalty since both the air flow and the velocity increase add to the cooling drag. Experience on reciprocating engines has indicated that cowl flaps are required to achieve adequate cooling with low drag over a large range of flight speeds. It would appear that some similar provision of variable geometry may become a necessity for high-speed turbojet cooling.

OPERATIONAL PROBLEMS

Speed Stability. A well-known characteristic of present-day airplanes, particularly those powered by turbojets, is their lack of speed stability when flying at relatively low indicated speeds (14). To the pilot, the difficulty appears as a wandering of the flight speed. This may become worse in supersonic flight. "Speed stability" is used in the sense that once the airplane is trimmed with fixed controls to hold a certain speed, there must be restoring forces which after a small disturbance in speed, will bring the speed back toward the trim value. Conventional subsonic airplanes equipped with reciprocating engines and propellers inherently have this characteristic in the cruising and high-speed regions since any increase in speed from the trim position results in an increased drag and a decreased thrust, both of which changes tend to reduce the speed. If the speed is reduced below the trim value, there is a decrease in drag and an increase in thrust, which again accelerates the airplane back toward the trim speed. This situation is, in general, a satisfactory one, and it is noteworthy that special thrust regulators are not required. The power plant - propeller combination provides a stabilizing force by virtue of its characteristic of holding the product of speed and thrust essentially constant. Fig. 15 shows this situation diagrammatically.

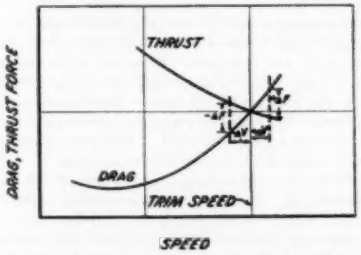

FIG. 15 THRUST-DRAG INTERSECTION FOR PROPELLER-DRIVEN AIRPLANE

The characteristics of supersonic airplanes powered by turbojets are considerably different from those of propeller-driven aircraft. The thrust variation with speed is such that an increase in speed produces little, if any, decrease in thrust. Furthermore, when flying in the subsonic long-range cruising condition, the drag may not decrease at all below the cruising speed. An additional possible source of difficulty may occur in approaches to landings where the pilots of present-day turbojet-powered aircraft have reported difficulty in establishing proper speed trim during instrument approaches. At supersonic speeds, in addition, the drag curve roughly parallels the thrust curves for constant fuel-air ratio. Thus at both subsonic and supersonic speeds, it is believed that constant fuel-air ratio regulation will not be satisfactory. Curves demonstrating these conditions for the high-speed plane are shown in Fig. 16.

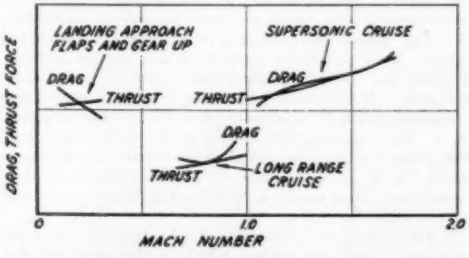

FIG. 16 THRUST-DRAG INTERSECTIONS FOR SUPERSONIC TURBOJET AIRPLANE

It is suggested that to meet the minimum requirements of a highly loaded supersonic airplane, thrust should be regulated approximately according to the following principles:

(*a*) At subsonic speeds the product of the thrust and speed should stay constant.

(*b*) At supersonic speeds a constant thrust might be adequate.

Analytical studies and flight experience will be needed to verify these intuitively derived rules. It is understood, of course, that the regulation described is an automatic transient thrust variation. This should not be confused with the maximum thrust which remains controllable through the pilot's throttle.

Jet Interference. Many turbojet-powered airplanes have tailpipe outlets ahead of the tail surfaces. Such an arrangement has several important advantages, but it also introduces problems which may be of crucial importance in supersonic designs. Some of the problems arising in that arrangement are concerned with heating of the fuselage and tail, buffeting of fuselage and tail, and aerodynamic interference of the jet on the tail. A study of these problems might begin with an examination of the exhaust jets alone. Unfortunately, the basic information needed to cope with all of these problems has not yet been obtained. Of aid is the recent review of the present state of knowledge on jets by Squire (15). Aspects of several jet problems not considered in that paper will be discussed here.

There are several important characteristics displayed by jets. To help understand these phenomena, tests were made with two pairs of circular nozzles which were supplied from a nitrogen tank. Figs. 17 and 18,[7] are Schlieren pictures taken when the

FIG. 17 EXPANSION PATTERN FROM TWO JETS ISSUING FROM CONVERGENT NOZZLES
(Pressure ratio = 0.111.)

FIG. 18 EXPANSION PATTERN FROM TWO JETS ISSUING FROM STEPPED NOZZLE, SIMULATING EJECTOR
(Pressure ratio = 0.111.)

jets were exhausted with a fractional pressure ratio of $^1/_9$ into quiescent air. Reference to Fig. 13 shows that ratio to correspond to flight near a Mach number of 2.0. Thus the external air flow is not properly simulated. Study of Fig. 17 reveals the following properties:

(*a*) The jets expand toward ambient pressure with the usual wave pattern.

(*b*) The jets spread immediately on issuing from the nozzle. This is due to the incomplete expansion in the nozzle.

(*c*) Additional spreading takes place in the jet-ambient air mixing region.

(*d*) The jet axes are displaced outward by interference between the jets.

(*e*) The jets coalesce finally into one jet.

This pair of nozzles would approximate the actual geometry of an airplane installation only crudely, since no diameter change was made in the nozzle to simulate a jet pump. The effect of a step in the nozzle simulating a jet pump is seen in Fig. 18 to be very important. With that configuration, the spreading is reduced and the interference is eliminated.

The twin jets just discussed, when passing under tail surfaces, could introduce various interferences with the tail. One type is demonstrated in Fig. 19, where in a supersonic flow, an airfoil is placed behind and above the wake of another airfoil (16).[8] It is seen that the leading-edge shock of the tail intersects the wake, forms reflected and transmitted waves, and deflects the wake. To investigate this phenomenon for the tail-jet case a calculation was made for a two-dimensional tail in a supersonic flow over a two-dimensional jet. The result obtained for that simple case indicated the effect of interference to be small, but

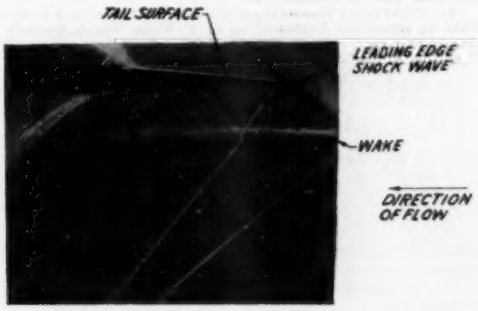

FIG. 19 INTERSECTION OF SHOCK-WAVE AND WAKE

possibly of significance. It seems likely that power-on wind-tunnel tests would be needed to determine the importance of this effect.

CONCLUSIONS

The flight-speed trend was examined to show that supersonic airplanes with turbojet engines are to be expected soon. An analysis was made which showed that supersonic wave drags will cause an increase in drag near sonic speed and a thrust increase requirement for the turbojet.

The performance requirements of a turbojet installation were considered from the point of view of an aerodynamicist whose task is to see that an installed turbojet engine develops as nearly as possible its ideal thrust. It was shown that the difficulty and importance of this task increased with airplane speed. Thus, at a Mach number of 2.5, a normal shock inlet lost 0.60 of the thrust obtainable with an ideal inlet. The losses in the exit nozzle likewise assumed an increase in importance with higher airplane speeds. Whereas at subsonic speeds the inlet size was not very critical (providing a minimum size was ex-

[7] Figs. 17 and 18 were made by Drs. H. W. Liepmann and John Laufer at the Guggenheim Aeronautical Laboratory of the California Institute of Technology.

[8] The wake simulates the jets in the sense that both are regions in the flow passing the tail with velocities differing from the free-stream velocity.

ceeded), at supersonic speeds large drag increments, whose magnitude may be estimated, resulted from an oversize inlet. These scoop drags may be avoided by an adjustable inlet, and an analysis was made of the salient factors governing the matching of the inlet size and the engine. It was shown that the mass-flow ratio, the criterion used for subsonic speeds lost much of its significance at supersonic speeds.

The ability of a supersonic turbojet-equipped airplane to stably hold a desired speed with a fixed throttle setting was compared to that of a subsonic propeller-equipped airplane, and it was indicated that careful consideration of the engine controls on a supersonic airplane was necessary to avoid the tendency toward instability created by the parallelism of the thrust and drag curves against speed.

A discussion of jet interference was given, and several illustrations of interference phenomena for supersonic jets were shown.

BIBLIOGRAPHY

1 "Predictions of Supersonic Airplane Performance," by H. Luskin, *Journal of the Aeronautical Sciences*, vol. 17, January, 1950, pp. 5–12.

2 "Developments in High-Speed Aircraft," by E. H. Heinemann, *Mechanical Engineering*, vol. 69, 1947, pp. 805–812.

3 "Performance and Range of Application of Various Types of Aircraft-Propulsion Systems," Cleveland Laboratory Staff, NACA Technical Note 1349, August, 1947.

4 "Performance Possibilities of the Turbojet System as a Power Plant for Supersonic Airplanes," by G. P. Wood, NACA Research Memo. L7H05a, August, 1947.

5 "A Review of Aerodynamic Cleanness," by E. J. Richards, *Journal of the Royal Aeronautical Society*, vol. 54, March, 1950, pp. 137–172.

6 "Estimated Lift-Drag Ratios at Supersonic Speed," by R. T. Jones, NACA Technical Note 1350, July, 1947.

7 "A Method of Presenting the Performance of Turbojet Engines," by C. A. Meyer and H. F. Faught, Institute of the Aeronautical Sciences Preprint No. 293, July 12–13, 1950.

8 "Introduction to Aerodynamics of a Compressible Fluid," by H. W. Liepmann and A. E. Puckett, John Wiley & Sons, Inc., New York, N. Y., 1947.

9 "The Choice of Pressure Ratio in Aircraft Gas Turbine Power Plants," by C. Richard Soderberg, Institute of the Aeronautical Sciences, Preprint No. 218.

10 "Analysis of Turbojet Thrust Augmentation Cycles," by B. T. Lundin, Institute of the Aeronautical Sciences, Preprint No. 223, March 18, 1949.

11 "Pressure Recovery for Missiles With Reaction Propulsion at High Supersonic Speeds," by Kl. Oswatitsch, NACA Technical Memorandum 1140, June, 1947.

12 "The Calculation of the Scoop Drag for a General Configuration in a Supersonic Stream," by Harold Klein, Douglas Aircraft Company Report SM-13744, April 12, 1950.

13 "Increased Jet Thrust From Pressure Forces," by F. P. Durham, *Journal of the Aeronautical Sciences*, vol. 17, July, 1950, pp. 425–428.

14 "A Test Pilot Looks at the Jets," by Capt. F. M. Trapnell, *Aeronautical Engineering Review*, vol. 9, May, 1950, pp. 14–19 and 33.

15 "Jet Flow and Its Effect on Aircraft," by H. B. Squire, *Aircraft Engineering*, vol. 22, March, 1950, pp. 62–67.

16 "On the Reflection of Shock Waves From Boundary Layers," by H. W. Liepmann, A. Roshko, and S. Dhawan, Report submitted by Guggenheim Aeronautical Laboratory of the California Institute of Technology, to NACA under contract NAw-5631, August, 1949; being prepared for publication.

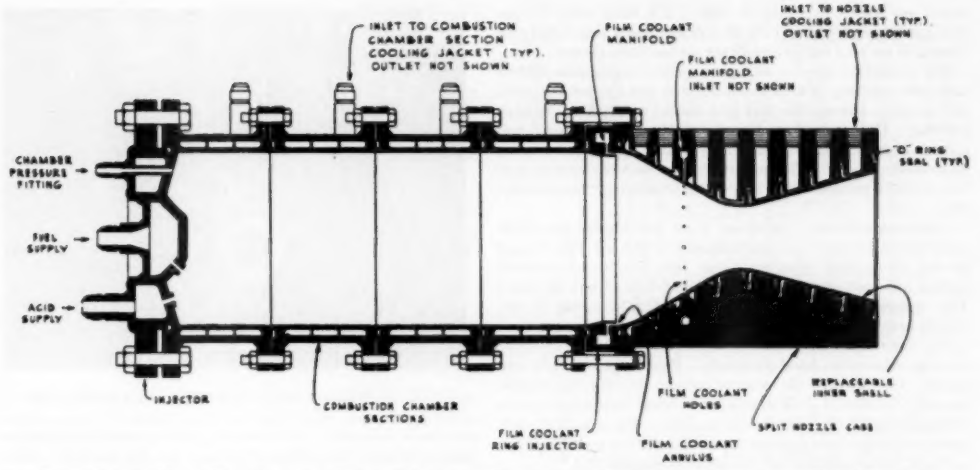

FIG. 1 ROCKET MOTOR WITH SECTIONAL COOLING JACKET AND FILM-COOLANT INJECTORS FOR QUANTITATIVE HEAT-TRANSFER ANALYSIS

Heat Transfer in Rocket Motors and the Application of Film and Sweat Cooling

BY R. H. BODEN,[1] YPSILANTI, MICH.

Heat transfer in rocket motors, as in all internal-combustion engines, is a major factor in determining the limiting performance of the power plant, and therefore establishes the limiting performance of the vehicle in which the motor is installed. This paper discusses the distribution of heat transfer in rocket motors, a number of factors which influence it, and finally, the experimental investigation of film cooling.

INTRODUCTION

HEAT transfer within the combustion chamber of a rocket motor has been found to be low. As the mass flow of the gases increases it increases rapidly, reaching a peak value at the minimum throat-area section of the nozzle, then rapidly decreasing as the gases pass through the expansion section. How the distribution of heat transfer changes under varying operating conditions is a detailed and difficult study within itself.

Among the factors which affect the studies we have made are convective and to a lesser extent radiation heat transfer within the motor. Their magnitudes are determined by the temperature, physical properties, and mass flow per unit area of the gases in the combustion chamber. Metallic contaminants in the propellants modify the chemical reactions taking place, resulting in greatly changed phenomena. The propellant-injector configuration establishes the nature of the resultant gas flow, further modifying the distribution of heat. As the hot gases leave the throat of the nozzle their expansion determines to some extent the heat transfer in the expansion section of the nozzle. Our problem is to control these factors within the limits which will allow application of available materials to the construction of rocket motors with the minimum loss in performance.

A definite limit exists which we can attain by design techniques and propellant selection in controlling the factors affecting heat transfer. A powerful method of supplementing them is to apply a liquid cooling film in the boundary layer between the high-velocity combustion gases and the rocket-motor walls. Film cooling reduces the heat transfer up to 70 per cent. Proper control of operating conditions and propellants gains an additional 10 to 15 per cent, an over-all reduction of between 80 and 85 per cent.

EXPERIMENTAL METHODS AND EQUIPMENT

Detailed analyses of the heat transfer within the combustion chamber and the nozzle of a rocket motor were necessary to understand fully the phenomena taking place and to compare the effects of the factors controlling heat-transfer distribution both before and after application of film cooling. Therefore a sectional motor was assembled, Fig. 1. The components were a multiorifice propellant injector, individually cooled combustion-chamber sections, a number of ring injectors for film coolant, and a Venturi nozzle. The nominal chamber pressure was 300 psia. The

[1] Supervisor of Combustion and Propulsion Activities, University of Michigan, Aeronautical Research Center, Willow Run Airport.

Contributed by the Heat Transfer Division and presented at the Annual Meeting, New York, N. Y., November 26–December 1, 1950, of THE AMERICAN SOCIETY OF MECHANICAL ENGINEERS.

NOTE: Statements and opinions advanced in papers are to be understood as individual expressions of their authors and not those of the Society. Manuscript received at ASME Headquarters, August 23, 1950. Paper No. 50—A-53.

thrust was 1000 lb at a mixture ratio of 2.8, when using 6½ per cent red fuming nitric acid for the oxidizer and a mixed fuel containing 80 per cent aniline and 20 per cent furfuryl alcohol.

The propellant injector had eight pairs of replaceable orifices and eight auxiliary orifices which directed fuel against the walls at the joint between the first and second combustion-chamber sections. Three orifice combinations, four-pair, eight-pair, and eight-pair with auxiliary fuel orifices, were obtained by using blank orifice inserts. The resultant propellant momentum was substantially parallel to the walls at the operating mixture ratio, 2.8.

Combustion-chamber sections were interchangeable. The inside diameter was 5 in., and a length of 2.9 in. was exposed to the combustion chamber. One test combustion-chamber section was built with a replaceable inner wall of porous metal. This replaced the section immediately adjacent to the nozzle. Porous-bronze and porous-copper liners were used.

The film-coolant injectors fitted between any of the combustion-chamber sections and the nozzle. Four units were built and tested. One directed the coolant radially into the combustion chamber. A second, J-92, directed the coolant tangentially to the circumference of the combustion chamber. The other two were radial and tangential types but both had deflecting vanes as shown in Fig. 1, which directed the coolant downstream.

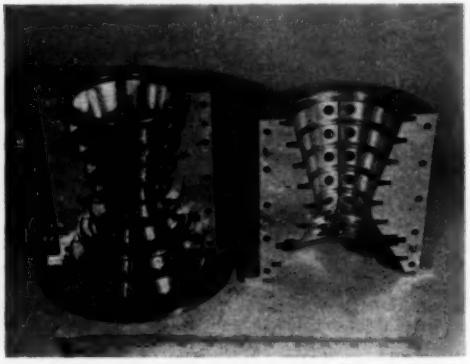

FIG. 2 SECTIONALLY COOLED NOZZLE FOR INVESTIGATION OF HEAT TRANSFER IN ROCKET MOTORS

The sectionally cooled nozzle, Fig. 2, had a split case and a replaceable inner shell. Cooling passages were separated by circumferential fins which fitted within mating grooves of the case. A longitudinal fin separated inlet and outlet passages. O-rings sealed between passages. Full expansion of the combustion-chamber gases into the atmosphere was attained for a chamber pressure of 330 psia. Therefore the experimental tests were conducted at this pressure. The thrust of the motor was then about 1150 lb.

A film-coolant manifold was built into this nozzle midway between the entrance to the contraction section and the throat. Film-coolant holes were drilled in the replaceable inner shell as needed.

The assembled motor was installed on a movable test stand so that the thrust could be measured, Fig. 3. Inlet lines, coiled to reduce restraint on the test stand, appear on the right of the illustration; thermocouple wells discharge cooling water at the left.

During a test, thrust, chamber pressure, and propellant flow rates were measured. From these operating parameters, characteristic velocity, c^*, average velocity, c, specific impulse, I_{sp}, and the thrust coefficient, c_f, were calculated. The chamber pressure and the propellant flow ratio were regulated automatically in order to obtain constant operating conditions. Heat-transfer data were obtained from records of the inlet and outlet temperatures and flow rates of the jacket coolant from each section of the motor.

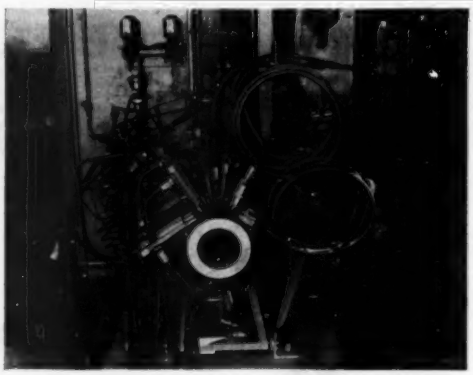

FIG. 3 SECTIONALLY COOLED ROCKET MOTOR ON TEST STAND

OPERATING PARAMETERS AND HEAT TRANSFER

The operating parameter, which is a measure of the efficiency of combustion of the propellants, is the characteristic velocity, c^*. It has the dimensions of a velocity and is defined as

$$c^* = \frac{p_c f_t g}{w} \text{ fps}$$

in which

p_c = chamber pressure, psia
f_t = throat area, sq in.
w = total weight rate of flow of propellants through injector, lb per sec

A second characteristic velocity, defined as $c^{*\prime}$, is calculated from the total weight of fluids flowing through both the propellant injector and the film-coolant injector

$$c^{*\prime} = \frac{p_c f_t g}{w'}$$

in which

w' = total weight rate of flow of propellants and film coolant, lb per sec

The average velocity, c, of the exhaust gases across the exit section of the nozzle is directly proportional to the thrust

$$c = \frac{Fg}{w}, \text{ fps}$$
$$= c_f c^*$$

in which

F = motor thrust, lb
c_f = thrust coefficient

The thrust coefficient, c_f, is a nondimensional parameter which is a measure of the ability of the nozzle to convert the random thermal energy of the gases within the combustion chamber into

an ordered linear momentum which results in a directed thrust

$$c_f = \frac{F}{p_c f_t}$$

This parameter is substantially constant for a given nozzle and ratio of chamber pressure/atmospheric pressure over the range of mixture ratios investigated.

The mixture ratio, r, is defined as the ratio of the weight rate of flow of the oxidizer/weight rate of flow of fuel.

The specific impulse, I_{sp}, is the thrust obtained per unit weight of propellants consumed. The dimensions are those of a time which is the period for which the rocket motor will produce its rated thrust from a weight of propellants equal to the rated thrust

$$I_{sp} = \frac{F}{w}, \text{ sec}$$

$$= \frac{c}{g}$$

Detailed discussions of these parameters are beyond the scope of this paper. Excellent accounts of their derivation are given in the references.

The heat transfer, q, Btu/in.^{2}/sec, was calculated from bulk temperatures, flow rates, and specific heats of the jacket coolant and the area of the combustion-chamber wall exposed to the hot gases

$$q = \frac{w_c(t_o - t_i)c_p}{A_w}, \text{ Btu/in.}^2\text{/sec}$$

where

w_c = coolant flow rate, lb per sec
t_i = inlet bulk temperature of coolant, deg F
t_o = outlet bulk temperature of coolant, deg F
A_w = wall area exposed to hot gases, in sq in.
c_p = specific heat of coolant, Btu/lb /deg F

Heat flow between cooling jackets of the combustion-chamber sections was minimized by nonconducting asbestos-fiber gaskets between them. In the nozzle, Fig. 2, heat flow across the circumferential fins between cooling-jacket sections was minimized by controlling the coolant flow to obtain the least possible temperature difference between the coolants on each side of the fins. Heat transfer from the fins to the coolant was small in comparison to that through the motor walls.

Heat Transfer and Factors Affecting It

The first step in this research program was to determine as accurately as possible the heat transfer along the length of the rocket motor, Fig. 4. This figure shows the average heat transfer over each section of the motor. No film coolant was used, the injector being replaced by a blank ring. The heat-transfer bar graph indicated by the dashed lines shows what can be expected with a good commercial grade of red fuming nitric acid. Along the combustion chamber $^1/_2$ Btu/in.^{2}/sec is a fair average value. As the gases enter the nozzle their velocities increase with a corresponding increase in the heat transfer. As they travel into the nozzle the rate of change of heat transfer increases very rapidly, reaching a maximum value just upstream of the minimum throat-area section. After passing through the throat, the heat transfer decreases at a relatively rapid rate.

One of the first anomalies which we detected was the wide variation in heat transfer with acid density and ambient temperature. Fresh acid always produced low heat transfer. As it aged, dissolving Fe, Cr, and Ni from the shipping containers, its density increased. The motor performance shifted to lower values and the heat transfer increased remarkably. These effects reached maxima for acid densities in the range from 1.59–1.60, then decreased again as the density increased further. Typical analysis of the red fuming nitric acid for a range of oxidizer densities is summarized in Table 1. The results summarized in Fig. 4 for three different acid densities indicate that the plane of maximum heat transfer is also shifted a short distance toward the throat. A 50 per cent increase in heat transfer can be anticipated from the presence of Fe, Cr, and Ni in the oxidizer.

TABLE 1 COMPOSITION OF RED FUMING NITRIC ACID

Specific gravity	Weight per cent of components					
	HNO_3	NO_2	H_2O	$Fe(NO_3)_3$	$Cr(NO_3)_3$	$Ni(NO_3)_2$
1.539	91.51	6.90	0.92	0.50	0.13	0.04
1.548	90.25	7.62	0.40	1.36	0.26	0.11
1.559	90.14	7.58	0.43	1.38	0.36	0.11
1.573	86.54	8.15	1.45	2.87	0.76	0.23
1.592	80.10	9.24	3.90	5.03	1.53	0.40
1.619	75.25	11.67	3.63	7.03	1.86	0.56
1.620	73.76	11.54	3.68	8.20	2.17	0.65

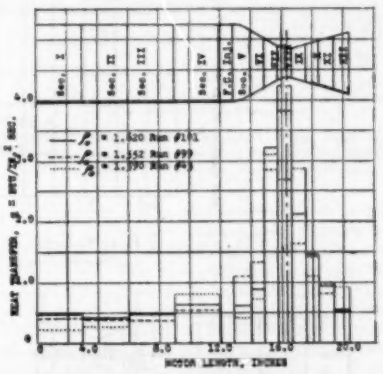

FIG. 4 EFFECT OF ACID COMPOSITION ON HEAT-TRANSFER DISTRIBUTION IN ACID-ANILINE ROCKET MOTOR

A second factor which greatly affected the heat transfer was the operating mixture ratio. The theoretical combustion-chamber temperature increases rapidly from 3200 F (2000 K) for a propellant mixture ratio of 2.0 to approximately 5120 F (3100 K) over the range from 2.8–3.4. This change is reflected in the heat-transfer curves which are summarized in Fig. 5. The heat transfer increases at a steady rate at the lower mixture ratios over all sections of the motor. Over the range of mixture ratios for which maximum motor performance is obtained, a sharp increase in the rate occurs, particularly in those sections of the rocket motor which are in the neighborhood of the throat. The characteristic velocity, c^*, calculated from the propellant consumption, is also plotted in Fig. 5. The characteristic velocity $c^{*\prime}$ is calculated from the total flow rate of propellant and film coolant. A constant flow of film coolant was used for these tests in order to minimize chances of burning out the nozzle. From these data it is clear that the heat-transfer problems encountered in normal rocket-motor operation can be diminished with insignificant loss in performance by designing for a mixture ratio slightly lower than that for maximum motor performance.

A third factor which greatly affects the heat-transfer rates in the rocket motor is the propellant-injector design. The heat-transfer data in Fig. 6 were obtained under the same operating conditions. The solid curve summarizes the results for a four-pair injector; the corresponding heat transfer for an eight-pair unit is shown by the dotted line. A major difference is apparent in the combustion-chamber sections of the motor and at the

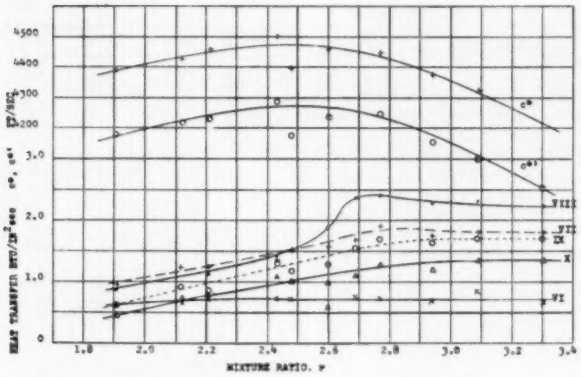

FIG. 5 VARIATION OF HEAT TRANSFER IN ROCKET-MOTOR NOZZLE WITH PROPELLANT-MIXTURE RATIO
(Chamber pressure 329 psi; film coolant 0.298 lb H_2O/sec.)

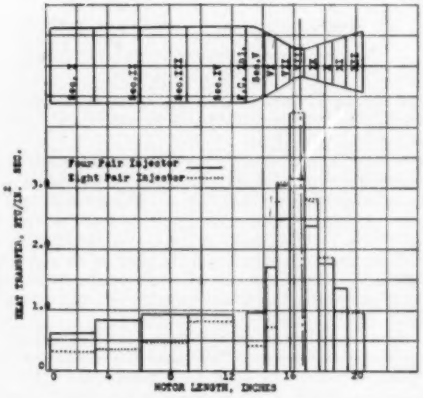

FIG. 6 COMPARATIVE HEAT TRANSFER FROM MULTIORIFICE INJECTORS

throat. The differences are not entirely attributable to the injector since there was some variation in the oxidizer composition between tests.

Two minor factors affected the test results. In the combustion chamber the resultant momentum of the propellant streams increased the heat transfer if it was directed toward the combustion-chamber walls. In the expansion section of the nozzle the heat transfer was somewhat greater for overexpansion of the combustion gases than for underexpansion. These are minor effects and can be handled effectively by proper design.

The preliminary data which have been presented indicate clearly that the major region of attack is the throat section of the nozzle in which the maximum heat transfer can reach values between 4 and 5 Btu per sq in. per sec. Full account must be made of the propellant-injector design, and the possibilities of contamination of the propellants.

FILM AND SWEAT COOLING

Since the region of maximum heat transfer in rocket motors occurs in the throat, the problem of cooling this section was attacked first. Film-coolant injectors were fitted at the entrance to the contraction section of the nozzle, and at a plane midway between the entrance and the throat.

The heat-transfer data which we are about to discuss was obtained in all cases using water for the film and sweat coolant. The rocket motor was operated at a chamber pressure of 330 psia to obtain full expansion in the nozzle. Mixture ratios were maintained within the range 2.8–3 because heat transfer is little affected from changes within these limits.

The least effective method of film cooling was by radial injection at the entrance to the nozzle. A reduction of less than 20 per cent at the throat was obtained. Directing the coolant along the walls proved several times more efficient. Flow along the walls was accomplished by injecting the coolant tangentially to the circumference of the combustion chamber and by deflecting the flow with a thin annular ring.

Heat-transfer curves for the nozzle sections adjacent to the throat are given in Fig. 7. In this case the film-coolant injector was a deflector type as shown in Fig. 1. Coolant was injected radially against the deflector. An unexpected result was the increase of heat transfer for flow rates between 0 and 0.1 lb per sec. The oxidizer used in these tests had a specific gravity of 1.62, indicating a large amount of Fe, Cr, and Ni in solution. The maxima occurred in all tests with contaminated acid and are believed to result from the presence of the metallic materials. The heat transferred rapidly decreased with flows greater than 0.15 lb per sec, and little was gained by injecting more than 0.6 lb per sec. The greatest reduction was obtained in those sections for which the mass flow of combustion gases per unit cross-sectional area was greatest. At the throat with 0.6 lb of water per sec the reduction is from 70 to 75 per cent of the value with no film coolant.

The effect on motor performance was small. An increase occurred at low flows, then it decreased again to substantially the same value for no film coolant.

The film-cooling method which we have just discussed dealt with an injector which delivered discrete streams of water into the combustion chamber after being spread in a fairly uniform layer by a deflecting ring. By injecting coolant through a porous-metal wall a continuous film was satisfactorily developed over the entire inner surface of the combustion chamber. Two advantages result. The porous metal wall is satisfactorily cooled and the heat transfer is controlled below the porous section by excess coolant.

Preliminary tests on the sectionally cooled rocket motor were recently completed with distilled water as the sweat coolant. The

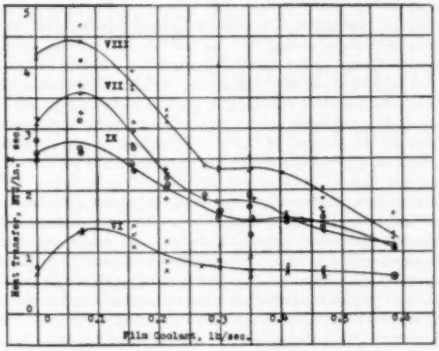

FIG. 7 HEAT TRANSFER IN NOZZLE WITH FILM COOLING

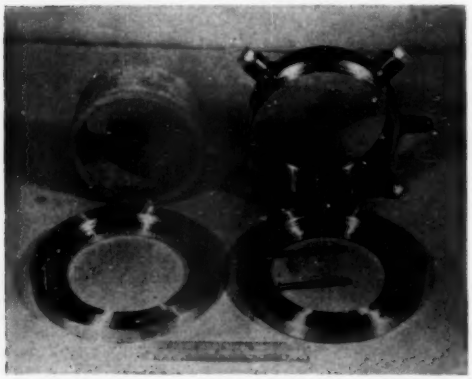

(a) Components

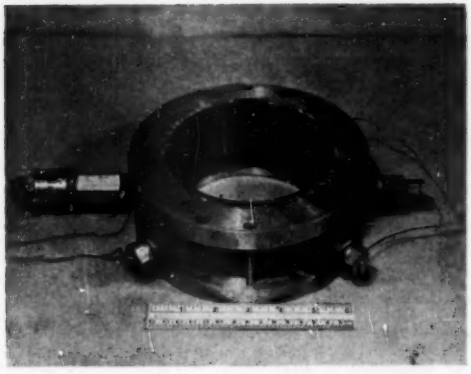

(b) Assembly

FIG. 8 SWEAT-COOLED COMBUSTION SECTION FOR 1000-LB-THRUST ROCKET MOTOR

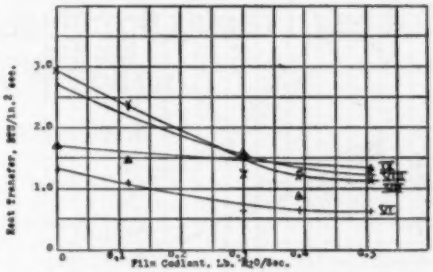

FIG. 9 REDUCTION OF HEAT TRANSFER WITH FILM COOLANT INJECTED THROUGH POROUS-COPPER COMBUSTION-CHAMBER SECTION AT ENTRANCE TO CONTRACTION SECTION OF NOZZLE

combustion-chamber section immediately adjacent to the nozzle was replaced by a porous-metal section which is shown in Fig. 8. The liners were of copper and bronze having a porosity of approximately 50 per cent. They were arbitrarily made $^1/_2$ in. thick for the first tests. The inside diameter was the same as the other combustion-chamber sections. A length of $2^3/_8$ in. was exposed to the combustion chamber. Thermocouples were inserted at four points, equally spaced, on the inner surface of the liners.

The temperatures measured within the porous metals indicated large temperature gradients. These resulted because of nonuniform flow in the liners, nonuniform flow and temperatures of the gases in the combustion chamber and probably variations in the porosity of the metal. Temperature rise did not exceed 193 deg F at the lowest flow rate, 0.11 lb per sec. The minimum change was 48 deg F for 0.51 lb per sec of coolant. No serious plugging occurred during the tests which lasted $2^1/_4$ min. The copper liner cracked at the thermocouple wells. The bronze liner withstood two tests without damage and suffered a reduction in porosity of approximately 30 per cent.

Effective cooling persisted through the nozzle from the sweat coolant. The heat transfers, Fig. 9, for coolant flows of 0.11 and 0.4 lb per sec were obtained with the porous-copper liner, and for flows of 0.30 and 0.51 lb per sec were obtained with the bronze liner. Propellants had very little metallic contamination; therefore heat-transfer values were low with no coolant. The decrease in heat transfer observed was of the same order of magnitude as those which were observed from the other types of film-coolant injectors with the exception of the radial-type unit having no deflector ring. The maximum heat-transfer reduction observed was 60 per cent.

Comparative heat transfers at the throat section of the motor are summarized in Fig. 10. The greatest heat transfer resulted when a high-specific-gravity oxidizer was used and the propellant injector was fitted with a set of auxiliary fuel orifices. When the red fuming nitric acid contained only small amounts of metallic contaminants, the magnitude of the decrease in heat transfer with film-coolant flow was substantially the same for all types of film-coolant injectors which spread a uniform film over the motor walls. The greatest reduction for the least film coolant was obtained with the film-cooled nozzle.

The film-cooled nozzle injected coolant in a region where the rate of change of heat transfer was increasing rapidly. The coolant was injected radially. Nevertheless, this nozzle required the least coolant flow to obtain the maximum cooling effect, and reached the lowest heat-transfer rate of all the methods applied. For coolant rates greater than 0.35 lb per sec, the heat-transfer rate stabilized at a constant value 26.5 per cent of that reached with no coolant.

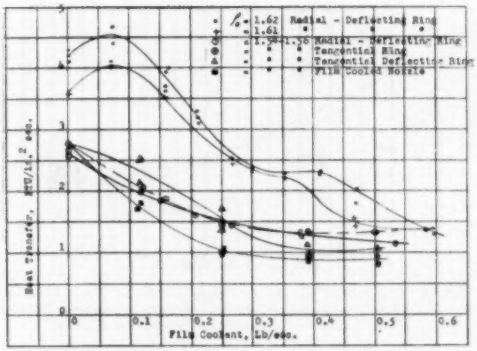

FIG. 10 HEAT TRANSFER AT NOZZLE THROAT WITH FILM COOLING

sweat cooling clearly indicates the effectiveness of these methods of cooling, particularly when applied in those regions of the motor where the rate of change of heat transfer is increasing rapidly. For the motor under discussion maximum cooling effect was achieved with 5 per cent of the total weight of propellant used. This percentage will change with the size of the motor approximately in proportion to the square root of the thrust ratios. Therefore $^1/_2$ per cent of the total propellant weight is sufficient coolant for a 100,000-lb-thrust motor, a small cost for the results gained.

Other data which we have obtained lead us to believe that fuel and water are equally effective in accomplishing film cooling. Therefore incorporation of special tanks and supply systems is unnecessary in a vehicle. Much research remains to be done in this regard, particularly correlating the cooling effects of the many different propellants with their physical and chemical properties. These detailed analyses, and a number of others, are now in process from which we shall gain a clear insight into the many phenomena involved.

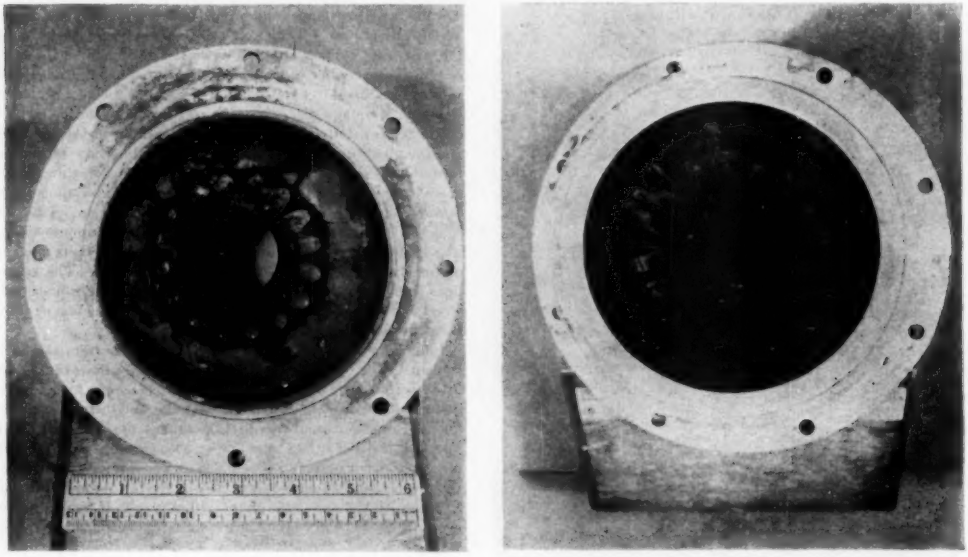

(a) Contraction section (b) Expansion section

FIG. 11 COOLANT TRACES ON FILM-COOLED NOZZLE

The effect of the film coolant persisted through the throat of the nozzle. Photographs of the coolant traces are shown in Fig. 11. It is evident from the photographs that additional film-coolant holes would result in full coverage of the throat and in further reduction of heat transfer.

Comparison of the data, summarized in Figs. 9 and 10, shows that injecting a uniform film of coolant by the methods described or by means of a porous-metal section are equally effective in reducing heat transfer downstream of the injectors. In all cases a 50 per cent reduction in heat transfer can be accomplished with 0.021 lb of cooling water per linear inch of injector circumference.

CONCLUSION

The brief survey of this experimental investigation of film and

ACKNOWLEDGMENT

The studies presented in this paper were performed at the Jet Propulsion Laboratory of the California Institute of Technology. They were jointly sponsored by the Army Ordnance Department and the Air Materiel Command. The author wishes to acknowledge the interest and support of these agencies and particularly of Dr. Louis G. Dunn, Director of the Jet Propulsion Laboratory.

REFERENCES

1 "The Physics of Rockets," by H. S. Seifert, M. M. Mills, and M. Summerfield, *American Journal of Physics*, vol. 15, January–February, 1947, pp. 1–21; March–April, 1947, pp. 121–140, and May–June, 1947, pp. 255–272.

2 "Rocket Propulsion Elements," by G. P. Sutton, John Wiley & Sons, Inc., New York, N. Y., 1949.

Centrifugally Cast Bronze-Back Bearings for Heavy-Duty Operation

By L. M. TICHVINSKY,[1] BERKELEY, CALIF.

The art of centrifugally casting bronze-backed bearings for use in heavy-duty Diesel engines is only 4 to 5 years old and was introduced by the United States Navy at the end of the last war. Steel-backed bearing material will withstand any actually applied loads in operation without permanent deformation, because of adequate physical properties. However, sand-cast bronze-backed bearings did not operate satisfactorily when subjected to high cyclic loads. The introduction of centrifugally cast bronze for that purpose made it possible to use successfully bronze-backed bearings for heavy-duty application. This paper describes the performance and the salient points of manufacture of centrifugally cast bronze-backed bearings. Comparison of the sand-cast and of centrifugally cast bronzes are discussed and the advantages of the latter are mentioned. Methods of rational casting of bearing-back-bronze material are also discussed in detail and steps for the improvement of their physical properties are indicated.

Introduction

THIS paper describes briefly the occurrences of bronze-backed bearing failures due to the inherent weakness of the sand-cast bronze material. Pertinent high points of centrifugal-casting technique of heavy-duty Diesel-engine bronze bearings are mentioned and comparison is made of the physical properties of these two materials. It is shown that centrifugally cast bronze is considerably superior to the sand-cast bronze because of fine and homogeneous grain structure which results in high physical properties. This permits its use in heavy-duty bearing applications.

The paper also indicates a number of improvements in the casting technique which will make the manufacture of such bearings more rational and economical.

Operation of Heavy-Duty Diesel-Engine Bearings

Connecting-rod bearings of modern Diesel engines operate under heavy-duty conditions because of high cyclic loads, producing sometimes pressures in excess of 3000 psi on the bearing projected area (1, 2, 3).[2] The loading of such bearings depends upon the interrelation of all acting forces which are plotted in Fig. 1, showing diagrammatically an elementary crank mechanism. It is seen that there are three sources of loading, as follows:

F_p = force due to gas pressure
F_{rec} = inertia force of the reciprocating masses
F_{cen} = centrifugal force due to rotating masses

The sketch in Fig. 1 is for a two-cycle engine, and the three forces given are for the 45-deg position of the crank. It is realized that the first two forces, the gas and the inertia forces, vary, whereas the third force, the centrifugal, remains constant for any operating speed. The vectorial summation of these three forces for the 45-deg position is indicated by F_{res}. The interrelation of these forces for all positions of the crank is of great importance because it is possible to determine the maximum resultant force, or perhaps several resultant forces of high magnitude, together with their directions; the latter indicates at what position of the upper or of the lower bearing shell the high-intensity forces are acting.

The gas force in an internal-combustion engine depends on the compression ratio and, of course, on the position of the piston; this force reaches its maximum value near the end of the compression and the beginning of the expansion strokes, usually a few degrees past the top dead center. The gas force acts downward and is directly transmitted by the connecting rod to its bearing. (The force along the connecting rod is equal to the gas force acting downward, divided by the cosine of the angle formed by the vertical and the connecting-rod center line.)

The inertia force is equal to the mass of the reciprocating parts times the acceleration; therefore this force depends on the speed of rotation of the crank and the l/r ratio (where l is the length of the connecting rod and r is crank radius). This force is largest where the piston speed is zero, i.e., at the top and bottom dead centers. At the beginning of the power stroke the inertia force is acting opposite to the gas force; then it gradually diminishes and slightly before one half of the stroke, it changes sign and acts in the same direction as the gas force, increasing numerically toward the bottom dead center. The mass of the reciprocating parts is usually composed of the following weights: Piston, piston pin and bushing, compression and oil rings, and one third of the connecting rod.

The centrifugal forces are equal to the mass of the rotating parts times the angular acceleration and are, therefore, different for the main and the connecting-rod bearings. These forces for the connecting rod depend on the weights of the two connecting-rod bearings and two thirds of the connecting-rod weight. This force acts radially along the crankshaft crank and is constant for a given engine speed.

All these three types of forces may be computed by the use of formulas indicated in Fig. 1. It is evident from this figure that the resultant connecting-rod-bearing force will be obtained by geometrical summation of the centrifugal force, as one component, with the sum of the gas and inertia force as the other component. The resultant force so obtained is defined as to its magnitude and its direction; besides, the position of the crank angle at these conditions is also known (45 deg for the case shown in Fig. 1). The procedure of so evaluating the connecting-rod-bearing resultant force is repeated for all positions of the crank at intervals of 10 or 15 deg. One revolution (or 360 deg) is considered for a two-cycle engine and 2 revolutions (or 720 deg) for a four-cycle engine. If the resultant forces so constructed were indicated as vectors acting at the bearing center, and if their end points were connected, a polar diagram of the bearing loads would be obtained. Such a polar diagram indicates at a glance the magnitude of the

[1] Professor of Mechanical Engineering, University of California. Mem. ASME.

[2] Numbers in parentheses refer to the Bibliography at the end of the paper.

Contributed by the Oil and Gas Power Division and presented at the Annual Meeting, New York, N. Y., November 26–December 1, 1950, of The American Society of Mechanical Engineers.

 Manuscript received at ASME Headquarters, September 18, 1950. Paper No. 50—A-106.

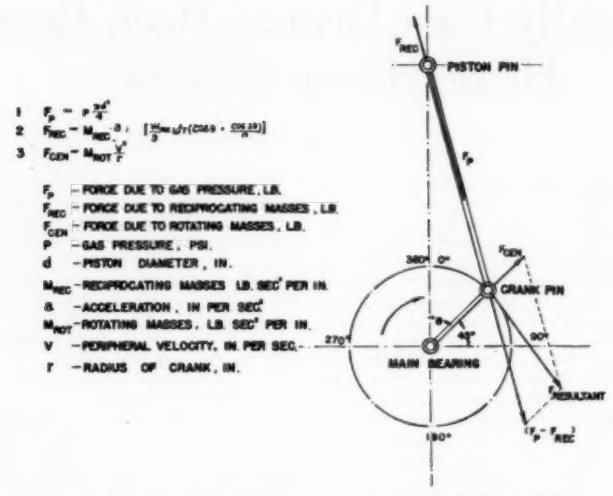

Fig. 1 Forces on Connecting-Rod Bearing at 45-Deg Crank Angle

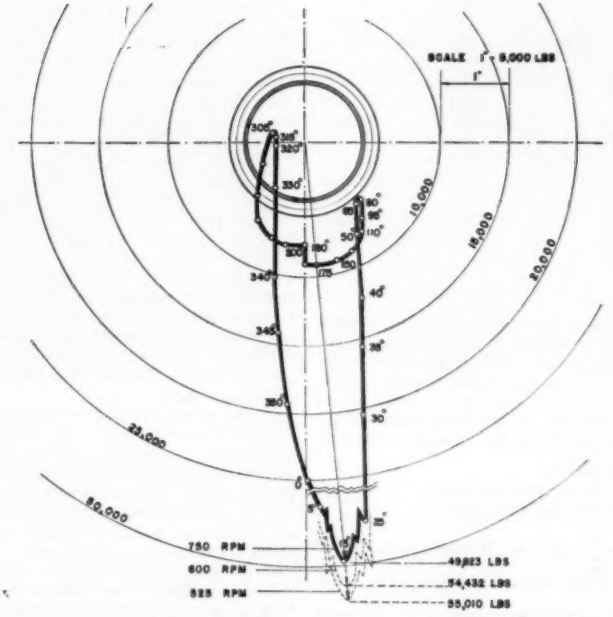

Fig. 2 Polar Diagram of a Connecting-Rod Bearing; Two-Cycle Diesel Engine

load at any position of the upper or of the lower bearing half, together with the respective crank angle. Thus Fig. 2 shows a polar diagram constructed for a heavy-duty two-cycle Diesel engine operating at 750 rpm. It is interesting to note (this may be easily understood by following the procedure of constructing a polar diagram with the help of the sketch shown in Fig. 1) that slight decrease in engine speed might increase the bearing load. Two such conditions are indicated by dotted lines in Fig. 2. (4).

Fig. 2 at once shows the high magnitude of a nearly vertical force which acts downward and which imposes high stresses on the upper shell of the connecting-rod bearing. The peak force at the rated speed of 750 rpm is close to 50,000 lb which results in a pressure of approximately 3000 psi on the bearing projected area. Such excessive loading caused bearing failures of bronze-backed bearings. A typical example of such failure is represented in Fig. 3 where extrusion of the weak bronze back into the connecting-rod oilhole took place (1, 4). No similar failure occurred when steel-backed bearings were used, because of the high modulus of elasticity of the steel back. Attention was then directed to the improvement of standard bearing bronze which is highly desirable as a bearing-back material because of easy machining (no grinding is necessary of the OD) and because of easy long-term storage (no corrosion of the bronze back). A marked improvement was achieved by casting bronze bearing shells centrifugally instead of using the old method of sand casting. Because of this, centrifugally cast bronze-back bearings may be used successfully for all encountered heavy-duty applications.

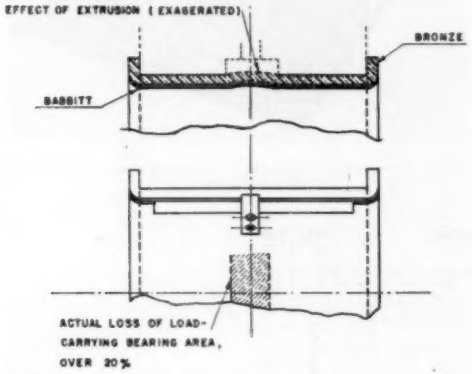

FIG. 3 EXTRUSION OF DEFECTIVE BRONZE BEARING BACK INTO CONNECTING-ROD OIL GROOVE

METHODS OF CENTRIFUGAL-CASTING BRONZE BEARING SHELLS

Most of the Diesel-engine bearings with bronze backs are manufactured with the Navy "M" bronze (U. S. Navy 46B8, Federal QQ-B-691a, Composition 1). Other bronzes such as SAE 65 and SAE 620 are sometimes also used. Chemical and physical properties of these three bronzes are tabulated in Fig. 4. Hardness for centrifugally cast bronzes for bearing backs should be minimum 55 Bhn (500 kg) for Navy "M" and minimum 35 Rockwell number for SAE 65 and SAE 620. Different hardness scales are used on account of different characters of these bronzes, the SAE 65 and SAE 620 being solid solutions, while the Navy "M" is an alloy where lead might be locally segregated.

Because of special requirements imposed by the heavy-duty performance, new specifications have been prepared which include progressive tests made at different predetermined stations during the centrifugal-casting process as well as during the manufacture of bearings. For example, it is required to break some castings and a few unfinished and finished bearing halves in order to ascertain by visual examination the soundness of the bronze.

Centrifugal castings may be spun on vertical, horizontal, and inclined casting machines (5, 6). A casting for one bearing shell (for two bearing halves) can be obtained on a vertical machine, such as shown in Fig. 5,[3] while a casting for several bearing shells may be obtained on a horizontal machine, such as shown in Fig. 6.[4] Such and similar centrifugal-casting machines were used successfully for manufacturing large numbers of castings varying in sizes from approximately 4 in. OD, to approximately 12 in. OD.

A good and sound casting will be obtained when such variables as spinning speeds, casting temperatures, rate and amount of pour are determined properly (2, 7). Besides, experience may indicate the desirability of different methods in line with personal experience which may vary considerably. In addition to these obvious methods of casting bearing shells satisfactorily, it became

[3] The illustration was supplied by Mr. G. W. Bingham of the Centrifugal Machine and Engineering Company, Kalamazoo, Mich.

[4] The illustration was supplied by Mr. Nathan Janco of the Centrifugal Casting Machine Company, Tulsa, Okla.

	CU	Sn	Zn	Pb	Fe MAX	Ni MAX	Ph MAX	AL MAX	TENS. STR'GTH PSI	ELONGATION %
NAVY M	86-91	5.5-6.5	1.5-5	1-2	0.15	1.0	0.05	—	34,000	22
SAE 65	88-90	10-12	0.5*	0.5*	0.15	TR*	.1-.3	.005	35,000	10
SAE 620	88-89	7.5-9	3-5	0.3	0.15	1.0	—	—	40,000	20

* TOTAL LEAD, ZINC, NICKEL 1.0% MAX

SUB-SIZE TEST SPECIMEN

SIZE IN INCHES

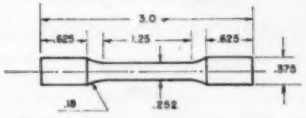

FIG. 4 SPECIFICATIONS OF BRONZES

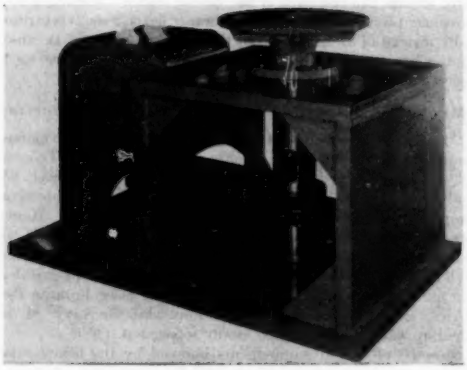

FIG. 5 VERTICAL CENTRIFUGAL MACHINE USED FOR BRONZE BEARING CASTINGS

imperative to decrease the amount of waste material usually formed on the inside of a centrifugally cast shell, and to select long-life mold materials.

Typical molds or dies for centrifugally casting bronze bearing shells may be of the type shown in Fig. 7. Dies mounted on vertical machines are made of suitable high-grade steel or of special cast-alloy materials. The molten bronze is poured vertically and is held in the mold by a clamped cover. Sometimes permanent carbon molds are used in horizontal machines; such molds are inserted into the spinning tube and the molten bronze is held by two side covers provided with orifices for side pouring Fig. 7.

The required periodical tests of centrifugally cast bronze shells chosen at random from one or two heats consist of visual examination of the fracture. The examination of the fracture may indicate such easily detectable defects as axial stratification, coarse

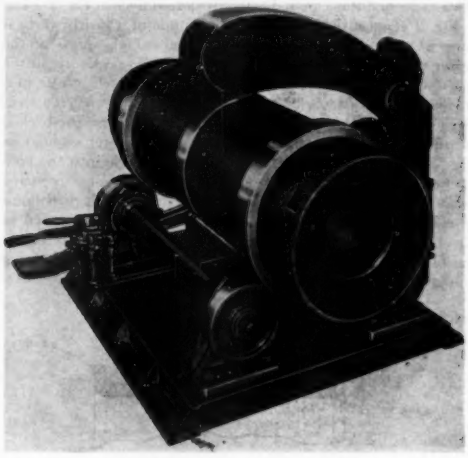

FIG. 6 HORIZONTAL CENTRIFUGAL MACHINE USED FOR BRONZE BEARING CASTINGS

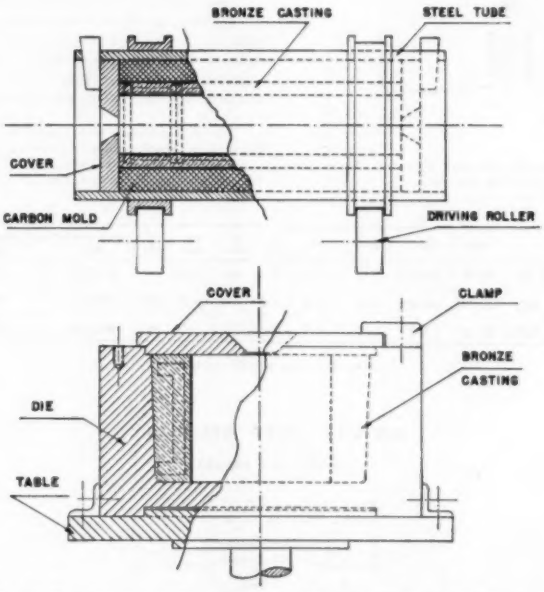

FIG. 7 HORIZONTAL AND VERTICAL MOLDS USED FOR CASTING CENTRIFUGALLY BRONZE BEARING SHELLS

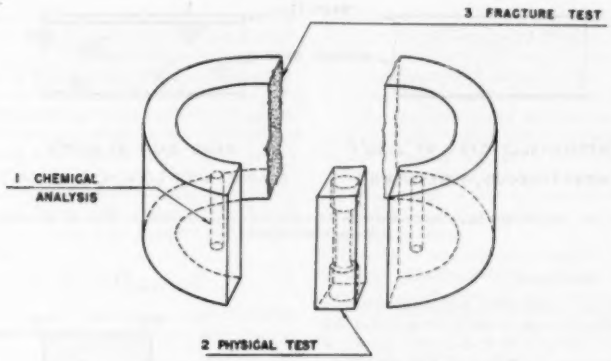

FIG. 8 TEST OF CENTRIFUGALLY CAST BRONZE BEARING SHELL

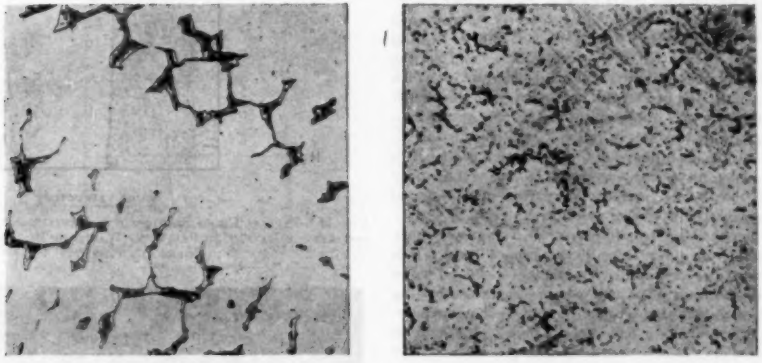

Sand cast — Centrifugally cast

FIG. 9 PHOTOMICROGRAPHS OF SAND AND CENTRIFUGALLY CAST BRONZE; CAST AT 2150 F; SAE 620 BRONZE; ×100

and heterogeneous structure, excessive porosity, especially on the inside diameter, and radial gas holes, which are frequently on the outside diameter of the casting. If these defects are found and are beyond prescribed limits, all castings from the corresponding heat are rejected. Castings which reveal positive fracture test are then tested further for chemical composition and for physical properties. If all these tests are positive, i.e., the centrifugal casting meets the required specifications, all the shells of the representative heats are released for manufacture of bearings.

The method for these tests is as follows: A blank for the physical test is cut from a casting which was selected for the fracture test. The fracture test is then made and, if positive, chips are secured for the chemical test and a test specimen machined from the blank. This procedure is schematically represented in Fig. 8.

Since many centrifugal castings are short, subsize test specimens are used for the determination of the tensile strength and the elongation, Fig. 4.[5]

The advantages of centrifugally cast bearing-back bronzes over similar ones cast in sand (static casting) are numerous. It has been shown that for the case of the widely used Navy "M" bronze, the tensile strength of a centrifugal casting is 17.7 per cent above that of the sand casting; similarly, the per cent of elongation increase amounted to 54 per cent (2, 7). Satisfactory centrifugally cast bronzes should have fine grain size and their structure must be homogeneous, without any sign of porosity. Localized porosity is practically always encountered in sand-cast bearing bronze; it is of interest to note that hydraulic test will show positive results of such sand-cast bronze which may contain a considerable amount of widely dispersed porosity. It can be stated that superior quality of centrifugally cast bronze is almost entirely due to controlled rapid solidification, which is an integral part of the centrifugal method of casting. The two photomicrographs taken at ×100 and shown in Fig. 9, reveal the marked difference between the coarse structure of the sand-cast bronze and the fine and homogeneous structure of the centrifugally cast bronze, both poured at the same temperature.

It is the author's opinion that the use of centrifugally cast bearing-back bronzes will increase and will ultimately spread into the field of medium and low-duty application, and will thus almost entirely eliminate the use of sand-cast bearing-back bronzes.

[5] General Specifications for Inspection of Material. Appendix II, Metals, Part A. Issued by the Navy Department, June 1, 1941.

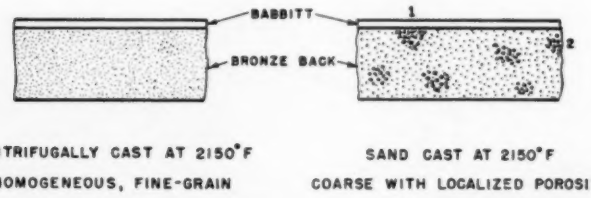

FIG. 10 SCHEMATIC REPRESENTATION OF SATISFACTORY AND DEFECTIVE BRONZE BEARING-BACK STRUCTURES

DISCUSSION

The description of the use, application, and manufacture of centrifugally cast bearing-back bronze as briefly presented in this paper would be incomplete without a short discussion in order to indicate rational and economical methods of casting such materials.

The desirablity of fine structure and homogeneity of the bronze back is necessary not only for the purpose of realizing high physical properties of the bronze material but also for securing a strong bond between the bronze surface and the bearing alloy. Bearing failures often have been attributed to "blistering" and peeling off of the thin layer of babbitt, an incipient case of which is schematically indicated in Fig. 10 (1). It is seen in this sketch that localized porosity of a sand-cast bronze may be on the babbitted surface (indicated by 1); in this case, the babbitt surface may be lifted during operation due to the trapped gases which expand at elevated temperatures; no similar trouble will occur on other parts of the bearing surfaces away from localized and totally enclosed porous areas (such as indicated by 2).

It is easily understood that periodical fracture tests are necessary during the manufacture of centrifugally cast bronze backs. It is realized that such tests are expensive because of increased waste material and of resulting wear and tear of centrifugal-casting machines. The question of great importance is how many bearing shells should be broken for such examination. This question is difficult to answer. It may be stated in a general way that minimum fracture tests will be required when carefully controlled conditions of centrifugal casting are rigorously maintained.

The examination of a fracture test will always reveal, as mentioned previously, porosity and coarse-grain structure on the inside diameter. They are due to excessive oxidation and low rate of solidification; the rate of solidification is high on the outside diameter, adjacent to the die material. The porous material will be removed during "rough-boring," the first manufacturing operation. The outside diameter is of fine-grain structure, but often small and medium-size gas holes may be found on that surface. The origin of these holes is mostly due to trapped water vapor which is formed when uneven and excessive amounts of mold wash are employed. In addition, the outside diameter may be rough, especially when old and partially cracked dies are still used. All such discontinuities and rough surfaces on the outside diameter are removed during "rough-turning," the second bearing manufacturing operation. Possible surface discontinuities also may be encountered on the top and on the bottom of the centrifugal castings. Therefore the sound structure for machining a good bearing such as schematically depicted in Fig. 11, will be found between two vertical lines, V_o and V_i, and two horizontal lines, H_b and H_t. A waste of over 50 per cent of the centrifugally cast bronze is a common occurrence, as indicated on that sketch. The cross sections of bearing backs, indicated by dotted lines in Fig. 7, are naturally in the region of sound bronze.

A gas hole, or radial crack, which was formed on the OD of a centrifugally cast Navy "M" bronze poured at 2150 F in an 8-in-diam steel mold, spinning at 750 rpm, is shown on a macrograph in Fig. 12. The structure of bronze is homogeneous and is fine except for the oxidized boundaries of the crack. Such casting will be rejected.

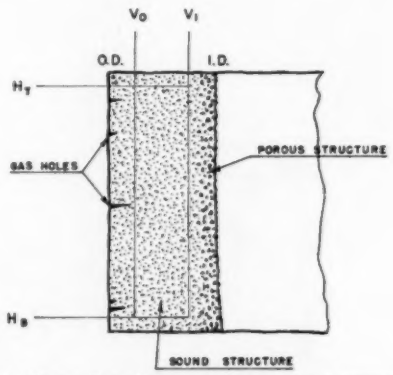

FIG. 11 TYPICAL CROSS SECTION OF CENTRIFUGAL CASTING SHOWING APPROXIMATELY 50 PER CENT WASTE OF BRONZE DUE TO GAS HOLES AND POROSITY

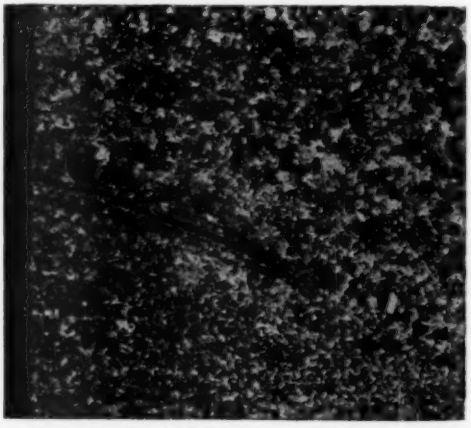

FIG. 12 RADIAL CRACK ON THE OD OF A CENTRIFUGAL CASTING; NAVY "M" BRONZE; ×6

Fracture tests reveal sometimes comparatively homogeneous structure with partially oxidized axial or longitudinal inside bands, such as sketched in Fig. 13. Macrophotographs of such dark bands are shown in Fig. 14 where, on the left macrophotograph, the band grain structure is considerably finer than on the right macrophotograph. Such conditions were sometimes encountered and were reproduced experimentally when the rate of pouring was changed, and when possible short-duration oxidation of a molten-bronze layer took place.

A macrophotograph of a good finished bearing is shown in Fig. 15. This photograph was taken from a section of a broken finished bearing picked at random after "inspection," the last manufacturing operation.

Conclusions and Recommendations

It has been shown that fine grain size and homogeneous structure are necessary for the bronze backs of heavy-duty bearings such as used in modern Diesel engines. The finer the grain structure the higher are the physical properties of the bronze; the same can be said with respect to the homogeneity. Only the centrifugal method of casting bronzes for bearing back produces a material possessing the required high physical properties.

It has also been shown that localized porosity of the bronze back may lead to ultimate bearing failure. The inside diameter of a centrifugally cast bronze is always porous. Such porosity penetrates to various depths and is removed by machining during the initial stages of bearing manufacture. It is evidently desirable to cast bronze shells under such conditions that will result in minimum porosity.

Because of all these requirements, centrifugally cast bronze shells are periodically broken for visual examination of the fracture. This will reveal to the inspector if the area of fine and homogeneous structure which will be left after rough-boring and rough-turning a casting will be sufficient for bearing manufacture.

For the purpose of economy, it is necessary to manufacture centrifugal castings with maximum sound material, i.e., minimum waste of defective bronze machined off on the four sides of a casting. Only well-controlled and rational methods of centrifugal casting will assure good product at reasonable cost.

The over-all efficiency of centrifugally casting bearing bronze back may be improved considerably if additional factors, which affect the manufacturing process, will be carefully considered, such as the following:

1 Temperature control should be as accurate as possible. Good pyrometers should be used; preferably not of the portable type because of easy damage. This also implies that molten metal should not be too long in the ladle where cooling rate is high.

2 Rate of pouring should be high and pouring should be continuous in order to prevent any incipient internal oxidation.

3 Pouring should be done in some inert atmosphere, such as

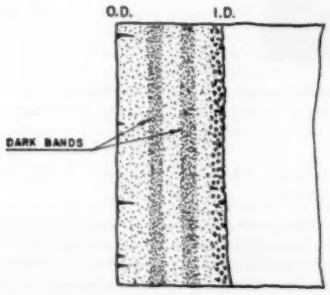

Fig. 13 Defective Centrifugal Casting Due to Localized Longitudinal Discoloration

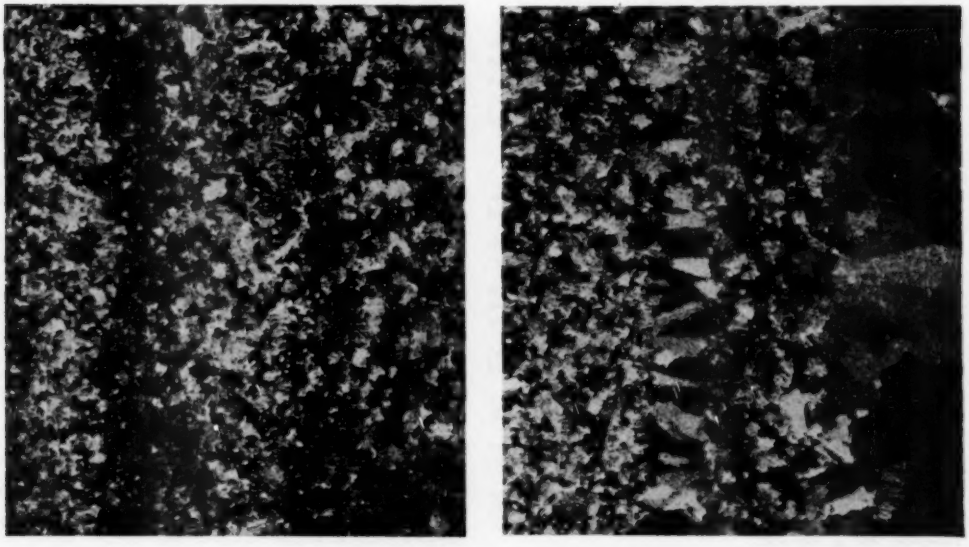

Fig. 14 Rejected Centrifugal Castings With Longitudinal Fine and Coarse-Grain Bands; Navy "M" Bronze; ×6

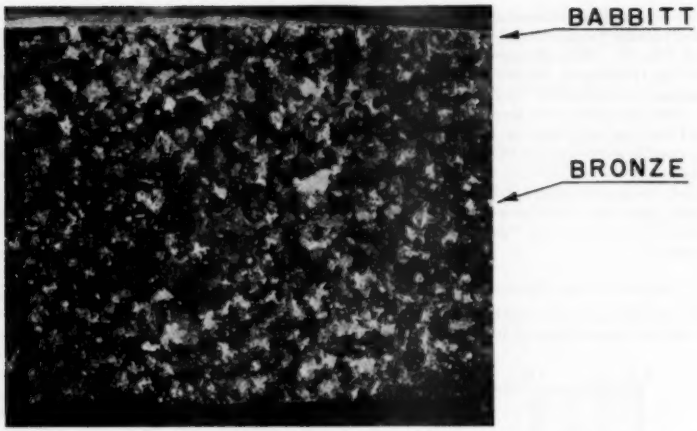

FIG. 15 MACROGRAPH OF CENTRIFUGALLY CAST FINISHED BEARING SECTION; NAVY "M" BRONZE; ×6

argon, in order to minimize or even eliminate porous bronze on the inside diameter; this would result in greatly reducing waste.

4 Suitable mold material should be developed to have a long life, i.e., the number of castings made should be substantially increased over the present limit which varies between 200 and 500, depending upon the die material and type of bronze poured.

5 Proper spraying, its technique and materials used for it, should be investigated also. This should be done in view of lengthening the mold life and also eliminating gas holes on the OD.

6 Rigid, sturdy, and reliable casting machines will secure continuous, economical, and safe operation.

ACKNOWLEDGMENT

Acknowledgment is due to Mr. J. F. Klement, Chief Metallurgist, Ampco Metal, Inc., Milwaukee, Wis., who prepared the photomicrographs shown in Fig. 9. Macrographs of test samples shown in Figs. 12, 13, 14, and 15, were made by Mr. R. C. Grassi, Assistant Professor of Mechanical Engineering, University of California.

BIBLIOGRAPHY

1 "Diesel Engine Bearings. Discussion of Failures and Progressive Inspection Methods," by L. M. Tichvinsky, *Mechanical Engineering*, vol. 67, 1945, pp. 297–308.

2 "Notes on Heavy-Duty Diesel Engine Bearings," by L. M. Tichvinsky, *Lubrication Engineering*, vol. 4, August, 1948, pp. 170–174.

3 "Basic Principles of Lubrication," by M. D. Hersey, Pre-Conference Lecture Course on "Lubrication," presented at the 20th National Oil and Gas Power Conference, May 19, 1948 (sponsored by the ASME), pp. 19–42.

4 Paper on "Diesel Engine Bearings," by L. M. Tichvinsky, presented at the meeting of the Baltimore Section of the Society of Automotive Engineers, February 10, 1944.

5 "Spinning Speeds of Centrifugal Casting Machines," by F. G. Carrington, Trans. American Foundrymen's Association, vol. 52, December, 1944, pp. 333–346.

6 "Eliminating Defects in Nonferrous Centrifugal Castings," by Nathan Janco, *The Foundry*, vol. 74, July, 1946, pp. 94–95 and 212–213.

7 "The Influence of the Centrifugal Process on the Physical Properties of Some Non-Ferrous Alloys," by W. W. Edens and J. F. Klement, Trans. American Foundrymen's Association, vol. 52, December, 1944, pp. 393–404.

Discussion

B. J. ESAREY.[8] The writer disagrees with the author on two points as follows:

1 Centrifugally cast bronze-back bearings for use in Diesel engines in Navy service were first made in 1941. Production quantities of lead-bronze centrifugal castings were made from that time on as reported in I. E. Cox's paper.[7] Properties of these and other alloys were given in a paper on bronze-back bearings in 1946.[8]

2 The control of centrifugally cast bearings has progressed to the point that it is not necessary to fracture any number of pieces. Normal test-bar procedures, in addition to chemical control, have eliminated the necessity for more than an occasional fracture.

All of the author's recommendations are necessary in the control production of good centrifugal castings.

AUTHOR'S CLOSURE

The author is in agreement with the points indicated by Mr. Esarey. In connection with the fracture test, however, it appears necessary to consider the interest of the manufacturer as well as the interest of the user of bronze-backed bearings. The manufacturer resents the expensive technique of fracture tests, while the purchaser of bearings wants to be sure of the satisfactory quality of the bronze material below the bearing lining, and, therefore, may insist on the continuance of these tests. It should be noted that during the mass production of bronze-backed bearings at the peak of the last war, bearing manufacturers, because of limited foundry facilities, were obtaining centrifugal castings by subcontracting. The author's experience indicates that more fracture tests were necessary of the subcontracted castings than of castings made by bearing manufacturers.

---

[8] Chief Engineer, National Bearing Division, American Brake Shoe Company, St. Louis, Mo.

[7] "The Centrifugal Casting of Non-Ferrous Metals," by I. E. Cox, Proceedings, American Foundrymen's Society, 1941.

[8] "Bronze Back Bearings," by B. J. Esarey, Sleeve Bearing Metals Lectures, American Society for Metals, 1946.

A Study of Head Loss in Venturi-Meter Diffuser Sections

By JOEL WARREN,[1] PROVIDENCE, R. I.

There has been considerable experimental and analytical work done, pertaining to diffuser action, both in this country and abroad. The research discussed in this paper was undertaken to furnish additional information with reference to the relative performance of various shapes of diffuser sections in Venturi tubes.

DATA presented in the paper indicate that the minimum per cent head loss for recovery cones in Venturi meters installed in 6-in. pipe lines depends upon both the cone angle and the ratio of cone entrance diameter to exit diameter (β). Concerning per cent head loss, cones with a small value of β seem to be quite sensitive to cone-angle change, whereas the per cent head loss changes a relatively small amount in cones with a large value of β as the cone angle is changed. In certain instances, shortening of recovery cones by cutting off small portions at the large end resulted in decreased per cent head loss when compared with full length cones of the same angle.

Test Program

All tests were made with water and were conducted at the hydraulic laboratory of Builders-Providence, Inc. Fig. 1 is a schematic sketch showing the initial test setup. However, due to excessive fluctuations at the manometer when data were being taken, the arrangement shown in Fig. 2 was constructed. Almost complete elimination of manometer fluctuations, especially at low flow conditions, and faster recording of data resulted in tests run on this system. The test equipment was designed originally so that investigations could be made concerning flow coefficients as well as head loss. All data reported were taken on the system shown in Fig. 2.

Fig. 3 is a schematic sketch of the special Venturi-meter test rig used in these tests. The test rig consisted of four sections; the inlet section, the approach section, the throat section, and the recovery section. Each of these sections could be changed independently of the other sections. The joining surfaces of any two adjacent sections were designed with rabbeted joints to a tolerance of ± 0.002 in. measured on a diameter.

The inlet section consisted of a flanged Meehanite casting with a honed bronze bushing at the downstream end through which pressure taps fed into an annular chamber, which, in turn, had openings in its outer wall which were connected to the manometer.

The approach sections were Meehanite castings, machined to templates of specified shapes as follows: $1^1/_2$ in. throat, reverse curve $4^7/_8$ in. long; 3 in. throat, uniform velocity head increase per unit length, $1^1/_2$ in. long; 4.5 in throat, same type $1^1/_2$ in. long. The inner surfaces of the approach sections were painted with two coats of spar varnish to retard rusting. The initial use

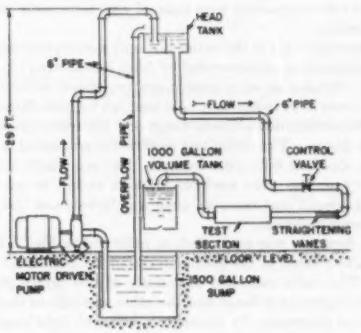

Fig. 1 Initial Arrangement of Test Equipment

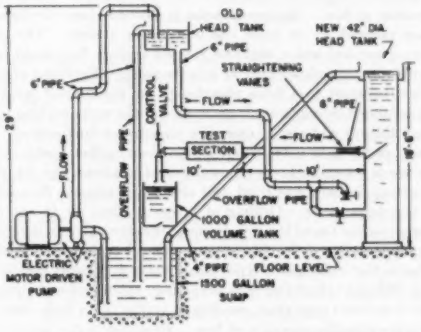

Fig. 2 Final Arrangement of Test Equipment

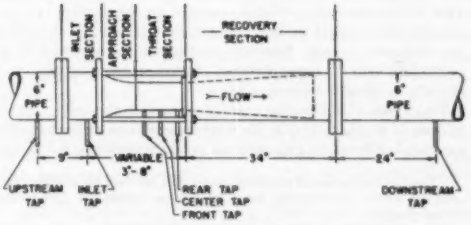

Fig. 3 Venturi Test Rig

[1] Assistant Professor of Mechanical Engineering, Brown University. Jun. ASME. Consultant to Builders-Providence Inc.

Contributed by the Fluid Meters Research Committee and presented at the Annual Meeting, New York, N. Y., November 26–December 1, 1950, of The American Society of Mechanical Engineers.

Note: Statements and opinions advanced in papers are to be understood as individual expressions of their authors and not those of the Society. Manuscript received at ASME Headquarters on September 12, 1950. Paper No. 50—A-65.

of bitumastic paint was discontinued due to excessive flaking of the paint.

The throat sections were Meehanite castings about $2^1/_2$ in. long with honed bronze liners and with pressure taps arranged in a manner similar to the inlet section.

The recovery section consisted of a flanged Meehanite casting of 6 in. ID, into which flanged diffuser or recovery cones[2] of varying shapes and cone angles could be inserted. All recovery cones and the recovery section were painted with bitumastic paint to retard rusting.

All pressure taps in the entire test unit were square-edged, carefully prepared as recommended by Allen and Hooper (1).[3]

The combination of approach section, throat section, and recovery cone to be tested were held together by bolts fitted between the inlet-section downstream flange and the recovery-section upstream flange. The entire test section was connected in the 6-in. line to standard 6-in. pipe flanges. The same inlet section and recovery section were used for all tests except in one instance when a special cast recovery cone was tested, and this replaced the recovery section.

The flow rate was controlled, as indicated in Fig. 2, by a control valve located at the discharge end of the horizontal flow system. The valve consisted essentially of two orifice plates, one fixed to a loose pipe flange and the other so designed that it could be moved externally, by means of a lever, at right angles to the fixed plate, and hence to the flow, thus permitting maximum flow when the two plates were in alignment and almost no flow, except that due to leakage, when the movable plate was at its extreme outer position. A downspout consisting of a wooden box, which surrounded the valve, was also fastened to the loose pipe flange. A deflector plate was installed in the box to aid in changing the direction of flow. Numerous holes in the box above the deflector plate allowed air to enter the downspout system. The entire downspout and valve could be rotated so that flow could be directed into the volume tank or into the sump. Early use of a gate valve, fastened to a loose pipe flange, at the control point was discontinued owing to the large weight of the valve making movement difficult and also to excessive manometer fluctuations. Location of the gate valve about 7 pipe diam further upstream and the use of a standard pipe elbow fastened to a loose pipe flange for diverting the flow was tried, but also gave excessive fluctuations at the manometer. Drilling of holes to allow air to enter the system on the top of the pipe leading from the valve to the diverting elbow reduced the fluctuations somewhat, but was much inferior to the orifice-plate-type control valve previously mentioned.

A 1000-gal cylindrical tank previously calibrated and equipped with a vertical gage glass, reading in tenths of an inch, was used for measuring the quantity of flow. Readings to the nearest 0.02 in. could be made by interpolation. One tenth of an inch on the gage glass was equivalent to 1.77 gal of water. A minimum of 350 gal per test run was established when actual measurement of flow quantity was necessary.

Flow time was measured by an electric timer which was actuated by two mercury switches mounted on the wooden box surrounding the control valve. The smallest division on the dial of the clock was $^1/_{10}$ sec; however, readings to the nearest 0.02 sec could be made by interpolation. A stop watch was used periodically to check the action of the unit.

Two types of differential gages were used in the tests. Heads of from 15 in. Hg to $1^1/_4$ in. Hg were measured on a direct-reading mercurial differential gage with an inside diameter of 0.5 in. and with a vulcanite float on top of the mercury. The smallest division on the scale was $^1/_{10}$ in. Heads below $1^1/_4$ in. Hg were measured on a 3-in. air-differential hook gage, equipped with a vernier scale which could be read directly to 0.01 in. water and interpolated to the nearest 0.005 in. of water. A number of readings of the manometer were taken and averaged at each flow rate.

All pressure connections were by means of transparent tubing, which was arranged so that any air in the leads would collect at a high point and be observed readily. In some of the testing, valves located in the manometer circuit made it possible to switch quickly from one pressure tap to another and from one manometer to another. However, the use of interconnecting valves was decreased as the tests progressed. The valves were replaced by unions which made possible changeable direct leads between the pressure taps and the connections to the manometers.

Test Results

Test methods and calculations concerning flow followed, in general, the procedure outlined in reference (2). However, the per cent heat loss was calculated as the ratio of the "local pressure loss" of the Venturi to the differential pressure. The total pressure loss was measured between the upstream and downstream taps located as shown in Fig. 3. Local pressure loss was determined by subtracting from the total pressure loss a calculated loss due to the straight portions of the test section, not including the throat and approach sections, using data from available tables on head loss in straight pipe (3). In instances where a single value of per cent head loss has been reported for each cone tested, this value is the minimum per cent head loss reached on a graph of per cent head loss versus differential pressure. Complete rechecks of data were made in a number of instances, and in all cases the original and the new data were well within accepted experimental limits.

Fig. 4 indicates that the minimum per cent head loss for recovery cones in Venturi meters installed in 6-in. nominal diam pipe

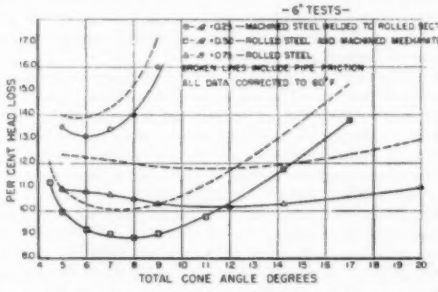

Fig. 4 Effect of Recovery Cone Angle on Per Cent Head Loss

lines depends upon both the cone angle and the value of β. Cones with a small value of β seem to be quite sensitive to cone-angle change. However, the per cent head loss of cones with a large value of β seems to be affected relatively little by changes in cone angle. There seems to be no reasonable explanation at this time as to why the lowest per cent head-loss points go through a minimum as the value of β is changed. An attempt was made to explain this fact by taking into consideration the variation in the approach coefficients as β is changed, but, whereas this helped between two cases, it worked in the wrong direction for the third.

Of considerable importance is the fact that the foregoing head-loss data are in disagreement with information published by Gibson (4, 5) who reported minimum per cent head loss for cones

[2] The nomenclature of recovery cones will be used to include those sections which are actually cones and those which are special machined shapes.

[3] Numbers in parentheses refer to the Bibliography at the end of the paper.

with numerous values of β as occurring at an angle of about 5° 30′. In addition, the general slopes of the per cent head-loss curves for different values of β were nearly the same up to total cone angles of 35°. The discrepancy with the data shown in Fig. 4 may be due to differently designed test equipment. Gibson inserted a test unit, similar to but shorter than that shown in Fig. 3, into a 2-in. pipe line. Hence flow into and out of the test section was always through a pipe of 2 in. diam, regardless of end diameters of the cone being tested. It is believed that such a design would result in poorer velocity distribution than the normal Venturi meter for throat diameters in the vicinity of the 2-in. pipe size. His experiments also were on machined brass sections with throat diameters of from 0.65 in. to 2.00 in. and with values of β from 0.30 to 0.67, thus being on generally smaller pipe sizes and covering a smaller range in β.

Beckman (6) has indicated that a truncated[4] conical diffuser of greater than 8° total angle and with a β of 0.5 gives equal or less per cent head loss than the longer Herschel-type recovery cone. Fig. 5 shows the effect on per cent head loss of truncating an 8° rolled-steel recovery cone. In this instance, in which $\beta = 0.5$, truncating was found to produce an increase in per cent head loss when compared to the full-length 8° cone. In these tests, truncating was accomplished by cutting off successively given lengths of the original cone at its downstream end, which left this end of the cone submerged in water. The welding of a full-diameter collar on the downstream end had no measurable effect on per cent head loss in the instances tried.

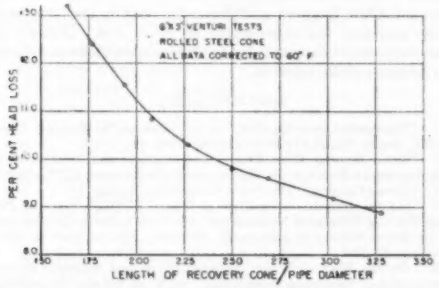

Fig. 5 Effect on Head Loss of Truncating an 8° Recovery Cone

Fig. 6 shows that for large angles of 6-in. × 3-in. recovery cones, truncating did result in a smaller per cent head loss. However, the per cent head loss was, in all instances tested, larger than the minimum found in Fig. 4 for the 6-in. × 3-in. cones. Except for the 8° cone, truncating was accomplished by making one cut in length on each of the cones of the different angles reported. It is realized that truncating in each instance by a series of steps would be more desirable; however, in support of the data shown in Fig. 6, the data in Fig. 5 indicate that the per cent head loss may change at a fairly uniform rate when changes are made near the original length. Hence it is believed that Fig. 6 may be representative of the general trend for the cone angles reported.

Fig. 7 indicates that for a given length of recovery cone, there may be a certain cone angle that will give a minimum per cent head loss. Truncated cones of 1.37 D and 1.88 D in length and of about 13° and 11° total angle, respectively, show smaller per cent head loss than full length cones of the same indicated lengths.

[4] "Truncated" as used here and later indicates that a portion of the large end of the recovery cone has been cut off.

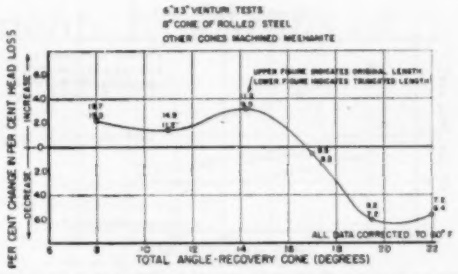

Fig. 6 Per Cent Change in Per Cent Head Loss Per Inch Decrease in Length

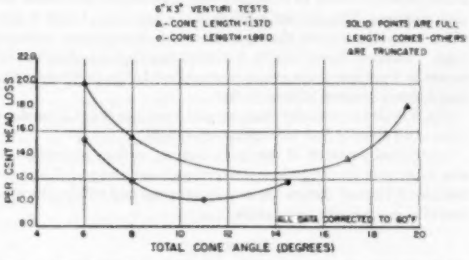

Fig. 7 Per Cent Head Loss of Cones of Same Length But With Different Cone Angles

Three large angle diffusers, each 0.78 diam long, with $\beta = 0.5$ and with curved walls instead of cones, were tested. A circular curve gave 30.5 per cent head loss, an elliptical curve, 27.2 per cent, and a curved surface designed to give a uniform decrease in velocity head per unit length of diffuser, the smallest head loss or 25 per cent. Gibson (4) recommends that for best conditions the curvature should begin gradually leaving the throat and should end with a straight line. The elliptical section reported had the most gradual curvature leaving the throat, but did not give the lowest head loss. Apparently, separation of the fluid from the wall surface is less with the uniform velocity-head decrease curve than with the others of the same length tested. However, regardless of the shape, recovery cones with total angles greater than 30° gave excessive manometer fluctuations.

The results reported in Fig. 4 indicated that a total cone angle of about 8° would give minimum per cent head loss for cases where $\beta = 0.5$. Since the cones used were of rolled steel and hence had quite smooth wall surfaces, a comparison test was run on a cast Meehanite 8° total angle cone in which the wall surface was left unmachined but was coated with bituminastic paint. The cast section replaced the entire recovery section in Fig. 3. Fig. 8 indicates that the cast cone had but slightly higher per cent head loss, especially at conditions of relatively large flow rate. Since the coating of the approach section with grease during additional testing gave some effect on the flow coefficient, tests were run on a number of cones to determine the effect of grease on head loss. As noted in Fig. 8, the addition of light grease, wiped off to a thin coating with a piece of cloth, caused an increase in per cent head loss, with the greater effect produced on the smoother rolled-steel type of cone.

Additional tests of like nature on other cones produced similar results. Tests on a straight length of 6-in. pipe with a distance of

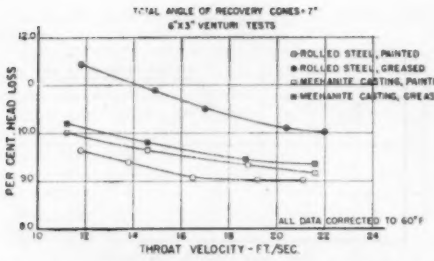

FIG. 8 EFFECT OF SURFACE CONDITION ON PER CENT OF HEAD LOSS

6.6 pipe diam between pressure taps indicated that the addition of a thin layer of grease to straight rough pipe tends to increase the pipe friction. The greased portion of the pipe was at least 1 pipe diam away from both the upstream and downstream pressure taps. Based on these results, it is probable that the observed increase in head loss when grease was applied to the recovery cones was due to increased friction to flow.

Fig. 8 is also a reminder that per cent head loss is not a constant ratio at all rates of flow for a given cone angle.

Additional research of the same nature as that reported and also some new investigations concerning head loss and flow coefficients of Venturi meters are now in progress and will be the subject of a report in the near future.

SUMMARY

1 The minimum per cent head loss for recovery cones in Venturi meters installed in 6-in. pipe lines depends upon both the cone angle and the ratio of the cone entrance diameter to exit diameter (β). Table 1 shows the cone angle at which the minimum per cent head loss occurred for different values of β.

TABLE 1 CONE ANGLE FOR MINIMUM PER CENT HEAD LOSS

β	Approx total cone angle, deg-min	Minimum per cent head loss
0.25	6–15	13.1
0.50	8–0	8.9
0.75	11–30	10.2

In addition, cones with a small value of β are quite sensitive to change in cone angle, whereas for large values of β a change in cone angle causes a much smaller change in per cent head loss.

2 Truncating of conical diffusers may result in decreased or increased per cent head loss dependent upon the cone angle, the prospects for decreased loss seeming to be greater at large values of cone angle.

3 At a cone length of 1.37 diameters when $\beta = 0.5$, a truncated cone of about 13° total angle gave minimum per cent head loss. Likewise, a truncated cone 1.88 D long and of about 11° total angle gave minimum per cent head loss. In both instances, full-length cones of the lengths indicated gave higher per cent head losses. Thus for certain lengths of recovery cones including truncated cones there is a certain cone angle that will give minimum per cent head loss.

4 Diffusers of curved walls instead of cones, but of the same length, can be expected to give different per cent head loss, with a uniform velocity-head decrease per unit pipe length of curved section, giving the minimum per cent head loss of those tested.

5 Unmachined cast 6-in. × 3-in. Meehanite cones may, in the vicinity of 8° total cone angle, be expected to give but slightly higher per cent head loss than smooth-surfaced rolled-steel cones of the same total angle.

6 Grease on the walls of certain recovery cones tends to increase the per cent head loss.

ACKNOWLEDGMENT

Sincere thanks are due Builders-Providence, Inc., for permission to present the results of the research done in their laboratories.

The author also wishes to acknowledge the many valuable suggestions and assistance given by Mr. Irving O. Miner, Vice-President and Chief Engineer of Builders-Providence, Inc., who originally proposed the experiments on head loss. Grateful acknowledgment is also extended to all who gave assistance during the progress of the research.

BIBLIOGRAPHY

1 "Piezometer Investigation," by C. Allen and L. Hooper, Trans. ASME, paper No. HYD-54-1, vol. 54, 1932, pp. 1–16.

2 "Fluid Meters, Their Theory and Applications," published by The AMERICAN SOCIETY OF MECHANICAL ENGINEERS, 1937 edition.

3 "Crane Catalog," The Crane Company, Chicago, Ill.

4 "On the Resistance to Flow of Water Through Pipes or Passages Having Divergent Boundaries," by A. H. Gibson, Transactions of the Royal Society of Edinburgh, Scotland, vol. 48, part 1, 1911–1912, pp. 97–116.

5 "On the Flow of Water Through Pipes and Passages Having Converging or Diverging Boundaries," by A. H. Gibson, Proceedings of The Royal Society of London, series A, vol. 83, May, 1910, pp. 366–378.

6 "The Proportions of Venturi Meters," by William Beckman, *Engineering*, vol. 140, November, 1935, pp. 489–490.

Discharge Measurements by Means of Venturi Tubes

By A. L. JORISSEN,[1] STATE COLLEGE, PA.

An attempt is made to present a comprehensive idea of the actual stage of development of the method of flow measurement by means of Venturi tubes. Use has been made here of (a) the latest available American and European Standards, published by the various national associations: The American Society of Mechanical Engineers, 1937; Ente nazionale per l'Unificazione nell' Industria, 1938; British Standards Institution, 1943; Verein deutscher Ingenieure, 1948; Association francaise de Normalisation, 1949. (b) The decisions taken at the international meetings of the Committees on Flow Measurement: ISA 30, Helsinki, 1939; ISO 30, Paris, 1948. (c) Published research reports. Both the nozzle-type and the Herschel-type Venturi are discussed from the viewpoints of discharge coefficient and pressure losses. The conclusions point out the need of further research and the necessity of an international standardization.

Nomenclature

The following nomenclature is used in the paper:

- D = diameter of the pipe
- A_1 = area of cross section of pipe
- d = diameter of throat section
- A_2 = area of throat section
- $m = \frac{A_2}{A_1} = \left(\frac{d}{D}\right)^2$ = opening ratio.[2]
- z_1 = elevation of center line of pipe at upstream pressure connection
- z_2 = elevation of center line of pipe at downstream pressure connection
- e = length of cylindrical throat section
- φ = angle of opening of diffuser
- a, b = cross-sectional dimensions of an annular pressure chamber
- s = thickness of slot connecting an annular pressure chamber to inside of pipe
- p_1 = pressure at standard upstream pressure connection
- p_2 = pressure at standard downstream pressure connection (throat)
- Q = volumetric rate of flow
- G = weight rate of flow
- w = specific weight of fluid
- w_0 = specific weight of fluid in undisturbed conditions (compressible fluids)
- T = temperature (absolute)
- g = acceleration of gravity
- k = adiabatic exponent
- V_1 = mean velocity in pipe
- V_2 = mean velocity in throat section
- α_1 = correction coefficient for nonuniform velocity distribution in pipe section
- α_2 = correction coefficient for nonuniform velocity distribution in throat section
- $(\mathrm{Re})_d$ = Reynolds number referred to throat diameter
- $(\mathrm{Re})_D$ = Reynolds number referred to pipe diameter
- C = discharge coefficient
- K_L = pressure-loss coefficient in converging portion
- α = discharge coefficient in old standards and publications
- J = roughness-effect coefficient
- ϵ = compressibility coefficient
- Δh = differential pressure of Venturi
- $\Delta' h$ = local Venturi loss
- λ = pressure-loss coefficient
- K = pressure-loss coefficient in Ferroglio's formula

Introduction

Since Clemens Herschel suggested, in 1887, making use of a long-known principle for a new type of flow-measuring device, much work has been done on Venturi tubes, both in this country and abroad.

American practice is codified in the publications of this Society (1, 2, 3).[3] Considerable work has been done in the last 40 years by Ledoux (26), Pardoe (30, 31, 32, 33, 34, 35), Stevens (47) and others. The ASME Special Research Committee on Fluid Meters has been very active in this field.

Pioneering work in Europe was done by Camichel in Toulouse, France (11, 12, 13), and by Schlag in Liége, Belgium (38, 39, 40). In 1932, at a meeting held in Milan, Italy, the Committee on Fluid Measurement of the International Federation of the National Standardizing Associations (ISA 30) pointed out the interest of systematic experimental research on Venturis. In the years preceding the second world war, numerous studies were undertaken, particularly in Belgium, France, Germany, Great Britain, and Italy, and results were published, susceptible of being used for a contemplated standardization. In 1938 the Italian Ente nazionale per l'Unificazione nell' Industria (UNI) submitted a project to a public inquiry (4), and this project served as a basis for discussion at the Helsinki, 1939, meeting of the ISA 30 Committee. It was at this meeting that, for the first time, international rules were established for flow measurements with Venturi tubes.

These rules were included in the standards of the Association française de Normalisation (5) and of the Verein deutscher Ingenieure (6). Finally, in May, 1948, the subject of Venturi tubes was one of the most important topics discussed at the Paris meeting of the Committee on Flow Measurement of the International Organization for Standardization (ISO 30). The latest published standards are the new standards of the Association française de Normalisation (8).

---

[1] Professor of Civil Engineering, The Pennsylvania State College. Mem. ASME.

[2] The author uses the European notation. In this country, the parameter $\beta = \left(\frac{d}{D}\right)$ is generally preferred ($m = \beta^2$).

Contributed by the Fluid Meters Research Committee and presented at the Annual Meeting, New York, N. Y., November 26–December 1, 1950, of The American Society of Mechanical Engineers.

Note: Statements and opinions advanced in papers are to be understood as individual expressions of their authors and not those of the Society. Manuscript received at ASME Headquarters, September 11, 1950. Paper No. 50—A-71.

[3] Numbers in parentheses refer to the Bibliography at the end of the paper.

The Venturi tubes belong in the category of the so-called pressure-difference devices for fluid-flow measurement in pipes. Like the orifices and the nozzles, they are based on the principle that, when the fluid is made to flow through a section of a diameter smaller than that of the pipe, the increase in kinetic energy is compensated by a decrease in pressure. By measuring the differential pressure thus obtained, one may evaluate the velocity and hence the rate of flow.

Essentially, a Venturi tube consists of the following:

1 A converging portion where the transformation of pressure into kinetic energy takes place. This is the essential part of the pressure-difference device. According to the shape of this portion, Venturi tubes are classified into:

(*a*) Herschel type, also called conical-entrance type or classical type, in which the entrance portion is a converging-entrance cone.

(*b*) ISA nozzle type in which the entrance portion consists of a standard ISA 32 nozzle.

2 A cylindrical throat section.

3 A divergent diffuser. This is the characteristic part of the Venturi tube. Its adjunction to the converging portion allows a partial recuperation into pressure energy of the kinetic energy existing in the throat section. This recuperation is progressive and is best effected when the eddying zone is small in the decelerating portion. The optimum value of the divergent angle is from 5 to 7 deg.

When the diameter of the downstream section of the diffuser is smaller than the diameter of the pipe, the Venturi is said to be truncated; when the two diameters are equal, the Venturi is nontruncated. Distinction is thus made between the following:

Venturi truncated with a divergent angle of 5 to 7 deg.
Venturi truncated with a divergent angle exceeding 7 deg.
Venturi nontruncated with a divergent angle of 5 to 7 deg.
Venturi nontruncated with a divergent angle exceeding 7 deg.

The following theoretical formula is readily derived from Bernoulli's equation and the equation of continuity for the case of incompressible fluids

$$V_2 = \frac{1}{\sqrt{\alpha_2 - \alpha_1 m^2 + K_L}} \sqrt{2g\left[\left(z_1 + \frac{p_1}{w}\right) - \left(z_2 + \frac{p_2}{w}\right)\right]} \quad \ldots\ldots [1]$$

This may be written

$$V_2 = \frac{C}{\sqrt{1 - m^2}} \sqrt{2g\left[\left(z_1 + \frac{p_1}{w}\right) - \left(z_2 + \frac{p_2}{w}\right)\right]} \ldots [2]$$

and the volumetric rate of flow is expressed by

$$Q = \frac{CA_2}{\sqrt{1 - m^2}} \sqrt{2g\left[\left(z_1 + \frac{p_1}{w}\right) - \left(z_2 + \frac{p_2}{w}\right)\right]} \ldots [3]$$

The so-called "coefficient of discharge" C makes allowance for frictional effects in the entrance cone or nozzle and nonuniform velocity distribution in the measuring sections.[4] The relation between C and K_L is easily found to be

$$C = \sqrt{\frac{1 - m^2}{\alpha_2\left(1 - \frac{\alpha_1}{\alpha_2}\right)m^2 + K_L}} \quad \ldots\ldots [4]$$

[4] In many older standards and publications, the coefficient of discharge is called α. The relation between C and α is $\alpha = \frac{C}{\sqrt{1 - m^2}}$.

Allowance also must be made for a possible roughness effect. Finally, the volumetric rate of flow is given by

$$Q = \frac{CJA_2}{\sqrt{1 - m^2}} \sqrt{2g\left[\left(z_1 + \frac{p_1}{w}\right) - \left(z_2 + \frac{p_2}{w}\right)\right]} \ldots [5]$$

When the fluid may not be considered as incompressible, an additional correction takes the compressibility effects into consideration. The weight rate of flow for compressible fluids is expressed by

$$G = \frac{C\,J\epsilon A_2}{\sqrt{1 - m^2}} \sqrt{2g(p_1 - p_2)\,w_0} \quad \ldots\ldots [6]$$

From Equation [4] it is evident that C is a function of m and, through α_1, α_2, and K_L, of the Reynolds number. At high Reynolds numbers, however, viscous effects are negligible and C is a function of the opening ratio m, only. The values of C are obtained experimentally. The roughness coefficient J, is also of an experimental nature and is found to be a function both of m and of D, increasing with increasing m and decreasing D. Finally, the expansion coefficient ϵ may be shown to be a function of m, p_2/p_1, and the adiabatic exponent k.

Tolerances and Errors

From Equations [5] and [6] it is seen that the value of Q or of G results from measurements of the geometric characteristics of the device and of the pressure difference $p_1 - p_2$ and from a knowledge of the physical characteristics of the fluid. The various standards give values of the tolerances and errors to be applied but much uncertainty still remains concerning the exact definition of these errors. At its Paris, 1948, meeting, the ISO 30 Committee was very much concerned with the establishment of definite rules, based upon the theory of probabilities. It appears to the author that tolerances and errors are best studied in the new French standards (8) and an attempt is made here to summarize this theory.

Errors have to be considered four times in the determination of the rate of flow with standard pressure-difference devices:

(*a*) A measurement is generally repeated several times; therefore, instead of one value of the pressure-difference associated with one group of data defining experimental conditions, one has a number of values of the pressure-difference and a number of corresponding data. The true values to be introduced in the formulas are the arithmetic means of the various characteristics. The difference is taken between each measurement and the true value. The mean quadratic error is the square root of the arithmetic mean of the squares of these differences.

(*b*) Measuring conditions themselves are uncertain; therefore, errors may result in the values of the physical constants and of the geometric characteristics of the device. Here again, the root-mean-square error is taken. Measurements of d, and, therefore, computation of A_2 generally may be made with a high degree of accuracy. The diameter of the pipe D, may not be so easy to determine; measurements are generally made of four diameters inclined at 45 deg, and the arithmetic mean computed. A common practice is to place a machined pipe section upstream from the device. The specific weight is known accurately for liquids, the admissible error being generally less than 1 per cent. For gases and vapors, w depends upon pressure and temperature. Pressure measurements are made with laboratory manometers with an accuracy of 0.5 per cent; with industrial manometers, a value of 1 per cent is common. According to Schlag, an accuracy of 0.5 per cent may be assumed for the measurement of the

temperature, whereas the law relating w, p, and T is exact within an approximation of about 0.7 per cent.[5]

(*c*) Coefficients such as C, J, and ϵ result from laboratory experiments and bear a certain degree of uncertainty. The various standards give the admissible tolerances, based on an analysis of the available experimental results. Concerning the coefficient of discharge, a so-called "basic tolerance" is given, but no precise definition of this expression is available. The new French Standards use again the notion of root-mean-square error. According to the theory, there is a probability of 5 per cent that the actual error will be equal to twice the root-mean-square error. Because it was not possible to recalculate older experiments, it was assumed that the basic tolerance and the root-mean-square error were the same.

(*d*) Errors in the measuring instruments must also be taken into consideration, but generally these do not obey the laws of probabilities. It can be expected that these errors will be smaller in laboratory experiments than in industrial practice. In the latter case, the over-all tolerance is generally increased by 50 per cent of its value, computed by taking the root mean square of all tolerances.

The ISO 30 Committee recommended that the various standards no longer use terms such as error, approximation, tolerance, without giving them a precise definition and that, in future experiments, the root-mean-square error be always given.

It appears that in this country, the probable error is preferred by some.

Nozzle-Type Venturi Tubes

As explained, a nozzle-type Venturi consists of a standard ISA 32 nozzle, followed by a cylindrical throat and a diffuser. Fig. 1 shows the principal characteristics of this device and makes apparent the essential differences between this type of Venturi tube and the standard nozzle. It will be noticed that, whereas in the latter, the downstream pressure hole is located on the downstream face of the nozzle, in the Venturi, it is situated in the throat, immediately following the nozzle profile and preceding the cylindrical section.

To the knowledge of the author, the first systematic study of this type of Venturi tube was made by Schlag (38). The early experiments (40) dealt with nozzle Venturis having no cylindrical throat section ($c = 0$). It appeared later that a cylindrical section of length between $0.2d$ and $0.4d$ was advantageous. In various publications, Schlag (38, 40) and Schlag and Jorissen (44) give results of nozzle-Venturi calibrations effected between the years 1934 and 1947. Their results are summarized in Table 1 which shows that, for all values of $c \geq 0.2d$, the differences between the Venturi and the nozzle coefficients are well below 1 per cent. The International Recommendations allow an approximation for the nozzle coefficients of between 1 per cent at small values of m and 1.7 per cent at high values of m. It thus appears that for $c \geq 0.2d$, the difference between the coefficients of the nozzle Venturi and the standard nozzle is well within the tolerated approximation.

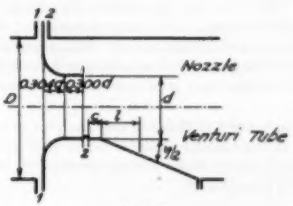

Fig. 1

When c is smaller than $0.2d$, greater deviations may be expected, principally, as remarked by Witte (49), when the angle of opening of the diffuser is great.

The results of Schlag and Jorissen are confirmed by experiments by Wentzell and Groessle (48) with values of m between 0.05 and 0.58, $c = 0.2d$, and pipe diameters up to 275 mm (10.8 in.).

Ruppel (37), however, found that the Venturi coefficients were smaller than the nozzle coefficients for $m \leq 0.3$ and larger for $m > 0.3$. Except for one value of m ($m = 0.57$), however, the differences are well within the tolerated approximations.

Ferroglio (14, 15, 16) experimented with $c = 0.296d$, $D = 80$ mm (3.2 in.), $\varphi = 7$ deg and $m = 0.1$, 0.3 and 0.5, He concluded that, for all values of m, greater coefficients were needed for the Venturi than for the nozzle. The UNI standards (4), recommended that slightly higher values be chosen for the Venturi than for the nozzle and the ISA Recommendations (Helsinki 1939) endorsed this viewpoint. Nozzle Venturis were thus standardized for use with liquids only and diameters D between 50 mm (2 in.) and 500 mm (20 in.) (41, 42, 43). (Table 2).

The Helsinki Recommendations further stipulate that the angle of opening of the diffuser may not be greater than 60 deg and that, in the case of a truncated Venturi, the length of the diffuser may not be smaller than d (42).

The upstream pressure connection is made through an annular chamber or individual bores; the diameter of these bores or the width of the slot, connecting the chamber with the inside of the pipe, may not be greater than $0.02D$. The downstream or throat

[5] These figures are given for average practice; it is certain that in laboratory experiments a much greater accuracy can be obtained.

TABLE 1 NOZZLE-VENTURI COMBINATIONS

D Millimeters	D Inches	m	$\frac{c}{d}$	$\frac{\varphi}{2}$ deg-min	C Venturi	C Nozzle	$\frac{C \text{ Venturi} - C \text{ Nozzle}}{C \text{ Venturi}}$ per cent
50	1.97	0.16	0	4-16	0.980	0.982	−0.2
100	3.94	0.16	0	2-50	0.982	0.982	0
50	1.97	0.25	0	2-55	0.975	0.975	0
100	3.94	0.25	0.1	5	0.962	0.975	−1.3
100	3.94	0.25	0.1	10	0.959	0.975	−1.6
100	3.94	0.25	0.2	5	0.977	0.975	+0.2
100	3.94	0.25	0.2	10	0.971	0.975	−0.4
100	3.94	0.25	0.3	5	0.969	0.975	−0.6
100	3.94	0.25	0.3	10	0.974	0.975	−0.1
100	3.94	0.25	0.4	5	0.973	0.975	−0.2
100	3.94	0.25	0.4	10	0.974	0.975	−0.1
100	3.94	0.26	0	2-50	0.974	0.974	0
50	1.97	0.36	0	1-53	0.959	0.961	−0.2
100	3.94	0.36	0	2-50	0.961	0.961	0
100	3.94	0.36	0.2	2-50	0.953	0.961	−0.8
50	1.97	0.49	0	1-15	0.965	0.939	+2.7
100	3.94	0.49	0	2-50	0.935	0.939	−0.4
100	3.94	0.49	0.2	2-50	0.946	0.939	+0.7

TABLE 2 NOZZLE-VENTURI COEFFICIENTS[a]

m	0.05	0.10	0.20	0.25	0.30	0.35	0.40	0.45	0.50	0.60
C_{Nozz}	0.986	0.984	0.979	0.975	0.970	0.964	0.956	0.947	0.936	0.914
C_{Ventu}	0.986	0.985	0.981	0.978	0.973	0.968	0.960	0.953	0.948	0.924

[a] These values are included in the German standards of 1948 (6).

pressure connection is by means of bores, preferably connected to an annular chamber. The diameter of these bores may not be greater than $0.13d$ and must be between 3 and 6 mm ($^1/_8$ and $^1/_4$ in.). The slot was prohibited, the committee judging that there could be danger of a faulty centering of the upstream and downstream parts of the device. Schlag and Jorissen (44) succeeded in avoiding this by an appropriate construction of their Venturis and obtained very good results with a pressure-connection slot.

It was recommended at Helsinki that the area of the meridian cross section of the annular chamber be at least as large as the area of the total section of the passage between the chamber and the inside of the pipe (Fig. 2)

$$a\,b > \pi\,D\,e$$

This rule was adopted after study of a paper by Beckmann (10) on pressure-balancing in annular chambers. For large values of D, however, this requires unusually large chambers. Furthermore, the author has shown (24) that when the device is well centered, the width of the pressure slots is of little importance. The ISO 30 Committee finally decided at the Paris meeting that when D is greater than 200 mm (8 in.), it is enough that the cross section of the annular chamber satisfy the relation

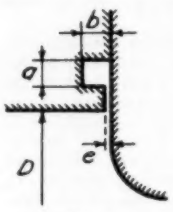

Fig. 2

$$a\,b > \frac{1}{2}\,\pi\,D\,e$$

Even at Helsinki, the advisability of choosing different coefficients for the Venturi and for the nozzle was questioned. The British Standard Code of 1943 (7), recommends the use of the same coefficients for the two devices. Schlag has shown (45) that the differences in the Helsinki coefficients are always well within the admissible approximation. Furthermore, it appears that Ferroglio's experiments were not decisive in this matter; for $m = 0.1$, sufficiently high Reynolds numbers were not attained for the discharge coefficient to be a constant; for $m = 0.30$ the value of C appears to be 0.973 whereas the corresponding value for standard nozzles is 0.970 (a difference of 0.3 per cent). Finally, for $m = 0.50$—to which corresponds a nozzle coefficient of 0.936—two Venturis were studied, one of them nontruncated, the other one truncated. The average value of C for the first one is estimated, from Ferroglio's diagram, at 0.948 (a difference of 1.3 per cent). For the truncated Venturi, the results are not as definite, but the average value of C may be estimated at 0.940 (a difference of 0.4 per cent).

As shown by Schlag, (45), Ferroglio's additional results on large-diameter industrial pipes (16) are too unreliable to be taken into consideration. Furthermore, they were all obtained with Venturis having small values of c/d. Ferroglio's analysis of Witte's measurements of pressure distribution downstream from a standard nozzle and the computation of the discharge coefficient of a Venturi by that method must also be questioned, due to the essential difference between the flow conditions in the diffuser of the Venturi and in the eddy-creating expansion downstream from the nozzle.

It appears to the author, therefore, that the decision of Helsinki was hasty and based on insufficient experimental evidence. At the Paris meeting (1948), the ISO 30 Committee decided that, temporarily, the same coefficients should be used for the nozzle Venturis and for the standard nozzles, but that the length of the throat section should be maintained between $0.2d$ and $0.4d$. The necessity of additional experiments was stressed.

The values of C adopted at the Paris meeting and endorsed by the new French Standards (8) are given in Fig. 3 and Table 3. These values differ only slightly from those of the British

TABLE 3 VALUES OF C

m	C	m	C
0.05	0.986	0.35	0.964
0.10	0.984	0.40	0.956
0.15	0.982	0.45	0.947
0.20	0.979	0.50	0.936
0.25	0.975	0.55	0.925
0.30	0.970	...	...

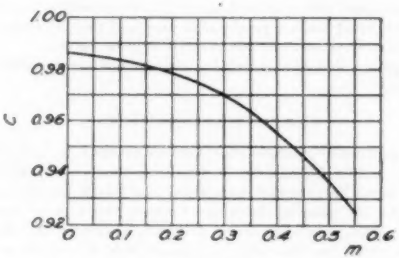

Fig. 3

Standard Code (7). They apply, naturally, only to high Reynolds numbers. According to the French Standards, the limiting values of Re are as given in Table 4.

TABLE 4 LIMITING VALUES OF REYNOLDS NUMBER[a]

m	$(Re)_D$	$(Re)_d$
0.05	60000	268000
0.10	63000	199000
0.20	90000	201000
0.30	120000	219000
0.40	165000	261000
≥ 0.50	200000	283000

[a] In the French Standards (8), as in most European standards and publications, Reynolds number is expressed as a function of the pipe diameter D. The relation between this Reynolds number and the Reynolds number expressed in function of the throat diameter d may be written $(Re)_D = (Re)_d\sqrt{m}$. This, however, is only approximately true in the case of compressible fluids.

It is recommended not to use the nozzle Venturi at smaller Reynolds numbers; if this cannot be avoided, viscous effects must be taken into consideration, and a correction factor must be applied to the value of C. Fig. 4 gives the correction factors found in the British Standards (7). Corresponding factors, expressed as functions of $(Re)_D$ are given in the French Standards (8).

The roughness coefficient J, has equivalent values in both standards. These are given on the diagram, Fig. 5.

Neither the International Recommendations, nor the French Standards (8) extend the use of the nozzle Venturis to incompressible fluids. The German standards (6) specify that, although all

experimental results have been obtained with liquids, there is no apparent reason to prevent using these results for vapors and gases. The British Standard Code (7) adopts the values of the

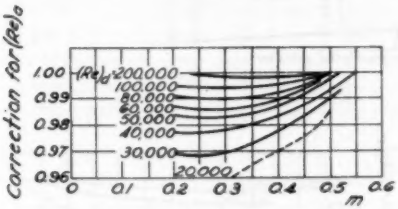

FIG. 4

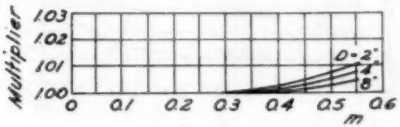

FIG. 5

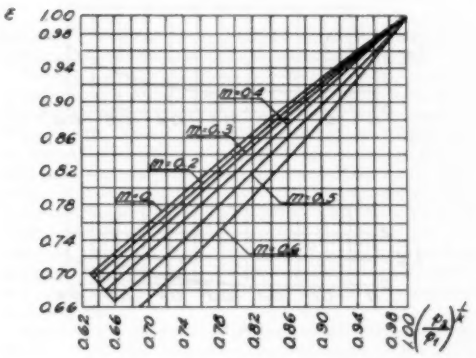

FIG. 6

expansion coefficients for nozzles. Fig. 6 allows computation of these coefficients. Restrictions are made for the case where $p_2/p_1 < 0.98$.

Figs. 7, 8, and 9 give the values of the basic tolerance as established by the International Recommendations and of the extra tolerances for $(Re)_d$ (viscous effects) and for D (roughness effects) from the British Standard Code (7). In the French Standards (8), the basic tolerance varies from 1 per cent for $m = 0.1$ to 1.7 per cent for $m = 0.65$. The extra tolerances for viscosity and roughness effects are very nearly the same as those of the British Standards (7). The roughness coefficients, however, may be considered as only temporary values and it is highly desirable that new experiments be undertaken to study the effects of roughness.

According to the British standards (7), an additional tolerance must be applied in the case of compressible fluids; this is due to uncertainties in the knowledge of ϵ. This extra tolerance is equal to $^1/_3$ the percentage correction in the case of gases, and $^1/_4$ the percentage correction in the case of vapors.

HERSCHEL-TYPE VENTURI TUBES

Herschel-type Venturi tubes are not yet standardized internationally, but they are included both in the British Standards (7) and in the French Standards (8). According to these stand-

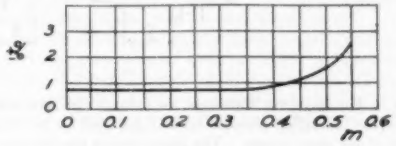

FIG. 7

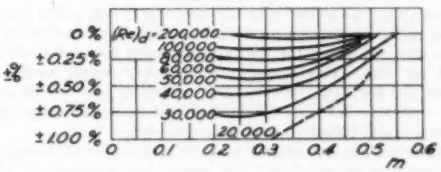

FIG. 8

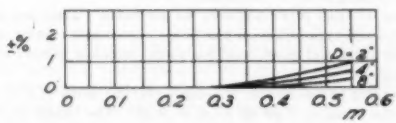

FIG. 9

ards, a Herschel-type Venturi, as represented in Fig. 10, consists of the following:

An entrance cone of 21 deg angle.
A cylindrical throat section of length d.
A diffuser of angle φ, generally equal to 7 deg.

The angle of 21 deg for the entrance cone is chosen both in the British and the French standards. Experiments have indicated a considerable variation of the coefficient of discharge with different angles. Schlag and Jorissen (44) have shown that this coefficient increases by approximately 1 per cent when the angle increases from 12 to 15 deg. It is therefore essential that the standard angle of 21 deg be maintained when the standard coefficients are used. Fig. 10 points to the existence of transition curves both at the entrance and exit of the entrance cone. The radius of these curves is not given in the standards. Schlag has shown (39) that an exit transition curve increases the coefficient of discharge by 1 to 1.5 per cent and gives a sharper variation with Reynolds number.

If a relatively high pressure loss may be tolerated, the angle φ of the diffuser may be greater than 7 deg, but never greater than 30 deg.

The same distinction between truncated and nontruncated devices applies as for other Venturis.

The upstream pressure connection is situated at a distance $D/2$ upstream from the entrance cone, and the downstream pressure connection is at the middle of the throat section. A common practice is to use annular chambers with a machined stainless lining. The diameter of the pressure holes in this lining must not be smaller than 4 mm ($^5/_{32}$ in.) and the number of holes at least 4. Distance between two holes may not be greater than 160 mm

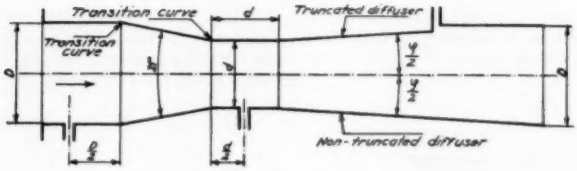

FIG. 10

(6.3 in.). For very large diameters, the annular chambers may be replaced by individual pressure holes distributed on the circumference of one cross section. The lining insures smooth entrance and throat sections. The influence of roughness in the entrance cone is very marked. Schlag has proved (38) that, by proper machining of a cast-iron entrance cone of $m = 0.26$ and $D = 100$ mm (4 in.), the coefficient of discharge could be increased by 1 per cent. Rust, on the contrary, decreased the coefficient by 1.5 per cent. This is confirmed by experimental results of Camichel and Teissié Solier (12) on a Venturi of $m = 0.25$ and $D = 80$ mm (3.15 in.). Rust decreased the coefficient of discharge of this Venturi by more than 2 per cent.

Herschel-type Venturis are now standardized for all diameters greater than 50 mm (2 in.), and values of m ranging from 0.15 to 0.60 according to the French standards (8) and from 0.10 to 0.55 according to the British standards (7).

These Venturi tubes are used for all fluids. They are made of a material appropriate to this fluid; cast iron for water, sheet iron for water and gases, steel for vapor, stainless metal for corroding gases.

According to the British standards (7), the value of C is constant and equal to 0.99 up to $m = 0.50$. The values of J are given in Fig. 11. The French standards (8) give slightly different values of C and J. These differences were discussed at the Paris meeting of the ISO 30 Committee. Slight differences in the values of CJ result from the use of both standards. The French standards do not give any limiting value of Reynolds number; according to the British standards, this is slightly above 100,000. For smaller Reynolds numbers, corrections are necessary; they are given in Fig. 12. The same values of ϵ may be used as for nozzle Venturis.

The basic tolerance and the additional roughness tolerance (diameter effect) result from Figs. 13 and 14, taken from the

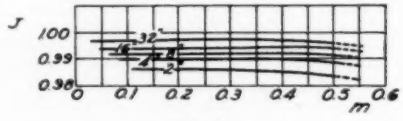

FIG. 11

British Standards (7). Slightly different results are obtained from the use of the French Standards (8). These state that, in the horizontal portion of the curve, the basic tolerance is 0.5 per cent for $D > 500$ mm (20 in.) and 1 per cent for $D < 500$ mm. In the nonhorizontal portion, the basic tolerance is 1.5 per cent. Extra tolerances are applied for Reynolds numbers below the limiting value, Fig. 15. The same tolerance on ϵ is taken as for nozzle Venturis.

Diffuser

As stated previously, the conical diffuser is the characteristic part of the Venturi tube. It allows a substantial part of the differential pressure to be regained. In the first Venturi tubes,

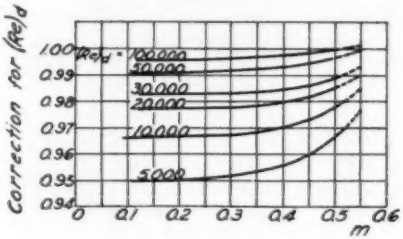

FIG. 12

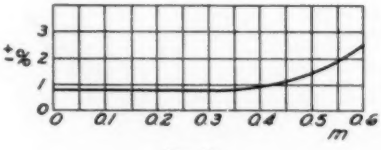

FIG. 13

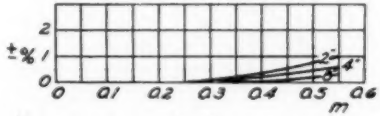

FIG. 14

built according to the specifications given by Herschel, the total angle of opening of the diffuser was from 5 to 7 deg. This small value led to fairly long devices. For a long time, diffusers were built with an angle not exceeding 8 deg. The choice of such a small value was justified by the necessity of maintaining low losses in the transformation of kinetic into pressure energy. These losses are principally due to the eddies that are created when the flow separates from the wall in the diffuser. Frictional and internal losses must also be considered; these losses being proportional to the square of the velocity, are greater in a small-angle than in a large-angle diffuser. Ruppel has shown (37) that a balance may be attained between the various losses, giving optimum conditions and a minimum loss. It was recommended at Helsinki that the total angle of the diffuser not exceed 30 deg.

A few years before the war, German manufacturers suggested cutting the diffuser at a downstream diameter smaller than the diameter of the pipe. According to the terminology of the Paris meeting, this is the truncated Venturi, Fig. 10. Beckmann has shown (9) that such a truncated diffuser may allow the same amount of recuperation as a nontruncated type. This is also confirmed by some of Ruppel's experiments (37). The truncated diffuser is, of course, more advantageous both for space and

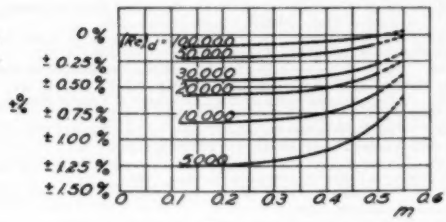

FIG. 15

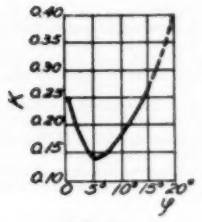

FIG. 16

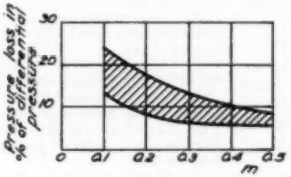

FIG. 17

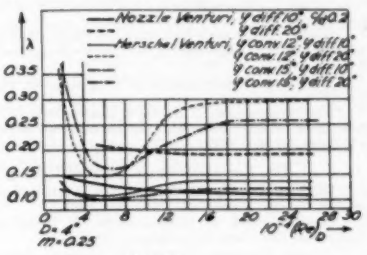

FIG. 18

economy. The length of the standard truncated diffuser, however, may not be smaller than the throat diameter d.

The rating of various diffusers is largely dependent on the residual pressure loss of the Venturi. This quantity is defined differently in the German (6) and in the Italian publications (4). In Germany, a differential pressure is measured between piezometer openings situated at a distance D upstream from the upstream standardized pressure connection and a distance of 7, 6, or 4 times D downstream from the downstream standardized pressure connection for $m = 0.1$, 0.25, or 0.50, respectively, for truncated Venturis, and D downstream from the Venturi for nontruncated Venturis. The ratio of the differential pressure thus obtained to the differential pressure between the two standardized connections is conventionally called "ratio of permanent head loss."

It seems more rational to adopt the method recommended by Marchetti (28) and Ferroglio (15). The pressure difference is measured between a section situated upstream and a section downstream from the Venturi. These sections are chosen far away from the device, so that its disturbing influence is not felt and normal flow conditions may be expected to prevail. From this differential pressure is subtracted the friction loss in a pipe of diameter D and length equal to the distance between the two sections. The difference is called "local Venturi loss," $\Delta' h$. This loss is generally expressed, not in absolute value, but by its ratio to the differential pressure Δh of the Venturi

$$\lambda = \frac{\Delta' h}{\Delta h}$$

The Venturi pressure loss is a function of Reynolds number; according to Marchetti (28), its value is

$$\left[0.052 - 0.25\, m^2 + \frac{1.25}{(\mathrm{Re})_D^{0.25}}\right]\left(\frac{1}{m^2} - 1\right)\frac{V_1^2}{2g}$$

for diffusers of 7 deg opening. Ferroglio (15) suggests using the formula

$$\left[0.02\left(\frac{1}{m^2} - 1\right) + K\left(\frac{1}{m} - 1\right)^2\right]\frac{V_1^2}{2g}$$

which is somewhat less accurate than Marchetti's but may be applied to diffusers of from 5 to 14-deg opening. This formula was endorsed at Helsinki. The coefficient K is given by Fig. 16.

Both Marchetti's and Ferroglio's formulas are for nontruncated Venturis; for truncated Venturis, the Recommendations of Helsinki give the diagram, Fig. 17, which allows an approximate computation of the pressure loss as a function of m.

In their experiments, Schlag and Jorissen (44) systematically measured the pressure loss and computed the pressure-loss coefficient. A typical diagram of λ as a function of Reynolds number is shown in Fig. 18. It appears that, whereas the angle of opening of the diffuser cone has little influence on the value of the coefficient of discharge, the pressure-loss coefficient λ, on the contrary, varies appreciably with this angle, increasing with increasing φ. In Herschel-type Venturis, the influence of the angle of the converging cone is small.

Conclusions

As appears from this report, considerable effort has been devoted to the study of Venturi tubes. Their standardization is now in progress. Although much information is still needed, it is certain that enough data are available to justify the attempts of the various national standardizing associations and of the ISO 30 Committee.

Concerning nozzle-type Venturis, experiments are in progress, to decide, once and for all, whether the same coefficients may be used for them as for the standard ISA nozzles. At the Paris meeting of the ISO 30 Committee, the delegations stressed the need for laboratories to continue experimental work on this subject.

The study of Herschel-type Venturis is also continued. It is expected that at the next meeting of the ISO 30 Committee, enough information will be available to lift the slight discrepancy between the British and the French standards.

The notions of tolerances and errors are well clarified; it is hoped that the analyses of future experiments will take the recommendations on this subject into consideration.

Remaining to be studied are the effect of transition curves in the entrance cone and the diffuser, as well as a comprehensive analysis of the effect of roughness. Flows at small Reynolds numbers are also of great interest.

Little information is at present available on measurements in pulsating flows or with heterogeneous fluids.

Acknowledgments

Figs. 4, 5, 7, 8, 9, 11, 12, 13, 14, and 15 are reproduced from Figs. 17 and 20 of B.S. 1042: 1943 "Code for Flow Measurement." They are included by permission of the British Standards Institution, 24/28 Victoria Street, London, S.W.1, who reserve all copyright.

Figs. 3, 6, and 10 are reproduced from Figs. 34, 42, and 51 in "Mesure des débits instantanés des fluides," with the kind permission of the Association française de Normalisation, 23 rue Notre Dame des Victoires, Paris, France, 2e.

BIBLIOGRAPHY

I National Standards

1 "Fluid Meters. Description of Meters," ASME Research Publication, 1931.

2 "Fluid Meters. Their Selection and Installation," ASME Research Publication, 1933.

3 "Fluid Meters. Their Theory and Application," ASME Research Publication, 1937.

4 "Venturimetri-unificati e relative regole per la misura di portata di liquidi," *Ente nazionale per l'Unificazione nell' Industria*, August, 1938.

5 "Régles unifiées pour la mesure des débits des fluides à l'aide de tubes de Venturi," *Association française de Normalisation*, March, 1939.

6 "VDI Durchflussmessregeln, DIN 1952," *Deutscher Ingenieur Verlag*, 1948.

7 "Flow Measurement," British Standard Code 1042, 1943.

8 "Mesure de débits instantanés des fluides," *Association française de Normalisation*, 1949.

II Publications on Venturi Tubes

9 "Die zweckmassige Gestaltung von Venturirohren," by W. Beckmann, *Gas und Wasserfach*, December, 1933.

10 "Druckausgleich in Ringkammern von Drosselgeräten," by W. Beckmann, *Forschung*, July–August, 1937.

11 "Tarages d'ajutages Venturi par jaugeage direct en regime permanent," by C. Camichel and M. Teissié Solier, *Association française de Normalisation*, May, 1939.

12 "Etudes d'ajutages Venturi de 80 m de grand diamètre par jaugeage direct a l'aval," by C. Camichel and M. Teissié Solier, *Association française de Normalisation*, May, 1939.

13 "Résultats obtenus dans les études d'ajutages Venturi effectuées aux laboratoires de Beauvert et de Toulouse," by C. Camichel and M. Teissié Solier, *Association française de Normalisation*, May, 1939.

14 "Ricerche sperimentali per la normalizzazione dei Venturimetri," by L. Ferroglio, *Ricerche di Ingegneria*, 1937.

15 "Per la normalizzazione dei Venturimetri," by L. Ferroglio, *Ente nazionale per l'Unificazione nell' Industria*, 1937.

16 "Sull' applicazione del Venturimetro unificato a grandi condotte," by L. Ferroglio, *L'Energia elettrica*, June, 1938.

17 "Sulla unificazione dei Venturimetri," by L. Ferroglio, *La Ricerche scientifica*, December, 1938.

18 "Per la unificazione dei methodi di misura della portata delle corrente fluide," by L. Ferroglio, *La Ricerche scientifica*, October, 1939.

19 "Prove su Venturimetri unificati ISA, Venturimetri con strozzatura 200/64," by L. Ferroglio, *La Ricerche scientifica*, July–August, 1940.

20 'Sul funzionamento idraulico del Venturimetro unificato ISA 30," by L. Ferroglio, *L'Energia elettrica*, December, 1940.

21 "Flow Through Standard Nozzles, Orifice Plates, and Venturi Tubes," by J. R. Finniecombe, *Engineering*, May 28, 1948.

22 "The Venturi Meter," by C. Herschel, Trans. ASCE, 1887–1888.

23 "The Measurement of the Flow of Gases and Liquids by Means of Orifices, Nozzles, and Venturi Tubes," by J. L. Hodgson, *World Engineering Congress*, Tokyo, Japan, 1929.

24 "Contribution a l'étude des pertes de charge continues dans les conduites circulaires," by A. L. Jorissen, *Bulletin du Centre d' Études des Constructions du Génie civil et d'Hydraulique appliquée de l'Université de Liége*, 1949.

25 "Mesure et régulation des débits gazeux," by H. Laplanche, *Mesures*, n°100, 101, 102, 103, 1945.

26 "Venturi Tube Characteristics," by Ledoux, Proceedings of the ASCE, December, 1927.

27 "Normung von Venturirohren zur Durchflussmessung," by H. Lohmann, *Zeitschrift des Vereines deutscher Ingenieure*, May, 1938.

28 "Venturimetri con convergente foggiato come il boccaglio unificato," by M. Marchetti, *L'Energia elettrica*, October, 1938.

29 "Beeinflussung der Anzeige von Venturimessern durch vorgeschaltete Krümmer," by H. Mueller, *Mitteilungen der Hydraulischen Institut der technischen Hochschule*, Munich, Germany, 1928.

30 "The Effect of Installation on the Coefficients of Venturi Meters," by W. S. Pardoe, Trans. ASME, vol. 58, 1936, p. 677.

31 "Effect of Installation on the Coefficients of Venturi Meters," by W. S. Pardoe, Trans. ASME, vol. 59, 1937, p. 750.

32 "Effect of High Temperatures and Pressures on Cast-Iron Venturi," by W. S. Pardoe, Trans. ASME, vol. 61, 1939, p. 247.

33 "Effect of Ambient Temperature on the Coefficients of Venturi Meters," by W. S. Pardoe, Trans. ASME, vol. 63, 1941, p. 457.

34 "Effect of Installation on the Coefficients of Venturi Meters," by W. S. Pardoe, Trans. ASME, vol. 65, 1943, p. 337.

35 "The Coefficient of Herschel-Type Cast-Iron Venturi Meters," by W. S. Pardoe, Trans. ASME, vol. 67, 1945, p. 339.

36 "La mesure des débits par Venturi classique," by R. Rousselet, *Chaleur et Industrie*, August–September, 1946.

37 "Vorarbeiten zur Normung der Venturi Rohre," by G. Ruppel, *Prüfen und Messen*, 1937.

38 "Influence de la forme et de la rugosité du convergent sur le coefficient de débit des tubes de Venturi," by Alb. Schlag, *Annales des Mines de France*, August, 1934.

39 "Expériences sur les tubes de Venturi avec convergent tronconique," by Alb. Schlag, *Revue générale de l'Hydraulique*, November–December, 1938.

40 "Expériénces sur les tubes de Venturi avec convergent en forme de tuyère normale," by Alb. Schlag, *Revue universelle des Mines*, January, 1939.

41 "L'état actuel de la normalisation des mesures de débits en conduites," by Alb. Schlag, *Standards*, n°8, 1939.

42 "Normalisation des mesures de débits par tubes de Venturi," by Alb. Schlag, *Revue universelle des Mines*, March, 1940.

43 "La mesure des débits par appareils à étranglement (Tuyères, diaphragmes et tubes de Venturi)," by Alb. Schlag, Descer, Liége, Belgium, 1943.

44 "Contribution à la normalisation des tubes de Venturi," by Alb. Schlag and Andre Jorissen, *Revue générale de l'Hydraulique*, January, February, March, April, 1947.

45 "Les appareils deprimogènes de mesure des débits: le coefficient de débit des Venturi à tuyère normalisée," by Alb. Schlag, Hommage de la Faculté des Sciences appliquées de l'Université de Liége a l'Association des Ingénieurs de Liége, 1947.

46 "Beeinflussung der Anzeige von Venturimessern durch kleine Abweichungen in der Düsenform," by J. Spangler, *Mitteilungen der Hydraulischen Institut der technischen Hochschule*, Munich, Germany, 1928.

47 "Simpler and Better Venturi Tube," by J. C. Stevens, *Engineering News Record*, April 29, 1948.

48 "Venturiwassermesser fur geschlossene Leitungen," by Wentzell and Groessle, *Wasserkraft und Wasserwirtschaft*, n°10–11, 1937.

49 "Untersuchungen zur Normung von Venturirohren," by R. Witte, *Forschung*, July–August, 1939.

Discussion

I. O. Miner.[6] This paper is a valuable addition to the science of flow measurement. The remarkable similarity shown between American and European coefficients is a monument to the researchers who established the coefficients and a source of confidence to those using these coefficients. An example of the similarity is Table 2, herewith, which compares Venturi tube coefficients published by the Society,[7] with corresponding British coefficients CJ from the author's paper.

TABLE 2 VENTURI TUBE COEFFICIENTS

BRITISH		ASME	
Size Venturi tube	CJ	Size Venturi tube	C
32" × 16"	0.9875	30" × 15"	0.9872
16" × 8"	0.984	16" × 8"	0.9854
8" × 4"	0.9817	8" × 4"	0.9828
4" × 2"	0.9801	4" × 2"	0.9800
2" × 1"	0.9758	2" × 1"	0.9764

The greatest difference, namely, 0.14 per cent in the case of the 16-in. Venturi tubes, is little more than the total of possible reading errors even when values are taken carefully from the curves.

The author's statement, "The optimum value of the divergent angle is from 5 to 7 deg," is correct for $m = 0.0625$ ($\beta = 0.25$).

[6] Chief Engineer, Charge Design, Builders-Providence, Inc., Rumford, R. I. Mem. ASME.

[7] "Fluid Meters, Their Theory and Application," ASME Research Publication, 1937.

Investigations by Warren[8] show that the optimum angle is 8 deg at $m = 0.25$ ($\beta = 0.5$) and about 12 deg at $m = 0.5625$ ($\beta = 0.75$). At the latter value of m there is negligible change in loss for a considerable change in diffuser angle.

The British Standards give the same basic tolerance for all sizes of Venturi tubes with $m = 0.3$ or less, the value being 0.75 per cent. The French Standards give larger tolerances for small Venturi tubes, the values being 1/2 per cent for tubes over 20-in. line size, and 1 per cent for tubes of less than 20-in-line size. The French method appears to fit the facts more accurately. Tests made at the University of Pennsylvania, the University of Illinois, and Ohio State University on 49 Builders Venturi tubes of the design to which ASME coefficients apply show that of 14 which were 6 in. or smaller, one had a coefficient differing from standard[9] by 1.4 per cent, five by from 1/2 to 1 per cent, and eight by less than 1/2 per cent. Of 35 for line sizes of 7 in. to 16 in., two deviated by 1/2 per cent to 1 per cent and the remainder by less than 1/2 per cent. Of more significance is the fact that between $\beta = 0.45$, and $\beta = 0.68$, which included 26 tubes, the maximum error for 6-in. size and under was still 1.4 per cent, while for the larger tubes it was 1/2 per cent. A further study including a larger number of tubes will probably indicate that the French method with the dividing line made at about 8-in. size will apply to American tubes. Tolerances for extreme β and low Reynolds numbers will also be required.

The author has focused attention on the fact that the French and British have established tolerances for Venturi tube coefficients based on line size, Reynolds number, and m. Reliable data in this country should be correlated, and additional tests made where required. Complete methods of determining possible errors in Venturi tube coefficients can then be published by the Society.

Author's Closure

The author is grateful to Mr. Miner for his comments. A complete analysis of all available American Venturi-tube calibrations, including comparison with the French and British Standards, is now in progress. The results of this analysis will be published at a later date.

[8] "A Study of Head Loss in Venturi Meter Diffuser Sections," by Joel Warren, ASME Preprint 50—A-65, 1950.

[9] Builders-Providence, Inc. standard coefficients are those published in Trans. ASME, vol. 67, 1945, pp. 339–344, "The Coefficients of Herschel Type Cast-Iron Venturi Meters," by W. S. Pardoe. These differ from those given in Table 2 by a maximum of 1/4 per cent.

Controller Settings for Optimum Control

By W. A. WOLFE,[1] VANCOUVER, B. C.

When a controller is applied to a process, one set of problems that arises is the dynamic action of the controller. Problems of speed of return, stability, and accuracy of control are all involved. In a paper by J. G. Ziegler and N. B. Nichols,[2] a method of adjusting a controller was described. This method introduced and used concepts of time lag and reaction rate to arrive at satisfactory settings for the controller. The purpose of this paper is to study the problem of optimum settings and to develop criteria for obtaining the settings. In particular, the Laplace transform will be applied to an idealized plant and the resulting equations solved for optimum conditions.

SEVERAL writers[2,3] have shown that a process consisting of multiple capacities may be represented by a dead time and an inflection-point tangent. Fig. 1 illustrates the assumed response of the process to a step disturbance. The response is

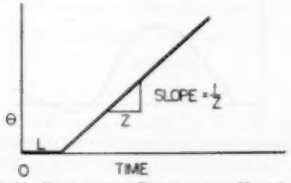

FIG. 1 IDEALIZED RESPONSE OF PROCESS TO A UNIT STEP DISTURBANCE, OCCURRING AT ZERO TIME

characterized by a delay or dead time of duration L, called the lag, and then a departure from the set value at a constant rate. The slope of the curve is equal to $1/Z$, where Z is the time required for the controlled variable to increase one unit. Such a process is termed "astatic with lag."

BLOCKING OUT THE SYSTEM

The combination of process and controller is conveniently represented by a block diagram such as Fig. 2. On this diagram the process, controller, and connections are shown. The process and controller are represented by their respective Laplace transforms, which effectively replace operations with differential equations in the original domain by algebraic operations in the subsidiary domain. The process and controller combination is considered to function as follows:

The output from the process θ is the variable whose value it is desired to maintain at the set point of the controller θ_{set}. The difference $\theta_{set} - \theta$ is measured by the controller and produces an output x, such that $x = \theta_{set} - \theta$. Further action within the

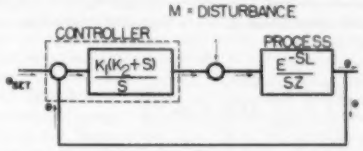

FIG. 2 BLOCK DIAGRAM SHOWING COMBINATION OF CONTROLLER AND PROCESS

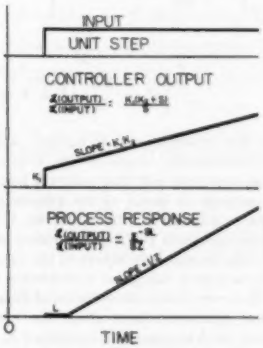

FIG. 3 RESPONSE OF CONTROLLER AND PROCESS TO A UNIT STEP CHANGE IN THEIR RESPECTIVE INPUTS

controller produces a response which is proportional to x and identified as K_1 in the diagram. If the controller has only proportional response, then the output K_1x is the corrective effect applied to the process. However, as will be shown later, proportional controllers are unable to remove completely the effect of a disturbance, and hence a further controller action called reset is frequently introduced. Reset action is idealized so as to modify the proportional response in such a manner that the output from the controller contains not only a proportional component, but also one that depends upon the $\int x dt$, multiplied by some constant determined by the controller setting.

Fig. 3 indicates the response of a proportional reset controller to a unit step change in the input. Expressing the controller action by a curve is very convenient, since a mathematical expression of the action of the controller can then be made without reference to the actual construction of the controlling mechanism.

It is well at this time to introduce the concept of a transfer function, which is defined[4] to be

$$\frac{\mathcal{L}(\text{output})}{\mathcal{L}(\text{input})}$$

Applying this definition and following the methods of Olden-

[1] Associate Professor of Mechanical Engineering, University of British Columbia.

[2] "Optimum Settings for Automatic Controllers," by J. G. Ziegler and N. B. Nichols, Trans. ASME, vol. 63, 1941, pp. 759–765.

[3] "The Dynamics of Automatic Controls," from the German "Dynamik Selbsttätiger Regelungen," by R. C. Oldenbourg and H. Sartorius) translated and edited by H. L. Mason, DSc, of Iowa State College, and published by the ASME in 1948, pp. 88–89 and 34.

Contributed by the Industrial Instruments and Regulators Division and presented at the Annual Meeting, New York, N. Y., November 26–December 1, 1950, of THE AMERICAN SOCIETY OF MECHANICAL ENGINEERS.

NOTE: Statements and opinions advanced in papers are to be understood as individual expressions of their authors and not those of the Society. Manuscript received at ASME Headquarters, July 10, 1950. Paper No. 50—A-22.

bourg and Sartorius,[3] the transfer function for the system in Fig. 2, is

$$\mathcal{L}(\theta - \theta_o) = \frac{Me^{-sL}}{s^2Z} + \frac{e^{-sL}(K_2 + s)K_1}{s^2Z}\,[\mathcal{L}(\theta_{set} - \theta)] \quad [1]$$

The transfer functions for the controller and for the process are shown in Fig. 3. For this investigation the disturbance M is assumed to have the step-change form.

Introducing the conditions that θ_o (the value of θ at the instant the observation is commenced) and θ_{set} be constants, and making the substitution $sL = q$ in Equation [1] gives the following equation

$$\mathcal{L}(\theta) = \frac{L\theta_o}{q\left[1 + \frac{K_1L}{Zq^2}(K_2L + q)e^{-q}\right]} + \frac{L\theta_{set}\left(\frac{K_1L}{Zq^2}(K_2L + q)e^{-q}\right)}{1 + \frac{K_1L}{Zq^2}(K_2L + q)e^{-q}} + L\frac{\frac{ML}{Z}e^{-q}}{\left[q^2 + \frac{K_1L}{Z}(K_2L + q)e^{-q}\right]} \quad [2]$$

The effect of this substitution is to replace t with the variable t/L. It also conveniently combines the controller constants with the process constants and thus makes it possible to express the controller settings in terms of the process characteristics. Two new constants will now be introduced; let $A = K_1L/Z$, $B = K_2L$. These new constants enable the solution of Equation [2] to be applied to the process irrespective of the values of L and Z.

It will be the purpose of this paper to determine suitable values of A and B. However, before the solution of Equation [2] is attempted, several significant facts about the controller-process combination may be determined by operations in the subsidiary domain by the application of the properties of the Laplace transform.

Operations in Subsidiary Domain

First consider a process-controller combination in which there is no reset action. Equation [2] is then modified by letting $K_2 = 0$, i.e.

$$\mathcal{L}(\theta) = \frac{L\theta_o}{q\left[1 + \frac{K_1L}{Zq}e^{-q}\right]} + \frac{L\theta_{set}\left(\frac{K_1L}{Zq}e^{-q}\right)}{1 + \frac{K_1L}{Zq}e^{-q}} + L\frac{\frac{ML}{Z}e^{-q}}{\left[q^2 + \frac{K_1L}{Z}qe^{-q}\right]} \quad [3]$$

To Equation [3] applying the relation[4]

$$\theta_\infty = \lim_{s \to 0} sF(s)$$

where θ_∞ indicates the value of θ at a large time after the disturbance, leads to the following equation

$$\theta_\infty = \theta_{set} + \frac{M}{K_1} \quad [4]$$

Thus the output θ finally comes to a steady value displaced by an amount M/K_1 from the controller setting θ_{set}.

When the same operation is performed upon Equation [2], which represents a controller with a proportional and reset response, the simple result

$$\theta_\infty = \theta_{set} \quad [5]$$

is obtained.

Thus, by the inclusion of the reset response, the offset has been removed and the effect of a disturbance produces a temporary deviation only. While the effect of a disturbance is eventually removed, there is no indication of the magnitude or duration of the deviation of θ from its set value. If the magnitude and duration are combined, there results a certain area of deviation between θ and θ_{set} shown schematically in Fig. 4. Useful results are obtained if this deviation area is made as small as possible.

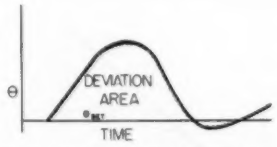

Fig. 4 Deviation Area Between Output Variable θ and θ_{set}

If in Equation [2] θ_o is assumed equal to θ_{set}, and both are assumed to be zero, a desirable simplification results, as follows

$$\mathcal{L}(\theta) = L\frac{\frac{ML}{Z}e^{-q}}{q^2 + A(B + q)e^{-q}} \quad [6]$$

Physically these changes assume that the process and controller have been in equilibrium for some time at θ_{set}, and that the scale of θ is equal to zero at the set point.

The value of $\int_0^\infty \theta dt$ is given by the relation[3]

$$\int_0^\infty \theta dt = F(s)\Big|_0^0$$

Applying this relation one obtains

$$\text{Deviation area} = \frac{ML^2}{Z\,AB} \quad \text{or} \quad \frac{ML^2}{2Z}\left(\frac{2}{AB}\right) \quad [7]$$

Since it will be found that A and B are constants independent of L and Z, and since M is a selected step disturbance, the deviation area is seen to vary directly as L^2 and inversely as Z. Some physical reasoning at this point may indicate the reason for the simple form obtained for the deviation area. It should be recalled that the disturbance M was applied at zero time. After a lapse of a period of time equal to the lag L, the effect of the disturbance will become apparent in the departure of θ from the set value of zero. Under the assumption of an astatic process, the deviation will follow a straight line of slope M/Z, and the deviation will follow this line for another period of time equal to the lag L. Since the controller action cannot start until the deviation has started, and the effect of the controller cannot become apparent until a further time equal to the lag has elapsed, it is

[4] "Transients in Linear Systems," by M. F. Gardner and J. L. Barnes, John Wiley & Sons, Inc., New York, N. Y., vol. 1, 1942, p. 226.

evident that, no matter what values of controller constants are selected, the first part of the deviation is a straight line of slope M/Z starting from zero at L units of time after the disturbance, and continuing for another period of time L.

Fig. 5 shows graphically the initial deviation just discussed. From Fig. 5 it is readily seen that the initial deviation area, which is independent of the controller, is equal to $(ML^2)/(2Z)$. After this period of $2L$, the shape of the curve depends upon the

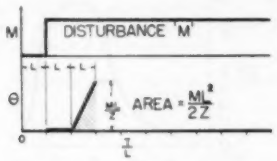

FIG. 5 INITIAL DEVIATION AREA

controller settings. Inasmuch as it seems reasonable to require the deviation area to be a minimum, it is evident that the product of the controller constants AB should be as large as possible.

SOLUTIONS OF STEM EQUATION

Several writers[3,5] have obtained graphical solutions of the stem equation

$$q^2 + A(B + q)e^{-q} = 0 \quad \ldots\ldots [8]$$

and the results of their solutions need only be indicated.

It is noted (1) that a necessary condition for stable solutions is $A > 0$ and $B > 0$, and (2) Equation [8] has one or three real negative roots and an infinite number of complex roots when the first condition is satisfied. Following Hartree[5] and others,[3] approximations for the real and imaginary parts of the complex roots are

$$\left.\begin{aligned} \delta &= \log_e \frac{\Omega}{A} \\ \Omega &= \left(2n - \frac{3}{2}\right)\pi - \frac{1}{\Omega}\left(B + \log_e \frac{\Omega}{A}\right) \end{aligned}\right\} \quad \ldots\ldots [9]$$

(n = harmonic number) where the complex root is of the form $q = -\delta + i\Omega$, and the real root is obtained from

$$A = \frac{\Delta^2}{(\Delta - B)e^{\Delta}} \quad \ldots\ldots [10]$$

where $q = -\Delta$.

From these approximations it is easy to show that the higher harmonics die away rapidly, and that after a small time the response curve of the controller-process combination may be approximated satisfactorily by the aperiodic and first harmonic terms. Oldenbourg and Sartorius[3] have shown that the ratio between successive amplitudes of the response curve depends upon the parameter δ/Ω. Actually, in using this parameter, the damping ratio of the first harmonic is specified. The initial response curve for small times is obtained by expanding the Laplace transform in a series form, which converges for large values of q, and then transforming back to the original domain term by term.

OPTIMUM SOLUTIONS

The problem now is to select some criterion (some relation between the roots of the stem Equation [8]) which will enable values of A and B to be calculated for an optimum response curve.

Since it has been shown that the selection of a specified damping ratio[3] provided a suitable criterion for the adjustment of the controller with proportional response, it is reasonable to inquire if the same criterion might not be valuable for the proportional-plus-reset controller. A further condition may then be imposed upon the stem equation. Recalling that the deviation area varies inversely as AB, the condition that AB be a maximum provides the second requirement. Upon substituting $q = -\delta + i\Omega$ in the stem Equation [8], there results

$$2\delta\Omega + ABe^{\delta}\sin\Omega - Ae^{\delta}(\delta\sin\Omega + \Omega\cos\Omega) = 0 \quad [11a]$$

$$\delta^2 - \Omega^2 + ABe^{\delta}\cos\Omega + Ae^{\delta}(\Omega\sin\Omega - \delta\cos\Omega) = 0 \quad [11b]$$

Solving Equations [11a, 11b] for AB results in

$$2\delta\Omega(\Omega\sin\Omega - \delta\cos\Omega) + (\delta^2 - \Omega^2)(\delta\sin\Omega + \Omega\cos\Omega) + ABe^{\delta}\Omega = 0 \quad \ldots\ldots [12]$$

The condition of a specified damping ratio requires that δ/Ω = constant; hence Equation [12] is rewritten as

$$\left(ABe^{\frac{\delta}{\Omega}}\right)e^{\Omega} = \Omega^2\left[\left(1 - \frac{\delta^2}{\Omega^2}\right)\left(\frac{\delta}{\Omega}\sin\Omega + \cos\Omega\right) - \frac{2\delta}{\Omega}\left(\sin\Omega - \frac{\delta}{\Omega}\cos\Omega\right)\right] \quad \ldots\ldots [12a]$$

The condition that AB be a maximum is

$$\frac{d(AB)}{d\Omega} = 0$$

Upon introducing this condition in Equation [12a], the following equation in Ω is obtained

$$\tan\Omega = \frac{\left[2\left(\frac{\delta}{\Omega}\right)\Omega - \Omega\left(1 - \frac{\delta^2}{\Omega^2}\right)\frac{\delta}{\Omega} + (\Omega - 2)\left(1 + \frac{\delta^2}{\Omega^2}\right)\right]}{\left[2\frac{\delta}{\Omega}(\Omega - 2) - \left(1 - \frac{\delta^2}{\Omega^2}\right)(\Omega - 2)\frac{\delta}{\Omega} - \Omega\left(1 + \frac{\delta^2}{\Omega^2}\right)\right]} \quad \ldots [13]$$

Hence, when a value of δ/Ω is selected, Equation [13] may be solved for Ω, and the values of A and B obtained from the Equations, [12a], and

$$A = \Omega e^{-\delta}\left[2\frac{\delta}{\Omega}\cos\Omega + \left(1 - \frac{\delta^2}{\Omega^2}\right)\sin\Omega\right] \quad \ldots [14]$$

Fig. 6 shows the response curve plotted for $\delta/\Omega = 0.4$, and the values for A and B are

$$A = 0.6, \qquad B = 0.36$$

One important feature of this response curve is the appearance of positive and negative areas. The response curve is found to cross the horizontal axis in its return to the set value. The maximum deviation is small, and the first return to the set value of the variable is rapid. If deviation on both sides of the set

[5] "Time Lag in Control Systems," by D. R. Hartree, A. Porter, A. Clalendar, and A. B. Stevenson, Proceedings of the Royal Society of London, Series A, vol. 161, 1937, p. 466.

value of the output variable can be tolerated, the criterion seems to be satisfactory.

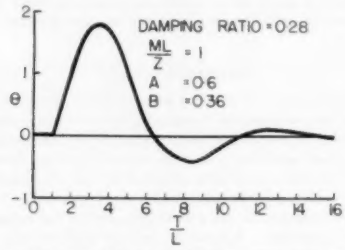

FIG. 6 RESPONSE OF PLANT TO STEP DISTURBANCE WHEN CONTROLLER HAS PROPORTIONAL AND RESET RESPONSE, AND SETTINGS ARE ADJUSTED TO PROVIDE SPECIFIED DAMPING RATIO

However, if it is desired to have the output variable return to the set value without crossing the set point to the same extent, another approach is necessary. Since the response for other than small times can be approximated by the aperiodic term and the first harmonic, the desired response might be obtained by requiring these components to have equal exponential terms. Further, the requirement that AB be a maximum will insure that the deviation area is a minimum.

The theory is developed as follows:

Rewriting the stem equation as

$$q^2 e^q + A(B + q) = 0 \quad \ldots\ldots\ldots\ldots\ldots\ldots [15]$$

and letting $q = -\Delta + i\Omega$, the following equations are obtained

$$(\Delta^2 - \Omega^2) \cos \Omega + 2\Delta\Omega \sin \Omega + ABe^{\Delta} - A\Delta e^{\Delta} = 0 \ldots [16a]$$

$$(\Delta^2 - \Omega^2) \sin \Omega - 2\Delta\Omega \cos \Omega + A\Omega e^{\Delta} = 0 \ldots [16b]$$

The equation for the aperiodic root is obtained from Equation [15] by substituting $q = -\delta$, resulting in

$$A(\delta - B)e^{\delta} = \delta^2 \quad \ldots\ldots\ldots\ldots\ldots\ldots [17]$$

Solving Equations [16a] and [16b] for AB gives the following equation

$$AB = e^{-\Delta}\left(\frac{\Delta}{\Omega}\right)[2\ \Delta\Omega \cos \Omega - (\Delta^2 - \Omega^2) \sin \Omega] - e^{-\Delta}\ [(\Delta^2 - \Omega^2) \cos \Omega + 2\Delta\Omega \sin \Omega] \ldots [18]$$

and from Equation [17] if the real parts of the aperiodic and first harmonic are equal, then $A(\Delta - B)e^{\Delta} = \Delta^2$, which upon substitution in Equation [16a] gives

$$\Delta^2 = (\Delta^2 - \Omega^2)\cos \Omega + 2\Delta\Omega \sin \Omega \quad \ldots\ldots\ldots [19]$$

and using Equation [19] in [18], a final relation for AB results

$$AB = e^{-\Delta}\left[\frac{\Delta}{\Omega}\ \{2\Delta\Omega \cos \Omega - (\Delta^2 - \Omega^2) \sin \Omega\} - \Delta^2\right] \ldots [20]$$

An arbitrary value of Ω now determines Δ from Equation [19], and these corresponding values of Ω and Δ will determine AB from Equation [20]. The desirability of making AB a maximum has been indicated before. However, the difficulties of performing the indicated differentiation of Equation [20], and the solution of the resulting equations lead to the adoption of the following procedure for the determination of the optimum value of Ω:

(*a*) Select a series of values for Ω, and solve Equation [19] for the corresponding Δ.

(*b*) Using these values of Ω and Δ, calculate AB from Equation [20].

(*c*) Plot the resulting values of AB on a base of Ω.

(*d*) Determine the maximum value of AB by inspection of the curve of (*c*).

Fig. 7 shows the resulting plot. From this plot values of $\Omega = 1.1$ and $\Delta = 0.304$ were selected. Fig. 8 shows the resulting

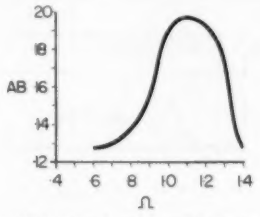

FIG. 7 PLOT OF AB VERSUS Ω FOR REAL PARTS OF APERIODIC AND FIRST-HARMONIC ROOTS EQUAL

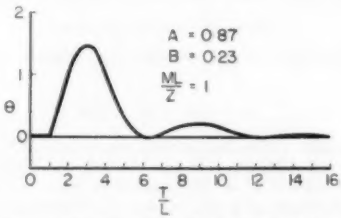

FIG. 8 RESPONSE CURVE FOR REAL EQUAL PARTS OF APERIODIC AND FIRST HARMONIC, WHEN PLANT IS DISTURBED BY A STEP INPUT

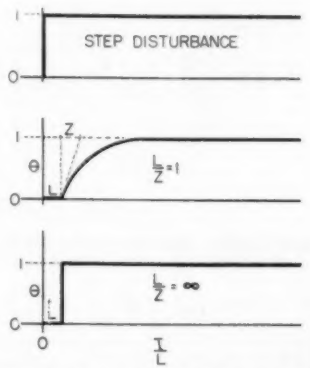

FIG. 9 RESPONSE OF PROCESS TO A STEP CHANGE, WHEN PROCESS IS APPROXIMATED BY A LAG AND AN EXPONENTIAL FUNCTION

response curve with

$$A = 0.87, \qquad B = 0.23$$

When the process contains self-regulation, the difficulty of controlling it is lessened. Such processes may be approximated by a lag and an exponential function.[3] Fig. 9 indicates the type of process response to a step change in the input for two values

of the parameter L/Z, where L is the lag, and Z is the time constant of the

$$\left(1 - e^{-\frac{t}{Z}}\right) \text{ function}$$

When the controller settings are determined from the criteria of equal negative real roots on the aperiodic and first-harmonic terms, it is found that the controller settings vary with the parameter L/Z. Table 1 gives the values of the proportional response K_1 and the reset rate K_2 for some values of L/Z. The previously defined values of A and B are not given because, in the case of $L/Z = \infty$, the constant A is not involved.

TABLE 1 CONTROLLER SETTINGS FOR PROCESS WITH SELF-REGULATION

($L = 1$)

L/Z	K_1	K_2
0.2	4.4	0.31
0.5	1.8	0.44
1	0.78	0.78
5	0.30	1.9
∞	0.2	3.3

Fig. 10 shows the response of the controller-process combination to a unit disturbance for two values of L/Z.

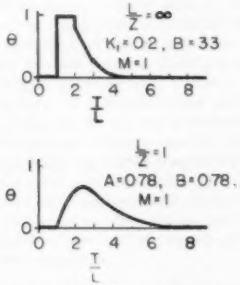

FIG. 10 RESPONSE CURVE FOR REAL EQUAL PARTS OF APERIODIC AND FIRST HARMONIC, WHEN PLANT IS DISTURBED BY A STEP INPUT (Self-regulated plant.)

CONCLUSION

In summary, a method of applying the Laplace transform to control problems has been demonstrated. The actual process has been replaced by the combination of a lag and an appropriate function. Solutions of the resulting equations have been obtained and criteria for controller settings developed from these solutions. The application of these results to an actual process will depend, of course, upon how well the assumed process represents the actual process.

Appendix

Summary of equations for drawing response curves for the "astatic with lag" process

Small Times

$$\theta = \frac{ML}{Z}\left[\left(\frac{t}{L} - 1\right) - \frac{A}{2!}\left(\frac{t}{L} - 2\right)^2 - \frac{AB}{3!}\left(\frac{t}{L} - 2\right)^3 + \frac{A^3}{3!}\left(\frac{t}{L} - 3\right)^3 + \frac{10\,A^3B}{5!}\left(\frac{t}{L} - 3\right)^4 + \frac{A^3B^2}{5!}\left(\frac{t}{L} - 3\right)^5 + \cdots\cdots\right]$$

Aperiodic Plus First Harmonic

$$\theta = \frac{ML}{Z}\left[\frac{e^{-\Delta\left(\frac{t}{L}-1\right)}}{A(1 + \Delta - B)e^{\Delta} - 2\Delta} + \frac{2e^{-\delta\left(\frac{t}{L}-1\right)}\sin\left[\Omega\left(\frac{t}{L} - 1\right) + \phi\right]}{\sqrt{a^2 + b^2}}\right]$$

where

$$a = Ae^{\delta}[(1 + \delta - B)\cos\Omega - \Omega\sin\Omega] - 2\delta$$
$$b = 2\Omega - Ae^{\delta}[(1 + \delta - B)\sin\Omega + \Omega\cos\Omega]$$
$$\tan\phi = \frac{a}{b}$$

Laplace transform (process with self-regulation)

$$(a)\quad \mathcal{L}(\theta) = L\,\frac{\frac{ML}{Z}e^{-q}}{q^3 + \frac{L}{Z}q + A(B + q)e^{-q}} \qquad 0 < \frac{L}{Z} < \infty$$

$$(b)\quad \mathcal{L}(\theta) = L\,\frac{Me^{-q}}{q + K_1(B + q)e^{-q}} \qquad \frac{L}{Z} = \infty$$

Small Times

$$0 < \frac{L}{Z} < \infty \quad (\theta) = \frac{ML}{Z}\left\{\frac{Z}{L}\left(1 - e^{-\frac{L}{Z}\left(\frac{t}{L}-1\right)}\right) - \frac{Z^3}{L^3}\left[\left(\frac{t}{L} - 2\right)\left(AB + A\left\{B - \frac{L}{Z}\right\}e^{-\frac{L}{Z}\left(\frac{t}{L}-2\right)}\right) + A\left(1 + e^{-\frac{L}{Z}\left(\frac{t}{L}-2\right)}\right)\right] + \frac{Z^3}{L^3}\left[2AB - 2A\left(B - \frac{L}{Z}\right)e^{-\frac{L}{Z}\left(\frac{t}{L}-2\right)}\right] + \text{etc.}\ \ldots\right\}$$

$$\frac{L}{Z} = \infty \quad (\theta) = M\left\{U\left(\frac{t}{L} - 1\right) - \left[K_1B\left(\frac{t}{L} - 2\right) + K_1\right] + \left[\frac{K_1^2B^2}{2!}\left(\frac{t}{L} - 3\right)^2 + 2K_1^2B\left(\frac{t}{L} - 3\right) + K_1^2\right] + \text{etc.}\ \ldots\right\}$$

where

$$U\left(\frac{t}{L} - 1\right) = 0 \text{ for } \frac{t}{L} < 1$$
$$= 1 \text{ for } \frac{t}{L} > 1$$

Aperiodic Plus First Harmonic

$$0 < \frac{L}{Z} < \infty \quad \theta = \frac{ML}{Z}\left\{\frac{e^{-\Delta\left(\frac{t}{L}-1\right)}}{A(1 + \Delta - B)e^{\Delta} - 2\Delta + \frac{L}{Z}} + \frac{2e^{-\delta\left(\frac{t}{L}-1\right)}\sin\left[\Omega\left(\frac{t}{L} - 1\right) + \phi\right]}{\sqrt{a^2 + b^2}}\right\}$$

where

$$a = Ae^{\delta}\left[(1 + \delta - B)\cos\Omega - \Omega\sin\Omega\right] + \frac{L}{Z} - 2\delta \qquad b = 2\Omega - Ae^{\delta}\left[(1 + \delta - B)\sin\Omega + \Omega\cos\Omega\right]$$

$$\tan\phi = \frac{a}{b}$$

$$\frac{L}{Z} = \infty \quad \theta = M\left\{\frac{e^{-\Delta\left(\frac{t}{L}-1\right)}}{1 + K_1(1 + \Delta - B)e^{\Delta}} + \frac{2e^{-\delta\left(\frac{t}{L}-1\right)}\cos\left[\Omega\left(\frac{t}{L}-1\right) + \phi\right]}{\sqrt{a^2 + b^2}}\right\}$$

where

$$a = 1 + K_1e^{\delta}\left[(1 + \delta - B)\cos\Omega - \Omega\sin\Omega\right] \qquad b = K_1e^{\delta}\left[(1 + \delta - B)\sin\Omega + \Omega\cos\Omega\right]$$

$$\tan\phi = \frac{b}{a}$$

Furnace Heat Absorption in Pulverized-Coal-Fired Steam Generator, Willow Island Station

Part I Furnace Heat-Absorption Efficiency as Shown by Temperature and Composition of Gases Leaving the Furnace

By J. W. MYERS[1] and R. C. COREY,[2] PITTSBURGH, PA.

As part of the comprehensive investigation of heat transfer in steam-boiler furnaces by the Special Research Committee on Furnace Performance Factors of the Society, the furnace heat-absorption efficiency and the distribution of heat absorption on the furnace walls were determined on boiler No. 1 at the Willow Island Station of the Monongahela Power Company, Willow Island, West Va. The unit is a single-drum boiler rated at 500,000 lb of steam per hr at 1350 psig and 950 F at the superheater outlet, with a water-cooled dry-bottom furnace that is fired through the roof with six multitip intertube burners. This paper presents the results of determination of furnace heat-absorption efficiency made by the Combustion Research Section of the Bureau of Mines, as part of the co-operative research program with the ASME Committee to study factors affecting furnace performance. The distribution of heat absorption in the furnace walls, investigated concurrently, is the subject of another paper, and together they comprise the third of a series[3] of reports of investigations sponsored by the committee.

THIRTEEN tests were made on boiler No. 1 of the Willow Island Station to determine the effect on furnace heat absorption of variations of load, excess air, and the arrangement of burners in service. The furnace heat absorption is defined as the heat transferred by convection to the furnace walls, not including the screen, and the heat transferred by radiation to the furnace walls, including the screen. The heat absorption in the furnace was obtained as the difference between the net heat available and the heat losses, including sensible heat in the products and radiation and convection losses. With slight modification, method *b*, paragraph 7, of the ASME Test Code for Stationary Steam-Generating Units was followed.

The sensible heat in the exit gas was calculated from the gas temperature and composition, which were determined by techniques and equipment developed by the Bureau of Mines for furnace testing.[4] The gas-temperature and composition data, and computed results, are tabulated completely in the paper.

The Code requires measurements to be made at a minimum number of locations, depending upon the area of the furnace outlet, to obtain satisfactory average values for the temperature and composition of the gases. However, location of the available doors in the furnace casing limited accessibility to less than the requisite number of sampling positions ahead of the screen, and it was necessary to calculate the average gas temperature at that location from complete surveys on the gas after passing through the screen, and computed heat-transfer rates to the screen tube bank. The basis for these calculations is described in detail later in the paper.

Methods of Test

Description of Furnace. Fig. 1 is a sectional side elevation of the unit, showing arrangement of the component parts. The furnace is approximately 84 ft high from the top of the hopper to the center line of the drum, 25 ft 3 in. wide, and 35 ft 4 in. deep from front wall to rear wall. All furnace walls are completely water-cooled, consisting of 3-in-OD tubes on 3-in. centers. The roof tubes are a continuation, through a header, of the front-wall tubes. The rear-wall tubes are bent forward and arranged in four rows to form the screen, with a spacing of 8 in. center to center between rows, and a spacing of 12 in. center to center between tubes in each row. From the screen the tubes are bent upward and brought into one plane to form the division wall between the furnace proper and the superheater and economizer section. The distance from the division wall to the rear wall is 14 ft, giving a horizontal projected furnace-outlet area of 353 sq ft, or, since the screen tubes are inclined at an angle of 15 deg from the horizontal, an actual furnace outlet area of 365 sq ft. The total projected area of radiant heating surface in the furnace is 8782 sq ft, including the actual furnace-outlet area.

The furnace is fired with six multitip intertube burners arranged in line across the width of the roof. Coal is supplied to groups of two burners by three B&W Type E pulverizers, designated in the paper as A, B, and C. Pulverizer A supplies the two burners near the right side, B the two burners near the center, and C the pair near the left side. The designation of the sides of

[1] Fuel Engineer, Combustion Research Section, Coal Branch, Bureau of Mines.

[2] Supervising Engineer, Combustion Research Section, Coal Branch, Bureau of Mines. Mem. ASME.

[3] "An Investigation of the Variation in Heat Absorption in a Pulverized-Coal-Fired Water-Cooled Steam-Boiler Furnace," Parts I–IV, Trans. ASME, v. d. 70, 1948, pp. 553–619.

"Furnace Heat Absorption in Paddy's Run Pulverized-Coal-Fired Steam Generator, Using Turbulent Burners, Louisville, Ky.," Parts I–III, Trans. ASME, vol. 72, October, 1950; Part I, by R. I. Wheater and M. H. Howard, pp. 893–923; Part II, by R. C. Corey and Paul Cohen, pp. 925–935; Part III, by H. H. Hemenway and R. I. Wheater, pp. 937–944.

Contributed by the Research Committee on Furnace Performance Factors, and Fuels, Power, and Heat Transfer Divisions and presented at the Annual Meeting, New York, N. Y., November 26–December 1, 1950, of The American Society of Mechanical Engineers.

Note: Statements and opinions advanced in papers are to be understood as individual expressions of their authors and not those of the Society. Manuscript received at ASME Headquarters, October 6, 1950. Paper No. 50—A-83.

[4] "Methods and Instrumentation for Furnace Heat-Absorption Studies: Temperature and Composition of Gases at Furnace Outlet," by P. Cohen, R. C. Corey, and J. W. Myers, Trans. ASME, vol. 71, 1949, pp. 965–978.

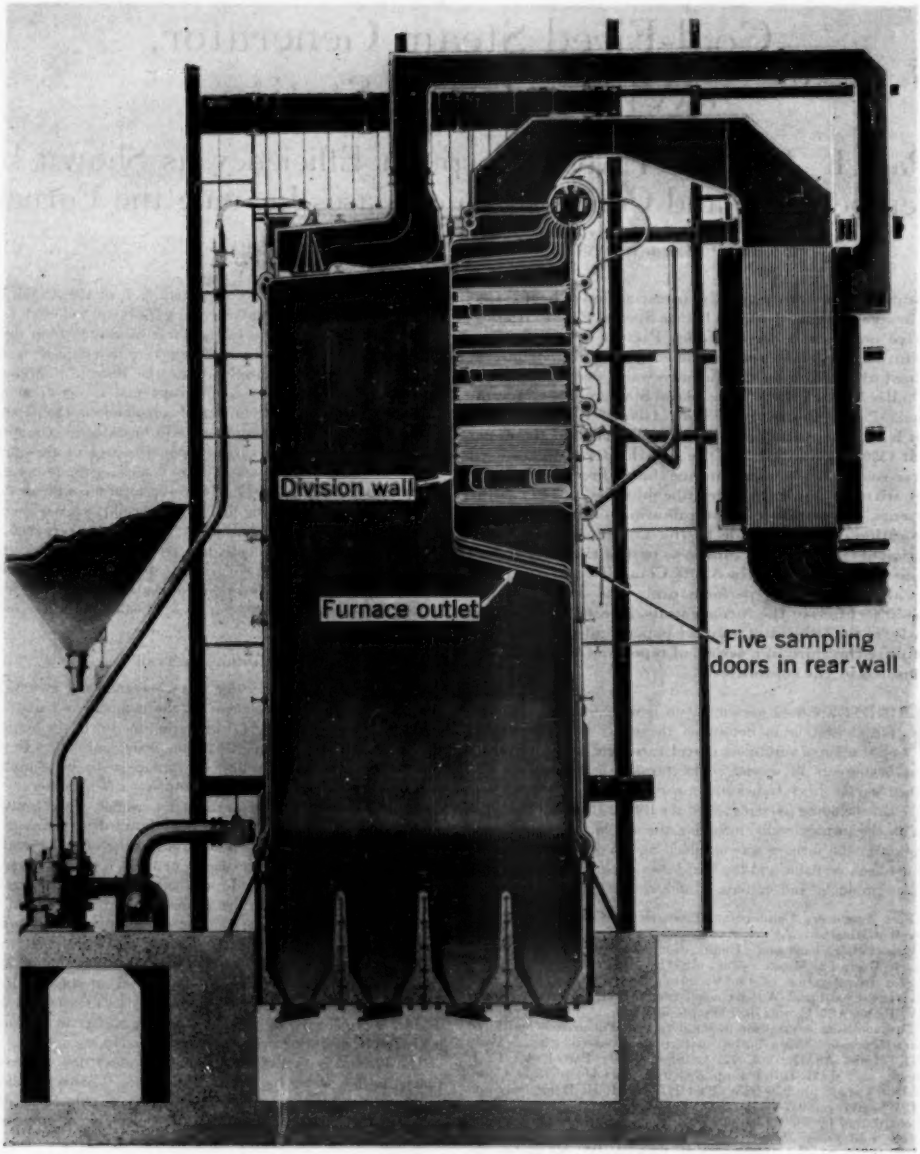

FIG. 1 SECTIONAL SIDE ELEVATION OF BOILER NO. 1, WILLOW ISLAND STATION

the unit, left and right, refers to the sides as seen by an observer facing the front wall of the unit.

Combustion air is supplied by two forced-draft fans and preheated in a tubular air heater. Superheat control is obtained by direct-contact spray-type desuperheater (attemperator) using feedwater as the cooling medium.

Location of Test Points at Furnace Outlet. The gas-temperature and composition surveys were made by means of a water-cooled high-velocity thermocouple probe inserted through five lancing doors on the rear wall of the furnace about 1 ft above the uppermost row of screen tubes. Measurements were made at five positions through each of the five doors, giving the distribution shown in Fig. 2, which is a diagram of the furnace outlet in a plane parallel to the screen tubes, as viewed from above and from the rear wall. The sampling doors are designated B-1, B-2, B-3, B-4, and B-5 from the left to the right of the furnace, and the arbitrary positions, chosen to represent equal area divisions, are numbered 1, 2, 3, 4, and 5 from the rear wall toward the division wall.

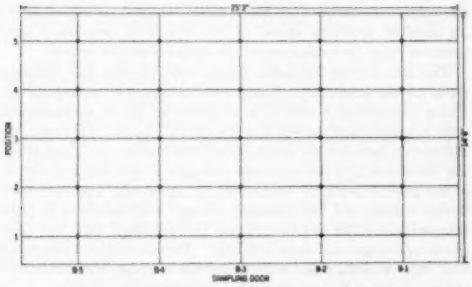

FIG. 2 DISTRIBUTION OF SAMPLING POINTS AT FURNACE OUTLET

In addition to measurements on the gas after passing through the screen at the 25 points shown, a partial temperature survey was made ahead of the screen by inclining the probe downward in the gas lanes of the tube bank until the thermocouple was in the plane of the first row of screen tubes. The space limitations mentioned previously made it impossible to sample more than 13 positions ahead of the screen.

The gas composition was also determined at the economizer outlet to provide data for calculating the enthalpy of the combustion air by means of a heat balance across the air heater. Samples were taken at 18 points, arranged in six groups of three across the economizer outlet, through sample lines that are part of the plant equipment. Individual samples were taken at the six center points and a composite sample from the other 12.

Instrumentation and Analytical Methods. The instrumentation and techniques employed, with some exceptions, were similar to those described and illustrated in recent publications.[4,5]

The temperature of the gas at the furnace outlet was determined with high-velocity thermocouples, consisting of platinum, 10 per cent rhodium-platinum elements, extending the full length of a water-cooled probe to an external terminal block. Previous experience showed the full-length couple to be the most expedient method of avoiding errors induced by excessively high temperatures at the junction between the noble metal and the compensating lead wires. A Bailey high-speed electronic recording potentiometer, used to record the emf of the thermocouples, gave representative average values of the temperature of the gas at a sampling point in a time interval of 1 1/2 min or less. An artificial cold junction, thermostatically controlled to a temperature higher than ambient, was used between the lead wires and the recorder. Fig. 3 shows the type E and G radiation shields used in making the temperature surveys. A considerable number of comparison tests were made between these shields and the B&W MHVT (multiple high-velocity thermocouple), also shown in Fig. 3, at various test conditions to furnish data for correcting the observed temperatures to the MHVT basis.

Gas analyses were made simultaneously with the temperature measurements by means of a Bailey oxygen recorder connected with the aspirating system of the high-velocity thermocouple. Satisfactory average values for the oxygen content of the gas could be obtained in approximately the same time interval required for the temperature record. Frequent complete Orsat analyses of the flue gas, sampled simultaneously with operation of the oxygen recorder, served both to calibrate the recorder and to give a relationship between the recorded oxygen content and that of the other constituents of the gases. The samples for complete analysis were obtained under reduced pressure by mercury-sealed aspirating bottles, which reduced the possibility of leakage and contamination by air, and partial solution of gas constituents, principally carbon dioxide, which may occur with the salt solution formerly used as a confining liquid.

The composition of the flue gas at the economizer outlet was also determined by the oxygen recorder, Orsat analyses also being made at regular intervals.

Fig. 4 shows the necessary equipment and instruments for measuring the gas temperature and composition, and for aspirating the gas at high velocity through the probe.

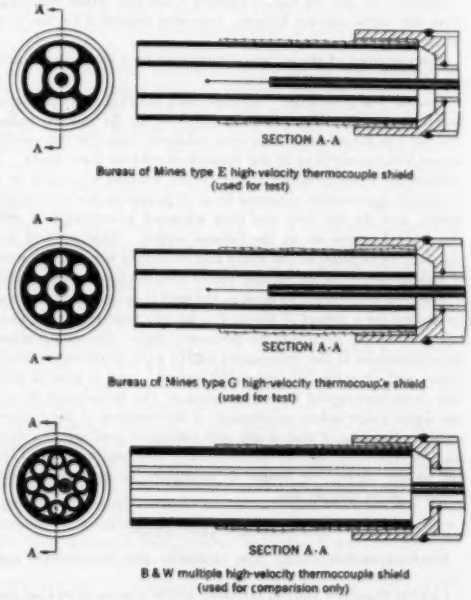

FIG. 3 RADIATION SHIELDS FOR HIGH-VELOCITY THERMOCOUPLE

[4] "Furnace Heat Absorption in Paddy's Run Pulverized-Coal-Fired Steam Generator, Using Turbulent Burners, Louisville, Ky. Part II—Furnace Heat-Absorption Efficiency as Shown by Temperature and Composition of Gases Leaving the Furnace," by R. C. Corey and Paul Cohen, Trans. ASME, vol. 72, 1950, pp. 925–935.

FIG. 4 VIEW OF INSTRUMENTS AND APPARATUS FOR MEASURING TEMPERATURE AND COMPOSITION OF GASES AT FURNACE OUTLET

All other observations pertinent to this part of the investigation were made with regular plant instruments. The temperatures of the flue gas and air entering and leaving the air heater were measured with resistance thermometers in the appropriate ducts and were recorded on the plant control board. The primary-air rate and temperature to each pulverizer were also recorded by plant instruments.

Coal-feed rates were determined by recording at regular intervals the time and number of the trip of the automatic scale discharging into each of the pulverizers in use. Increments of the coal were taken at the scales, following ASTM specifications,[6] and were stored during the test in covered milk cans. The gross samples from each test were reduced by crushing and riffling to a quantity sufficient to fill a 5-gal can and were sealed and shipped to the Coal Analysis Section of the Bureau of Mines for complete analysis.

Samples of the fly ash, obtained from the sluice discharge from the dust-collector hopper, were also analyzed by the Coal Analysis Section.

The humidity of the air was determined by a sling psychrometer at the forced-draft-fan inlet.

General Test Procedure. Routine soot blowing was completed before each test. The load was adjusted to the desired value, and the two forced-draft fans were balanced, from the differential across Venturi sections in the respective cold-air inlet ducts. A preliminary determination of the oxygen content was made on a composite gas sample obtained from 12 points at the economizer outlet, and the air flow was then adjusted accordingly to give the desired excess air at the furnace outlet. This method was satisfactory because of the small and relatively constant amount of leakage between the furnace outlet and the economizer outlet.

The test was started as soon as the unit was stabilized and was continued for a period of about 4 1/2 hr, the time required to obtain a complete set of all the necessary data. Gas-composition determinations at the economizer outlet were made immediately before and after the furnace-outlet survey; and in several tests that were interrupted before completion, the economizer survey was again made before resumption of the traverse at the furnace outlet. Reading of coal scales and taking of coal samples were started before the furnace-outlet survey and continued until the end of the survey, or longer if necessary, to give the recommended gross sample size.

METHODS OF CALCULATION

Gas-Composition Data. The complete gas composition and excess air at the furnace outlet and economizer outlet were calculated from arithmetical averages of the observed oxygen concentrations, corrected by appropriate factors for instrument calibration. It was shown in previous work[4] that this method is sufficiently accurate when the sample points are distributed properly over the area. The oxygen content at the furnace outlet was determined after the gas had passed through the screen, since the average composition will not be affected by the screen, although the distribution pattern may change considerably.

Flue-Gas Temperature. The definition of furnace heat absorption requires that the average flue-gas temperature ahead of the screen be known, but this was impossible to determine by direct measurement for reasons noted previously. It was planned originally to determine the temperature drop across the screen at one or two points and to apply this correction to the average of the temperatures obtained during a complete survey on the gases leaving the screen-tube bank. However, a few exploratory tests showed the temperature drop across the screen to vary widely at different points, probably as the result of complex gas-flow patterns and varying amounts of ash deposited on the tubes. Consequently, the temperature was measured at the 13 possible positions ahead of the screen to provide a more accurate basis for evaluation of the drop across the screen.

The data for the accessible points were plotted, and temperatures for the inaccessible points were obtained by extrapolation. These temperatures and those obtained by direct measurement were averaged and corrected to the MHVT basis. However, the differences between the averages so obtained for the gases entering the screen and the corrected averages of the complete survey of the gases leaving the screen did not agree well with estimated design values, and the enthalpy change corresponding to these temperature differences could not be correlated with the mean gas temperature and mass velocity. Therefore it was concluded that this procedure for calculating the average temperature of the gases ahead of the screen was not sufficiently accurate.

Accordingly, a method was devised for adjusting the average temperature ahead of the screen in such a manner that the enthalpy change of the gas passing through the screen, based on the *adjusted* temperature, would agree with the heat transferred from the gas to the tubes, which is calculated from convection and radiation coefficients. The adjustments were made to fit the following equation, the left term being the enthalpy change of the gas in passing through the screen and the right term expressing the convection and radiation heat transfer from the gas to the screen tubes

$$Wc_p(T_1 - T_2) = UA(T_m - T_s) + \sigma\epsilon AF(T_m^4 - T_r^4) \quad [1]$$

where

W = wet gases at furnace outlet, lb per hr
c_p = mean specific heat of gases, Btu per lb deg F
U = over-all convection heat-transfer coefficient, Btu/(hr) (sq ft) (deg F)
σ = radiation constant
ϵ = emissivity
A = developed area of screen tubes, sq ft
F = shape factor of radiation receiving surface (assumed at 1.0)
T_1 = adjusted average temperature of gas ahead of screen, deg R
T_2 = corrected average temperature of gas after screen, deg R
T_m = mean temperature of gas in screen $= \frac{T_1 + T_2}{2}$, deg R
T_s = temperature of saturated steam at operating pressure, deg R
T_r = temperature of tube surface, deg R

The value of U was assumed to be $2.2 + 0.00095\,G$ (G = mass

[6] ASTM Standard Method D492-46, ASTM Standards on Coal and Coke, August, 1947.

velocity of wet gases based upon free area between tubes), according to the work of Kreisinger,[7] and T_s and c_p were obtained with sufficient accuracy from the preliminary unadjusted temperature ahead of the screen. Other values were obtained from observed data for each test, leaving only T_1 and ϵ as unknowns in the equation. The emissivity ϵ is assumed to be constant for all tests.

An additional relationship is obtained by imposing the condition that the algebraic sum of the adjustments for the entire series of tests be zero, based on the assumption that the average of a large number of determinations should have greater precision than that of a single test, that is, $\Sigma(T_1 - T_2) = 0$, where T_2 is the average temperature, deg R, ahead of the screen before adjustment.

The adjusted temperatures for each test T_1 were found in the following manner: Different values for ϵ were substituted in Equation [1], which then was solved for T_1 for each test. The summation of the differences, $\Sigma(T_1 - T_2)$, was found to be zero when $\epsilon = 0.095$, which is similar in magnitude to Sherman's results for short beam lengths.[8] The final adjusted value of T_1 for each test was then computed from Equation [1] and used in all heat-balance equations.

In averaging the temperatures of the gases leaving the screen, the data from position 5 in each door were omitted because it was thought that the extremely large temperature gradient near the division wall in a number of the tests was due to very low gas velocity or even reversed gas flow induced by eddy currents. The entire gas stream would then be represented more adequately by positions 1 to 4 in each door, giving a total of 20 positions.

Furnace Heat Balance. The heat absorption in the furnace was calculated as the difference between the net heat available in the furnace and the heat lost from the furnace in products of combustion and by radiation and convection from the furnace casing. The net heat available is the sum of the lower heating value of the fuel fired (corrected for unburned combustible) and the enthalpy above 80 F of the air used for combustion. The combustible carbon losses were calculated from the fly-ash analysis, on the assumption that 80 per cent of the ash fired occurs as fly ash and that the remainder is carbon-free cinders. The enthalpy of the air was calculated from a heat balance on the air heater, using the recorded temperatures of the gas and air entering and leaving the air heater and the weight and average composition of the gases leaving the economizer. It was assumed that the composition was the same at the economizer outlet and the air-heater inlet, since air leakage between these points was negligible.

The enthalpy of the furnace-outlet gases was calculated from the quantities of the individual gas constituents and their heat content above 80 F, at the adjusted average temperature ahead of the screen tubes, obtained from the tables of Heck.[9] The quantities of the gas constituents were determined from the average flue-gas composition, the rate of fuel firing, and the ultimate analysis of the coal. It was assumed that all the ash left the furnace at the same temperature as the gases, and the heat content was calculated using a mean specific heat of 0.27 Btu per lb deg F. The heat loss from the furnace casing was taken as half that of the entire unit as given by the ABMA Standard Radiation Loss Chart, shown in the ASME Power Test Code for Stationary Steam-Generating Units (1946).

[7] "Heat Transfer in Air Heaters and Economizers," by Henry Kreisinger, *Combustion*, vol. 5, December, 1933, pp. 7–11.

[8] "Burning Characteristics of Pulverized Coals and the Radiation From Their Flames," by R. A. Sherman, *Combustion*, vol. 5, December, 1933, pp. 30–38.

[9] "The New Specific Heats," by R. C. H. Heck, *Mechanical Engineering*, vol. 62, 1940, pp. 9–12.

Results of Tests

Description of Tests. Six tests, Nos. 1, 2, 6, 7, 8, and 13, were made at full load; four tests, Nos. 3, 4, 5, and 11, at three-quarter load; and three tests, Nos. 9, 10, and 12, at half load. The object was to determine the effect on heat absorption of load, excess air, and burner arrangement. Only two values of excess air were used at each load, since the fan capacity established an upper limit at the full loads, and the ability to maintain stable ignition established a lower limit at the low loads. The pertinent operating data and results obtained in the thirteen tests are summarized in Table 1.

The fuel burned was a high-volatile A bituminous coal from West Virginia, from either of two mines or a mixture of the two. Except for the moisture content, the analysis was very uniform throughout the series of tests. However, the fineness of the coal as fired varied considerably between tests and between pulverizers during the same test.

Temperature and Gas Composition at Furnace Outlet. Because of previous interest in the distribution of temperature and composition of the gases at the furnace outlet, the data at each survey position, for the several tests, are presented in Tables 2, 3, and 4. The temperatures in Tables 2 and 3 are *observed* values, determined with the high-velocity thermocouple. For the heat-absorption calculations the averages, calculated according to the methods previously described, were converted to the B&W MHVT basis by adding the corrections shown in Table 5. Data for this table were obtained from thermocouple comparison tests mentioned previously.

The gas compositions in Table 4 are expressed as per cent excess air to provide more familiar values than the oxygen percentages recorded.

Distribution plots of the temperature and composition of the gas leaving the screen tubes, for typical full-load tests, are shown in Fig. 5. These plots illustrate the effect of burner arrangement on the distribution at a nominal excess air of 15 per cent, and may be characteristic of this method of firing.

The most uniform distribution of excess air was obtained in test No. 1, operating with the burners supplied by mills A-C. The use of mills A-B, test No. 7, also gave quite uniform distribution over the central portion of the furnace outlet, but high values occurred on one side and low values on the other side of the outlet. The excess-air pattern noted for test No. 6, with all burners in operation, may be caused by nonuniform distribution of secondary air to the burners or by nonuniform distribution of coal to the individual burner tips. It is conceivable that this uneven distribution of coal and secondary air may have occurred in all the tests, but when only two sets of burners are used the relative flame length and velocity are probably greater, causing the gases to travel farther toward the bottom of the furnace and achieve better mixing.

The temperature patterns in Fig. 5 probably have a complex relationship with the distribution of fuel and air to the burners, the velocity and path of the gas between the burners and the furnace outlet, and the location and extent of ash deposits on the walls. Although increase of gas residence time may improve mixing of gases and, therefore, produce uniform gas composition, it does not follow necessarily that the temperature distribution will also improve, since different streamlines of the gases may experience different histories of path length, velocity, and temperature of the heat-receiving surfaces. It is concluded, therefore, that rational explanation of the present temperature patterns would require more detailed analysis of the gases, in transit, than is required to determine the over-all heat absorption in the furnace.

The high temperature gradients near the division wall, dis-

TABLE 1 SUMMARY OF DATA AND RESULTS. ASME FURNACE HEAT-ABSORPTION TESTS. BOILER NO. 1, WILLOW ISLAND STATION, MONONGAHELA POWER COMPANY. JUNE 9-27, 1949

1	Test number	1	2	3	4	5	6	7	8	9	10	11	12	13
2	Date	6-9	6-10	6-14	6-15	6-16	6-17	6-20	6-21	6-22/23	6-23/24	6-25	6-25	6-27
3	Start of test, first economizer survey, Eastern standard time	9:05 AM	8:27 AM	10:34 AM	9:49 AM	8:51 AM	10:00 AM	2:14 PM	9:08 AM	11:51 PM	11:54 PM	12:09 AM	8:08 PM	9:54 AM
4	End of test, last economizer survey, Eastern standard time	3:18 PM	2:37 PM	4:32 PM	4:02 PM	2:12 PM	4:08 PM	8:08 PM	2:02 PM	4:00 AM	4:30 AM	4:55 AM	11:43 PM	5:03 PM
5	Actual duration of test, hr[a]	4.97	4.58	4.62	4.77	4.05	4.73	4.32	3.75	4.15	4.60	3.75	3.58	5.82
6	Corrected steam flow, M lb per hr	508	508	376	377	373	508	510	507	257	251	364	259	508
7	Superheater outlet header pressure, psig	1315	1315	1286	1285	1299	1295	1300	1300	1269	1270	1280	1275	1301
8	Steam temperature at superheater outlet header, F	958	956	954	954	956	957	955	949	921	925	947	958	956
9	Burner and pulverizer arrangement, (see text)	A-C	A-C	A-C	A-B-C	A-B	A-B-C	A-B	A-C	A-C	A-C	A-C	A-B	A-B-C
10	Coal feed rate, as fired weight, lb per hr	45,250	45,600	35,650	34,720	35,000	45,900	47,400	46,400	24,350	23,720	33,850	24,900	46,800
	Coal, proximate analysis, per cent as fired													
11	Moisture	1.6	1.5	6.1	2.8	2.2	2.4	4.4	3.1	3.4	3.3	3.6	3.2	5.2
12	Volatile matter	39.8	39.4	36.1	38.8	38.7	39.3	37.3	37.7	38.5	37.8	38.6	37.7	37.2
13	Fixed carbon	50.9	51.3	50.2	49.9	49.4	49.9	50.5	51.3	50.0	50.9	49.9	51.5	50.4
14	Ash	7.7	7.8	7.6	8.5	9.7	8.4	7.8	7.9	8.1	8.0	7.9	7.6	7.2
	Coal, ultimate analysis, per cent as fired													
15	Hydrogen	5.3	5.5	5.5	5.4	5.1	5.4	5.5	5.5	5.4	5.4	5.4	5.5	5.6
16	Carbon	75.7	75.7	72.3	74.2	71.8	73.1	73.0	73.9	73.6	74.0	73.8	74.5	73.2
17	Nitrogen	1.6	1.5	1.5	1.5	1.5	1.5	1.5	1.5	1.5	1.5	1.4	1.5	1.5
18	Oxygen	7.5	7.2	11.1	7.6	9.2	9.1	9.5	8.3	8.4	8.1	8.4	8.3	10.1
19	Sulfur	2.2	2.3	2.0	2.8	2.7	2.5	2.7	2.9	3.0	3.0	3.1	2.6	2.4
20	High heating value, as fired, Btu per lb	13,710	13,700	13,090	13,430	13,030	13,260	13,290	13,450	13,410	13,400	13,400	13,450	13,250
21	Grindability, Hardgrove index	54	52	57	57	54	53	56	56	56	59	60	57	57
	Ash cone fusion temperature, F (ASTM)													
22	I.D.T.	2030	2000	2030	1940	2040	2000	2000	2020	1970	1940	1990	2000	2000
23	S.T.	2050	2050	2080	2030	2120	2080	2050	2070	2030	2000	2030	2050	2050
24	F.T.	2260	2260	2380	2380	2390	2420	2260	2290	2260	2260	2130	2260	2260
	Screen analysis of pulverized coal[b]													
25	Per cent through 50 mesh	100.0	100.0	100.0	100.0	100.0	100.0	100.0	100.0	100.0	100.0	100.0	100.0	100.0
26	Per cent through 100 mesh	97.7	98.2	99.4	99.8	99.8	99.5	97.7	98.1	99.5	99.9	100.0	99.9	99.9
27	Per cent through 200 mesh	81.5	73.9	90.0	80.8	89.0	82.0	79.1	81.3	82.0	81.0	78.5	84.6	88.1
	Average temperature of gases at furnace outlet, F													
28	Ahead of screen[c]	2202	2150	2138	2155	2015	2298	2278	2042	1620	1691	1935	1722	2264
29	Leaving screen[c]	2110	2068	2038	2052	1928	2196	2181	1965	1552	1611	1858	1648	2172
30	Differential across screen	92	82	100	103	90	102	97	77	68	80	77	74	92
	Average composition of gases at furnace outlet, per cent dry gas[b]													
31	$CO_2 + SO_2$	16.06	14.74	14.88	14.85	14.87	16.12	15.93	16.07	13.38	14.63	13.52	13.34	14.84
32	O_2	2.62	4.22	4.11	4.12	4.18	2.69	2.96	2.71	5.90	4.89	5.43	5.91	4.19
33	N_2	81.32	81.04	81.01	81.03	80.95	81.19	81.11	81.22	80.72	81.08	80.79	80.75	80.97
34	Excess air at furnace outlet, per cent	13.0	24.0	23.4	23.4	23.9	13.9	15.2	13.8	37.5	24.1	36.0	37.9	24.1
35	Wet gas at furnace outlet, lb per lb coal as fired	12.71	13.90	13.71	13.57	13.11	12.42	12.50	12.58	14.79	13.65	14.79	15.12	13.48
36	Dry air for combustion, lb per lb coal as fired[d]	11.71	12.79	12.10	12.49	12.06	11.33	11.40	11.48	13.70	12.60	13.61	13.98	12.32
37	Total primary air through pulverizers, lb per lb coal as fired[e]	1.59	1.58	1.68	2.57	1.88	2.05	1.43	1.55	2.29	2.41	1.73	2.08	1.80
	Average composition of gases at economizer outlet, per cent dry gas[b]													
38	$CO_2 + SO_2$	15.89	14.71	14.77	14.67	14.82	16.03	15.83	15.95	13.38	14.58	13.52	13.34	14.69
39	O_2	2.81	4.25	4.24	4.32	4.24	2.79	3.07	2.85	5.90	4.35	5.73	5.91	4.36
40	N_2	81.30	81.04	80.99	81.01	80.94	81.18	81.10	81.20	80.72	81.07	80.75	80.75	80.95
41	Excess air at economizer outlet, per cent	14.2	24.2	24.3	24.9	24.3	14.5	15.9	14.6	37.5	24.5	36.0	37.9	25.3
42	Wet gas at economizer outlet, lb per lb coal as fired	12.83	13.93	13.30	13.72	13.15	12.48	12.57	12.67	14.79	13.69	14.79	15.12	13.61
43	Average temperature of gas entering air preheater, F	666	675	642	637	623	683	694	660	558	547	628	567	701
44	Average temperature of gas leaving air preheater, F	383	386	356	375	357	395	399	382	316	317	353	321	393
45	Average temperature of air entering air preheater, F	119	122	123	122	122	120	120	122	111	113	120	120	119
46	Average temperature of air leaving air preheater, F	530	530	513	525	506	547	550	525	460	459	501	465	546
47	Average temperature of tempered primary air (for all pulverizers), F	234	229	296	190	227	207	272	259	237	225	265	246	267
48	Low heating value of coal fired, kB per hr[f]	598,300	601,600	448,600	449,000	439,600	585,800	606,000	600,600	314,400	306,100	436,800	322,300	596,000
49	Sensible heat above 80 F in air, kB per hr	47,900	54,100	40,000	37,000	36,100	48,600	53,000	48,400	24,900	21,600	40,400	27,400	57,200
50	Heat loss due to unburned carbon, kB per hr	4,300	1,900	900	1,000	900	1,900	3,900	3,100	1,100	2,000	1,600	400	800
51	Net heat available in furnace, kB per hr	641,800	653,800	487,700	485,000	474,900	632,500	655,000	645,900	338,200	325,700	475,600	349,300	652,400
52	Sensible heat above 80 F in wet gas at furnace outlet, kB per hr	344,800	370,400	274,200	275,700	248,800	361,600	371,900	323,200	153,000	143,100	258,800	170,300	392,900
53	Sensible heat above 80 F in ash and fly ash leaving furnace, kB per hr	2,000	2,000	1,500	1,700	1,800	2,300	2,200	1,900	800	800	1,300	800	2,000
54	Heat loss by radiation from furnace, kB per hr	1,100	1,100	1,100	1,100	1,100	1,100	1,100	1,100	1,200	1,200	1,100	1,200	1,100
55	Total sensible heat and radiation losses, kB per hr	348,000	373,500	276,800	278,400	251,700	365,000	375,300	326,200	153,000	145,100	261,300	172,300	396,000
56	Heat absorbed in furnace, kB per hr	293,900	280,300	210,800	206,600	223,200	267,500	279,700	319,700	185,200	180,600	214,300	176,900	256,400
57	Net heat available in furnace, kB/(hr)(sq ft)	73.1	74.4	55.5	55.2	54.1	72.0	74.6	73.5	38.5	37.1	54.2	39.8	74.3
58	Heat absorption in furnace, kB/(hr)(sq ft)	33.5	31.9	24.0	23.5	25.4	30.5	31.9	36.4	21.1	20.6	24.4	20.1	29.2
59	Furnace heat absorption efficiency, per cent	45.8	42.9	43.2	42.6	47.0	42.3	42.7	49.5	54.8	55.5	45.1	50.7	39.3

a/ Not necessarily time from start to end; several tests were interrupted before completion
b/ Average for all pulverizers in service; determined by Babcock and Wilcox Company
c/ Corrected to R&W MSVT basis, see text for method of computation
d/ Average of twenty determinations, corrected to R&W MSVT basis by table 5, see text
e/ Average of twenty-five determinations
f/ Includes air from forced-draft fans plus leakage
g/ Includes preheated air and tempering air
h/ Average of determinations for six individual locations and a composite of twelve other locations
i/ This and subsequent figures were rounded after calculation

TABLE 2 OBSERVED[a] TEMPERATURE OF GAS, DEG F, LEAVING SCREEN AT FURNACE OUTLET, ASME FURNACE HEAT-ABSORPTION TESTS, BOILER NO. 1, WILLOW ISLAND STATION

Test No.		1	2	3	4	5	6	7	8	9	10	11	12	13
Door	Position													
B-1	1	1990	1880	1800	2080	1930	2150	2020	1710	1450	1440	1610	1520	1970
	2	1920	1940	1840	2120	2020	2290	2020	1750	1530	1560	1840	1610	2240
	3	1910	1940	1810	2140	2070	2290	2030	1780	1590	1660	1940	1580	2150
	4	1950	1960	1900	2160	1990	2280	2030	1780	1650	1770	1820	1540	2340
	5	1930	1960	1850	1740	2010	1760	1990	1810	1630	1690	1660	1510	1850
B-2	1	1950	1940	1950	2050	1960	2150	2170	1810	1520	1500	1850	1680	2130
	2	1990	1980	1980	2160	1970	2310	2240	1870	1590	1560	1890	1710	2240
	3	2020	1990	2020	2230	2020	2380	2290	1940	1620	1600	1890	1680	2200
	4	2060	1980	2070	2300	2040	2300	2290	2030	1660	1670	1880	1680	2190
	5	1900	2020	1900	1670	2020	1740	2350	2080	1690	1720	1860	1600	1800
B-3	1	2000	1960	1910	1970	1770	[c] 2200	2100	1930	1350	1370	1670	1620	2120
	2	2040	2030	2000	2050	1860	2180	2180	1950	1520	1550	1730	1710	2200
	3	2120	2040	2040	2150	1910	2060	2240	2000	1570	1560	1850	1720	2270
	4	2120	2060	2050	2200	1980	2080	2280	1950	1610	1630	1910	1700	2110
	5	1870	1910	1801	1730	1980	1880	2210	2050	1630	1650	1830	1680	1820
B-4	1	2070	2070	1960	1930	1750	2170	2080	1900	1490	1630	1820	1650	2090
	2	2210	2080	2030	1960	1830	2150	2150	1950	1550	1660	1830	1680	2080
	3	2200	2080	2090	2040	1870	2250	2210	2000	1520	1650	1860	1700	2080
	4	2120	2050	2040	1950	1960	2030	2240	2100	1540	1700	1880	1680	2030
	5	1780	1940	1790	1740	1990	1820	2220	2120	1560	1700	1790	1680	1830
B-5	1	2180	2090	2090	1800	1710	1950	2210	2040	1460	1530	1780	1630	1980
	2	2300	2190	2160	1840	1780	1990	2220	2070	1560	1680	1930	1640	1990
	3	2250	2270	2220	1780	1820	1950	2080	2120	1630	1720	1900	1630	1980
	4	2190	2160	2190	1790	1850	1900	2300	2090	1660	1800	1910	1600	1980
	5	1890	1900	1720	1800	1880	1870	2130	2170	1700	1800	1920	1570	1860

[a] Uncorrected; for corrections see table 5

TABLE 3 OBSERVED[a] TEMPERATURE OF GAS, DEG F, AHEAD OF SCREEN AT FURNACE OUTLET, ASME FURNACE HEAT-ABSORPTION TESTS, BOILER NO. 1, WILLOW ISLAND STATION

Test No.		1	2	3	4	5	6	7	8	9	10	11	12	13
Door	Position													
B-1	3	[b]	2040	1920	2220	1980	2330	2190	1930	1650	1740	1770	1630	2450
	4		2060	1890	2180	1960	2430	2230	2040	1810	1860	2020	1670	2460
	5		2050[b]	1930	2460	2270	2490	2280	1970	1770	1960	2080	1650	2500
B-2	3		2120	2070	2240	2060	2450	2330	1990	1700	1680	1940	1680	2480
	4	2210	2070	2090	2320	2170	2570	2440	2160	1770	1860	2110	1780	2480
	5		2150	2250	2470	2340	2610	2450	2280	1870	1900	2200	1770	2620
B-3	5		2260	2130	2220	2130	2150	2350	2170	1730	1670	1950	1760	2200
B-4	3	2420	2250	2080	2040	2000	2300	2180	2060	1570	1710	1900	1750	2030
	4		2290	2130	2150	2030	2280	2210	2100	1650	1680	1940	1770	2040
	5		2360	2320	2300	2120	2660	2490	2300	1780	1840	2060	1830	2280
B-5	3		2340	2140	1830	1840	2040	2100	2140	1640	1790	2080	1670	1960
	4	2513	2380	2360	1910	1950	2090	2350	2320	1770	1900	2190	1680	2100
	5		2390	2410	1940	2030	2160	2190	2400	1830	1990	2090	1700	2210

[a] Uncorrected; for correction see table 5 [b] Insufficient data taken for test No. 1 [c] No data taken; estimated value

TABLE 4 GAS COMPOSITION[a] AT FURNACE OUTLET, EXPRESSED AS PER CENT EXCESS AIR, ASME FURNACE HEAT-ABSORPTION TESTS, BOILER NO. 1, WILLOW ISLAND STATION

Test No.		1	2	3	4	5	6	7	8	9	10	11	12	
Door	Position													
B-1	1	15.4	24.9	25.5	22.3	22.6	20.7	19.5	17.5	41.3	26.7	45.0	56.9	24.1
	2	16.0	23.6	23.9	19.8	22.5	17.4	18.7	15.7	35.9	20.3	32.8	41.8	19.9
	3	15.2	24.3	26.6	17.0	24.6	14.5	21.0	13.9	34.1	16.3	27.6	39.9	15.1
	4	12.6	22.5	21.4	13.0	28.3	13.9	23.5	12.5	31.3	14.8	33.6	42.8	12.0
	5	10.0	22.5	21.0	10.9	29.2	11.8	21.7	12.3	32.7	17.3	33.2	45.9	18.1
B-2	1	15.7	24.5	20.5	24.3	24.3	20.0	15.3	17.0	37.2	29.7	34.8	38.5	25.5
	2	13.1	24.5	22.4	21.4	24.4	16.4	14.3	15.9	36.0	23.0	34.7	38.9	24.7
	3	13.6	24.0	21.7	18.4	22.8	14.4	13.7	13.0	37.7	23.8	35.6	39.1	23.5
	4	12.1	23.9	26.0	19.4	22.5	11.3	16.7	11.7	35.5	23.5	38.9	39.1	24.5
	5	10.2[b]	23.0	29.8	16.6	24.5	7.8	15.7	11.8	35.2	22.7	37.2	42.0	22.3
B-3	1	15.2	25.4	21.7	24.9	24.5	12.5	15.4	13.0	39.9	66.4	39.7	42.7	25.7
	2	13.9	23.5	14.1	24.8	23.4	13.4	14.4	15.2	37.3	25.1	38.6	34.5	26.8
	3	13.6	24.1	22.0	23.4	24.0	17.2	15.3	12.8	36.5	24.8	33.7	35.5	27.5
	4	13.2	23.9	25.2	22.7	23.1	13.0	15.0	13.6	35.1	25.6	36.5	37.3	24.5
	5	10.7	24.0	26.1	27.9	22.0	9.7	17.4	13.8	67.3	26.3	39.0	37.9	24.5
B-4	1	14.1	24.8	28.7	30.0	26.0	13.1	15.2	15.9	42.0	26.0	37.2	35.5	25.1
	2	14.0	24.3	23.6	29.0	21.9	14.6	15.9	14.4	39.2	24.2	38.2	32.9	23.4
	3	15.4	25.1	26.7	28.2	23.7	12.0	15.6	13.6	37.5	26.9	37.8	34.1	21.3
	4	16.1	25.2	25.8	28.1	22.6	16.9	16.1	14.7	36.4	24.3	37.0	34.7	24.3
	5	13.2	24.4	29.8	27.3	22.8	15.9	17.0	15.7	37.7	25.4	39.0	33.8	25.4
B-5	1	12.9	25.0	20.8	28.8	25.9	11.7	13.2	12.6	51.2	31.1	35.1	35.0	28.3
	2	12.8	24.8	18.2	29.1	24.7	12.7	13.9	14.3	36.2	22.9	32.1	31.0	29.8
	3	13.9	25.1	20.8	30.1	23.7	14.9	9.8	15.1	34.8	22.6	37.4	33.0	29.0
	4	15.2	26.4	20.3	30.9	24.8	16.9	12.5	16.4	34.4	23.5	38.2	35.5	32.3
	5	13.1	24.9	20.6	29.1	25.1	15.0	14.2	16.1	33.3	21.7	40.5	35.7	28.1

[a] Obtained from oxygen meter readings, corrected for meter calibration; see text [b] No data taken; interpolated value

cussed earlier in connection with the method of calculating the average gas temperature at the furnace outlet, are amply illustrated by the temperature-distribution plots for tests 1 and 6.

The distribution plots for other tests may readily be constructed from the data of Tables 2 and 4.

Due to the arrangement of the sampling doors with respect to the screen-tube bank, it was expedient to measure the gas temperatures after the screen either directly over the center line of the tubes or directly above the lanes between the tubes. To settle any question that the gas temperature at a given position would depend upon the location of the thermocouple with respect to the tubes, average temperatures above the tubes were compared with average temperatures above the lanes, and no significant difference was found.

TABLE 5 CORRECTIONS TO BE ADDED TO OBSERVED TEMPERATURES TO CONVERT TO B&W MHVT BASIS. ASME FURNACE HEAT-ABSORPTION TESTS. BOILER NO. 1, WILLOW ISLAND STATION

Observed temp, deg F	Correction, deg F[a]	Observed temp, deg F	Correction, deg F[a]
1600	0	2100	39
1700	7	2200	47
1800	15	2300	55
1900	23	2400	62
2000	31	2500	70

[a] Includes deviation of particular couple from standard tables.

Furnace Heat-Absorption Efficiency. The calculated furnace heat-absorption efficiency is plotted in Fig. 6 against excess air for several combinations of the other variables. An average value for the net heat available was chosen as a parameter for each load condition, high, medium, and low. The actual net heat available varied slightly, but since the furnace heat-absorption efficiency is not sensitive to these variations, this procedure was considered to be satisfactory.

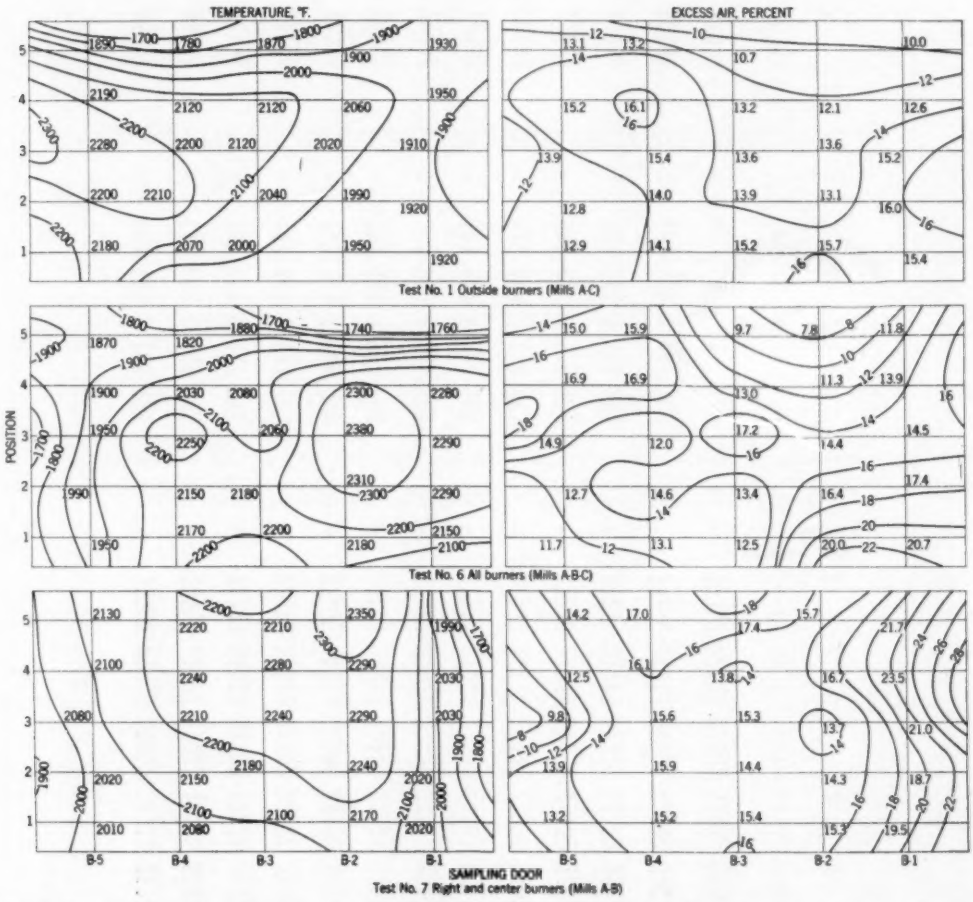

FIG. 5 DISTRIBUTION OF TEMPERATURE AND EXCESS AIR AT FURNACE OUTLET FOR FULL-LOAD TESTS WITH THREE DIFFERENT BURNER COMBINATIONS

(Measurements made on gas after passing through screen.)

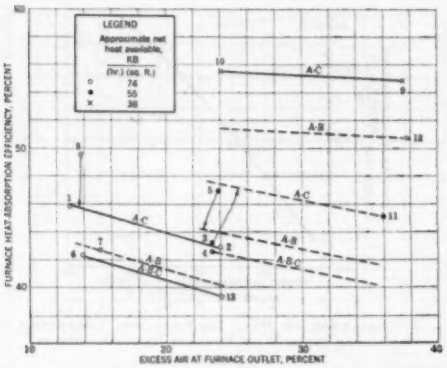

FIG. 6 FURNACE HEAT-ABSORPTION EFFICIENCY AS AFFECTED BY EXCESS AIR, NET HEAT AVAILABLE IN FURNACE, AND LOCATION OF BURNERS USED
(Numbers designate tests; letters designate burners used.)

At full load there were sufficient consistent data to establish the relation between heat-absorption efficiency and excess air. At medium load, however, a rational correlation is impossible, and it was concluded that variables other than those considered must have an important influence on the heat-absorption efficiency. Accordingly, the curves at medium load were constructed on the basis of previous experience with this type of correlation, rather than from the calculated results, and it is expected that the actual results would fall on these curves if all the conditions had been the same as for the high-load tests. Although the data at low loads also are insufficient for definite conclusions, the slope of the curve for tests 9 and 10 appears reasonable, being somewhat less than that at full load.

Although there are enough data at high loads to indicate that three-mill operation gives lower efficiency than using A and C, the effect of operating mills A and B is in doubt, the location of the A-B curves being determined from points 7 and 12, and the position of point 7 relative to A-C and A-B-C at full load. From the full-load tests, at least, it is apparent that the effect of excess air is independent of burner arrangement, the curves having the same slope, and this relation was used in constructing the other curves.

The discrepancies noted for tests 3, 5, and 8 may result from slag and ash accumulation or flame shape and area. These possibilities will be considered further later in the paper.

CORRELATION OF RESULTS

A condensed summary of test data and of results necessary for correlation is presented in Table 6, which includes furnace heat absorption and furnace heat-absorption efficiency corrected to clean wall conditions by use of effectiveness factors from Part II.

Relation Between Furnace Heat Absorption and Steam-Generating Duty. To seek a possible explanation for the poor correlation between furnace heat-absorption efficiency and operating variables for tests 3, 5, and 8, the furnace heat absorption calculated from the heat balance was compared with the heat required for steam generation. The heat absorbed by the steam was calculated from the enthalpy of the saturated steam at drum pressure, the enthalpy of the feedwater, and the total steam-flow rate, corrected for the attemperator water flow rate. These calculations were made from data reported in Part II, and the results are shown in Table 6 and Fig. 7. The heat required for steam generation is not equal to the furnace heat absorption for any of the tests owing to a consistent amount of heat absorption by the screen tubes, by the rear surface of the division wall, and by extended evaporating surface beyond the economizer. It is readily seen from the figure that the percentage of total evaporation occurring in the furnace is approximately 88.5 at full load, 90.0 at three-quarters load, and 93.2 at half load.

It will be noticed that good correlation occurs for all the tests except No. 8, suggesting the possibility that errors were made in the determination of heat absorption by the heat-balance data for this test. On the other hand, the good agreement for tests 3 and 5 shows the heat-absorption determination to be as reliable as that for the other tests, and the lack of correlation of heat-absorption efficiency with operating conditions for these two tests, shown in Fig. 6, was probably due to slag and ash deposits, or peculiarities of flame size and shape. Accordingly, the heat-absorption efficiencies were converted to theoretically clean conditions for subsequent correlations by the use of "effectiveness factors" reported in Part II, and obtained by the method of Mumford and Bice.[19]

Effect of Slag and Ash on Furnace Performance. The furnace heat-absorption efficiency, corrected to clean wall conditions, is shown in Fig. 8 as a function of operating conditions. The general trend of all the data was considered in constructing the figure. For example, the curve for operation with burners A-C at high load was located by test No. 1 only, in order that the relative positions of the three lines representing different burner arrangements would be consistent with the relative positions of the three corresponding curves at medium load. Test 8 was not used because the comparisons made in Fig. 7 suggested that it may be less reliable than the other tests. The slope of the A-C curve at full load was established by the slope of the A-B-C line at the same load. Similarly, the other curves through single points were constructed in such a manner that their slopes would be consistent with the slopes of the more completely defined curves. It will be seen that the slopes decrease with decreasing load, that is, the effect of excess air on furnace heat-absorption efficiency is less pronounced at the low loads.

Considerable improvement in correlation is noted for tests 3 and 5, although there is no change in test 8, and test 2 shows poor agreement in contrast with the results shown in Fig. 6. This discrepancy for test 2 may have been introduced by the interpretation of the slag and ash data, which consisted of qualitative descriptions of the amount and distribution of ash on the furnace walls, rather than quantitative measurements. The effect of burner arrangement shows better correlation, except at low loads, the heat-absorption efficiencies with mills A-B and with mills A-C being closer to each other and somewhat higher than the efficiency with all burners in service. At low loads, however, higher efficiencies are noted for burners A-C than for A-B, while for other load conditions the opposite is true.

The relationship between the variables can, perhaps, be more simply represented by Fig. 9 which shows the effect of net heat available on furnace heat-absorption efficiency for different burner arrangements and values of excess air. Data used in the construction of the curves were obtained from Fig. 8. The lower portion of the figure shows the heat-absorption efficiency with different burner arrangements at a single value (24 per cent) of excess air, while the upper part gives corrections to be added for operation at any excess-air value within the limits observed in the tests.

Data were available only at the points indicated and the

[19] "An Investigation of the Variation in Heat Absorption in a Pulverized-Coal-Fired Water-Cooled Steam-Boiler Furnace. IV—Comparison and Correlation of the Results of Furnace Heat-Absorption Investigations," by A. R. Mumford and G. W. Bice, Trans. ASME, vol. 70, 1948, pp. 601–614.

TABLE 6 CONDENSED SUMMARY OF OPERATING CONDITIONS AND RESULTS. ASME FURNACE HEAT-ABSORPTION TESTS. BOILER NO. 1. WILLOW ISLAND STATION

		1	2	3	4	5	6	7	8	9	10	11	12	13
1	Test number													
2	Steam generation, M lb per hr	508	508	376	377	373	508	510	507	257	251	364	259	508
3	Burner and pulverizer arrangement, (see text)	A-C	A-C	A-C	A-B-C	A-B	A-B-C	A-B	A-C	A-C	A-C	A-C	A-B	A-B-C
4	Excess air at furnace outlet, per cent	13.0	24.0	23.4	23.4	23.9	13.9	15.2	13.8	37.5	24.1	36.0	37.9	24.1
5	Net heat available in furnace, kB/(hr)(sq ft)	73.1	74.4	55.5	55.2	54.1	72.0	74.6	73.5	38.5	37.1	54.2	39.8	74.3
6	Heat absorption in furnace, kB/(hr)(sq ft)	33.5	31.9	24.0	23.5	25.4	30.5	31.9	36.4	21.1	20.6	24.4	20.1	29.2
7	Furnace heat-absorption efficiency, per cent	45.8	42.9	43.2	42.6	47.0	42.3	42.7	49.5	54.8	55.5	45.1	50.7	39.3
8	Heat absorption in furnace, millions of Btu/hr	294	280	211	207	223	268	280	320	185	181	214	177	256
9	Heat required for generation of saturated steam, millions of Btu/hr	324	314	238	239	246	305	312	332	194	191	231	194	291
10	Furnace heat absorption Effectiveness Factor[a]	0.92	0.89	0.84	0.89	0.89	0.91	0.85	0.90	0.99	0.98	0.96	0.97	0.93
11	Furnace heat absorption, corrected to clean conditions, kB/(hr)(sq ft)	36.4	35.8	28.6	26.4	28.5	33.5	37.5	40.4	21.3	21.0	25.4	20.7	31.4
12	Furnace heat-absorption efficiency, corrected to clean conditions, per cent	49.8	48.2	51.5	47.9	52.8	46.5	50.2	55.0	55.3	56.6	47.0	52.3	42.3
13	Average temperature of gas at furnace outlet, deg F[b]	2202	2150	2138	2155	2018	2298	2278	2042	1690	1691	1935	1722	2264
14	" " " " " " , T_o, deg R	2662	2610	2598	2615	2478	2758	2738	2502	2080	2151	2395	2182	2724
15	$\left(\frac{T_o}{1000}\right)^4$	50.2	46.4	45.6	46.8	37.7	57.9	56.2	39.2	18.7	21.4	32.9	22.7	55.1

[a] Data from Part II [b] Ahead of screen tubes, calculated by method described in text

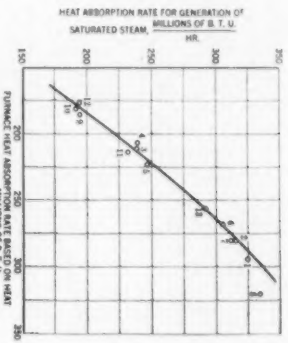

FIG. 7 COMPARISON OF HEAT REQUIRED FOR GENERATION OF SATURATED STEAM WITH FURNACE HEAT ABSORPTION (Numbers designate tests.)

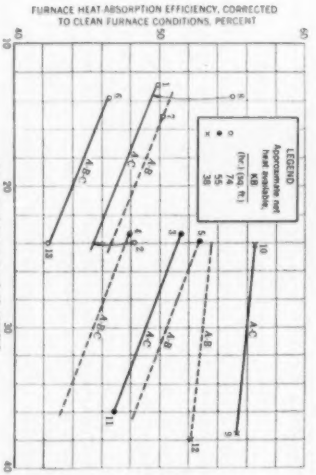

FIG. 8 FURNACE HEAT-ABSORPTION EFFICIENCY, CORRECTED TO CLEAN FURNACE CONDITIONS, AS AFFECTED BY EXCESS AIR, NET HEAT AVAILABLE IN FURNACE, AND LOCATION OF BURNERS USED (Numbers designate tests; letters designate burners used.)

dotted portions of the correction curves were located approximately by extrapolation, the magnitude of the corrections depending upon the slope of the curves in Fig. 8.

The heat-absorption efficiencies are for theoretically clean wall conditions, from which the actual efficiency at any condition may be found by multiplying by the appropriate effectiveness factor.

The reversal of the relative positions of the A-B and A-C curves in Fig. 8 is clearly shown by the crossing of the curves in Fig. 9 between medium and low load. The shape of the A-C curve agrees well with the curve of Broido, reported by Wohlenberg and Mullikin,[11] which shows a nearly linear relation between heat-absorption efficiency and heat input over the limited range of heat input shown in Fig. 9. For this reason, and the fact that the point on the A-C curve at low load was established by two tests while the A-B point was determined from one, it was assumed that the heat-absorption efficiency for the single test was influenced by some factor peculiar to this particular test. Actually this could be a condition which is inherent in all the low-load tests, but is compensated for in the A-C tests by an increase in the convection heat transfer when the burners near the side walls are used. Since it is unlikely that an appreciable error could be made in the slag and ash effectiveness factor for the nearly clean furnace conditions which occurred at all low-

[11] "Review of Methods of Computing Heat Absorption in Boiler Furnaces," by W. J. Wohlenberg and H. F. Mullikin, Trans. ASME, vol. 57, 1935, pp. 531–540.

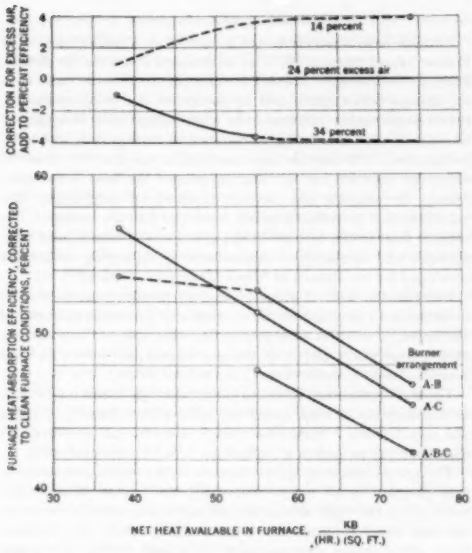

FIG. 9 EFFECT OF OPERATING CONDITIONS ON FURNACE PERFORMANCE

load tests, it is necessary to consider the effect of flame emissivity shape, and area for an explanation. However, since these factors are not amenable to quantitative evaluation at present, their effect upon heat absorption in cases where the flame does not fill the furnace can be estimated only by empirical methods.

Correlation Based Upon Radiant-Heat Transfer. Although several empirical equations have been proposed during the past 50 years to serve as a guide in furnace design, and in predicting furnace performance, it is generally agreed that none is applicable in all cases, which arises from the fact that not all the variables are or can be considered. The Wohlenberg method[11] takes into account the largest number of fundamental and independent parameters, but its usefulness is impaired by the inability either to predict in advance, or to measure accurately on operating units, such factors as area, volume, and emissivity of luminous flames, and the deposits of ash on furnace walls.

Nevertheless, certain empirical equations are useful for evaluating furnace heat absorption in terms of experimental data, and if full cognizance is taken of their limitations, the effect of certain variables can be more clearly interpreted. The simplest expression is that based on the Stefan-Boltzmann law, and proposed by other investigators.[12,13]

It is shown by Mullikin[13] that this is a rational treatment because empirical corrections are not great for a diversity of fuel types and firing arrangements.

The form of this expression used in the present investigation can be represented by the following equation

$$q = k\left[\left(\frac{T_o}{1000}\right)^4 - \left(\frac{T_w}{1000}\right)^4\right] \quad \ldots\ldots\ldots\ldots [2]$$

where

q = furnace heat absorption, KB/(hr)(sq ft)[14]
T_o = mean temperature of gases at furnace outlet, deg R
T_w = mean temperature of furnace walls, deg R
k = constant

Use of a mean radiant temperature between the adiabatic flame temperature and the exit-gas temperature is more desirable theoretically,[15] but the furnace-outlet temperature is used in this study because of its greater convenience and because it is doubtful that pulverized-coal flames reach adiabatic temperature in commercial practice.

Fig. 10 shows the furnace heat absorption, based on clean wall conditions, plotted against the fourth power of the absolute average temperature of the furnace-outlet gases. Although clean conditions did not actually occur in this investigation, it can be assumed that the same gas temperatures as observed in the tests could be maintained for clean conditions with a slightly greater heat-input rate without affecting the accuracy of this analysis. For comparison, the theoretical black-body radiation from a source at the average furnace-outlet temperature to clean furnace walls is also shown in the figure. For this comparison the walls were assumed to be at a uniform temperature of 1100 R, which is high enough to allow for the temperature drop through the wall tubes.

[14] KB = 1000 Btu

[15] "Absorption of Heat by Walls of a Furnace," by John Blizard, ASME Furnace Performance Factors Pamphlet, May, 1944, pp. 79–82. Bound with vol. 66, Trans. ASME, 1944.

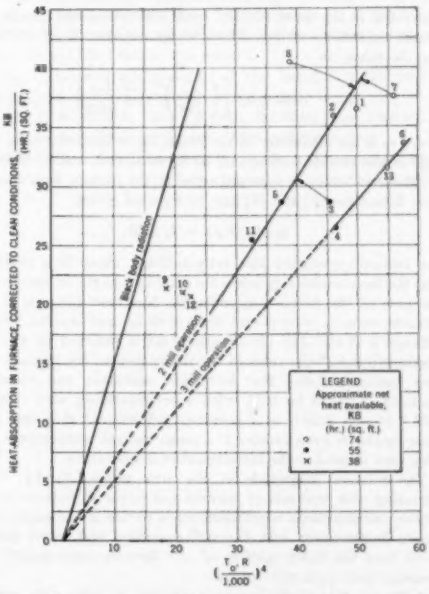

FIG. 10 CORRELATION OF HEAT TRANSFER IN FURNACE WITH FOURTH POWER OF ABSOLUTE TEMPERATURE OF GASES AT FURNACE OUTLET
(Numbers designate tests.)

[12] "An Investigation of Powdered Coal as Fuel for Power-Plant Boilers," by Henry Kreisinger, John Blizard, C. E. Augustine, and B. J. Cross, U. S. Bureau of Mines Bulletin No. 223, 1923.

[13] "Evaluation of Effective Radiant Heating Surface and Application of the Stefan-Boltzmann Law to Heat Absorption in Boiler Furnaces," by H. F. Mullikin, Trans. ASME, vol. 57, 1935, pp. 517–529.

The data can be fairly well represented by straight lines through the origin, that is, the point corresponding to the wall temperature, if the low-load tests are not considered. The low-load tests do not fit as well as the others, possibly because convection heat transfer accounts for a larger portion of the total heat absorption at the lower loads, and the furnace-outlet temperature used is farther from the mean radiant temperature. In addition, the furnace-outlet temperature ahead of the screen, which was calculated from heat-transfer rates to the screen, may be slightly in error owing to varying amounts of ash deposited on the screen tubes. While this error may have a relatively small effect on heat-absorption efficiency, it could have considerable magnitude when raised to the fourth power.

No distinction can be made in this figure between operation with mills A-C and operation with mills A-B, the data being insufficient and lacking the requisite degree of accuracy for any conclusions in this respect, but the difference between two-mill and three-mill operation is definitely indicated.

It will be noticed that the unit heat-transfer rate is considerably less than that calculated for a black body at the temperature of the gases at the furnace outlet, as shown by the reference line in Fig. 10. If the curves through the test points be represented by Equation [2], the value of k for two-mill operation is 786 and for three-mill operation 588, both being considerably lower than the theoretical radiation constant. For a similar case, it was shown by Corey and Cohen[5] that this deviation was due primarily to a flame area appreciably smaller than the furnace-wall area.

If the total heat absorption in the furnace is considered

$$Q_W = kA_W\left[\left(\frac{T_o}{1000}\right)^4 - \left(\frac{T_W}{1000}\right)^4\right] \quad [3]$$

where Q_W is the total furnace heat absorption and A_W is the area of the furnace walls. The total net radiation from the flame may be taken as

$$Q_F = 1730\,\epsilon_F A_F\left[\left(\frac{T_o}{1000}\right)^4 - \left(\frac{T_W}{1000}\right)^4\right] \quad [4]$$

where ϵ_F is the emissivity of the flame, A_F is the flame area, and 1730 is the radiation constant, all in consistent units. Then, if the flame radiation is assumed equal to the furnace heat absorption, Equations [3] and [4] may be equated giving

$$\epsilon_F(A_F/A_W) = k/1730$$

For two-mill operation this ratio is 0.45. Since it is probable that the flame emissivity is less than 1.0 and, as stated previously, the area of the flame is considerably less than the area of the furnace walls, it is apparent that both ϵ_F and A_F/A_W will lie between 0.45 and 1.0. If a value of 0.9 is assumed for ϵ_F from Sherman's data,[3] the ratio of the flame area to the furnace-wall area becomes 0.50. For three-mill operation the value of $\epsilon_F(A_F/A_W)$ would be 0.34, with a corresponding area ratio of 0.38. It was shown in a previous publication[5] that this area ratio would be even smaller if a mean radiant temperature had been used instead of the furnace-outlet temperature.

The relative magnitude of the area ratios, A_F/A_W, when operating with two sets of burners and when all burners are in service, substantiates conclusions made earlier in the paper, that longer flames occur with two-mill operation and travel farther down into the lower portion of the furnace, consequently increasing flame area and volume.

Although this study has been limited in scope, the results emphasize the fact that ash deposits and flame path and volume are exceedingly important, and their consideration is essential in evaluating the heat transfer in furnaces.

Summary and Conclusions

Furnace heat absorption was measured in a boiler furnace at Willow Island Station, W. Va., in co-operation with the ASME Furnace Performance Factors Committee, to provide basic data on furnace performance and to determine the relationship between heat-transfer rates and the temperature drop through the wall tubes, the latter being determined concurrently by other investigators. The furnace heat absorption was determined as the difference between the net heat input and the heat losses comprising the sensible heat in the products of combustion and radiation and convection losses from the furnace casing. The sensible heat in the furnace-outlet gases was obtained from temperature and composition measurements, employing techniques developed by the Bureau of Mines for furnace testing.

Because the lack of suitably located access doors prevented accurate determination of the average gas temperature ahead of the screen, it was necessary to calculate this quantity from a complete temperature survey of the gas leaving the screen and the computed heat-transfer rates to the screen tubes.

Thirteen tests were made to determine the effect on furnace heat absorption of load, excess air, burner arrangement, and slag and ash deposits. Only two values of excess air were used at each load due to capacity limitations of the forced-draft fans.

The gas temperature at the furnace outlet varied considerably with position in all tests. Generally, the highest temperature occurred on the right side of the furnace outlet and the lowest on the left when symmetrical burners (A-C) were in operation. With other burner arrangements (A-B and A-B-C), the maximum temperature occurred between the center and left side, and the minimum usually occurred between the center and right side. In several tests, particularly those with all burners in service, very low temperatures were observed near the division wall, which was ascribed to low gas velocities or eddy currents. Disregarding the low points at the division wall, the spread in the temperature of the exit gases varied from 200 to 460 deg F, the smallest occurring consistently in tests when mills A and B were in operation. It was concluded that the temperature-distribution patterns at the furnace outlet have a complex relationship with distribution of fuel and air to the burners, the velocity and path of the gas between the burners and the furnace outlet, and the location and extent of ash deposits on the walls.

The excess-air distribution also varied considerably with position. The minimum values occurred to the right of the center when operating with burners at the center and one side (mills A and B) and on the left of the center for the other burner arrangements. The maximum spread in values of excess air occurred during the low-load tests and the spread was a minimum in the full-load tests, using symmetrical burner arrangement (mills A-C). The maximum excess air is not significant due to leakage of air near the walls. It was concluded that there was nonuniform distribution of fuel and air to the burners, but any condition tending to produce longer flames of higher velocity would improve mixing of the gases and result in more uniform oxygen content.

Good agreement was noted, except for one test, between the furnace heat absorption calculated from heat-balance data and the heat required for generation of steam. Approximately 90 per cent of the evaporation occurs within the furnace, excluding the screen. However, correlation of the heat-absorption efficiency with operating variables was unsatisfactory. Accordingly, the heat-absorption efficiencies were corrected to theoretically clean wall conditions by the use of slag and ash effectiveness factors, which ranged from 0.84 at high load to 0.99 at low load. This procedure eliminated the effect of one variable and provided a more rational correlation. The maximum corrected furnace heat-absorption efficiency was 56.6 per cent at half load,

when operating with mills A and C and 24 per cent excess air. The lowest efficiency, 42.4 per cent, was obtained at full load with 24 per cent excess air and with all burners in service.

The furnace heat-absorption efficiency decreased with an increase of excess air in all cases, the decrease being more pronounced at the higher loads. For example, when the excess air increased from 14 to 24 per cent at full load, the efficiency decreased from 49.4 to 45.4 per cent. However, at half load an increase from 24 to 34 per cent excess air caused a decrease in efficiency from 56.6 to 55.6 per cent. Pulverizers A and C were in operation in both cases. Although it is not entirely conclusive, there is evidence that the effect of excess air on the heat-absorption efficiency is independent of the location of the burners in operation.

The burner arrangement has the same effect on efficiency at both high and medium loads. For example, at 24 per cent excess air, and at both load conditions, the efficiency with mills A and B is about 1.3 per cent higher than with A and C, and about 3.6 per cent higher than with all burners in service. At half load, however, the heat-absorption efficiency is higher with mills A and C than it is with mills A and B. This may be due to greater importance of convection heat transfer at low loads.

With all other conditions held constant, the heat-absorption efficiency decreased with increased values of net heat available, the relation being linear when burners A-C were used. With this burner arrangement, and with 24 per cent excess air, the efficiency varied from 56.6 to 45.4 per cent at unit net heat-input rates of 38 and 74 KB per hr, respectively.

The furnace heat absorption at medium and high loads was considerably lower than the theoretical radiation heat transfer from a black body with the area of the furnace walls and at the temperature of the gases at the furnace outlet. The actual heat absorption was 45 and 34 per cent of the theoretical radiation for two-mill and three-mill operation, respectively. It was concluded that these low values are due primarily to the flame being smaller in area than the furnace walls. If a flame emissivity of 0.9 is assumed, the ratio of flame area to wall area would be 0.50 in the case of two-mill operation. If the true mean flame temperature had been used, the ratio would have been even smaller. However, the mean radiant temperature can only be calculated readily when the fuel burns adiabatically, and it is doubtful if this ever occurs in pulverized-coal-fired furnaces.

This study shows the feasibility of a relatively simple correlation of the furnace heat absorption with a single variable, that is, temperature of the gases at the furnace outlet, and how this correlation may be used to evaluate the effect of other factors, such as flame area and emissivity. However, this is an empirical treatment at best, based upon dependent variables, and indicates that, in predicting furnace performance, it is of paramount importance to understand more fully how fundamental variables control the flame shape, ash deposits, and furnace-outlet temperature. The fundamental variables include furnace geometry, firing method, burner location, and fuel and air distribution.

Acknowledgments

The authors gratefully acknowledge, with appreciation and thanks, the contributions to this investigation made by the following:

The ASME Special Research Committee on Furnace Performance Factors, for the opportunity to participate in this project, and the individual committee members who gave advice and help whenever required.

Dr. A. C. Fieldner, Chief, Fuels and Explosives Division, and Dr. R. L. Brown, Coal Technology Coordinator, Coal Branch, Bureau of Mines, who authorized the Bureau's work and who made many helpful suggestions.

Mr. Paul Cohen, formerly Fuel Engineer, Combustion Research Section, for assistance and valuable suggestions in planning the test program and analyzing the test results.

Mr. C. B. Withers, Superintendent, and Mr. H. L. Webner, Plant Engineer, Monongahela Power Company, and their staff, for willing and able assistance in preparing for, and in conducting the tests.

The engineers and assistants of the Combustion Research Section: Messrs. J. Jonakin, C. H. Schwartz, J. J. Pfeiffer, and G. R. Kollar, who capably performed the difficult test work that formed the basis of this paper.

Dr. C. B. Anderson, formerly of The Babcock & Wilcox Company, for assistance in conducting the tests.

Mr. L. Hankison, formerly with the West Penn Power Company, for assigning personnel to assist in the test work.

The Bailey Meter Company, for the loan of a recording oxygen meter.

Furnace Heat Absorption in Pulverized-Coal-Fired Steam Generator, Willow Island Station

Part II Variation in Heat Absorption as Shown by Measurement of Surface Temperature of Exposed Side of Furnace Tubes

By F. G. ELY[1] AND N. H. TWYMAN,[2] ALLIANCE, OHIO

During the month of June, 1949, a series of thirteen furnace tests were conducted at Willow Island Power Station, a new plant on the system of The Monongahela Power Company, located at Willow Island, West Va. The test program was carried out under the auspices of the ASME Special Research Committee on Furnace Performance Factors, and represents the third in a sequence of field investigations undertaken by the committee for direct measurement of operating performance of commercially important furnace types, previous tests having been conducted at Tidd Station[3] in 1945, and at Paddy's Run Station[4] in 1947 and 1948. A companion paper[5] describing the tests at Willow Island, deals with the measurement of over-all furnace heat absorption by heat-balance method. The present paper is concerned with supplementary and independent measurements of furnace heat absorption obtained from special thermocouples installed in the furnace wall tubes.

TO those familiar with the problems of furnace design it is apparent that the prediction of furnace heat absorption has not yet been resolved to a fundamental basis, nor to clearly rational methods of calculation. The need for proceeding in advance of rational treatment calls for the use of empirical design factors which, in the past, have in some cases been very inadequate, although there is much evidence that recent design has been greatly improved through the better knowledge of values accumulated by experience and by test measurements comparable to those now being developed by the committee. Procurement of such data requires the use of special instrumentation and procedures which are not commonly available nor appreciated and which, in fact, are still in need of improvement.

Because of this situation, the committee has undertaken the program of developing such methods, and of measuring the performance of full-scale operating units in order to make these data available to the profession as a step toward practical advancement of the art of boiler-unit design, and to afford better ground work for an ultimate rational solution of the problem.

In a steam-generating unit the furnace structure serves not only as a boundary of the combustion space, but in present-day design, comprises a major portion of the steam-generating surface, and performs the important function of reducing the temperature of combustion products to acceptable values for entrance to the superheater. With close limitations on final steam temperature, it is apparent that the proportioning of heat-absorbing surface of furnace and superheater is critical, and that deviations in the functioning of either of these components must be accounted for quantitatively and provision made for positive compensation in the daily operation of the unit.

For this series of tests a plan of operation was outlined which would include the effects of major controllable factors such as variation of load and excess air, with various practical combinations of burners in service. The more obscure and less controllable factors of ash behavior were observed and noted as qualifying features of the tests.

Over-all measurement of furnace heat absorption was accomplished by the well-known heat-balance method, based upon traverses showing gas composition and temperature at the furnace outlet as reported in a companion paper, Part I of this report.[5]

Supplementary tests, showing the distribution of furnace heat absorption, were made by completely independent means of measurement, using a "sampling" arrangement of special thermocouples, installed in the furnace-wall tubes in such a manner that the temperature drop through the tube metal could be evaluated, at least relatively, in terms of heat flux. The present paper, Part II of the formal report, deals with this phase of the Willow Island tests, and includes further correlation of data from the

[1] Research Engineer, Research & Development Department, The Babcock & Wilcox Company. Mem. ASME.

[2] Test Engineer, Research & Development Department, The Babcock & Wilcox Company. Jun. ASME.

[3] "An Investigation of the Variation in Heat Absorption in a Pulverized-Coal-Fired, Water-Cooled Steam Boiler Furnace," by L. B Schueler, et al., Trans. ASME, vol. 70, 1948, pp. 553–619.

[4] "Furnace Heat Absorption in Paddy's Run Pulverized-Coal-Fired Steam Generator, Using Turbulent Burners, Louisville, Ky.," Parts I, II, and III, Trans. ASME, vol. 72, October, 1950; Part I, by R. I. Wheater and M. H. Howard, pp. 893–923; Part II by R. C. Corey and Paul Cohen, pp. 925–935; Part III by H. H. Hemenway and R. I. Wheater, pp. 937–944.

[5] "Furnace Heat Absorption in Pulverized-Coal-Fired Steam Generator, Willow Island Station, Part I Furnace Heat-Absorption Efficiency as Shown by Temperature and Composition of Gases Leaving the Furnace," by J. W. Myers and R. C. Corey, presented at the Annual Meeting, New York, N. Y., November 26–December 1, 1950, of THE AMERICAN SOCIETY OF MECHANICAL ENGINEERS.

Contributed by the Research Committee on Furnace Performance Factors, and Fuels, Power, and Heat Transfer Divisions and presented at the Annual Meeting, New York, N. Y., November 26–December 1, 1950, of THE AMERICAN SOCIETY OF MECHANICAL ENGINEERS.

NOTE: Statements and opinions advanced in papers are to be understood as individual expressions of their authors and not those of the Society. Manuscript received at ASME Headquarters on September 26, 1950. Paper No. 50—A-82.

[6] "Comparison and Correlation of Results of Furnace Heat-Absorption Investigations," by A. R. Mumford and G. W. Bice. Trans. ASME, vol. 70, 1948, pp. 601–614.

two methods of measurement. Consideration is also given to the effects of ash deposits, making use of the S-A factors developed in an earlier committee report.[6]

Description of Equipment

The boiler on which tests were conducted is a component part of the 40,000-kw single-boiler single-turbine initial installation at Willow Island Station, and was first placed in service February 20, 1949.

This unit, illustrated in Fig. 1, was designed for a steam-generating capacity of 500,000 lb per hr at 1350 psi and 950 F at the superheater outlet, with feedwater temperature of 416 F to the economizer. It is equipped with a completely water-cooled hopper-bottom furnace and is direct-fired by three pulverizers serving six multitip intertube burners located in the furnace

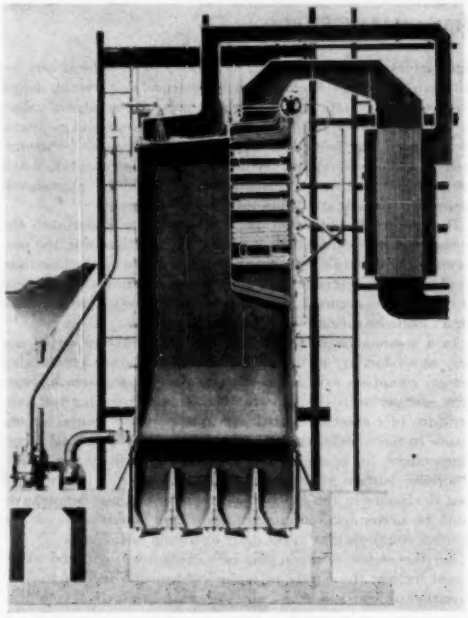

Fig. 1 Side Sectional View of Willow Island Unit

roof, and firing downwardly. The products of combustion leave the furnace by way of a bank of wide-spaced screen tubes and enter the convection superheater and economizer pass in vertically upward flow, then passing to a tubular air heater with gas flowing downward through the tubes and being delivered to a mechanical dust separator, induced-draft fan, and stack. Air from the forced-draft fans, after making four passes over the air-heater tube bank, is delivered as preheated air to the burner wind box at the top of the furnace. Preheated air and cold tempering air are supplied to the pulverizers, in controlled proportions, for drying the fuel.

Feedwater, entering the lower header of the economizer, is delivered with upward flow to the main steam drum. Saturated steam from the drum enters the upper header of the primary superheater, and flows countercurrent to the gases, leaving at the lower header and passing to the attemperator where feedwater, in the form of direct-contact spray, is used for interstage temperature regulation. Steam from the attemperator enters the lower header of the secondary superheater, passing through two loops of widely spaced elements and then through the remaining bank of closely spaced elements in parallel flow with the gases, to final discharge from the upper header of the secondary superheater. Final steam temperature is controlled by the amount of water used in the spray attemperator. Attemperating water is metered separately, but is included as an integral part of the total metered quantities of feedwater supply and superheated-steam output of the unit.

Raw coal from the plant bunker is delivered through automatic scales to three pulverizers, each of which serves two of the six burners arranged in a single row across the width of the furnace roof. The pulverizers are designated A, B, and C, as read from right to left and later referred to in this report. Pulverizer capacity is designed to permit operation of the furnace at full load with one pulverizer out of service.

In general dimensions the furnace is 25 ft inside width between vertical side walls, × 75 ft height between burners and hopper throat, with a depth of 22 ft from front wall to division wall in the upper part of the furnace, and 36 ft from front wall to rear wall of the lower part of the furnace. The hopper floors are sloped at an angle of 55 deg from horizontal.

Furnace construction consists of 3-in-OD bare water-cooled tubes on 3-in-center spacing in the four vertical walls and sloping hopper floors. Roof tubes are 3 in. OD, spaced on 6-in. centers, with flat-stud construction, forming a closed surface external to the wind box. The furnace-outlet screen is arranged in two staggered rows of two tubes each on 12-in. lateral spacing. Convection pass side walls and rear wall are water-cooled by tubes on 6-in. centers, backed by tile. Tubes of the division wall are arranged to form a small bank of generating surface at the top of the convection pass.

Retractable soot blowers are installed at the cavity spaces below and above the secondary superheater. No wall-cleaning blowers are provided in the furnace. Inspection or lance doors are located at three elevations at the corners of the furnace proper and at five positions across the rear wall above the furnace outlet screen. All test traverses of furnace-exit-gas temperature were taken at this latter set of doors.

Wall-Tube Thermocouples

Furnace-wall-tube thermocouples were installed during the course of erection of the new boiler unit. The pattern of thermocouple location is shown in Fig. 2, wherein the wall areas are represented as an unfolded or developed figure as viewed from the inside of the furnace. A total of 124 thermocouple stations are indicated, and these were connected by external lead wires to a Leeds and Northrup Speedomax recorder equipped with the special selector switch bank, used on previous committee tests, which permitted scanning the entire group of couples in approximately 24-min cycles. Thermocouple designations, used in Fig. 2, represent the corresponding printing points on the recorder chart.

The general pattern of thermocouple placement was intended to provide a sampling of the furnace-wall areas for measurement of, and to show the distribution of, heat-absorption rate. Some departure from previous practice was made in the type of thermocouple used for this purpose, in deference to the method developed by the boiler manufacturer for tube-thermocouple installation. Details of the thermocouple used are illustrated in Fig. 3. In this method, the thermocouple hot junction is formed by separately peening 22-gage chromel and alumel wires into notches cut by a sharp chisel in the tube surface center line exposed to the furnace. The Fiberglas insulated wires are extended

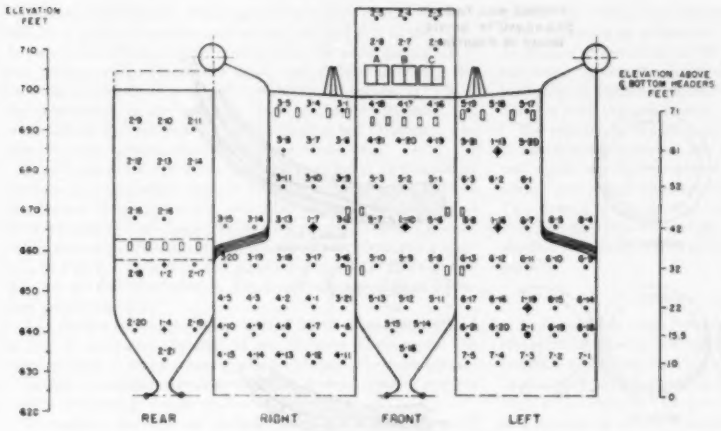

FIG. 2 (*left*) THERMOCOUPLE LOCATION DIAGRAM

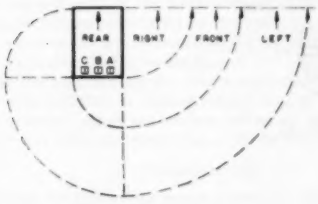

PLAN SHOWING DEVELOPMENT AND DIRECTION OF VIEWING FURNACE WALLS.

- FURNACE WALL DOORS.
- CHORD-HOLE TYPE SURFACE THERMOCOUPLE.
- GUARD RING AND CHORD-HOLE COMPARISON THERMOCOUPLES.
- CHORD-HOLE SURFACE AND DEPTH THERMOCOUPLE, AND GUARD RING THERMOCOUPLE.
- CHORD-HOLE SURFACE AND DEPTH THERMOCOUPLES.
- BURNERS A B C

FURNACE WALL TUBES
3" O.D. X 0.240" TH. SA-210
SPACED ON 3" CENTERS

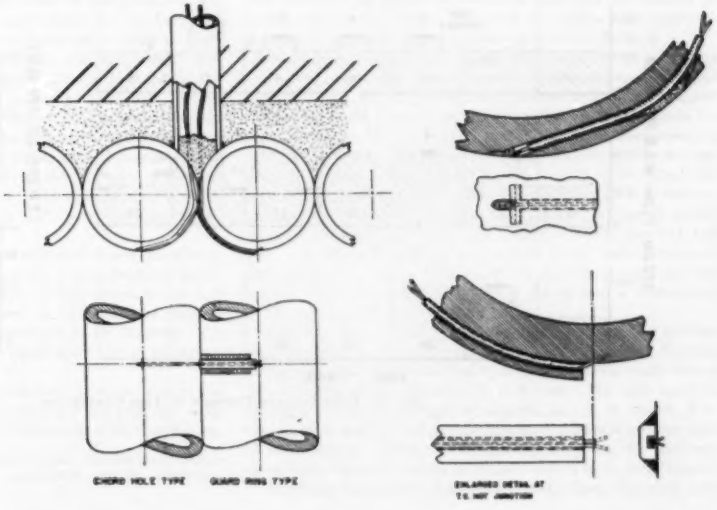

FIG. 3 (*right*) DETAILS OF TUBE-SURFACE THERMOCOUPLES

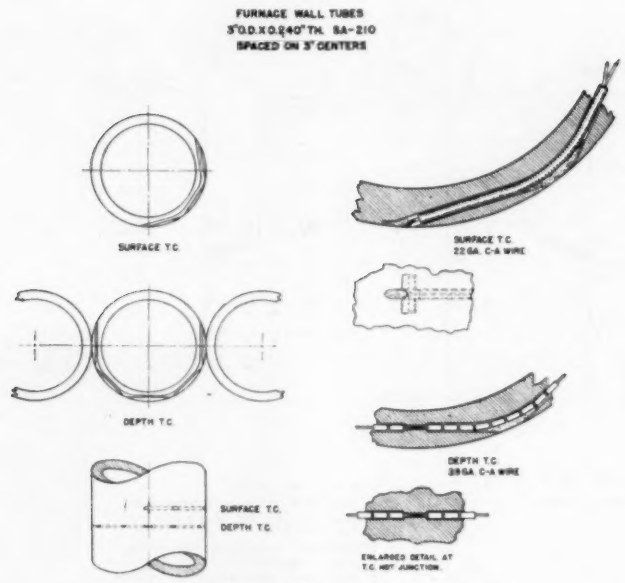

FIG. 4 DETAILS OF GRADIENT THERMOCOUPLES

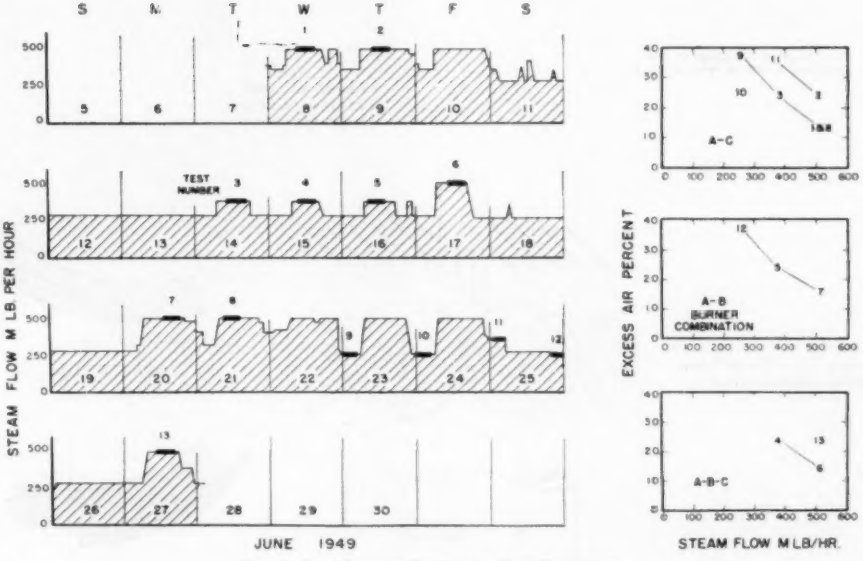

FIG. 5 LOAD LOG AND PATTERN OF TEST CONDITIONS

through a series of holes, drilled as chords in the metal of the tube wall, to a point of suitable exit on the shielded side of the tube. At each intersection of chord-drilled holes the small cavity space was packed with refractory cement, and in final assembly the tube surface presented a smooth uninterrupted contour on which the presence of the thermocouple could scarcely be detected. It is considered that the location of the effective hot junction is one wire diameter beneath the outer surface of the tube.

In addition to the chord-hole couples, installed at all designated stations, six comparison couples of the guard-ring type, as used in previous committee tests, were also installed for a check of their comparative readings. These were placed on tubes adjacent to the normal couples at the locations shown by identifying symbols in Fig. 2. Details of the guard-ring couple in this relative position are also illustrated in Fig. 3 and are described in literature references cited.[7]

As a further part of the study, special depth couples, illustrated in Fig. 4, were also installed at six different locations for the measurement of temperature gradients through the tube metal.

Results of comparative data from the several types of couples will be discussed in a later section of this report.

Throughout the test the recorder and switch bank operated in a dependable manner and consistent readings were obtained from practically all of the thermocouples involved. Two thermocouple failures were noted on the lower part of the division wall which could not be corrected during operation, and data from these areas had to be abandoned.

Two thermocouples for the measurement of saturation temperature were installed as surface-peened couples in the side-wall tube extension above the furnace roof at an elevation approximately 3 ft below the center line of the boiler drum.

Method of Test

During the four-month period following initial start-up, this unit remained in continuous service, with the exception of two 24-hr planned outages, carrying the entire station load at rates slightly in excess of design capacity through the day, and dropping to half or three-quarter load at night and on week ends, in accordance with system demand.

A log of operation covering the test period in June is shown in Fig. 5. It was planned to hold steady load for test measurements at low, intermediate, and full capacity, under the conditions of low, intermediate, and high values of excess air, in order to show the effect of these factors throughout the available range. Because the design permitted full load to be carried on two of the three pulverizers, as an expected method of operation, further tests were scheduled to show the influence of different pulverizer and burner combinations. For the standard basis of testing, the use of pulverizers A and C was adopted, since this appeared to represent a balanced condition between the two sides of the furnace. Supplementary tests were run with the combination of A and B pulverizers, and also with the ABC pulverizers and burners in service.

Test periods are identified by number in Fig. 5, and the scheme of operating conditions is indicated at the right side of the figure. Fan capacity limited the attainment of high excess air at full load, and the test with low excess air at half load was omitted because of anticipated unsteady conditions at the burners. Accomplished tests are grouped in the figure according to pulverizer combinations used.

Before the start of each test, soot blowers were operated in the screen and convection pass, and excess-air adjustments were stabilized and checked by gas-analysis traverse at the economizer outlet. No deliberate cleaning of the furnace walls was undertaken inasmuch as mechanical facilities for this were absent, and no practice of hand-lancing the furnace walls had been established nor found necessary. Natural shedding of ash from wall areas took place at various times and to varying extent in normal operation and with changes in load.

The scheduling of load sequence was co-ordinated with station and system requirements, and was affected by the occurrence of a coal strike during the period. Tests 1 and 2 were run with normal coal supply from the Pigott mine, Harrison County, West Va.; tests 8 to 13 with coal from stripping operations, Consolidation No. 32, Harrison County, and tests 3 to 7 with mixtures of the two. No conspicuous effects of these changes of fuel were apparent.

Method of Calculation

As in previous committee tests, it was considered that the ΔT elevation of tube-surface temperature above the saturation temperature of boiling liquid within the tube afforded a means of determining heat-flow rate at the local point of measurement, and that, with a sufficient number of measuring points, the pattern of distribution, as well as total furnace absorption, might be gaged.

With the recorder printing at 12-sec intervals, a complete survey of all thermocouples was made in approximately 24 min. Official time periods for the individual tests were taken from the chart record corresponding (to the nearest cycle) to elapsed time required for completing the gas-temperature traverses at the furnace outlet. On this basis, approximately twelve sets of readings were obtained for each test, of which the averaged values of ΔT for each point are recorded in Table 2. The recorder was kept in nominally continuous service, however, for the purpose of recording significant changes which might occur in normal operation of the furnace. On several occasions during nontest periods the switching mechanism was set for continuous record of a single thermocouple to permit observation of the range and frequency of temperature variation.

Tube surface temperatures were converted to ΔT equivalents by subtracting chart-recorded values of saturation temperature. To the average of these a somewhat arbitrary correction of —0.7 deg F was then subtracted as adjustment for static head difference between the mid-elevation of the unit and the location of saturation thermocouples. Resultant ΔT values were expressed to the nearest whole degree and are tabulated in Table 2.

For the complete furnace, a numerical average of all ΔT values was used, considering that all thermocouples represented equal increments of wall area, except that double weighting was given to the three division wall couples at elevation 681 to allow for that portion of the division wall area in which thermocouples had failed, and an addition of three hypothetical points was applied to represent the large area of rear wall at elevation 648 where structural interference prevented the installation of thermocouples, values for these being taken as the average of actual readings obtained from rear-wall couples at elevations 641 and 657. No thermocouples were installed in the screen tubes at furnace outlet; in all further use of the furnace average ΔT test values, it is tacitly assumed that the screen area is represented by the furnace average ΔT value.

Survey patterns of ΔT values are shown for each test in Figs. 6 to 18, inclusive, together with a graphic record of ash deposits on furnace-wall surfaces as interpreted from notes made during visual inspection in the course of each test. The code used for description indicates nature of deposit, i.e., L = liquid, P = plastic, S = sponge, and shows estimated thickness and per cent of area covered. Where no designation is shown, the tube surfaces were nominally clean or coated with a light dust deposit.

Following the practice of previous reports, these data have been

[7] "Thermocouples for Furnace Tube Surface Temperature Measurement," by C. G. R. Humphreys, *Combustion*, vol. 16, December, 1944, pp. 53–55.

TABLE 1 SUMMARY OF GENERAL AND CALCULATED PERFORMANCE DATA

Test Number		1	2	3	4	5	6	7	8	9	10	11	12	13
Date		6-9-49	6-10-49	6-14-49	6-15-49	6-16-49	6-17-49	6-20-49	6-21-49	6-22-49	6-23-49	6-24-49	6-25-49	6-27-49
Time: Start ΔT Test Record		10:20A	9:20A	11:00A	10:30A	9:42A	10:49A	2:58A	9:54A	12:13A	1:07A	1:03A	8:45P	11:02A
End ΔT Test Record		2:56P	1:30P	4:25P	3:33P	12:21P	3:29P	6:03P	12:13P	3:12A	3:49A	3:21A	11:27P	4:27P
Duration	hr	4.60	4.16	5.42	5.05	2.65	4.66	3.08	3.32	3.00	2.70	2.30	2.70	5.41
Number of Recorded ΔT Surveys		11	11	12	13	7	12	8	6	8	7	6	7	14
Burners in Service		A-C	A-C	A-C	A-B-C	A-B	A-B-C	A-B	A-C	A-C	A-C	A-C	A-B	A-B-C
Steam Flow	M-lb/hr	508	508	376	377	373	508	510	507	257	251	364	259	508
Attemperator Water Flow	M-lb/hr	30.4	38	34	34	21	53	45	20	0	0	30.2	0	64
Coal As Fired	lb/hr	45,250	45,600	35,650	34,720	35,000	45,900	47,400	46,400	24,350	23,720	33,850	24,900	46,800
Excess Air Furnace Outlet	%	13.0	24.0	23.4	23.4	23.9	13.9	15.2	13.8	37.5	24.1	36.0	37.9	24.1
Excess Air Economizer Outlet	%	14.2	24.2	24.3	24.9	24.3	14.5	15.9	14.6	37.5	24.5	36.0	37.9	25.3
Steam Pressure Drum	psig	1,384	1,380	1,327	1,325	1,325	1,350	1,357	1,360	1,294	1,287	1,305	1,295	1,355
Steam Pressure Leaving Attemperator	psig	1,340	1,340	1,305	1,304	1,300	1,319	1,321	1,325	1,275	1,279	1,290	1,280	1,321
Steam Pressure At Superheater Outlet	psig	1,315	1,315	1,286	1,285	1,299	1,295	1,300	1,300	1,269	1,270	1,280	1,275	1,301
Temperature Feedwater to Economizer	F	425	430	400	402	400	426	427	425	345	340	400	340	425
Temperature Feedwater to Drum	F	506	514	495	495	491	514	513	504	444	437	497	449	526
Temperature Saturation (Tables)	F	587	587	582	581	581	584	585	585	578	576	579	578	584
Temperature Saturation (Thermocouple)	F	580	586	580	578	581	586	582	581	576	580	580	575	581
Temperature Steam Leaving Primary Superheater	F	784	805	808	808	781	820	811	768	743	732	803	757	848
Temperature Steam Entering Secondary Superheater	F	708	704	682	681	707	682	690	721	734	723	703	746	674
Temperature Steam Leaving Secondary Superheater	F	958	956	954	954	956	957	955	949	921	925	947	958	956
Net Heat Available in Furnace	kB/hr	641,800	653,800	487,700	485,000	474,900	632,500	695,000	645,900	338,200	325,700	475,600	349,300	652,400
Heat Absorbed By Furnace	kB/hr	293,900	280,300	220,800	206,600	223,200	267,500	279,700	319,700	185,200	180,600	214,300	176,900	256,400
Heat Absorbed By Total Generating Surface	kB/hr	324,100	314,500	237,900	238,600	246,100	305,100	312,200	332,200	194,100	191,300	231,200	193,900	291,000
Heat Absorbed By Secondary Superheater	kB/hr	83,800	83,800	68,500	68,600	60,400	93,000	90,300	75,000	30,900	32,900	53,200	34,500	96,100
Gas Temperature Leaving Furnace	F	2,202	2,150	2,138	2,155	2,018	2,298	2,278	2,042	1,620	1,691	1,935	1,722	2,264
Gas Temperature Leaving Screen	F	2,110	2,068	2,038	2,052	1,928	2,196	2,181	1,965	1,552	1,611	1,858	1,648	2,172
Furnace Heat Absorption Efficiency (Test)	%	45.8	42.9	43.2	42.6	47.0	42.3	42.7	49.5	54.8	55.5	45.1	50.7	39.3
Furnace Effectiveness Factor	-	0.92	0.89	0.84	0.89	0.89	0.91	0.85	0.90	0.99	0.98	0.96	0.97	0.93
Furnace Heat Absorption Efficiency (Corrected)	%	49.8	48.2	51.5	47.9	52.8	46.5	50.2	55.0	55.3	56.6	47.0	52.3	42.3
Test Average ΔT	F	43.0	42.3	31.8	31.9	34.4	40.6	42.1	45.3	28.2	28.3	31.0	26.4	39.8
Furnace Wall Projected Area	sq ft	6,417												
Furnace Outlet Projected Area	sq ft	365												
Total Projected Area	sq ft	6,782												

TABLE 2 SUMMARY OF TEST AVERAGE ΔT VALUES FOR ALL TUBE THERMOCOUPLES

T.C.#	Elev.	Wall*	Test No. 1	2	3	4	5	6	7	8	9	10	11	12	13
1-2	33	B	57	53	47	51	50	70	70	53	26	29	35	28	68
1-3[d]	33	B	33	30	28	28	28	40	39	31	15	18	22	17	39
1-4	16.8	B	44	43	33	33	46	47	60	48	24	23	29	29	45
1-5[d]	16.8	B	28	27	22	22	28	30	36	31	17	16	19	18	28
1-6[d]	42	B	29	27	22	23	27	24	34	35	18	14	21	20	32
1-7	42	B	39	34	23	10	46	31	31	34	12	12	19	36	53
1-8[d]	42	B	29	26	18	9	37	23	20	30	11	30	14	22	33
1-9[d]	42	F	60	59	26	20	41	36	25	47	11	32	47	39	40
1-10	42	F	75	75	41	25	34	25	37	75	10	36	36	42	57
1-11[d]	42	F	42	41	22	15	20	17	22	40	7	20	20	24	35
1-12[d]	61	L	34	37	23	37	17	32	32	37	42	16	13	26	29
1-13	61	L	53	64	33	51	21	46	40	56	50	32	23	33	46
1-14[d]	61	L	29	33	15	27	12	24	22	29	28	22	12	17	24
1-15[d]	42	L	60	54	20	35	39	54	23	47	38	32	54	31	48
1-16	42	L	70	61	34	36	50	70	24	47	42	59	62	36	37
1-17[d]	42	L	35	27	22	17	33	44	16	31	26	38	39	22	27
1-18[d]	22	L	43	45	36	44	53	42	75	71	36	33	38	32	45
1-19	22	L	40	44	30	37	43	39	68	67	32	33	33	28	38
1-20[d]	22	L	22	25	18	22	28	23	37	38	21	19	19	16	23
1-21[g]	15.5	L	35	40	32	36	48	33	61	58	27	17	31	32	41
2-1	15.5	L	42	46	37	42	57	40	69	67	28	19	34	35	44
2-3		T	36	34	34	35	29	37	32	35	21	30	36	21	42
2-4		T	36	43	36	35	30	38	39	37	22	31	36	24	42
2-5		T	39	35	37	33	29	33	31	31	19	25	28	20	34
2-6		T	46	40	43	45	34	46	37	48	30	41	42	27	47
2-7		T	56	49	39	41	34	48	28	24	30	39	43	31	47
2-8		T	41	39	40	40	35	41	37	24	33	40	37	33	45
2-9	66.5	B	46	41	27	30	19	29	16	20	28	24	23	18	28
2-10	66.5	B	52	45	30	45	30	37	19	19	27	35	34	27	45
2-11	66.5	B	41	30	33	36	24	39	34	24	9	21	31	22	35
2-12	56.7	B													
2-13	56.7	B	81	78	43	17	51	44	29	26	31	44	47	30	51
2-14	56.7	B	73	66	33	15	38	39	54	26	33	43	47	28	44
2-15	44.1	B	39	69	32	29	39	27	32	16	34		33		
2-16	44.1	B	41	52	28	33	17	69	84	45			21		86
2-17	33	B	62	56	56	68	64	85	87	82	32	33	48	34	87
2-18	33	B	65	59	52	40	40	62	60	56	24	28	41	25	59
2-19	16.8	B	51	52	36	31	40	43	54	98	54	28	37	32	46
2-20	16.8	B	33	34	27	30	40	40	56	40	20	19	26	27	40
2-21	9	B	30	30	22	23	30	32	39	30	15	13	24	22	29
3-1	71	R	24	50	34	47	33	50	44	25	15	43	29	39	35
3-2[d]	81	R													
3-4	71	R	31	28	21	34	22	38	26	24	26	21	16	32	30
3-5	71	R	38	33	27	34	24	28	21	17	6	22	25	18	30
3-6	61	R	56	34	39	34	28	55	62	53	61	34	57	26	22
3-7	61	R	22	26	27	15	25	52	35	45	19	14	22	38	36
3-8	61	R	54	50	36	28	17	24	29	18	20	28	16	17	23
3-9	52	R	46	20	19	35	26	43	45	30	52	60	68	26	31
3-10	52	R	31	27	17	34	23	33	37	68	45	49	37	40	38
3-11	52	R	61	57	41	37	29	39	38	14	24	33	37	23	41
3-12	42	R	86	68	43	19	12	50	34	68	45	54	58	49	51
3-13	42	R	45	59	36	31	45	40	29	16	24	33	12	23	40
3-14	42	R	20	21	17	15	19	27	30	28	14	18	19	11	28
3-15	42	R	37	29	26	19	19	30	28	26	11	15	20	13	30
3-16	32	R	56	60	33	24	25	24	27	77	36	31	39	38	30
3-17	32	R	57	50	41	33	35	38	19	41	38	41	44	36	40
3-18	32	R	65	57	48	36	39	47	32	13	7	3	17	26	47
3-19	32	R	63	60	44	32	36	51	46	90	21	31	38	22	48
3-20	32	R	48	43	35	28	30	45	44	40	18	22	29	19	44
3-21	22	R	35	38	22	13	20	19	33	52	23	15	18	24	18
4-1	22	R	48	52	26	20	35	30	48	72	33	27	31	32	31
4-2	22	R	50	49	26	18	31	33	30	64	31	31	33	27	34
4-3	22	R	51	50	31	22	30	37	43	45	24	24	29	23	38
4-5	22	R	35	31	23	20	23	32	38	36	17	18	22	17	33
4-6	15.5	R	34	43	26	18	28	22	44	68	25	12	23	30	25

T.C.#	Elev.	Wall*	Test No. 1	2	3	4	5	6	7	8	9	10	11	12	13
4-7	15.5	R	22	54	32	20	35	38	49	38	22	16	29	35	33
4-8	15.5	R	52	59	37	24	34	34	35	9	30	19	36	28	37
4-9	15.5	R	53	56	40	29	37	43	53	62	26	25	37	27	45
4-10	15.5	R	40	38	31	25	32	42	45	37	12	14	26	19	41
4-11	10	R	26	32	21	17	27	20	38	50	19	14	17	21	20
4-12	10	R	34	43	26	23	36	27	58	70	26	12	22	38	35
4-13	10	R	40	48	29	25	41	35	46	26	28	13	28	38	38
4-14	10	R	43	44	30	25	38	38	58	59	24	17	26	31	37
4-15	10	R	32	31	25	22	30	36	42	32	13	9	20	18	36
4-16	71	F	29	15	51	49	31	52	17	45	17	54	16	4	46
4-17	71	F	8	3	10	80	75	95	79	98	36	38	13	45	80
4-18	71	F	21	65	38	63	53	69	53	35	60	52	55	36	48
4-19	61	F	37	39	28	50	55	42	55	107	73	68	33	24	67
4-20	61	F	25	26	55	62	42	117	63	31	62	34	20	14	85
4-21	61	F	90	68	61	75	63	123	112	96	85	31	35	34	94
5-1	52	F	59	25	59	59	48	60	34	72	51	58	67	27	45
5-2	52	F	85	77	28	35	80	72	58	97	49	51	42	43	85
5-3	52	F	60	39	30	35	47	59	79	45	58	61	77	30	34
5-4[g]	81	R													
5-6	42	F	49	46	39	43	22	55	22	84	38	42	44	28	45
5-7	42	F	72	80	36	18	10	32	35	65	45	47	56	45	47
5-8	32	F	35	34	24	28	32	26	50	61	32	32	29	26	31
5-9	32	F	33	36	25	23	30	27	20	14	27	25	24	30	27
5-10	32	F	43	42	30	23	26	26	21	57	30	32	27	33	30
5-11	22	F	18	20	14	17	21	16	38	43	21	17	15	19	19
5-12	22	F	32	32	19	18	24	22	43	45	24	19	18	27	21
5-13	22	F	21	29	21	15	22	21	28	35	24	17	19	23	19
5-14	15.5	F	19	23	15	14	20	17	27	30	18	14	16	21	17
5-15	15.5	F	16	21	14	10	16	14	23	30	16	10	12	18	15
5-16	10	F	16	20	14	11	18	12	29	36	13	10	12	18	15
5-17	71	L	39	36	28	23	19	17	9	18	7	15	25	14	29
5-18	71	L	19	18	18	37	14	32	15	21	26	13	16	7	32
5-19	71	L	33	18	37	63	20	36	44	65	51	52	24	26	49
5-20	61	L	41	34	20	27	22	25	12	15	13	31	36	18	40
5-21	61	L	81	52	54	113	61	95	35	127	60	80	34	30	71
6-1	52	L	45	37	25	29	28	33	26	18	20	36	40	19	35
6-2	52	L	39	26	38	53	15	31	23	31	35	45	44	14	22
6-3	52	L	24	29	37	75	51	82	59	81	63	97	65	25	40
6-4	42	L	21	20	20	25	20	33	29	19	8	10	17	10	35
6-5	42	L	25	21	21	23	25	24	29	26	12	12	17	9	29
6-7	42	L	62	49	39	34	34	42	30	7	24	34	41	14	39
6-8	42	L	33	33	25	39	32	39	12	73	33	37	41	20	39
6-9	32	L	36	34	31	37	32	46	46	34	17	17	24	19	47
6-10	32	L	44	43	42	48	46	54	52	55	25	28	35	23	55
6-11	32	L	43	43	44	50	52	56	47	60	4	8	10	25	55
6-12	32	L	36	38	34	39	43	47	51	61	32	34	32	26	36
6-13	32	L	33	33	28	37	44	44	52	83	39	36	33	30	41
6-14	22	L	30	30	23	23	29	34	43	33	17	16	23	20	35
6-15	22	L	38	38	30	32	37	37	54	48	25	22	26	25	38
6-16	22	L	27	31	21	26	40	31	99	68	31	25	24	29	32
6-17	22	L	21	25	20	24	37	28	56	62	27	21	22	28	29
6-18	15.5	L	34	33	27	27	33	39	45	33	19	14	24	21	38
6-19	15.5	L	35	39	31	35	49	38	66	46	19	12	26	26	39
6-20	15.5	L	32	41	32	36	56	34	74	69	31	17	27	39	35
6-21	15.5	L	26	36	27	29	47	28	71	70	31	18	26	38	31
7-1	10	L	34	35	26	27	32	34	43	34	16	12	25	21	63
7-2	10	L	42	44	32	30	43	37	58	51	19	14	27	23	37
7-3	10	L	35	43	28	27	44	30	56	54	17	11	28	29	32
7-4	10	L	32	40	25	27	42	26	68	59	21	10	26	37	35
7-5	10	L	25	30	21	21	34	20	44	53	22	13	19	29	32

(d) Depth thermocouple
(g) Guard-Ring thermocouple
(s) Saturation thermocouple
All other thermocouples are chord-hole surface type.

* B - Rear Wall
F - Front Wall
L, R - Left and Right Walls
T - Roof

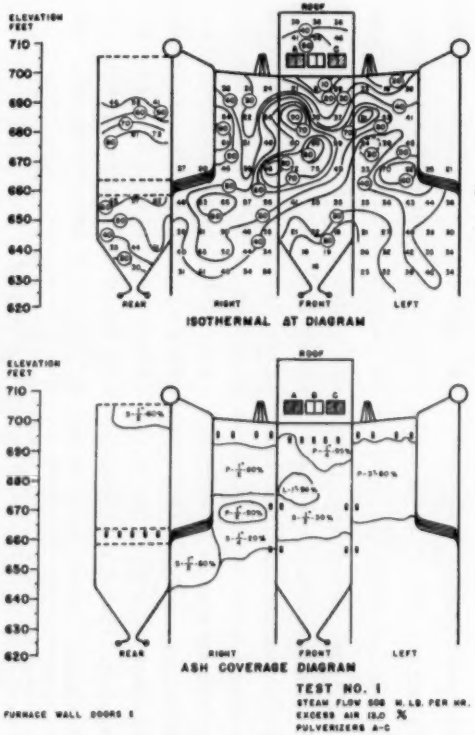

FIG. 6 DISTRIBUTION PLOTS OF ΔT AND ASH COVERAGE FOR INDIVIDUAL TESTS 1 TO 13, INCLUSIVE

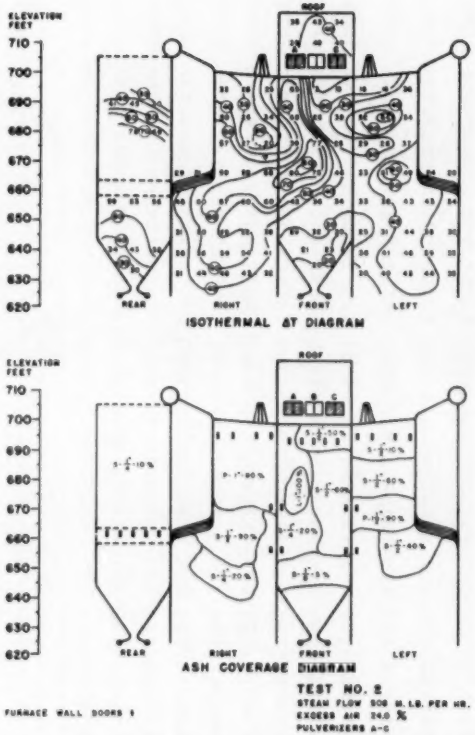

FIG. 7 DISTRIBUTION PLOTS OF ΔT AND ASH COVERAGE FOR INDIVIDUAL TESTS 1 TO 13, INCLUSIVE

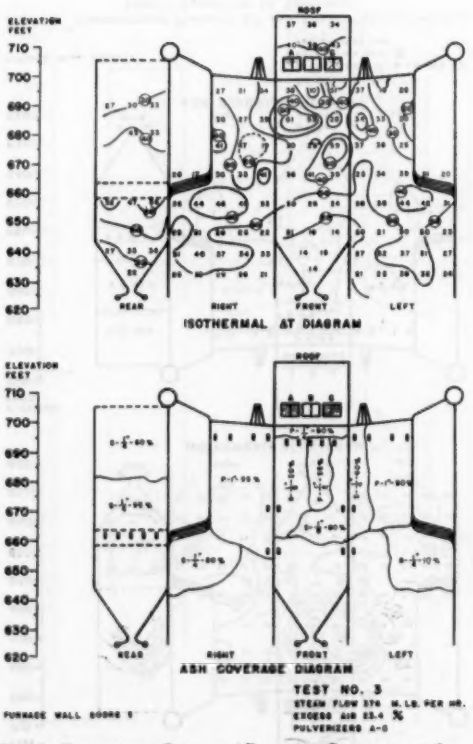

FIG. 8 DISTRIBUTION PLOTS OF ΔT AND ASH COVERAGE FOR INDIVIDUAL TESTS 1 TO 13, INCLUSIVE

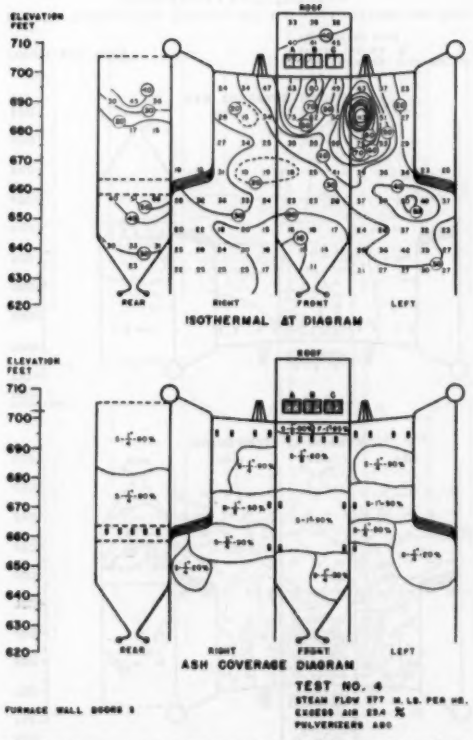

FIG. 9 DISTRIBUTION PLOTS OF ΔT AND ASH COVERAGE FOR INDIVIDUAL TESTS 1 TO 13, INCLUSIVE

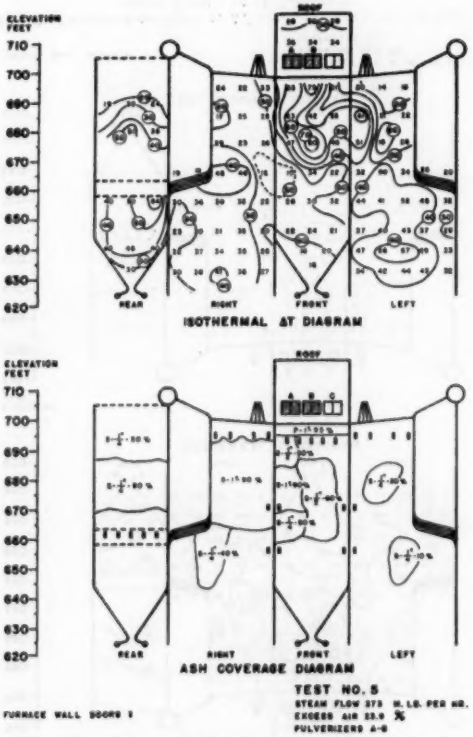

FIG. 10 DISTRIBUTION PLOTS OF ΔT AND ASH COVERAGE FOR INDIVIDUAL TESTS 1 TO 13, INCLUSIVE

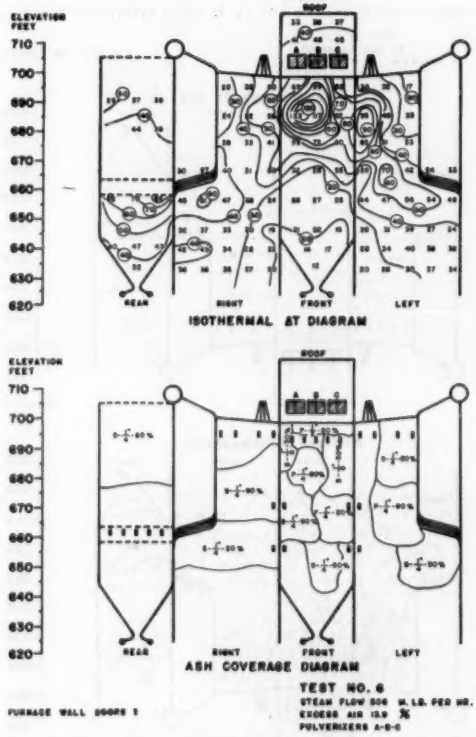

FIG. 11 DISTRIBUTION PLOTS OF ΔT AND ASH COVERAGE FOR INDIVIDUAL TESTS 1 TO 13, INCLUSIVE

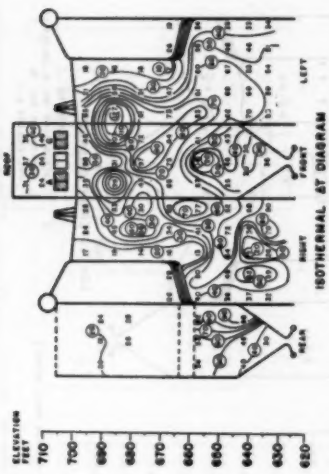

FIG. 12 DISTRIBUTION PLOTS OF ΔT AND ASH COVERAGE FOR INDIVIDUAL TESTS 1 TO 13, INCLUSIVE

FIG. 13 DISTRIBUTION PLOTS OF ΔT AND ASH COVERAGE FOR INDIVIDUAL TESTS 1 TO 13, INCLUSIVE

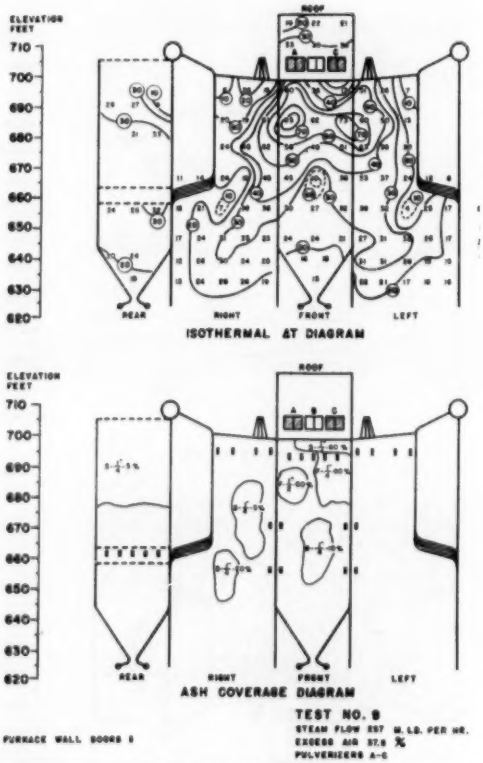

Fig. 14 Distribution Plots of ΔT and Ash Coverage for Individual Tests 1 to 13, Inclusive

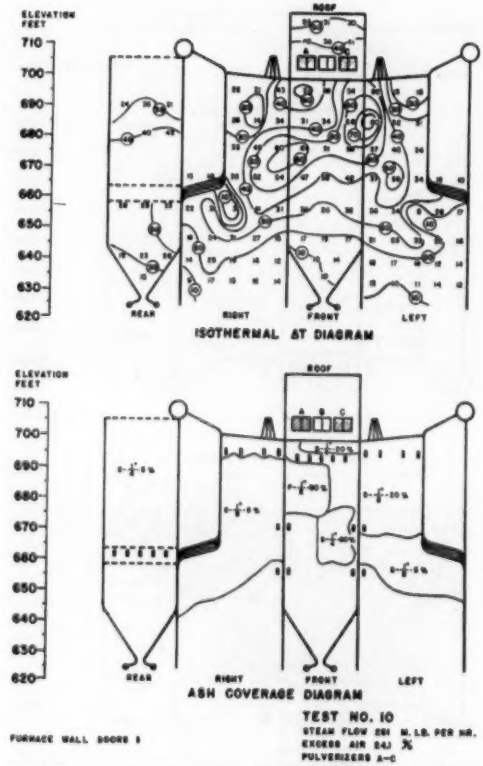

Fig. 15 Distribution Plots of ΔT and Ash Coverage for Individual Tests 1 to 13, Inclusive

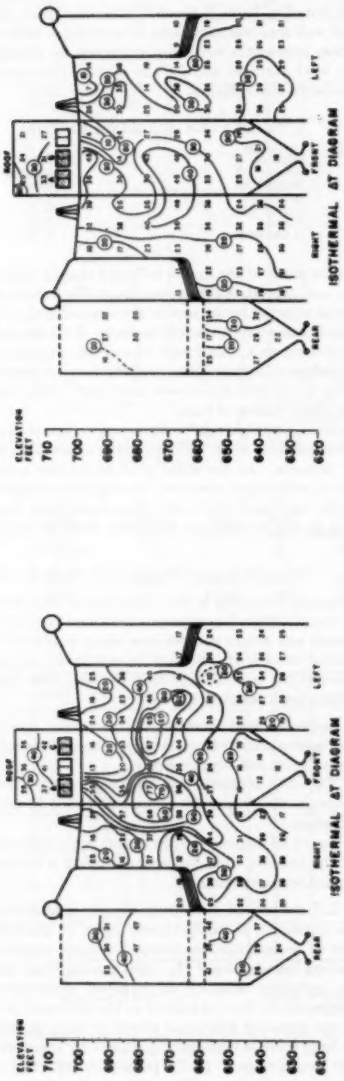

FIG. 16 DISTRIBUTION PLOTS OF ΔT AND ASH COVERAGE FOR INDIVIDUAL TESTS 1 TO 13, INCLUSIVE

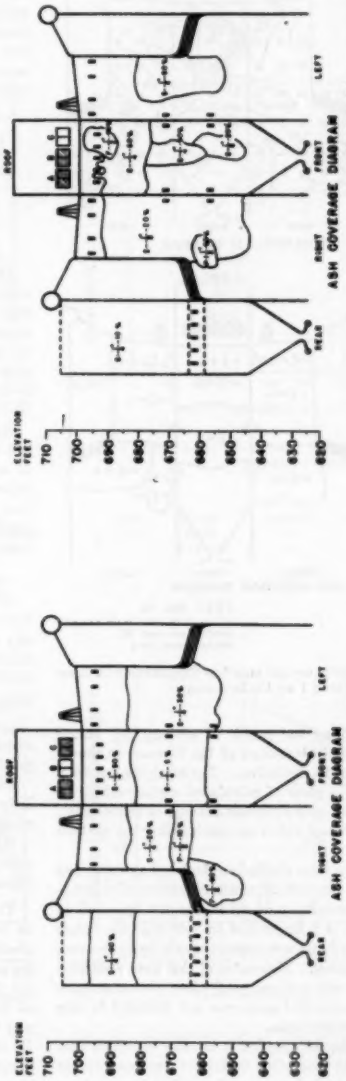

FIG. 17 DISTRIBUTION PLOTS OF ΔT AND ASH COVERAGE FOR INDIVIDUAL TESTS 1 TO 13, INCLUSIVE

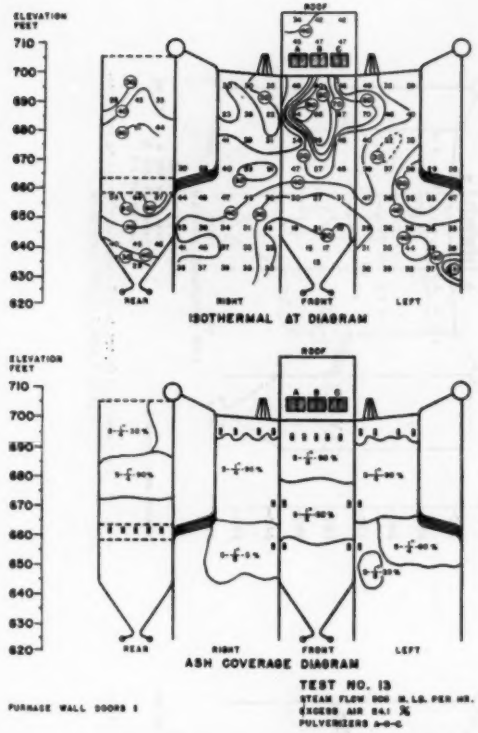

FIG. 18 DISTRIBUTION PLOTS OF ΔT AND ASH COVERAGE FOR INDIVIDUAL TESTS 1 TO 13, INCLUSIVE

analyzed further by plotting the profile of average ΔT values for bands taken at different elevations of the furnace as shown graphically in Figs. 19 to 29, inclusive. The analysis has been extended to include profile plots of calculated surface effectiveness for these bands, which give a further concept of the location and effect of ash deposits, and aid in comprehending the pattern of ΔT distribution.

Level average ΔT values were similarly calculated as numerical averages, using the data for each separate elevation of thermocouple placement. No weighting of areas was incorporated in this calculation, although it is important to note that the bands in the lower portion of the furnace represent nearly twice the area of those in the upper portion. Estimates of ΔT were made for those sections of division wall and rear wall where thermocouples were absent. The furnace-outlet area was not included in this level-average treatment of the data.

In a first appraisal of the ΔT profiles, it became apparent that conditions, other than the controlled factors of load and excess air, were exerting important influence, and an effort was made to show in a more quantitative manner the occurrence and magnitude of ash in related zones of the furnace.

Evaluation of wall cleanliness or surface effectiveness factor was calculated by the method proposed by Mumford and Bice[8] and is based upon the estimated values of ash coverage and thickness shown in Figs. 6 to 18, inclusive. In that method it is considered that clean wall surface, as a standard of reference, has a heat-absorbing effectiveness of 1.0, and that ash deposits of increasing extent or thickness decrease the heat-absorbing effectiveness of the surface to lower values. Using their range of factors, as reproduced in Table 3, the S-A (slag-ash) factor of each increment of wall area was calculated in accordance with the method, and these increments were then combined for evaluation of the several level averages and for the over-all furnace effectiveness factors shown in the figures.

TABLE 3 S-A (SLAG-ASH) FACTORS

Average thickness of slag or ash deposit, in.	S-A multiplying factor
0 to 1/32	1.0
1/32 to 1/4	0.7
1/4 to 1	0.5
1 and over	0.3

Detailed study of the figures indicates that as a normal characteristic, ash deposits were present upon the front-wall and side-wall areas adjacent to the zone of active combustion, where flame from the burners swept the wall surfaces. Less ash was deposited on the division wall. Roof surfaces and side walls adjacent to the roof remained relatively clean, and the lower portion of all walls including the hopper slopes were essentially clean, being covered by a nominal coating of dust.

In general, the higher ΔT values occur in the combustion zone, but some patterns show included areas of low ΔT, attributable to ash deposits. In the areas of clean surface a more regular pattern of isotherms is observed, having fairly consistent correlation with load and other operating conditions, but being influenced by ash on surfaces preceding them in the path of gas travel.

DISCUSSION AND CORRELATION OF RESULTS

As grouped according to the conditions of load, excess-air and burner combination, it is apparent that the effects of ash materially distort any simple comparisons which might be drawn from this limited number of tests, and in some cases appear to exceed the effects of the controlled primary factors. The following generalizations seem justified, however:

(*a*) Increased load increases the maximum rate of heat absorption, and markedly increases absorption of the ash-free lower portions of walls and hopper section.

(*b*) The effect of change in excess air is obscure, but may similarly increase the proportion of heat absorbed in the lower part of the furnace.

(*c*) Use of all burners ABC transfers more duty to the upper part of the furnace, while the opposite effect is indicated for the unbalanced arrangement AB.

The ΔT method of measuring furnace heat-absorption rate, as here employed, is conspicuously open to question as to its absolute or quantitative accuracy, for many reasons, as noted by previous investigators.[3,4,8] Chief among these questions are (*a*) the sampling accuracy of localized temperature reading, at the tube center line, as related to the full contour of the tube and to the extent of wall areas served by each measuring point; (*b*) the large error in heat-flux equivalent for small errors in temperature measurement; (*c*) the pronounced effect of ash deposits in shielding local areas. Nevertheless, the ability to use this tool, with due allowance for its shortcomings, permits a breakdown of the over-all performance into smaller increments which are revealing in nature and provide insight into the underlying factors affecting general performance. The method of testing, therefore, becomes a fitting supplement to other methods and provides a basis for cross-check of results.

TEST NO.	STEAM FLOW M LB/HR.	EXCESS AIR %	PULV.	FURN. EFF. %	FURN. EFFECTIVENESS FACTOR
○ 2	508	24.0	A-C	42.9	0.89
△ 3	376	23.4	A-C	43.2	0.84
□ 10	251	24.1	A-C	55.5	0.98

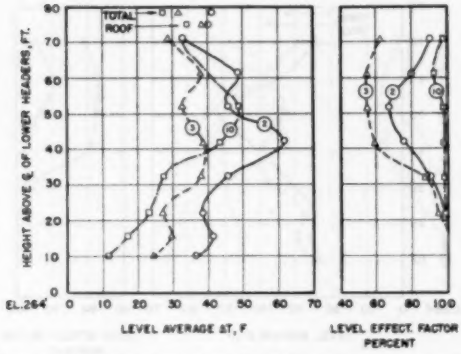

FIG. 19 COMPARISON OF ΔT AND ASH-DEPOSIT PROFILES IN RELATION TO LOAD

TEST NO.	STEAM FLOW M LB/HR.	EXCESS AIR %	PULV.	FURN. EFF. %	FURN. EFFECTIVENESS FACTOR
□ 9	257	37.5	A-C	54.8	0.99
△ 11	364	36.0	A-C	46.1	0.96

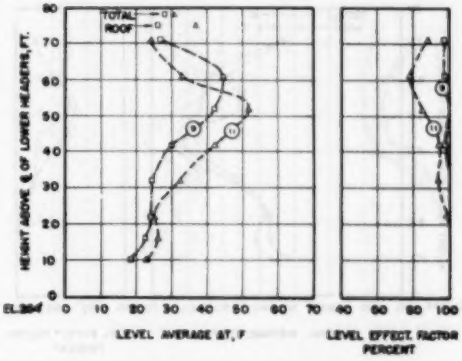

FIG. 20 COMPARISON OF ΔT AND ASH-DEPOSIT PROFILES IN RELATION TO LOAD

TEST NO.	STEAM FLOW M LB/HR.	EXCESS AIR %	PULV.	FURN. EFF. %	FURN. EFFECTIVENESS FACTOR
△ 4	377	23.4	A-B-C	42.6	0.89
○ 13	506	24.1	A-B-C	39.3	0.93

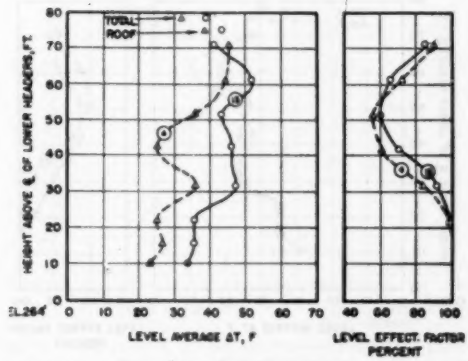

FIG. 21 COMPARISON OF ΔT AND ASH-DEPOSIT PROFILES IN RELATION TO LOAD

TEST NO.	STEAM FLOW M LB/HR.	EXCESS AIR %	PULV.	FURN. EFF. %	FURN. EFFECTIVENESS FACTOR
○ 1	508	13.0	A-C	45.8	0.98
△ 8	507	13.8	A-C	49.5	0.90

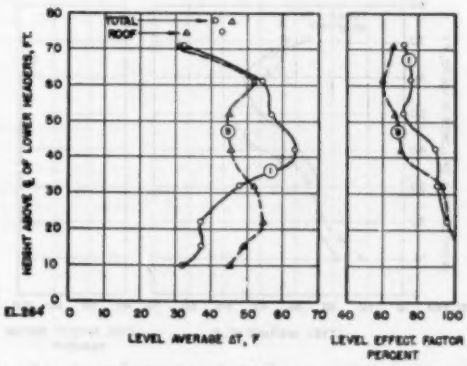

FIG. 22 COMPARISON OF ΔT AND ASH-DEPOSIT PROFILES IN RELATION TO LOAD

	TEST NO.	STEAM FLOW M LB/HR.	EXCESS AIR %	PULV.	FURN. EFF. %	FURN. EFFECTIVENESS FACTOR
□	1	508	13.0	A-C	45.8	0.92
△	2	508	24.0	A-C	42.9	0.89

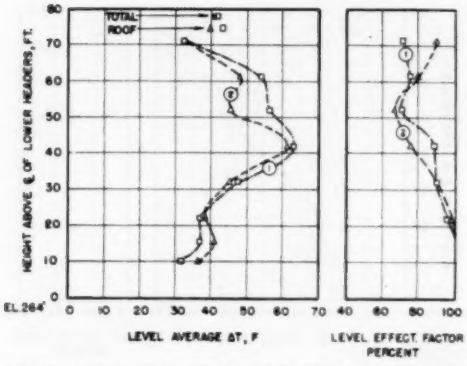

FIG. 23 COMPARISON OF ΔT AND ASH-DEPOSIT PROFILES IN RELATION TO EXCESS AIR

	TEST NO.	STEAM FLOW M LB/HR.	EXCESS AIR %	PULV.	FURN. EFF. %	FURN. EFFECTIVENESS FACTOR
△	3	376	23.4	A-C	43.2	0.84
○	11	364	36.0	A-C	46.1	0.96

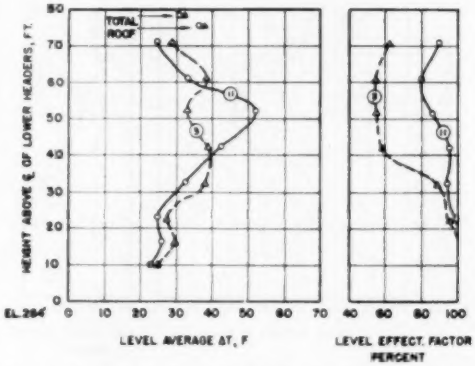

FIG. 24 COMPARISON OF ΔT AND ASH-DEPOSIT PROFILES IN RELATION TO EXCESS AIR

	TEST NO.	STEAM FLOW M LB/HR.	EXCESS AIR %	PULV.	FURN. EFF. %	FURN. EFFECTIVENESS FACTOR
○	9	257	37.5	A-C	54.8	0.99
△	10	251	24.1	A-C	55.5	0.98

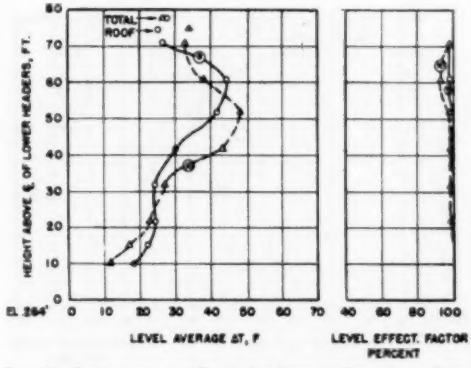

FIG. 25 COMPARISON OF ΔT AND ASH-DEPOSIT PROFILES IN RELATION TO EXCESS AIR

	TEST NO.	STEAM FLOW M LB/HR.	EXCESS AIR %	PULV.	FURN. EFF. %	FURN. EFFECTIVENESS FACTOR
□	6	508	13.9	A-B-C	42.3	0.91
△	13	508	24.1	A-B-C	39.3	0.93

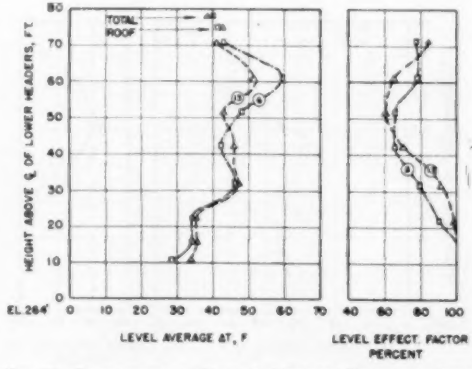

FIG. 26 COMPARISON OF ΔT AND ASH-DEPOSIT PROFILES IN RELATION TO EXCESS AIR

TEST NO.	STEAM FLOW M LB/HR.	EXCESS AIR %	PULV.	FURN. EFF. %	FURN. EFFECTIVENESS FACTOR
○ 1	508	13.0	A-C	45.8	0.92
□ 6	508	13.9	A-B-C	42.5	0.91
△ 7	510	15.2	A-B	42.7	0.85

TEST NO.	STEAM FLOW M LB/HR.	EXCESS AIR %	PULV.	FURN. EFF. %	FURN. EFFECTIVENESS FACTOR
○ 3	376	23.4	A-C	43.2	0.84
□ 4	377	23.4	A-B-C	42.6	0.89
△ 5	375	23.9	A-B	47.0	0.89

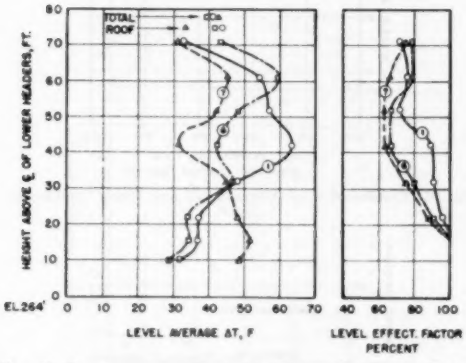

FIG. 27 COMPARISON OF ΔT AND ASH-DEPOSIT PROFILES IN RELATION TO BURNER COMBINATIONS

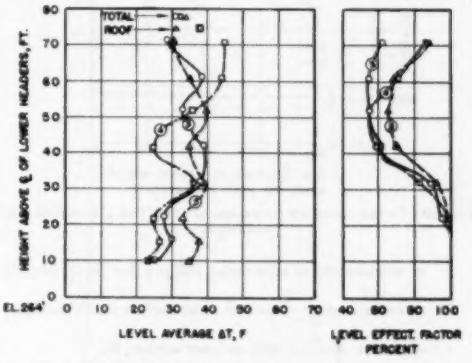

FIG. 28 COMPARISON OF ΔT AND ASH-DEPOSIT PROFILES IN RELATION TO BURNER COMBINATIONS

TEST NO.	STEAM FLOW M LB/HR.	EXCESS AIR %	PULV.	FURN. EFF. %	FURN. EFFECTIVENESS FACTOR
○ 9	257	37.5	A-C	54.8	0.99
△ 12	259	37.9	A-B	50.7	0.97

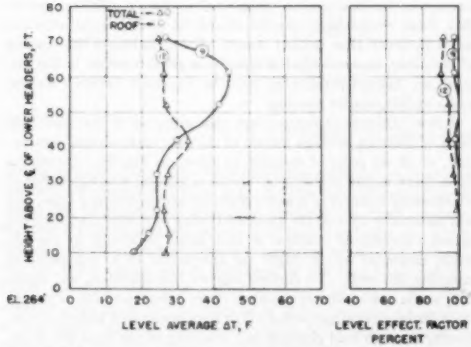

FIG. 29 COMPARISON OF ΔT AND ASH-DEPOSIT PROFILES IN RELATION TO BURNER COMBINATIONS

The heat-balance method, as reported in Part I[4], is likewise subject to inherent and experimental inaccuracies, but appears to be more definitely adjustable to absolute values, and has been adopted here as the criterion or basis for comparison.

Inasmuch as the furnace-wall areas of this unit comprise nearly all of the total generating surface, a further independent means of cross-checking the consistency of test results was made available by calculating the "steam-generating duty" of the unit from metered quantities of steam output, corrected for attemperator flow, and the change in enthalpy from water entering the drum to steam at saturated condition.

Data from the ΔT measurements are plotted against each of these references in Figs. 30 and 31, and show remarkably good correlation or consistency among the individual test runs.

Empirical values of U_o, the over-all conductance coefficient from tube surface to boiling liquid, as calculated from the heat-balance measurement of total furnace absorption, are plotted in Fig. 32, and show a similarly good correlation. These values were calculated by the equation

$$U_o = \frac{\text{Total furnace absorption (Btu per hr)}}{8782 \text{ (sq ft)} \times \text{furnace average } \Delta T \text{ (F)}}$$

Excluding test No. 8 the deviation is within plus and minus 4 per cent of the average 755 Btu per (hr) (sq ft) (deg F).

Direct calculation of over-all conductance, from tube outer surface to boiling liquid, involves several factors not clearly established for which values must be assumed. These include the following:

(*a*) Actual thickness of tube wall.
(*b*) Location of thermocouple with respect to tube surface.
(*c*) Conductivity of tube material.
(*d*) Conductance at the inner surface of the tube.

The general relationship is shown by

$$U_o = \frac{U_M\, U_S}{U_M + U_S}, \text{ and } U_M = \frac{k}{R \log_e \frac{R}{r}}$$

where

U_o = over-all conductance, tube surface to boiling liquid, Btu per (hr) (sq ft) (deg F) referred to outer surface
U_M = conductance of tube wall, Btu per (hr) (sq ft) (deg F)
U_S = conductance at inner surface, Btu per (hr) (sq ft) (deg F)

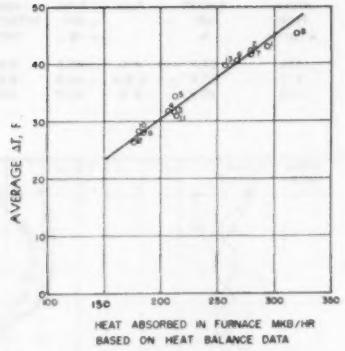

FIG. 30 CORRELATION OF AVERAGE ΔT AND TOTAL FURNACE ABSORPTION

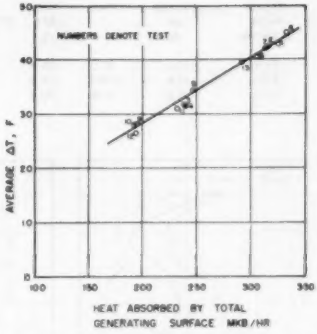

FIG. 31 CORRELATION OF AVERAGE ΔT AND STEAM GENERATING DUTY

k = conductivity of tube metal, Btu per (hr) (sq ft) (deg F/in.)

R = radius, center of tube to outer surface or TC location, in.

r = radius, center of tube to inner surface, in.

For a tube 3 in. OD and 0.240 in. specified thickness we have assumed, for mill tolerance, an actual thickness 15 per cent greater, and an ID of 2.45 in. With the chord-hole thermocouple embedded 1 wire diam (0.0253 in.) beneath the outer surface, the effective radius at thermocouple location is 1.4747 in. In previous reports, K has been taken as 348 Btu per (hr) (sq ft) (deg F per in.), whereas the ASM value for SA-210 steel at 650 F is given as 300. Recognizing the significance of this factor, both values of U_c have been calculated for comparison as shown in Table 4, using the previously assumed value of 5000 Btu per (hr) (sq ft) (deg F) for film conductance at the inner surface.

TABLE 4 CALCULATED WALL-TUBE CONDUCTANCE

R	1.4747	1.4747
r	1.224	1.224
k	348	300
U_M	1272	1097
U_S	5000	5000
U_c	1015	901

It will be noted that the test average of 755 Btu per (hr) (sq ft) (deg F) is appreciably lower than either of the calculated values, which lack of agreement may perhaps be attributed to inexactness of measurement or to other factors involved in the assumption that the center-line couples are representative of the equivalent flat projected area of the walls.

COMPARISON OF THERMOCOUPLES

As stated previously, the type of thermocouple used for general furnace survey of this unit was of the chord-hole type illustrated in Fig. 3. With this type of couple, no projection nor disturbance of the normal surface contour of the tube is created by the measuring device, upon which localized deposits of ash might tend to lodge or accumulate. In this respect, the chord-hole thermocouple differs from the guard-ring type used in previous committee tests, and it has been expressed by the authors of those papers that some question might exist in regard to the representative measurement of temperature by the guard-ring thermocouple employed.

For the purpose of comparing the two thermocouple types, guard-ring thermocouples were installed in the Willow Island

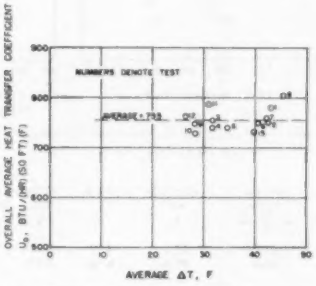

FIG. 32 TEST AVERAGE WALL-TUBE CONDUCTANCE

furnace at six locations as designated in Fig. 2. It was agreed that these comparison couples should be placed upon adjacent tubes in order that neither couple should influence the reading of the other, and considering that for a given location in the furnace, no distinct differences need be expected between similar tubes at 3-in. center spacing.

A first attempt at comparison was made upon the statistical basis of plotting average values of ΔT, for each formal test period, of all six pairs of couples, as shown in Fig. 33. On such a basis there might perhaps be drawn a general average factor of relationship indicating lower values for the guard-ring type, but it is disturbing to note the great scattering of points that occurred between individual couples, in such close proximity to one another, either of which might be acceptable as a test point of sampling the wall. To further explore this question, we, therefore, made use of the continuous chart record of tube temperatures during operating period other than prescribed tests and continuing through load changes and shedding of ash from the walls.

Studies were made for each of the various localities in the furnace where comparative couples were installed. One of the most revealing examples is illustrated in Fig. 34, showing the temperature record of thermocouples 1–6 and 1–7 on the right side wall during the three days from June 9 to June 11, which period of time included tests 1 and 2.

Scrutiny of this chart will indicate that prior to test No. 1, the chord-hole surface couple showed a reading 20 deg higher than its companion guard-ring couple, but exhibited a slowly declining value in the course of the test until a period of exact agreement occurred after about 12 hr. This continued for 4 hr, to the point

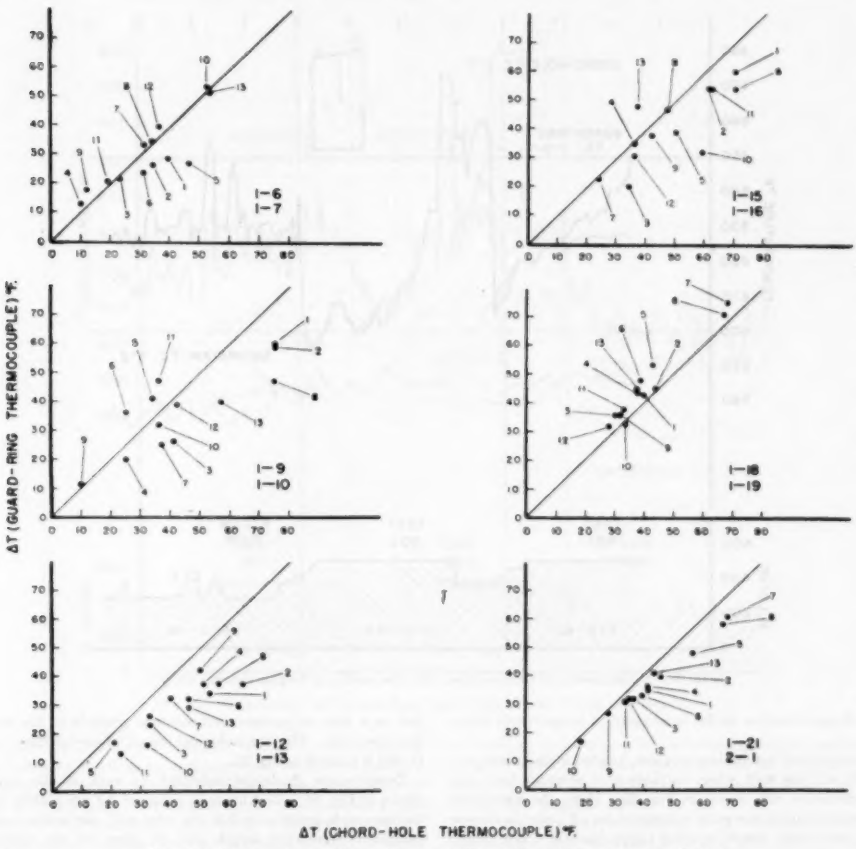

FIG. 33 COMPARISON OF GUARD-RING AND CHORD-HOLE THERMOCOUPLE DATA

of drop in station load, when the difference between readings was reversed by approximately 4 deg. At the lowest point of load, when one might expect minimum readings on both thermocouples, a sudden increase occurred in both readings, and a difference in temperature of 20 deg is again re-established between the two, with higher values indicated by the chord-hole couple. Upon resuming full load rating at 5 a.m. on June 10, both couples again show abrupt increase in value, followed by a more or less rapid decrease, until both couples are again at the same reading near the end of test 2, and subsequently, reverse this difference by a matter of about 2 deg, which is held persistently for 8 hr, when upon drop in load both couples again reach higher values and show a consistent spread of 10 deg between their readings, the chord-hole couple being at the higher temperature.

Our interpretation of this sequence is as follows:

During the early part of June 9, and throughout the course of test 1, ash was accumulating upon the chord-hole thermocouple to the point of equaling the ash that existed upon the guard-ring couple on the adjacent tube. It might be assumed that ash accumulation had reached a point of equality on the two tubes at this time, although no direct evidence of that condition is at hand. With decrease in load, the temperature of both couples diminished, but upon reaching the lowest point of load, ash was shed from the wall, exposing both couples and causing the sudden rise in temperature of each. This cleaning action appears to have been more complete on the smooth chord-hole couple than upon the guard-ring couple, resulting in a fairly high difference between them, which difference was further increased at the time of load pickup at 5 a.m. on June 10.

With continued full load on the furnace, ash accumulation on this area again took place and, during the course of test 2, attained the condition of complete coverage of both couples, persisting throughout the remainder of full-load operation on June 10. With the drop-in load at midnight, shedding of ash from the wall again took place, exposing both couples, in a nominally clean condition, to radiation from the furnace at a rating lower than the previous night load.

Conclusions which might be drawn from this example are that the ΔT values shown by either type of couple are subject to wide variation caused by ash deposits, and that the guard-ring couple tends to indicate lower values than the chord-hole type, possibly

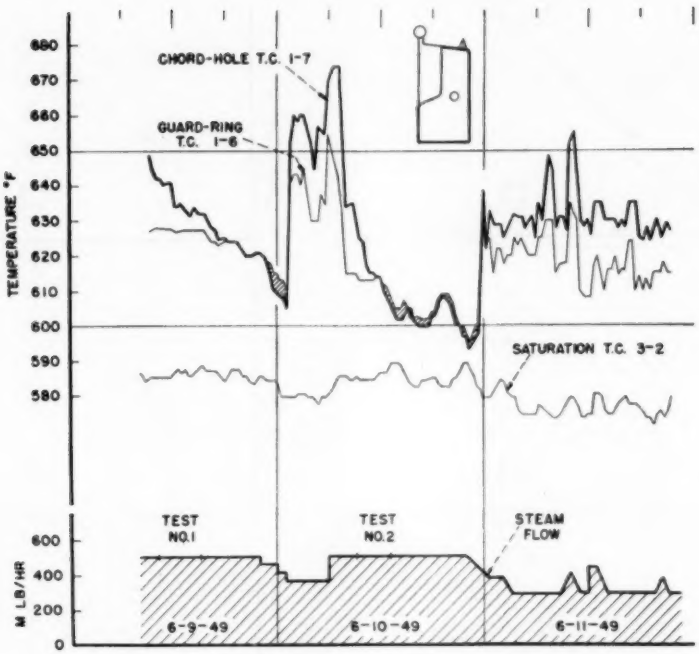

FIG. 34 COMPARISON OF GUARD-RING AND CHORD-HOLE THERMOCOUPLE DATA

because of ash retention at the local point of temperature measurement.

Two examples of comparison couples, located in the lower portion of the left side wall, where surfaces were normally free from ash accumulation, are shown in Fig. 33. Here, the agreement of the thermocouples was quite consistent for all tests; in the one case the chord-hole couple reading approximately 5 deg higher than the guard ring, while in the other case the chord-hole couple was approximately 3 deg lower than the guard-ring type. A detailed plot of temperatures for the second pair is shown in Fig. 35, which indicates close agreement and similar response of both couples to load change or other major influences in furnace operation.

It may well be argued that in a dry-ash furnace, where no true equilibrium point of ash deposit is attained, there is opportunity for radically different rates of heat absorption to occur at local points of adjacent tubes, or along the length of the same tube depending upon the shadowing influence of scattered ash deposits as they are prone to exist in this type of furnace. For the cleaner zones perhaps no choice exists between the two types of thermocouples. For the zones susceptible to ash accumulation, we believe that the chord-hole type is more likely to be representative of the normal furnace wall.

GRADIENT THERMOCOUPLES

For further study of the ΔT method of measurement, special depth thermocouples were installed at seven locations shown in Fig. 2 and illustrated in Fig. 4. The hot junction was placed at measured depth beneath the surface of the tube, in close relation to the chord-hole surface couple so that the two would function as a pair, to measure temperature gradient in the metal of the tube wall. The chronological record of one of these couples (1–20) is plotted in Fig. 35.

Temperature gradients indicated by each of the pairs are shown in Fig. 36. Test average values of ΔT are plotted against thermocouple position within the tube wall, the latter being calculated as equivalent length (Le) to adjust for the radial path of heat flow and permit gradients to be drawn as straight lines through the test points. Equivalent length (Le) = $R \log_e (R/r)$. Positions of the thermocouples are based upon assumptions that the effective hot junction exists at the center of the wire; that the center of the surface couple is embedded 1 wire diam beneath the tube surface; and that the depth couple is correctly represented by the depth of chord hole as measured in the field at the time of installation. Unfortunately, no measurement of actual tube-wall thickness, at the points of application, was undertaken at that time. The probable location of inner surface is shown on the chart by two lines, one representing specified thickness and the other representing 15 per cent excess thickness of tube wall.

It will be seen from Fig. 36 that the temperature-gradient lines exhibit general convergence toward the inner surface, showing intercepts in fairly close relation to saturation temperature. The slope of the lines is proportional to rate of heat flow, and the point of convergence is in reasonable relation to the probable thickness or inner surface of the tube.

Considerable study has been given to these temperature-gradient data, in the hope of deriving values of inner surface conductance (U_s) which might be used in quantitative calculation of over-all furnace absorption by the ΔT method. It was concluded that they provide general confirmation of high values, but that

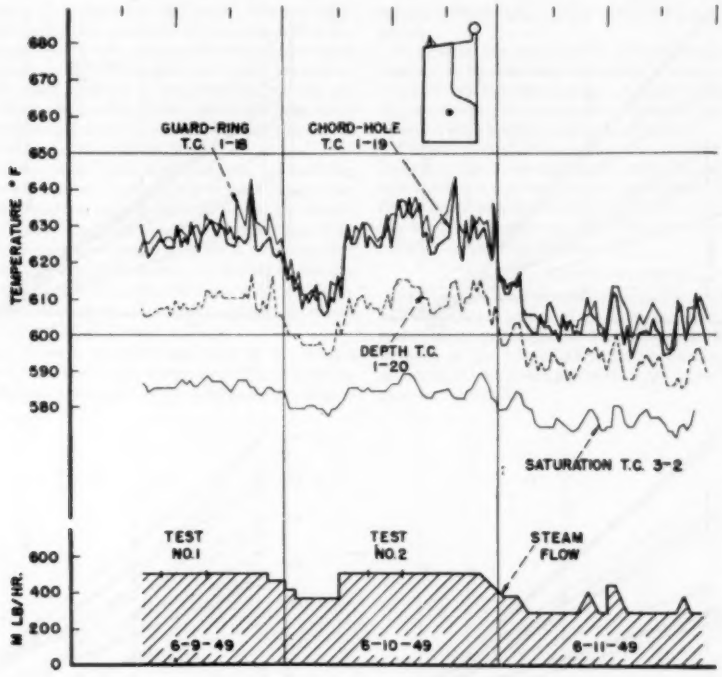

FIG. 35 COMPARISON OF GUARD-RING AND CHORD-HOLE THERMOCOUPLE DATA

lack of precision in measurements and variations caused by time interval between readings in unsteady-state conduction, as well as the possible effects of localized ash deposits, prohibit authentic evaluation of this item. The measurement of temperature gradient is shown to be practicable, and can be expressed in terms of heat-transfer rate, qualified by the consideration that it represents the localized position at tube center line where the thermocouple hot junctions were placed.

For future work it is believed that improvement can be made in thermocouple application. Even with the present coarse indication, the gradient readings are capable of detecting the presence of internal scale, or deposits having positive thermal resistance which might lead to overheating of the tubes, and thus provide the operator with a means for checking internal cleanliness conditions in high-duty zones of the furnace.

CONCLUSIONS

Measurement of furnace performance is simple in principle, but difficult of attainment, partly because of physical size, limited accessibility, and dependence on the sampling of large quantities; partly because of problems encountered in taking measurements at high temperature with accuracy, and partly because of diverse and intangible factors which can exert important influence upon the over-all performance, but yield only to statistical or indirect evaluation.

For lack of an absolute standard, the most acceptable basis for appraising test results is by correlation with major variables and by judging the trends and consistencies shown among individual test points. Validity is enhanced when points can be reproduced by check test under the same operating conditions, and is further enhanced when agreement can be indicated by other measurements obtained through independent means or methods of approach to the problem.

The generally good consistency of ΔT values, plotted against heat-balance data on over-all furnace absorption, is gratifying in this respect, as is the similarly good agreement of both methods with the independent calculation of steam-generating duty. Less satisfaction can be taken from the disagreement between tests 1 and 8 which were intended to be duplicate runs under similar operating conditions.

While the effects of heat release, excess-air, and burner combinations are of primary importance, it is obvious that ash deposits on the absorbing surface impose a fourth factor of great significance, which should be quantitatively taken into account, both for appraisal of test data and for consideration in future design.

The use of (S-A) and effectiveness factors is a partial recognition of this variable, and has been employed for conversion of test results to the hypothetical "clean-furnace" condition, from which other factors might be more logically compared. While this fails to account directly for the self-compensating effects of increased heat absorption by clean surfaces following the ash-covered areas, it makes quantitative adjustment for gross differences in furnace cleanliness and shows an improvement in the correlation of test points of furnace heat-absorption efficiency, as plotted in Fig. 8 (Part 1).[8]

No conclusive explanation is apparent for the discrepancy between tests 1 and 8. From a comparative study of Fig. 7, (Part

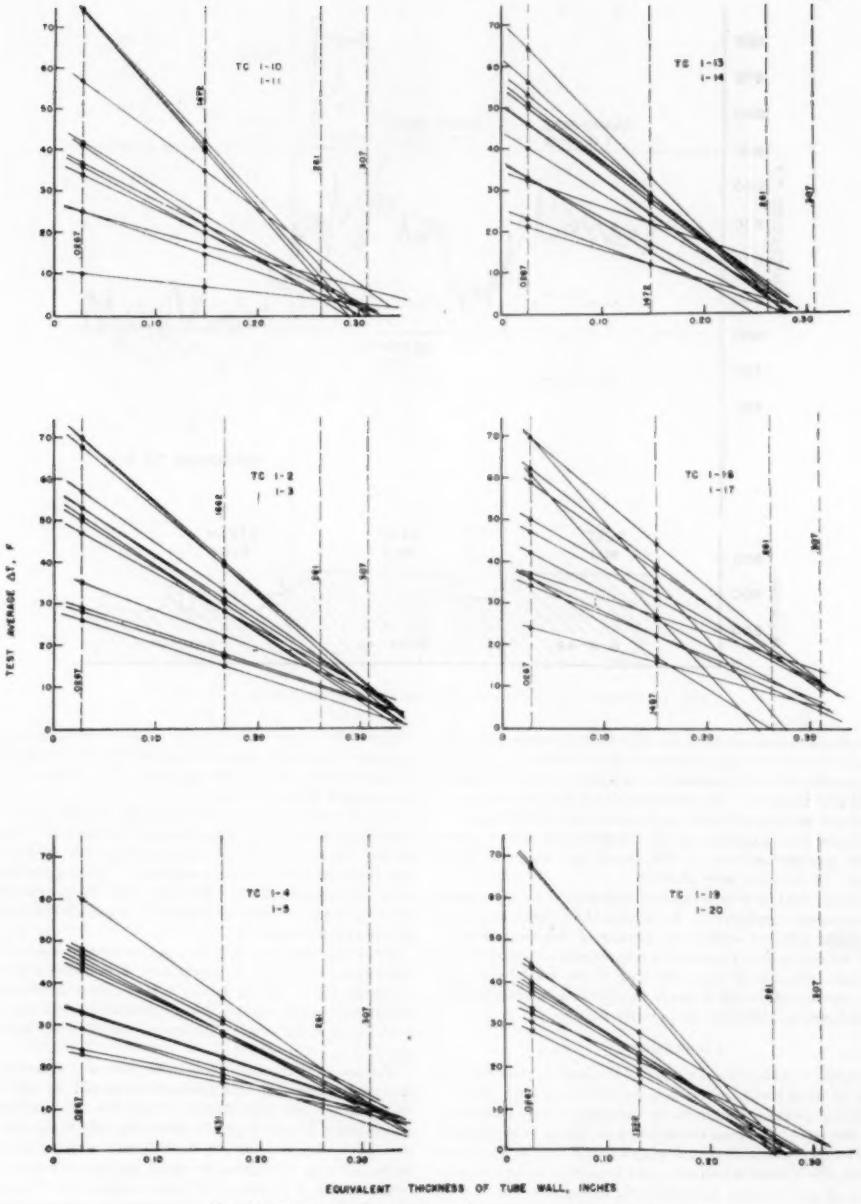

FIG. 36 MEASURED TEMPERATURE GRADIENTS IN TUBE WALL

I),[4] and Figs. 30 to 32, inclusive (of this paper), it would seem that the ΔT value for test 8 is confirmed by the independent calculation of steam-generating duty, whereas the heat-balance value of furnace absorption is high. The difference of 3.7 per cent in furnace heat-absorption efficiency is equivalent to 145 deg gas temperature at the furnace outlet, which seems too large to be ascribed to error in actual measurements, but might possibly be attributed to weighting of the traverse points.

Testing procedures would have been improved by including measurements of gas-mass-flow distribution at the furnace outlet for more accurate weighting of heat capacity of the gas stream. The exclusion of traverse position No. 5, in calculating average gas temperature, is an approximation of such weighting and seemed to be justified in most instances, by studies of the gas-temperature pattern at the rear of the division wall. Inclusion of all traverse points in the average for tests 1 and 8 would reduce the discrepancy to half of its present value.

Conclusiveness of results would be improved by procuring a greater number of check tests to show reproducibility of performance for a specified operating practice, or to measure the range of deviation which might occur with changes in the uncontrolled factors.

In general, the tests disclose a characteristic performance of decrease in furnace heat-absorption efficiency with increase of load and with increase of excess air, and show higher temperature of gases entering the superheater when using all burners or an unbalanced combination of two sets of burners.

The ΔT method of measuring furnace performance, when calibrated by the more quantitative heat-balance test, appears to give consistent measurement of furnace heat absorption, and offers a ready means for procuring further analysis of trends in day-by-day performance, or the effects of change in fuel characteristics or operating practice.

Acknowledgments

The authors wish to express appreciation of the co-operation and assistance extended to the committee and its individual representatives, by Messrs. W. V. Drake, C. B. Withers, and L. R. Webner, of the Monongahela Power Company, as well as to members of its operating personnel for accommodating the program of these tests.

Furnace Heat Absorption in Pulverized-Coal-Fired Steam Generator, Willow Island Station—Discussion

G. W. Bice.[1] The authors of both parts of this report are to be complimented for the excellent papers produced. There is no doubt that the data presented, together with their skillful analysis, will represent a valuable addition to the slow but steady accumulation of reliable data on the performance of large pulverized-coal-fired steam-boiler furnaces.

The very real need for such basic information by both boiler manufacturers and operating companies cannot be questioned, at least until such time as specified superheater and reheater outlet steam temperatures can be obtained on every new unit without the need to resort to field alterations in order to correct for erroneously estimated furnace heat-absorption values.

There is no indication in the text of Part II that any attempt was made either to confirm or to re-evaluate the S-A (slag-ash) factors developed during the Tidd tests.[2] Data such as those illustrated in the steady-load portions of Fig. 34 of Part II, together with corresponding estimates of slag or ash thicknesses at the thermocouple location, afford an excellent opportunity for check-computation of S-A factors. It is suggested that the data and furnace observation reports be re-examined with a view toward obtaining as many such check points as possible. Because of the empirical nature of these factors, a large number of points obtained by different observers on different furnaces will be necessary before they can be accepted as reasonably accurate and generally representative of bare-tube furnace-wall surface.

In examining the furnace-performance data, and adding them to those previously obtained at Paddy's Run[3] and Tidd,[4] the question might be asked: "Is any information of immediate practical value available from these studies?" The answer should certainly be in the affirmative. For one thing, it is obvious that furnace heat absorption (and indirectly superheater and reheater absorption) is controllable within certain limits by adjusting the following specific variables: (1) Excess air; (2) furnace-wall cleanliness; (3) burner flame geometry; (4) load.

The use of high excess air to increase superheat (through decrease of furnace heat absorption) has been widely used for many years and is, therefore, nothing new to either boiler manufacturers' service engineers or users' operating engineers. Data on variable excess air obtained during these furnace-performance tests therefore serve only to explain, perhaps a little more fully, the reasons why raising excess air increases superheat and lowering excess air decreases superheat, within limits generally covered by these tests.

The effect of furnace-wall cleanliness on furnace heat absorption has also been recognized almost since the first water-cooled furnace was placed in operation and, during much of this time, has also been utilized as a means of controlling furnace and superheater heat absorption, although to a somewhat more limited extent than excess air. Control of furnace-wall cleanliness can be accomplished in many ways, some of the more common of which are manual lancing with steam, air, or water; use of manually operated or automatic wall blowers, employing steam or air as the cleaning medium; controlled load changes; careful adjustment of furnace atmosphere (excess air); and more recently, skillful manipulation of burner flames.

Although previously recognized and used by a few operating engineers, the potentialities of burner-flame adjustment for controlling furnace heat absorption has only recently been made available and understood widely. The first positive step in this direction came with the application of vertically adjustable burners to corner-fired tangential-flame furnaces, as described in the Tidd reports.[3,4] Control of furnace absorption through variation in flame shape, rather than direction of firing, by adjustment of vane opening in horizontal turbulent burners was described in the Paddy's Run reports.[3] In the present reports on tests at Willow Island, it has been demonstrated that some degree of furnace-absorption control can be obtained with single-directional nonadjustable burners, by varying the number of burners in operation. Effective use of this method of control requires that more burners than are necessary to carry full load be installed. However, with the definite trend toward higher capacity boilers in the single boiler-single turbine combination, maintenance economics frequently dictate the installation of an extra pulverizer and burners over and above those required to carry full load.

Use of load variation to control furnace heat absorption indirectly through furnace wall-deposit shedding has been employed by various operating companies for many years. The possibilities of furnace-wall cleaning by this method increased materially with the advent of closely spaced bare-tube walls as compared with the once popular refractory-covered or water-cooled metal-block walls. Under many conditions, a drop to 50 or 60 per cent of full load for a short period (often 1 hr or less) will cause wall deposits to peel off in sheets, especially if these deposits are composed of semifused slag as usually found in dry-ash-removal furnaces with closely spaced bare-tube walls.

Looking into the future just a little, it seems apparent that, at least in central-station design, superheat and reheat temperatures will soon be in the 1150–1250 F range. If steam temperatures such as these are to be obtained, it will undoubtedly be found impractical to attempt to place all superheating and reheating surface in convection banks beyond the furnace. Thus, as more and more of the furnace heat-absorbing areas change from saturated steam-generating surface to superheating and reheating surface, the control of both quantity and distribution of radiant heat absorption will assume greater importance. Flame geometry through location and adjustment of burners, furnace cleanliness through control of wall deposits, and excess air (or possibly flue-gas recirculation) will have to be understood thoroughly and controlled rigidly if anticipated performance is to be realized. It is believed that a considerable potential of fundamental information along the lines required for such future design is available from the combination of data collected and presented here and in the Tidd and Paddy's Run reports.

In order to realize fully all of the potential benefits contained in the considerable volume of data so far obtained, it is strongly recommended that the Research Committee on Furnace Per-

[1] Engineer, Mechanical Engineering Division, American Gas and Electric Service Corporation, New York, N. Y. Mem. ASME.

[2] "An Investigation of the Variation in Heat Absorption in a Pulverized-Coal-Fired Water-Cooled Steam-Boiler Furnace, Part IV—Comparison and Correlation of the Results of Furnace Heat-Absorption Investigations," by A. R. Mumford and G. W. Bice, Trans. ASME, vol. 70, 1948, pp. 601–614.

[3] "Furnace Heat Absorption in Paddy's Run Pulverized-Coal-Fired Steam Generator, Using Turbulent Burners, Louisville, Ky.," parts I, II, and III, by R. I. Wheater, et al., Trans. ASME, vol. 72, 1950, pp. 893–947.

[4] "An Investigation of the Variation in Heat Absorption in a Pulverized-Coal-Fired Water-Cooled Steam-Boiler Furnace," parts I, II, III, and IV, by L. B. Schueler, et al., Trans. ASME, vol. 70, 1948, pp. 553–614.

formance Factors sponsor a fourth paper, in which correlation of data from all three series of tests together with additional rational or more readily usable empirical relationships among variables can be obtained.

C. G. R. HUMPHREYS.[5] In November, 1949, the writer installed at Sewaren Station, eight CE-S type thermocouples, two per wall, to compare this method, which was applied also at Tidd Station and Paddy's Run Station, with the method used at Willow Island.

As can be seen only slight differences in temperatures were found (Table 1).

TABLE 1

Date	Steam, M lb/hr	Drum, psi	Steam, deg F	Couple no.	CE surface type, deg F	PS surface type, deg F
1/13/49	820	1685	995	17	729	720
				19	732	742
				20	868	—
				21	748	—
				22	786	790
1/19/49	780	1675	1042	17	700[a]	695
				18	785	780
				19	705	700
				20	782	780
				21	720	—
				22	765	785[a]
				23	702	710
				24	760	740

[a] Loose connection at Speedomax.

Note that during the few data shown, the boiler was oil-fired and walls were clean. As can be seen the couples checked to within 5 F average, and CE type showed 5 F higher.

EARLE C. MILLER.[6] These papers, which are the result of careful testing, once again point up the difficulties experienced in obtaining reproducible data in commercial furnaces. It is noted that certain corrections had to be applied to the data before the results could be established. Concerning these corrections the writer has a few questions:

1 What is the basis for assuming temperatures needed any adjustment when average measured drop through *part* of screen appeared consistent?

2 What is the magnitude of the error in heat absorption caused by a given error in gas temperature at the furnace outlet?

3 How does measured drop through part of screen compare with predicted value?

4 In calculating radiation to the screen tubes, from gas passing through the screen, what effect does magnitude of the emissivity have on the corrections to the temperature? Also, could the emissivity have been estimated by an independent method?

5 From visual observation did the gas and flames appear to go farther toward the bottom when only two sets of burners were used, as compared to all burner operation? What was effect of load on flame length?

6 What was the magnitude of the adjustments made on the temperature ahead of the screen?

JOINT CLOSURE BY J. W. MYERS, R. C. COREY, AND F. G. ELY

The authors are indebted to Mr. Bice for his supplementary and interpretive comments on furnace performance, with which they are in general agreement.

With regard to the evaluation of S-A factors; it is possible to find a few instances in the Willow Island record where confirming evidence may be inferred. Thus, in Fig. 34, a maximum ΔT of 90 deg is indicated for thermocouple 1-7 immediately preceding test No. 2 which might be considered to represent a clean-surface condition in this locality, following the shedding of ash from the wall. Compared to this, the ΔT value of 34 deg during test No. 2, with ash deposit of $^1/_2$ to 1 in. thickness (see Fig. 7), indicates an effectiveness factor of 37.8 per cent, which is in substantial agreement with the data previously developed from the tests at Tidd Station.

It will be appreciated that in the Willow Island tests there were relatively few occurrences of ash dislodgement from the furnace walls during periods of test when the surveys of ash distribution were made and recorded in quantitative manner. Two additional points, as disclosed by further study of the charts, have indicated values of 59.5 per cent for $^1/_2$ in. thickness, and 41.5 per cent for $1^1/_2$ in. thickness of ash, and lie close to the original curve of S-A factors reported for the tests at Tidd Station.

The temperature comparisons presented by Mr. Humphreys show similar readings for the guard-ring and chord-hole types of thermocouples, for the condition of clean tube surface in an oil-fired unit. This comparison is consistent with the record shown in Fig. 35 of Part II where the tube surfaces were nominally free from ash deposit. It is of interest that this relationship holds in a temperature range considerably higher than that observed at Willow Island.

With reference to Mr. Miller's comments, we are submitting Table 2 of this closure which includes supplementary comparisons of gas-temperature data at the furnace outlet screen as derived from Tables 2 and 3 of Part I.

From furnace observation it was apparent that the direction of gas flow approaching the screen was not uniformly normal to the plane of the tubes. The gas flow was, in general, upset toward the rear of the furnace, and penetrated farther into the hopper section as the load was increased, and also with the use of two sets of burners as compared to the use of three sets of burners.

It was therefore considered illogical to use direct comparison of the geometrically similar traverse points for determining gas-temperature drop through the screen, which values are shown in Table 2 to be extremely scattered.

Considerable study was given to plotted temperature profiles of this section, in an effort to estimate fair values for the areas ahead of the screen that were not accessible for direct traverse measurement.

TABLE 2 COMPARISON OF TEMPERATURE DROP THROUGH SCREEN OBTAINED FROM DIRECT TRAVERSE READINGS WITH THAT OBTAINED FROM THE ADJUSTED TEMPERATURE VALUES

Test No.	Steam-flow rate, Mlb/hr	Excess air at furnace outlet, per cent	Temperature drop across screen, deg F: From observations during traverse[a]	From extrapolated profile plots[b]	From adjusted temperature values[c]
1	508	13.0	...	...	92
2	508	24.0	200	172	82
3	376	23.4	178	68	100
4	377	23.4	278	53	103
5	373	23.9	104	112	90
6	508	13.9	316	149	102
7	510	15.2	125	46	97
8	507	13.8	138	90	77
9	257	37.5	258	71	68
10	251	24.1	112	98	80
11	364	36.0	168	69	77
12	259	37.9	79	50	74
13	508	24.1	209	132	92

[a] Obtained by difference between the average of the values in Table 3 and the average of values at corresponding points in Table 2.
[b] Obtained by difference between the average of values in Table 2 and the average of profile plots from data of Table 3 extrapolated to include traverse points 1 and 2.
[c] Obtained from adjusted temperatures used for the furnace heat-absorption calculations. See text of Part I for method of computation.

These studies for which the average values are also shown in Table 2 were inconclusive, however, and necessitated an approach

[5] Combustion Engineering-Superheater, Inc., New York, N. Y. Mem. ASME.
[6] Design Engineer, Riley Stoker Corporation, Worcester, Mass. Mem. ASME.

by heat-balance calculations as described in the text. The values of temperature drop through the screen resulting from this calulation are reasonably consistent and are in fair agreement with the predicted value of 80 deg at full-load operation.

The magnitude of the error in heat absorption for a given error in the gas temperature may be calculated readily. The quantity of heat in the gases leaving the furnace (above the base temperature of 80 F) is given by

$$Q = \frac{W}{1000} c_p (T_1 - 80)$$

where Q = Heat in gases leaving furnace, kB/hr
W = Quantity of gas leaving furnace, lb/hr
c_p = Mean heat capacity of gas (above 80 deg), BTU/(lb)(deg F)
T_1 = Temperature of gas at furnace outlet, deg F

Partial differentiation of the above equation gives

$$\partial Q = \frac{W}{1000} c_p \partial T_1$$

Taking test number 1 as a typical example, substituting appropriate values for W and c_p gives $\partial Q = 174.8\ \partial T_1$. Therefore, an error of 100 deg in T_1 will result in an error of 17,480 kB/hr. Based upon the calculated value of net heat available for this test, 641,800 kB/hr, the error would be 2.7 per cent. Since the furnace heat-absorption efficiency is also based upon the net heat available, the absolute error in that quantity would likewise be 2.7 per cent. Thus, an increase of 100 deg in the temperature of the exit gas would lower the furnace heat-absorption efficiency from the calculated 45.8 per cent (Table 1, Part I) to 43.1 per cent.

Concerning the effect of the magnitude of the emissivity on the calculated temperature of the gas ahead of the screen, it can be shown that the allowable variation in the former must be confined to very narrow limits to obtain results consistent with the criterion cited in Part I when making the temperature adjustments.

It will be recalled that the adjustment was made with the aid of Equation [1]

$$Wc_p(T_1 - T_2) = UA(T_m - T_s) + \sigma\epsilon AF(T_m^4 - T_r^4)$$

Since $T_m = \frac{T_1 + T_2}{2}$, T_1 may be replaced by $2T_m - T_2$. By partial differentiation and substituting appropriate values in the resulting equation we may determine the variation in T_m for a given change in ϵ. When typical data from test number 7 are used

$$\partial T_m = 292\ \partial\epsilon$$

or

$$\partial T_1 = 584\ \partial\epsilon$$

Thus, for a change in ϵ of 0.1 (for example, from 0.095 determined empirically to 0.195) a corresponding change of 58 deg in T_1 would occur. Since this change is greater than the largest adjustment made to the temperature, T_1, it is apparent that the emissivity could not have been estimated from any observations with sufficient accuracy to be used in calculating the temperature drop through the screen.

In spite of the complexities involved in the evaluation of this increment of heat absorbing surface, it is believed that the test measurements as related to the plane above the screen tubes are valid and well within attainable limits of accuracy for this type of furnace-performance test.

Stress Distribution in the Continuous Chip—A Solution of the Paradox of Chip Curl

By E. K. HENRIKSEN,[1] ITHACA, N. Y.

This paper is intended to throw light upon the hitherto unsolved problem of chip curl. The chip passes along the tool face for a certain distance before it leaves the tool and then curls through space. The author assumes that a sudden drop in pressure occurs at the point of ultimate contact, which combines with a single force at this point. The physical origin of this system of forces is explained by surface roughness of the tool, which leads to an explanation of the sharp boundary line for the area of wear on the tool face. Distribution of pressure between chip and tool follows an exponential law. Methods of stress analysis are explained which should be useful in further investigations.

Introductory Observations

THE curling of the chip is an everyday phenomenon, and various attempts have been made to explain it. The most logical explanation, hitherto published, is the one given by Ernst and Merchant,[2] according to which the rate of deformation ("the cutting ratio") and hence the instantaneous velocity of the chip, vary across the root of the chip ("the plane of shear"), Fig. 1, in such a manner that the face of the chip which is in contact with the tool will be longer than the outer side of the chip. This will give the chip a tendency to curl away from the tool. In close connection herewith is the fact that the plane of shear normally is slightly curved and will be concave downward when cutting under steady conditions.

One might, so far, expect the chip to curl away from the tool face, immediately above the cutting edge, following a circular or helical path.

A closer observation, however, will show that the curling does not occur immediately after the chip has passed through the plane of shear. On the contrary, the chip passes along the face of the tool for a certain distance even when the tool is ground with a plane surface, and then it suddenly will leave the tool face, curling through space. In the following, the point where the chip leaves the tool face will be called "the point of ultimate contact."

In other words, the chip is "born curled," but it moves in a straight line for a certain distance, clinging to the tool face; then, first, it starts curling.

This fact is proved by several observations. Many micrographs of chips in connection with the workpiece and the tool, and many high-speed photographs will show it. The same conclusion is supported by the fact that the tool wear is distributed over an area of the tool face of a definite width, with a sharp and well-defined boundary line, Fig. 2.

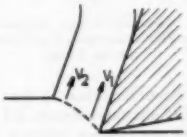

Fig. 1 Continuous Chip Formation, Showing Variation of Velocity of Chip Across Plane of Shear ($V_1 > V_2$)

Fig. 2 Wear on Tool Face, Showing Sharp Border Line of Worn Area

The Chip as a Cantilever Beam

In order to explain this observation we must assume that the chip is subjected to a load having a resultant bending moment of such a direction that it will tend to bend the chip back to the tool face.

In this paper orthogonal cutting is assumed, and only a plane tool face will be considered. It is, however, possible to give analogous solutions to the same problem, involving a tool, ground or worn to a circular groove, a "crater," or with a built-up edge, and an investigation shows, in principle, results similar to those obtained for a plane tool face.

The chip, as emerging from the plane of shear, with its inborn tendency to curl, may already contain a set of stresses "A." Another set of stresses "B" will be superimposed on the chip by the load from the contact with the tool face. After having passed the point of ultimate contact, and curling through space, no longer subjected to any load at all (ignoring its weight) it may still contain a set of stresses "C."

Between the plane of shear and the point of ultimate contact the total stress in the chip is determined by $A + B$, provided all stresses stay within the elastic range. If so, the stress C, in the curling chip beyond the point of ultimate contact, is equal to the "inborn" stress A. If the stresses $A + B$ exceed the elastic range some modification will take place. If A is zero, and B does not exceed the elastic range, then C must be zero; in other words, the curling chip must be stress-free. Whether such a condition exists or not is yet unknown.

The present investigation is limited to the stresses B. No assumption is made as to whether A is zero or not, but it is assumed that A + B stays within the elastic range.

Two sets of forces are at work between the chip and the tool face, a normal pressure and a frictional force. The normal pressure p between tool face and chip cannot possibly bend the chip backward, if anything it would tend to bend the chip away from the tool face; the conclusion would, therefore, be that the frictional forces μp must be strong enough to bend the chip backward to the tool face and hold it there, in equilibrium with the normal pressure p (see Fig. 3, where this system of forces is shown in full lines).

When the chip is considered as a cantilever beam, we get the load picture shown in full lines in Fig. 4, and we can write an

---

[1] Professor, Head of Materials Processing Department, College of Engineering, Cornell University. Mem. ASME.

[2] "Chip Formation, Friction and Finish," by H. Ernst and M. E. Merchant, Surface Treatment of Metals, ASM, Cleveland, Ohio, 1941, pp. 335–336.

Contributed by the Production Engineering Division and presented at the Semi-Annual Meeting, St. Louis, Mo., June 19–23, 1950, of The American Society of Mechanical Engineers.

Note: Statements and opinions advanced in papers are to be understood as individual expressions of their authors and not those of the Society. Manuscript received at ASME Headquarters, April 27, 1950. Paper No. 50—SA-9.

equation for the bending moment M_x in a point at a distance x from the point of ultimate contact.

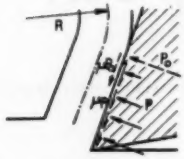

FIG. 3 FORCE SYSTEM BETWEEN CHIP AND TOOL FACE

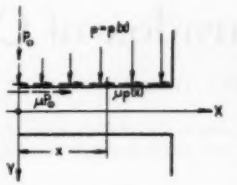

FIG. 4 SAME FORCE SYSTEM AS IN FIG. 3, ACTING ON A CANTILEVER BEAM

We will assume that R is the radius of curvature in the chip when it curls away beyond the point of ultimate contact, and the equation must express the fact that the bending moment M_x must have such a value for any x that it bends the chip straight; in other words, imposes a curvature of radius R on the curled chip in the opposite direction of the natural curl. This leads to the equations

$$\frac{d^2y}{dx^2} = -\frac{M}{EI}$$

$$\frac{M}{EI} = \frac{1}{R}$$

where R is the radius of curvature in the chip after it has started curling away from the tool face, in other words, the equation says: M = const. Assuming the coefficient of friction μ constant and p being an unknown function of x, we can transform the equation into a differential equation for p, which, by the way, is of first order only and easy to solve, giving p as an exponential function of x.

This solution is, however, so far only a solution of the differential equation in p, and it is necessary to make a test by inserting it into the original equation M = const, and when doing so we will find that the solution to the differential equation in p can by no means satisfy the original equation in M.

The conclusion is that a load system as that shown in full lines in Fig. 3 or Fig. 4, cannot hold the chip in equilibrium against a straight-line tool face.

This might be interpreted as a result of oversimplified mathematical assumptions. This is, however, not the case. A more complete investigation that takes into account the contribution of the shearing stresses to the deflection gives the same result, and so does an investigation of the chip flow over a tool face curved to a circle.

A well-fitting solution is, however, rather easily obtained if we assume that the load on the chip (and hence on the cantilever beam) is composed of two systems:

(*a*) A continuously distributed load $p(x)$ and a friction $\mu p(x)$, as before.

(*b*) A single, concentrated, normal force P_0 and a friction μP_0 located at the point of ultimate contact, as shown in dotted lines in Figs. 3 and 4.

Solution of the equations gives

$$p(x) = p_0 e^{\frac{2}{t}\frac{x}{t}}$$

$$P_0 = \frac{\mu t}{2} p_0$$

where p_0 is the unit pressure at the point of ultimate contact, and t the thickness of the chip.

FORCES BETWEEN CHIP AND TOOL FACE

The necessity for assuming a concentrated force P_0 at the point of ultimate contact may seem rather startling at first; as explained previously, it is not just some mathematical trick, introduced in order to find a nice and simple solution, but it must have a physical reason.

The validity of this statement can be supported in several different ways.

A consequence is that $p(x)$ does not decrease gradually to zero with x; it decreases only to a certain definite value p_0 which occurs at the point of ultimate contact. This is in accordance with the observation on a worn tool face; it seems difficult to understand the sharp boundary line of the worn section if there was a gradual decrease of pressure right down to zero.

Another way of looking at the problem is the following:

Let us follow the chip backward, from the free-curling state through the point of ultimate contact and further on, along the tool face. When passing the point of ultimate contact the curvature changes suddenly from R (natural curl) to infinity (straight line). At the point of ultimate contact, a load must be applied quite suddenly and with a bending moment of a definite value, equivalent to the sudden change in curvature, and such a load cannot start gradually from a zero value. However, a continuously distributed load, no matter how large it is, cannot suddenly generate such a bending moment of a definite value; this must require a concentrated single force.

This side of the problem may be rather difficult to grasp at first sight. Perhaps the matter can be clarified by reference to a somewhat related problem, that of a belt over a pulley. If the weight of the belt is ignored (which is usually the case), it is not possible to generate any tractive force by friction between belt and pulley unless there is a tension in the so-called "slack" side of the belt. With a zero stress in the belt, no traction can be built up.

These attempts to clarify the problem may be said to be rather on the mathematical side. Let us, therefore, try to find an explanation of a physical nature.

No tool face, no matter how well ground, and lapped, and polished, is straight. It has a certain roughness, and the chip has to pass a large number of small irregularities in the surface. When passing over each of them the chip is subjected to a variation in pressure, not sufficient to "throw the chip off," but, as the distance from the root of the chip increases, the tendency to "throw-off" is increased. Finally, one of these irregularities will be large enough to force the chip so far out that it is not "caught in" again by the friction on the next irregularity, and this constitutes the point of ultimate contact (see Fig. 5).

FIG. 5 MECHANISM OF CHIP FLOW OVER TOOL FACE AND "THROW-OFF ACTION"

A conclusion to be drawn from this explanation is that the location of the point of ultimate contact is, to some extent, a matter of chance, and also a matter of wear on the tool face. This is in

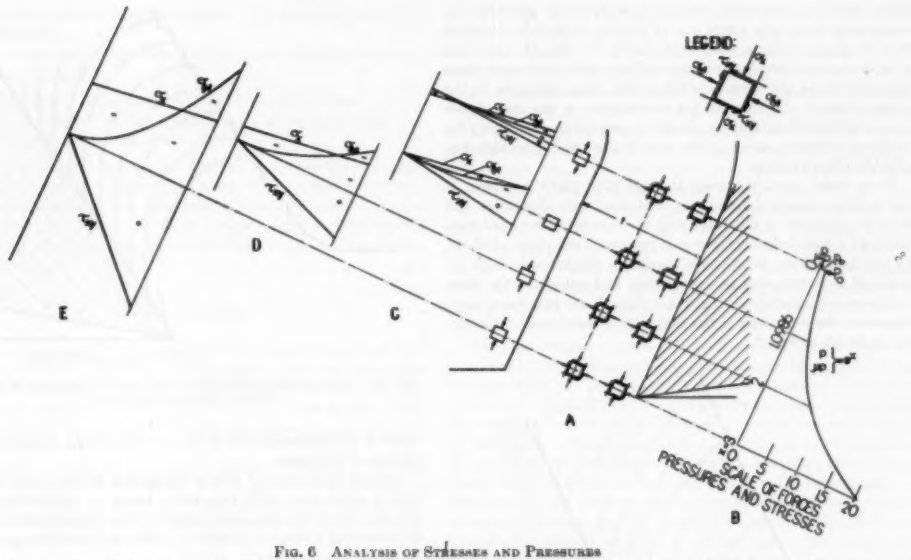

FIG. 6 ANALYSIS OF STRESSES AND PRESSURES

(*A*. Section through chip and tool, showing conventional signature for longitudinal, transverse, and shearing stresses. *B*. Distribution of pressure over tool face. *CDE*. Curves for longitudinal, transverse, and shearing stresses at four different sections of chip.)

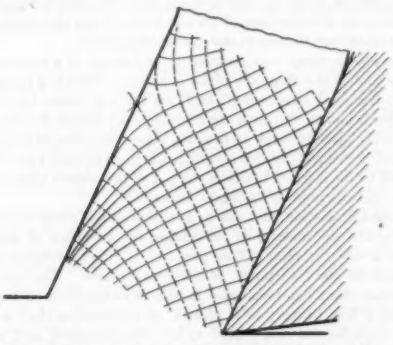

FIG. 7 TRAJECTORIES FOR PRINCIPAL STRESSES IN CHIP

(Dotted lines: Maximum principal stress σ_1. Full lines: Minimum principal stress σ_2.)

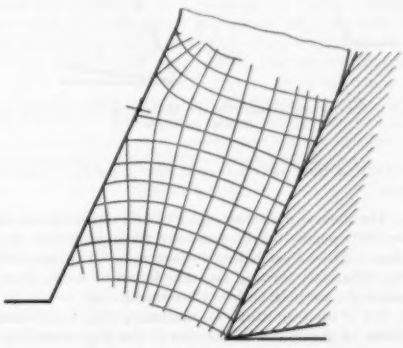

FIG. 8 TRAJECTORIES FOR MAXIMUM SHEARING STRESS τ_{max}

accordance with the observation that the chip, sometimes, may change its curvature and path quite suddenly, the reason being that the point of ultimate contact is changing from one high spot to another, due to local wear, perhaps only of a microscopic order.

ANALYSIS OF STRESSES AND DEFORMATIONS

Once the function $p = p(x)$ has been established, the further analysis is fairly conventional and simple. It is possible to determine the longitudinal and transverse normal stresses σ_x and $\sigma_{(y)}$ and the shearing stresses $\tau_{x,y}$. Diagrams are shown in Fig. 6, giving values for these stresses, and the forces and pressures between chip and tool face. Of more interest are the values of the principal (normal) stresses, maximum σ_1 and minimum σ_2, and the maximum shearing stresses τ_{max}, which occurs at a 45-deg angle to σ_1 and σ_2. The stress trajectories for the principal stresses and the maximum shearing stress are shown in Figs. 7 and 8.

It should be emphasized, in order to avoid misunderstanding, that the values for pressures and stresses shown in these figures are derived from some simple basic values, such as $\mu = 1$, $t = 2$, and $p_0 = 1$, just in order to illustrate the nature of the variation of these components and their mutual relations, rather than to give true numerical values.

Besides these stress trajectories, it will be of interest to determine the trajectories for the direction of maximum elongation of the material in the chip. Maximum elongation occurs in the direction of maximum principal stress when the material passes through the plastic range. Now, this investigation does not, in

effect, deal with the plastic range. It is, however, generally assumed that the plastic range is very narrow, essentially identical with the plane of shear, and, when that is the case, the direction of the stresses in the plane of shear will not differ very much from the direction of the stresses in the elastic range adjacent to the plane of shear. In order to get the location of the trajectories for maximum elongation, we, therefore, assume the trajectory for maximum shearing stress at the root of the chip to be identical with the plane of shear.

As a metal particle passes through this plane of shear, it will undergo plastic deformation, and maximum elongation will be in the direction of the tangent to the corresponding maximum (normal) stress trajectory where it intersects the plane of shear. By this method the directions of maximum elongations can be determined for every point across the chip, and, subsequently, these directions are transferred lengthwise through the chip where they determine the directions of the tangents to the desired trajectories, as shown in Fig. 9.

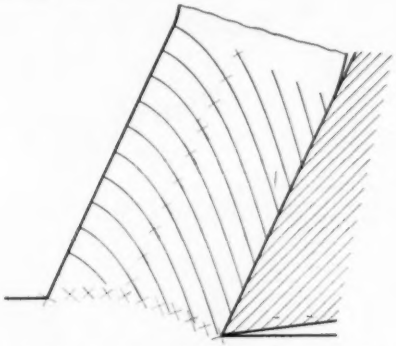

FIG. 9 CURVES FOR DIRECTION OF MAXIMUM ELONGATION OF MATERIAL IN CHIP

A study of these curves reveals several points of interest, as follows:

(*a*) The lines of maximum shear have a direction almost, but not entirely, parallel to the surface of contact between chip and tool face. These lines indicate where material is being sheared off the chip, thus forming the thin layers or laminations that constitute the essential body of the built-up edge.

(*b*) One of the trajectories for maximum shear must constitute the plane of shear, and at the root of the chip these trajectories have the same concave form as found from experience for the plane of shear.

(*c*) The lines of maximum elongation coincide very closely with one of the patterns for chip structure found by Oldacre and Erickson.[1] Under certain cutting conditions the chip elements would be continuously curved, such as is shown in Fig. 10. The resemblance to the curves in Fig. 9 is striking.

ASSUMPTIONS AND LIMITATIONS

No conclusion is valid beyond its assumptions. This fact imposes several limitations.

Only orthogonal cutting and a plane tool face is considered here. It is assumed that the chip has a solid cross section throughout; hence a discontinuous chip is not, or only partly, covered by the findings of this paper.

Another limitation of this investigation results from the fact that it deals only with the elastic range of deformations and stresses, one of the principal reasons for this being the desirability of preserving a relative simplicity in the mathematical apparatus involved.

This limitation is, however, not too serious, because the pattern of trajectories of elastic stresses, although certainly modified when passing from the elastic range into the plastic range, will still serve as an indication of the character (if not the magnitude) of the stress distribution in the plastic range itself.

The plastic range was assumed to be limited to a narrow zone at the root of the chip (the plane of shear). This is a fairly generally accepted assumption; still, we do not know for certain whether it is entirely correct or whether some plastic deformations are taking place through an interval above the plane of shear. If so, then the validity of this investigation in its present state will be limited to the interval between the end of the plastic deformation range and the point of ultimate contact.

A third limitation, also due to a mathematical simplification, is involved in the method of calculating the variation of shearing stress across the chip. This problem is closely related to the question of the "warping" of the cross section. The usual assumption (that has been used in this investigation) is that the section is free to warp as it pleases, an assumption that may be fairly true for the major part of the chip involved, and which, therefore, leads to a fairly true pressure distribution between chip and tool, but which is not entirely correct in the close vicinity of the plane of shear, where the distribution of shearing stress may have to be modified.

Finally, the coefficient of friction is assumed constant, and any effect of temperature variation and of work hardening is ignored; so is any effect of time lag.

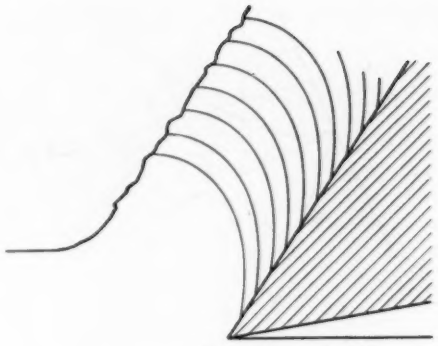

Courtesy Oldacre and Erickson

FIG. 10 CURVES FOR DIRECTION OF MAXIMUM ELONGATION, DRAWN AFTER A PHOTOMICROGRAPH

CONCLUSIONS

The fact that a chip passes along the tool face for a certain distance before it leaves the tool and curls through space has been investigated and leads to the assumption of a sudden drop in pressure at the point of ultimate contact, combined with a concentrated single force at this point.

The physical origin of this system of forces is explained by surface roughness of the tool, and it leads to an explanation of the very sharp boundary line for the area of wear on the tool face.

[1] "Mechanisms of Metal Cutting. Frozen Motion or Chip Contours as a Clue to Process of Chip Formation," by W. H. Oldacre and H. A. Erickson, *Mechanical Engineering*, vol. 69, 1947, pp. 655–657.

The distribution of pressure between chip and tool follows an exponential law.

A stress analysis for the chip gives an explanation of the following three phenomena:

The downward concave curvature of the plane of shear.
The "chipping off" of thin layers forming the built-up edge.
The structure of deformation in the chip.

It is the belief of the author that the paper has thrown some light upon a hitherto unsolved problem, but he is also aware that many more problems in this field still remain unsolved. He hopes, however, that methods of analysis, such as described in this paper, or related hereto, may be found useful in further investigations.

Discussion

H. A. Erickson.[4] We believe with the author, that the chip "is born curled." However, it appears to us that he contradicts his own assumption inasmuch as he hypothecates the curl as a secondary operation occurring not at "birth" but shortly thereafter, through interference from an obstructive "high spot" on the tool surface.

The effect of such a high spot is indicated clearly in the use of chip breakers. These result not in further curling, but in breaking the chip, as the chip rigidly resists further deformation after it is born curled in passing through the narrow zone of formation.

We wish, however, to compliment the author on his studied and careful approach to this complex problem. In view of the importance of the metal-cutting process, many more scientific researchers should be investigating the intriguing problems of chip formation and structure.

M. E. Merchant.[5] It is evident that the author has spent considerable time in the development of the theory presented in this paper and has carried through a considerable amount of mathematical analysis. His efforts are to be commended, and we congratulate him on his interest in tackling this particular problem in the mechanics of chip formation. It is certainly true that, as the author puts it, "the chip is born curled" at the shear plane and yet remains in contact with the flat tool face for some little distance above the cutting edge before peeling away from it. The main questions which concern the author are how and why the naturally curled chip remains in contact with the flat tool face for a time before peeling away.

We feel that in searching for an answer to these questions, the author somehow "got off on the wrong foot" at the start. He considers the problem as involving the gross stressing of a beam (comparing the chip to a beam) and tries to determine the type of force system that would bend the curved beam into contact with the flat tool face for some distance above the cutting edge. This results in the necessity for an artificial assumption regarding the stress distribution at the chip-tool interface, making it necessary to suppose that there is a residual force P_0 at the point where the chip peels away from the tool face, rather than a stress distribution of the type which approaches a value of zero stress at this point. Such an assumption is in direct contradiction to the actual behavior of elastic bodies which are in contact.

It is this very matter of the behavior of elastic bodies in contact which is the crux of the present problem. Instead of the problem being one concerning the "gross" stresses in a beam, it is essentially one involving the "surface" stresses in two elastic bodies which are in contact. In essence, the chip, as it leaves the shear plane, is a cylindrical body, and the tool face which contacts the chip is a normally plane surface. Thus the problem is essentially one of elastic contact between a plane and a cylinder. The surface of the cylinder (back surface of the chip) and the plane tool face deform together elastically to develop a definite area of contact above the cutting edge, which supports the resultant force which the tool exerts on the chip. Thus, instead of treating the flattening of the chip against the tool as the deformation of a curved cantilever beam, a very much better approximation would be to treat this flattening as one involving surface-stressing due to elastic contact, similar to that described by Herts's equations for elastic contact. In fact, the Herts equations for elastic contact between a cylinder and a plane can be directly applied, as a fair approximation, to the analysis of the problem of elastic contact between chip and tool.

When the foregoing approach is used, the conclusions drawn are in harmony with observed facts about the process of machining. For one thing, the artificial supposition of a residual force at the point where the chip peels away from the tool face is eliminated. The contact pressure at the chip-tool interface decreases to zero at that point of separation, in a normal manner. In addition, the equations of elastic contact show that the point of maximum pressure between chip and tool will lie, not at the cutting edge, as predicted by the author's theory, but at a point some distance above the cutting edge; the location of that point is determined by a line through the center of curvature of the chip and perpendicular to the tool face. That this point of maximum pressure is actually somewhat above the cutting edge in practice is borne out by the way in which the tool face wears or craters. This cratering of the tool face always begins at a location somewhat above the cutting edge and then spreads out from that point toward the cutting edge and toward the point where the chip peels away from the tool face. Such a behavior occurs even in cases where no built-up edge is present, as in machining with sintered-carbide tools at very high cutting speeds. On the other hand, according to the author's theory, which predicts that the contact pressure would be a maximum at the cutting edge, wear and cratering should start there, contrary to actual fact.

Author's Closure

The straight form of the chip before it reaches the point of ultimate contact is an effect of the force system described. Take this force system away and the chip will curl, following its inborn tendency. This is what the high spot does. It lifts the chip off the tool face so that no further forces will act upon it and prevent it from taking its natural curl.

In the comparison with the chip breaker: The chip breaker is a large obstruction above the road, that dents your fenders, while the high spot is only a surface bump that just makes your wheels bounce from the ground.

The force P_0 can hardly be said to be "residual," because it may change its value, due to transient variations in the tool surface. Actually it is a mathematical simplification for a localized peak on the curve for $p(x)$ which may take a form as shown in Fig. 11. Similar peaks in pressure-distribution curves are known from other cases of bodies in contact.

It is a general rule that when direct normal loads and bending loads occur on the same structure, then the bending loads will produce more deformation, and normally, higher stresses; in other words, they will predominate over the normal loads, which are frequently ignored completely. Hence the gross bending can definitely not be ignored.

Dr. Merchant's contribution is valuable because it points to two factors, both of which have been considered to some extent,

[4] D. A. Stuart Oil Company, Ltd., Chicago, Ill.
[5] Research Physicist, Research Department, The Cincinnati Milling Machine Co., Cincinnati, Ohio. Mem. ASME.

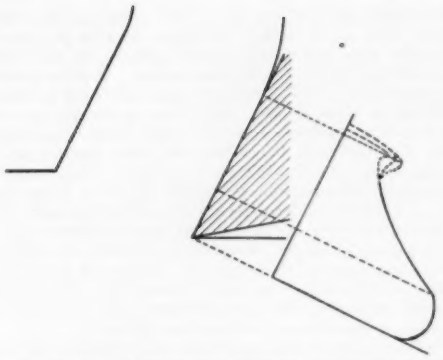

FIG. 11 PRESSURE DISTRIBUTION OVER ELASTIC RANGE (UPPER PORTION OF TOOL) AND PLASTIC RANGE (LOWER PORTION, ADJACENT TO THE CUTTING EDGE)

and which will be considered in future developments of the study of chip stress.

The most important point brought out by Dr. Merchant is the question of the location of the pressure maximum. This is the only point where the theory presented in this paper did not, so far, receive confirmation from common observations, but the answer hereto is already implied in the author's repeated statements that the validity of the theory is limited to the elastic range, in other words, to the interval between the point of ultimate contact and the point where plastic deformation begins.

The theory presented in this paper has, however, already been extended into the plastic range. One of the results found is that the steep rise of the pressure curve, according to the exponential function, does not continue beyond the elastic range; after the plastic range has been entered the contact pressure curve will reach a maximum and then again decrease, approaching the cutting edge, as shown in Fig. 11. It is of interest to note that the shape of the pressure curve is not symmetrical, as it would have been according to an application of Hertz's equations.

The second point raised by Dr. Merchant is the effect of localized surface pressure, and this to some extent has already entered the picture in the curves for $\sigma_{(y)}$ (see Fig. 6, *CDE*). A complete analysis should further consider a superposition of this effect on the effect of gross bending. The full effect of localized pressure would, however, have to be calculated by other methods than by Hertz's equations, for the following reasons:

(1) Hertz's equations assume a body system with symmetrical support; the chip is unsymmetrical, supported on the one side, and entirely free on the other side.

(2) Hertz's equations assume a symmetrical load system, and in particular, no tangential force. The chip load is composed of normal and tangential forces of equal order of magnitude.

(3) Hertz's equations assume a thickness of metal in the direction of pressure, that is, infinity as compared with the width of the area of contact; the thickness of the chip and the width of the area of contact are of the same order of magnitude.

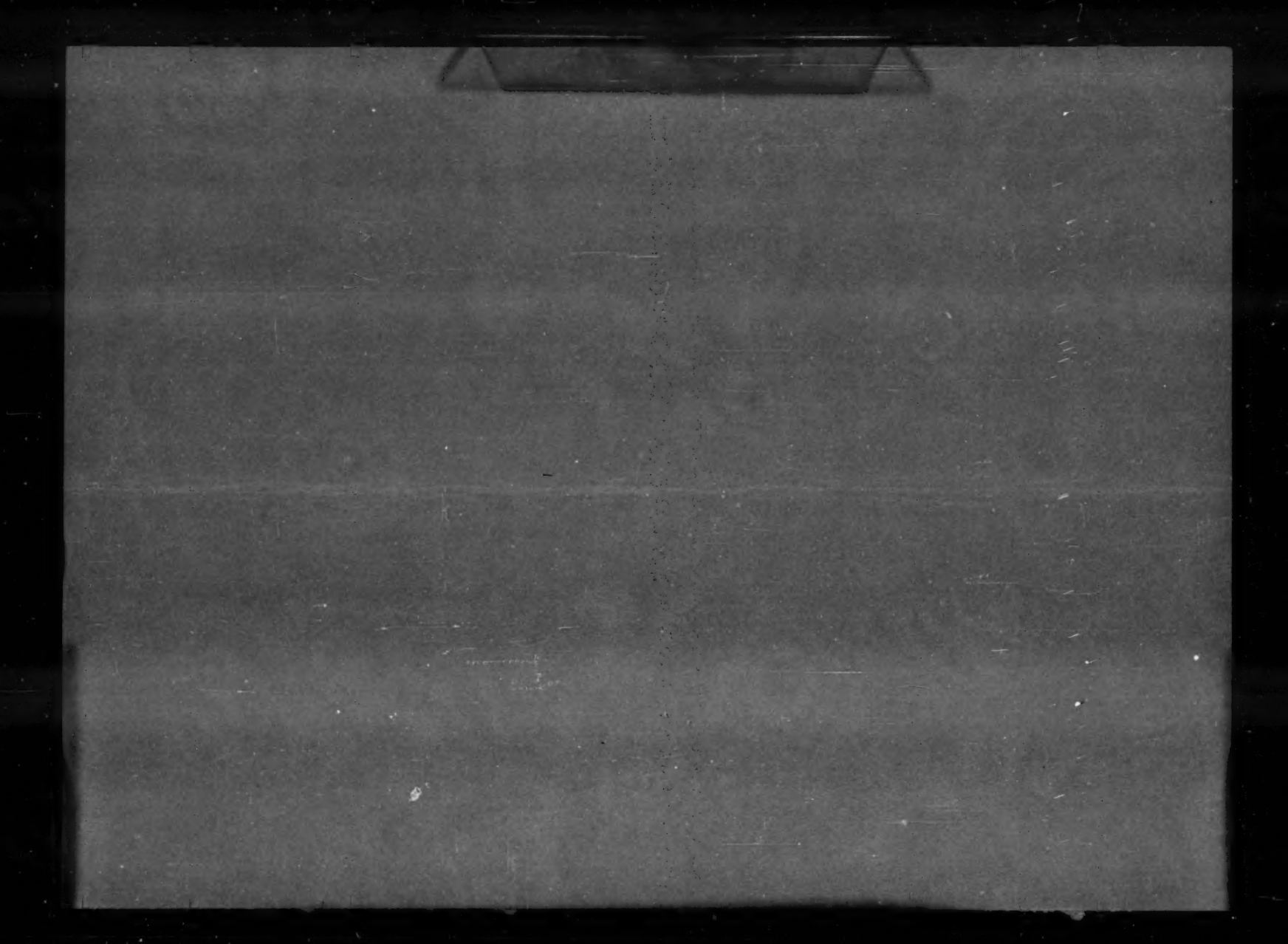

AN ASME PAPER

Its Preparation, Submission and Publication, and Presentation

To a large degree the papers prepared and presented under the ASME sponsorship are evidence by which its professional standing and leadership are judged. It follows, therefore, that to qualify for ASME sponsorship, a paper must not only present suitable subject matter, but it must be well written and conform to recognized standards of good English and literary style.

The pamphlet on "AN ASME PAPER" is designed to aid authors in meeting these requirements and to acquaint them with rules of the Society relating to the preparation and submission of manuscripts and accompanying illustrations. It also includes suggestions for the presentation of papers before Society meetings.

CONTENTS

Price 35¢. No discount allowed. *A remittance must accompany all orders for $3.00 or less. U.S. Postage Stamps are acceptable.*

THE AMERICAN SOCIETY OF MECHANICAL ENGINEERS

29 West 39th Street, New York 18, N. Y.